SYNTHESIS AND CHARACTERIZATION OF HEALABLE WATERBORNE POLYURETHANES

Roberto Hernández Aguirresarobe

Supervisors

Prof. María José Fernández-Berridi Taberna

Prof. Lourdes Irusta Maritxalar

POLYMAT, Polymer Science and Technology Department,

Faculty of Chemistry, University of the Basque Country

(UPV/EHU)

Donostia 2016

Al final de este largo camino toca escribir la última página (y posiblemente la más leída) de esta tesis y agradecer a toda esa gente que ha estado a mi lado durante este tiempo.

En primer lugar, quiero darles las gracias a Josepi y a Lourdes la oportunidad de trabajar con ellas y por todo lo que he aprendido. También quiero reconocer a Yanko, María Eugenia y Alba el apoyo tanto científico como personal que me han dado durante mi estancia en el laboratorio. Así mismo, no quiero olvidarme de Loli, por su proximidad y ayuda cuando hemos necesitado de su buena mano con la microscopía.

Tengo que acordarme de la gente que me acogió cuando entré en el laboratorio: Marina, Lorea, Haritz, Marian, Itziar, Itxaso y de toda la gente de los diferentes departamentos con los que he ido coincidiendo (Ingeniería, Catálisis, Reología, Ensayos) que siempre han estado ahí cuando he necesitado ayuda.

Qué puedo decir de toda la cuadrilla de becarios, tanto los de mi generación (Alex, Jorge, Maite, Eneko, Ana, Andrea, Nora, Asier, Pablo, Ibai, Ion, Marije, María) y los que se han ido incorporando (Oihane, June, Ane, Nerea, Idoia, Jordana, Itziar, Bea,…). Juntos hemos compartido muchos buenos momentos y superado los baches que tiene esta etapa.

A mi familia, especialmente a mi Ama y a mi Aita, por apoyarme siempre. Y a toda la gente que me ha dado fuerzas para continuar en este camino.

Por último, a Izaskun, por los litros de café y kilómetros en bici que (implícitamente) lleva esta tesis.

Esta tesis ha sido un reto muy personal que he llevado adelante con mucho esfuerzo y perseverancia. Sin embargo, tengo que decir que los resultados más importantes del trabajo no se recogen en estas páginas.

Eskerrik Asko!

GENERAL INDEX

CHAPTER 1

Introduction

1.1 General introduction

This work, entitled "Synthesis and characterization of healable waterborne polyurethanes", has been carried out at the University of the Basque Country in the Polymer Science Group with funding from the Basque Government.

This group has wide experience in the synthesis and characterization of different types of polyurethanes, both solventborne and waterborne polyurethane resins as well as polyurethane foams and nanocomposites. However, this is the first attempt of the group in the field of stimuli-responsive and healing materials.

1.2 Background

1.2.1   Healable polymeric materials

One of the most interesting characteristics of natural tissues is their ability to self-repair damaged structures. Inspired by this ability of living organisms and natural materials, researchers are trying to incorporate the same concept to develop manmade materials able to restore their structural integrity in case of deterioration or failure.

In general terms, self-repairing or self-healing can be defined as the ability of certain materials to *autonomically* repair (heal or recover) damage without losing their physical properties.

In biological systems, the self-reparation phenomenon is triggered by chemical signals released in the site of the damage. As a consequence of these signals, an orchestrated series of reactions occurs, which implies different stages of transport, deposition and assembly of healing agents [1–3]. However, mimicking the natural self-repairing mechanisms is an extremely challenging issue.

Research has been carried out in the field of healable materials based on metals, ceramics and polymers. Among these, polymers seem to be the most suitable candidates owing to their intrinsic physical properties and the ease by which they can be functionalized [4–6].

Generally, healable polymers incorporate active elements (embedded in the polymer matrix or attached to the polymer structure), which can act as sensing and/or reactive components. Ideally, these components would be able both to sense and repair invisible pinholes and microcracks over the lifetime of materials with no or minimum intervention. Hence, they make materials safer, more reliable and durable and reduce maintenance costs.

1.2.2 Damages

In general terms, damages are usually described as changes introduced in the material structure, which negatively affect their function and/or performance. The appearance of these defects can be due to different factors:

- Harmful environmental conditions, substances or agents, such as oxygen, oxidizing agents, water, solvents, heat, visible light or living bodies such as fungi, bacteria, insects, animals and others [7].

- The result of actions during their lifetime, such as impact, fatigue, fracture or puncture [8,9].

The presence of these defects can promote a degradation process, which implies different stages of coalescence, crack propagation and finally the failure of the material [10,11]. This degradation process is affected by the crack depth, material/crack geometry and applied stress as well as by the nature of the polymeric system. Figure 1.1 shows different types of damages affecting structural polymers and polymer composites.
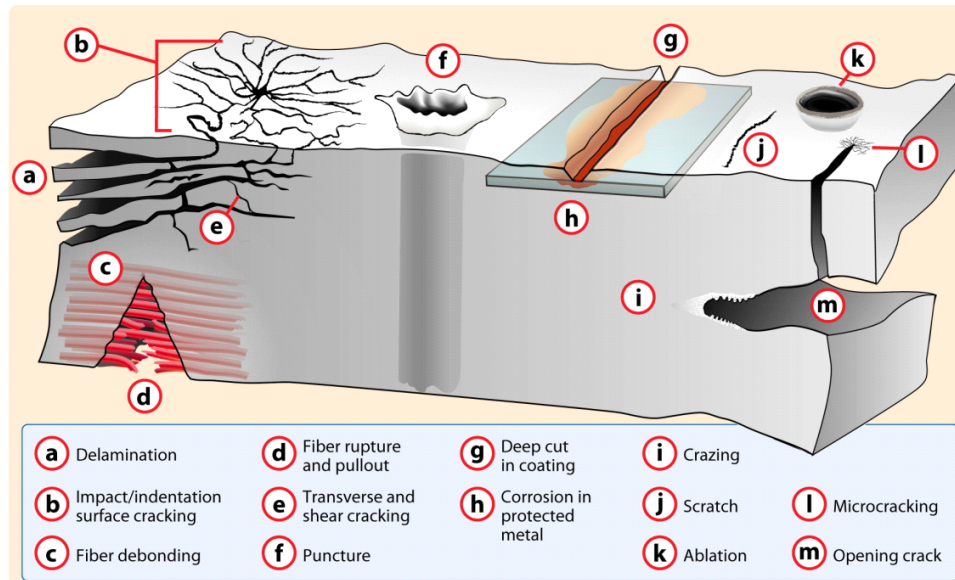
Figure 1.1 *Types of damages affecting polymers and polymer composites [9].*

As shown, polymers can present a wide variety of damages, which are directly affected by their nature and function. For example, when applying an impact, the resultant damage is different in coatings or reinforced materials. In the former, the impact can provoke surface cracking whereas in the latter, the fibers rupture. Hence, it is necessary to foresee the type of damage that can be present in a material according to its nature and application.

Unfortunately, deterioration of materials is difficult to avoid, perceive and repair as damages are typically a local phenomenon, often formed deep inside the structure [12].

1.2.3   Healing mechanisms in polymers

Although most of the recent developments focus on synthetic aspects, it is important to take into account the role of the physical properties of the polymer network in the healing process. A prerequisite for the healing process to occur is the generation of a mobile phase, which will contribute to the diffusion of active elements to the damaged surface and promote the damage refilling. Therefore, a

well thought out material design with the appropriate physical and rheological properties is necessary.

A widely accepted theory involving crack healing in polymers is that put forward by Wool et al. [13,14], who proposed a polymer diffusion model in terms of five stages: surface rearrangement, surface approach, wetting, diffusion and randomization (Figure 1.2).
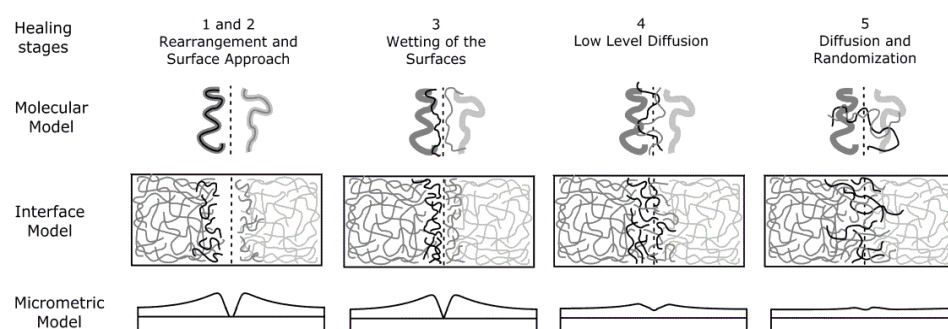

Figure 1.2 *Healing mechanism via molecular interdiffusion.*

According to this theory, when the crack is generated, polymer chain-ends are available in the newly formed surfaces. These chain ends are susceptible both to rearrange themselves in the bulk polymer (1) and/or start the healing process. The rearrangement in the bulk will delay or hinder the healing process. However, if the chain-ends initiate a reptation into the opposite side of the crack, a surface approach occurs (2) leading to a wetting process (3). As a consequence, the diffusion of the polymer chains occurs first (4) and finally a randomization of the healed material takes place (5).

It should be mentioned that the last two stages are strongly dependent on the diffusion coefficient of the interpenetrating chains and, therefore, of the nature of the polymer. In the case of thermoplastic polymers, for $T_{healing} > T_g$, the whole material can initiate the healing process. However, in the case of vitreous and thermostable polymers, only the free chain-ends generated as a consequence of the crack are responsible for the polymer self-diffusion [15–17].

Additionally, after the randomization process, an immobilization process occurs, resulting in the partial or full restoration of the mechanical properties. This immobilization process could be related to the decrease of the material temperature or to physical or chemical reaction produced by the healing agents [17,18].

Although this theory provides general considerations regarding physical polymer network requirements, the healing mechanism should take into account the damage characteristics, such as the nature, depth or geometry, in order for the repair to be successful. Damages involve different physical and/or chemical degradation processes depending on the scale of the damage, from Angstrom level to nano-, micro- and millimeter range. Accordingly, researchers have developed different healing strategies based on interactions capable to take action at different length scales. Figure 1.3 illustrates different physicochemical processes that can occur during the damage of materials and some of the repair mechanisms depending on the dimensions of the damages.
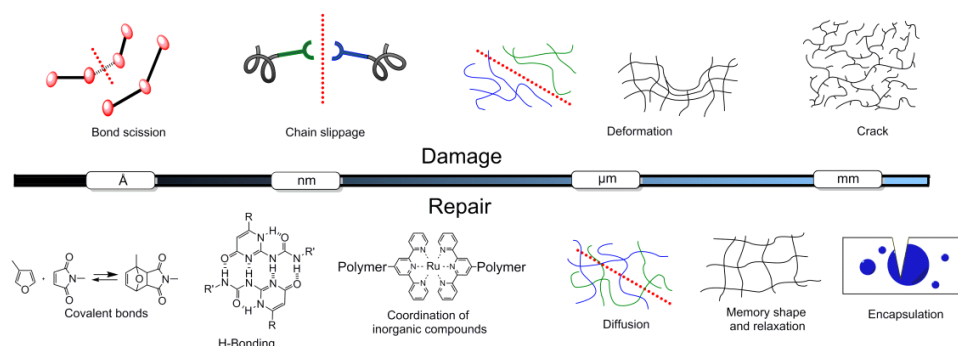
Figure 1.3 *Damage and repair mechanisms in terms of length scale [3].*

As shown, the appearance of damages involves specific degradation processes at each scale. However, the damage formation is a dynamic process. Thus, damages in the Angstrom scale provoke the rupture of covalent bonds of the polymer chains and progress to higher scales, producing polymer chain slippage, material deformation and finally the appearance of cracks. In the same manner,

damages produced in a higher scale involve the material degradation in lower levels.

In general, synthetic healing approaches focus on interactions that act at one specific scale and take advantage of molecular diffusion or shape memory effects to produce repairs at higher scales. However, these alternatives are not able to superimpose different individual events across different scales, as occur in biological systems.

1.2.4   Classification of healing mechanisms in polymers

The classification of different healing mechanisms in polymeric materials has been a difficult issue due to the inherent multidisciplinary nature of the field. Hence, classifications based on the triggering process of the healing, the chemistry involved in the healing process, the intrinsic or extrinsic nature of the healing or the reversibility have been proposed [4,19–23]. Scheme 1.1 provides a general overview of the healing process regarding the different aspects mentioned above.
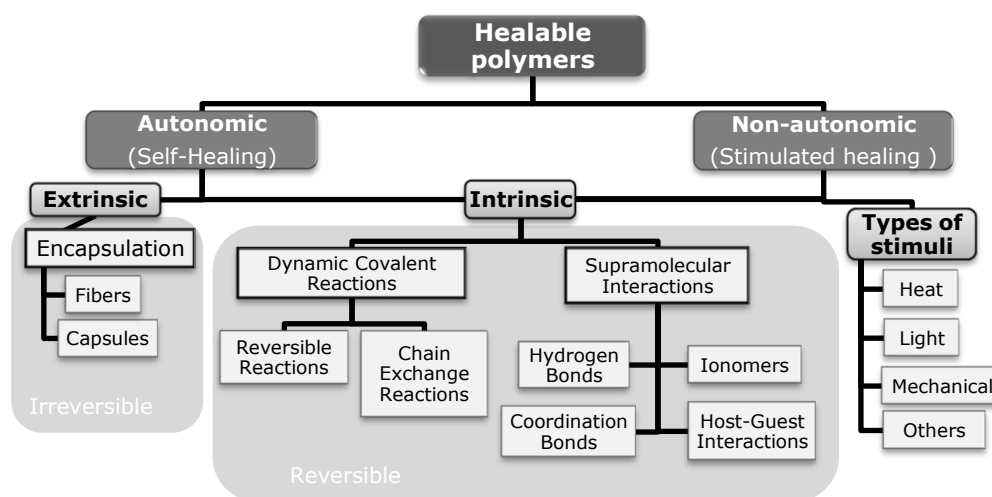
Scheme 1.1 *General classification of self-repairing polymers.*

Essentially, two main groups can be distinguished according to the autonomic or non-autonomic behavior of the healing mechanism. The difference between these two groups is the process by which the healing process is triggered.

Autonomic healable materials are the ones that can repair damages without any intervention; that is, the damage generation itself is responsible for the activation of the healing mechanism. Thus, this type of materials can be repaired without the intervention of humans and, for this reason, they are called self-healing materials.

Non-autonomic healable materials can be defined as those, which need external intervention to be repaired. For this reason, these materials are also called assisted or stimulated healable materials, as the healing mechanisms do not start themselves but operate in response to a certain stimulus.

In the following sections, the most relevant synthetic approaches regarding both autonomic and non-autonomic healable alternatives are summarized. In addition, the most common stimuli used in non-autonomic healable materials are also described.

1.2.5 Healing reactions in polymers

A general healing strategy should take into account not only aspects such as material properties and function but also the damages that they could suffer during their lifetime. In order to provide healing abilities to different types of materials, a wide variety of synthetic alternatives have been applied. These synthetic alternatives can be divided into extrinsic or intrinsic according to the intervention of the polymer matrix in the healing process.

Extrinsic healing materials incorporate liquid healing agents such as monomers or catalysts, within brittle vessels into the polymeric matrix. These vessels are able to migrate to the crack and release the healing agent, promoting the crack refilling and the material curing.
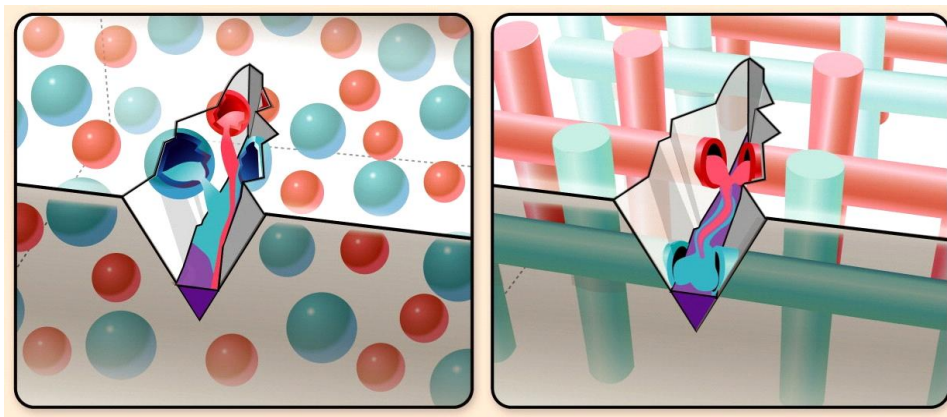
Figure 1.4 *Schematic representation of self-healing concept using microcapsules and hollow fibers [9].*

This repairing alternative has mainly been used for thermoset and polymer composites. The healing process in highly crosslinked polymer structures is hindered owing to the low molecular mobility they present. However, the low viscosity of the healing agents enables them to reach the damaged area and refill the crack. Figure 1.4 shows the way of acting of extrinsic self healing polymer composites containing liquid active agents embedded in microcapsules (left) and hollow fibers (right) [24,25]. This process is only effective when healing agents are available on the crack's surface and as such, is considered irreversible.

In order to develop polymeric materials capable of undergoing repeated healing events, researchers have focused on intrinsic healing materials. This concept requires the presence of "weak linkages" in the polymer network capable of breaking in response to the stress or the appearance of defects, and able to recombine afterwards. Selecting the appropriate chemistry, these "weak linkages" can recombine to reform the virgin polymer structure and lead to the healing process. This approach can be applied to both thermoplastic and thermoset polymers and elastomers.

Depending on the molecular principle used in the healing process, they can be grouped into dynamic covalent reactions and supramolecular interactions.

1.2.5.1 Dynamic covalent reactions

This category comprises different strategies, which involve the reversible rupture and formation of covalent bonds. These dynamic structures, being part of a crosslinked polymer structure, provide the necessary chain mobility for the healing process to occur. Interest in this field has grown due to its versatility and easy implementation in different polymeric networks.

Two main groups of dynamic covalent reactions have been applied in the field of healable polymers: reversible crosslinking reactions and chain exchange reactions. Table 1.1 summarizes several chemistries used to provide healing properties in polymers.

a) *Reversible crosslinking reactions*

The formation of crosslinked structures *via* reversible covalent reactions have led to healable polymeric materials. The majority of these materials do not present healing properties by their own, and an external stimulus, such as heat or light, is needed to activate the reversibility.

The most studied reversible system is the one based on the Diels-Alder (DA) reaction. The adduct formation between furan (diene) and maleimide (dienophile) has been utilized to reversibly crosslink different materials [26]. Similarly, photoinduced [2+2] cycloaddition reaction of cinnamic acid derivatives as well as [4+4] cycloaddition reaction of anthracene derivatives offer reversible crosslinking alternatives [27,28].

Table 1.1 *Different chemistries involving dynamic covalent reactions [3,17,26,27,29–33].*
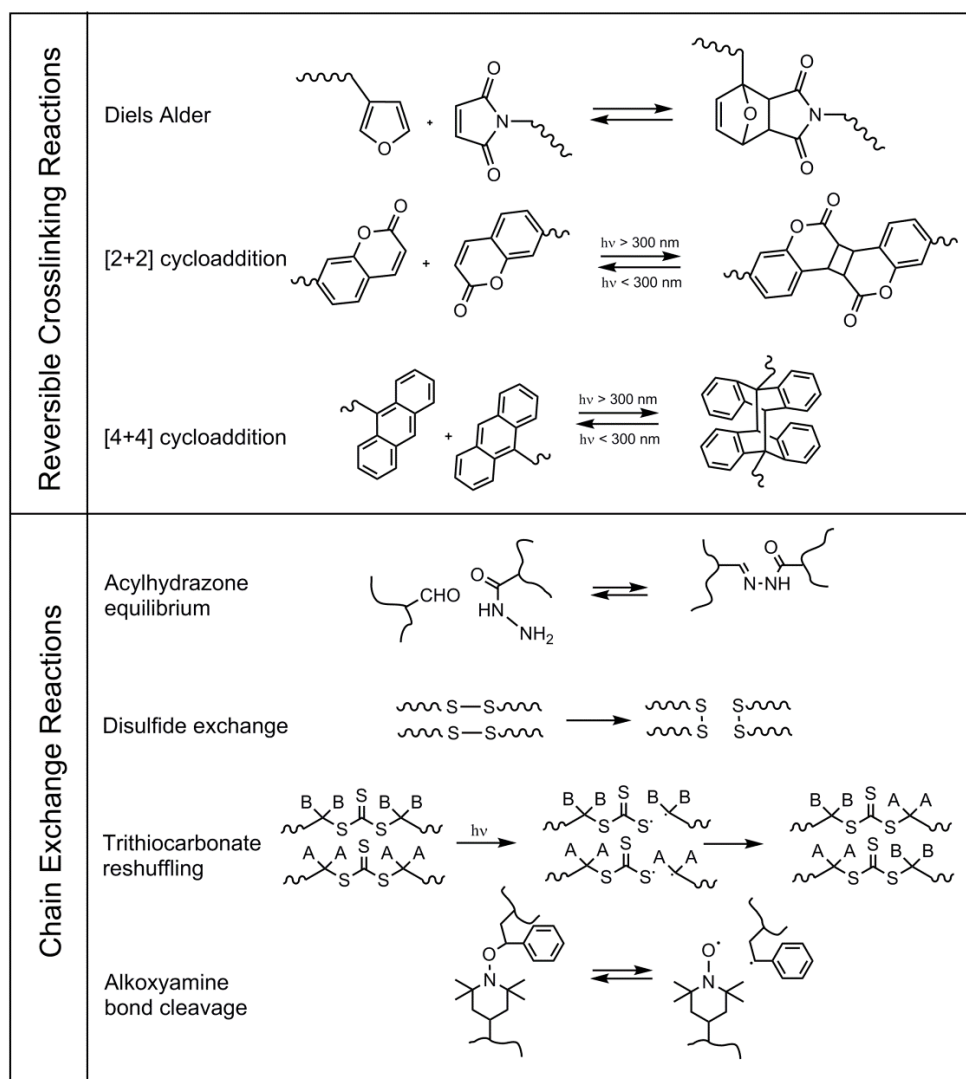
b) Chain exchange reactions

Another approach utilized in crosslinked healable polymers is the introduction of monomers capable of giving chain exchange reactions. This concept takes

advantage of the dynamic rupture/formation equilibrium occurring in certain functional groups, many of which occur *via* radical mechanisms.

Thus, acylhydrazone equilibrium, siloxane and disulfide exchanges, trithiocarbonate reshuffling reactions or alkoxyamine bond cleavage and reformation have been applied to produce healable polymers [17,31–33].

1.2.5.2 Supramolecular interactions

Supramolecular interactions impart to the material the capability of self-assembly and self-healing due to highly directional and reversible non-covalent interactions [34,35]. Different types of non-covalent reactions have been reported to create supramolecular polymers with repairing abilities. The most common interactions are shown in Table 1.2.
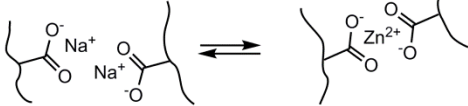
a) Ionomers
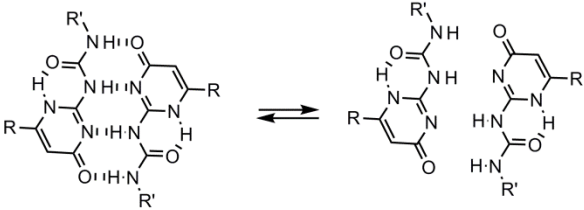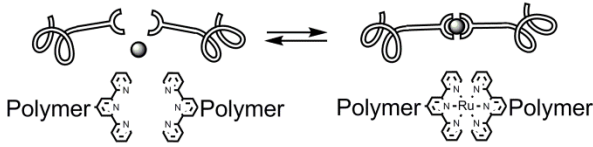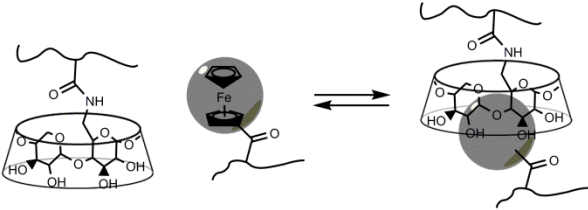
Ionomers are a special class of polymers, which contain a certain amount of acid groups, partially or fully neutralized in the form of salts. The ion content is usually up to about 15 mol% [40]. The electrostatic interactions between different polymer chains are the driving force behind the repairing process.

This approach has been applied to poly(ethylene-co-methacrylic acid) samples and has exhibited remarkable healing abilities not only in small cracks but also in several millimeter holes [4,11].

b) Hydrogen bonding

Despite not being one of the strongest non-covalent interactions, hydrogen bonds between neutral organic molecules have been studied to incorporate healing abilities into different polymer matrixes [41]. Several studies of Meijer and coworkers [37,42] have shown that the multiple H-bonding interaction of ureidopyrimidinone (Upy) units provides self-healing and self-assembly properties to low T_g polymer thermoplastics and elastomers.

Table 1.2 *Supramolecular chemistries used in self-healing polymers [3,17,36–39].*

Ionomers	Acid Groups Interactions	
Hydrogen Bonding	Multiple H-Bonding of Ureidopyrimidinones	
Coordination Bonds	Terpyridine-Ru Complex	
Host-Guest Interactions	Cyclodextrin-Ferrocene Interactions	

c) Coordination bonds

Similar to H-Bonding, metal-ligand interactions can be used to design supramolecular repairing polymers, incorporating ligand substitutes into the polymer backbone [43]. The formation of cracks involves the rupture of these coordination bonds, which can autonomically reform to restore the initial structure. Additionally, the metal-ligand interaction can be externally triggered by light, heat or pH [38,44,45].

d) Host-guest

The application of host-guest interactions is the most recent approach for intrinsic healing materials [46]. In this case, the reversible interaction between macrocycles, such as cyclodextrines or crown ethers, and specific guest groups, such as ferrocene or organic salts, is responsible for the healing process [47,48]. The main advantage is the high selectivity of the interaction, which prevents the passivation of the healing process. However, this development is at an early stage.

In addition to the examples mentioned above, healing alternatives from a different point of view have been proposed. Among them, one interesting alternative is based on the modification of nanoparticles with reversible healing agents such as ureidopyrimidone or coumarin moieties [49,50]. These modified particles are able to reinforce the material structure and additionally take part in the healing process.

1.2.6 Types of stimuli

As mentioned in section 1.2.4, some healing mechanisms do not work autonomically but operate upon external stimulation. In non-autonomic healing materials, the healing process occurs as a consequence of physicochemical reactions promoted by the application of a certain stimulus. These reactions can lead to the crosslinking and decrosslinking of samples, the polymer self-assembly or the generation of active species.

One of the main drawbacks of recent autonomic healable alternatives is the passivation of the fracture surfaces. In these approaches, active species such as free radicals are formed as a consequence of the damage. However, the reaction of these species in the generated surfaces leads to their passivation, especially for exposed areas, which limits the effectiveness of the healing process [46,51]. In this sense, non-autonomic healable materials succeeded in reactivating non-reactive surfaces by applying the appropriate stimulus to the material. In fact, to avoid these problems, most of the aforementioned autonomic healing

mechanisms have been directly applied or modified to be triggered by an external stimulus.

Non-autonomic healing materials can be classified within the larger group of stimuli-responsive materials. These materials present the ability to change their physical properties in a predictable manner when they are exposed to external or internal stimuli. In non-autonomic healing materials, a wide range of stimuli have been used to activate the healing mechanism:

- *Heat*

Some of the most common non-autonomic healing materials are those with thermal-responsive abilities. In this case, heat is responsible for starting the healing process. However, the temperature must be selected accurately as the temperature range should be low enough not to degrade the material, but high enough not to compromise the material integrity or functionality.

- *Light*

Light induced healing is advantageous as the damaged area can selectively be activated, although side reactions as well as local temperature can adversely affect the overall process [52]. This feature also allows the healing of the polymer under load. However, the inherent characteristic of the interaction restricts this stimulation to transparent polymers and/or polymeric surfaces.

- *Mechanical stimulation*

This stimulation process is based on the presence of mechanophores incorporated in the polymer matrix. These compounds are designed to remain dormant when unperturbed but activated under stress [53]. Many mechanophores generate active molecules, mainly metals, used as catalysts of the healing process. Some examples are silver complexes for transesterification reactions or ruthenium bis-carbene complexes for olefin metathesis [54].

- *Other stimuli*

Despite being less studied, other stimuli have been used to trigger healing mechanisms. Some examples are polymeric materials exhibiting healing characteristics upon exposure to a moisture environment [55] or conductive polymers and polymer composites repairing themselves when an electrical failure occurs [56,57].

1.2.7 Polyurethanes

Since the publication of the first work by Bayer et al. over 75 years ago, polyurethanes have become one of the most versatile polymers ever synthesized. The presence of the urethane group in their structure is the main characteristic of these modular-like polymers, which can be developed with very diverse physicochemical properties [58]. For this reason, polyurethanes have been formulated for a wide range of applications, including adhesives, elastomers, composites or foams, as shown in Figure 1.5.
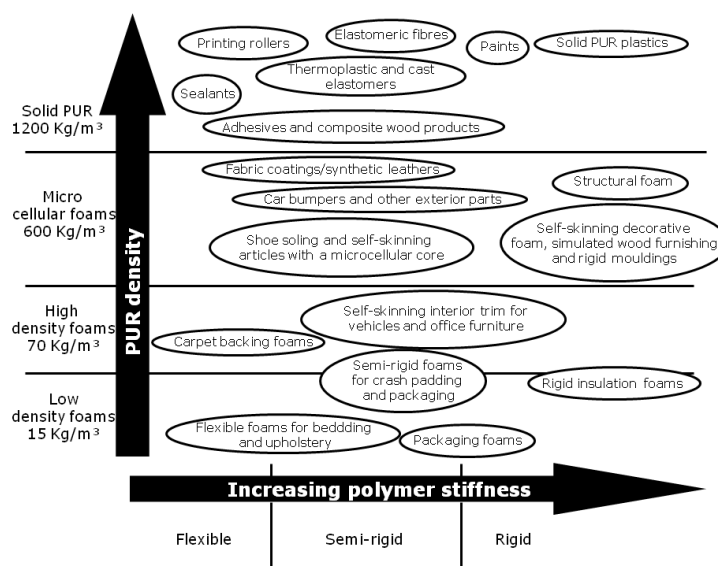
Figure 1.5 *Different applications depending on the density and stiffness of polyurethane resins.*

The synthesis of these polymers is based on the polyaddition reaction taking place between isocyanates and polyols whereby the urethane groups are formed. Given that the monomer nature, cristallinity, composition and crosslinking degree directly affects the material properties, this reaction allows the tailoring of the polymer physical properties for an specific application. In addition to the polyurethane formation reaction, reactions involving hydrogen-containing nucleophiles are common in polyurethane chemistry, as can be seen in Scheme 1.2. Thus, the reaction of isocyanate groups and water, amine, carboxylic acid and so forth can give rise to different products, such as urea, amine, amide and others.
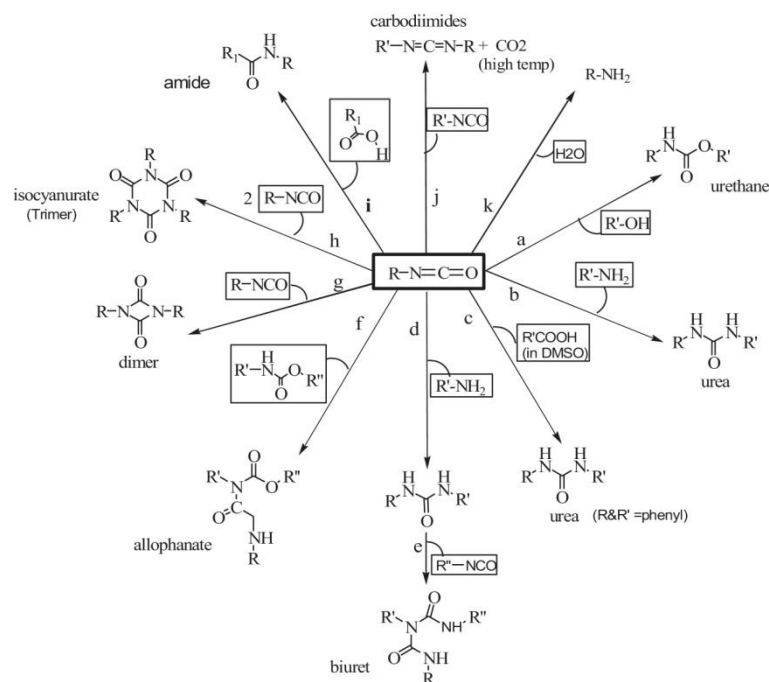

Scheme 1.2 *Isocyanate-polyol polyaddition reaction and different isocyanate reactions [59].*

Polyurethane synthesis generally involves the reaction of low molecular weight isocyanates with macropolyols in order to obtain macromolecular structures. These macropolyols are usually polyether or polyester based polyols with

molecular weights ranging from 300 to 18000 g mol^{-1}. Apart from these, many polyurethanes incorporate short-chain diols or diamines as chain extenders in their polymer structure. Hence, this allows either functionality to be incorporated into the polymer backbone or precise adjustments to material properties.

The combination of low and high molecular weight polyols in the polyurethane synthesis gives rise to segmented polyurethanes. The polymer chain structure can be separated into two segments: a high T_g segment, usually termed hard segment, which includes the urethane groups as well as isocyanate and chain extender moieties, and a low T_g segment, also called soft segment, formed by the macropolyol moiety [60,61]. Owing to the different nature of both segments, polyurethanes present a phase-separated morphology. Hence, hard segments tend to aggregate forming hard domains, which are connected by soft segments, as can be seen in Figure 1.6.
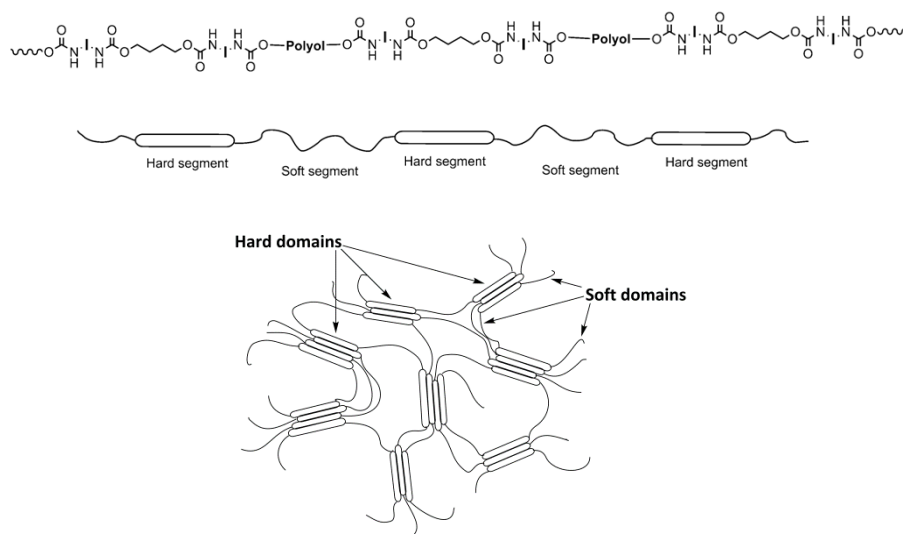
Figure 1.6 *Structure of segmented polyurethanes and phase-separated morphology.*

The phase separated morphology leads to an elastomeric behavior, which is particularly appealing for the synthesis of healable materials. The interactions between hard domains generates physical joints in the material while the low T_g

of the soft segment will provide the necessary chain mobility for the healing process to occur.

1.2.7.1 Waterborne polyurethanes

The reaction between isocyanates and alcohols occurs rapidly and with high yields in presence of organic solvents. However, owing to environmental concerns, this solventborne technology has been progressively replaced by waterborne polyurethanes. The implementation of this technology has to overcome different aspects. The main problem refers to the high reactivity of the isocyanate groups to water [61]. For this reason several reaction alternatives have been developed in order to obtain waterborne polyurethanes (WPUs), including miniemulsion polymerization, prepolymer mixing process and others [62–64].

Among these strategies, one of the most appealing synthetic routes to obtain waterborne polyurethane dispersions is the so called "acetone process" [62,65,66].This process, represented in Scheme 1.3, is divided into three different steps.
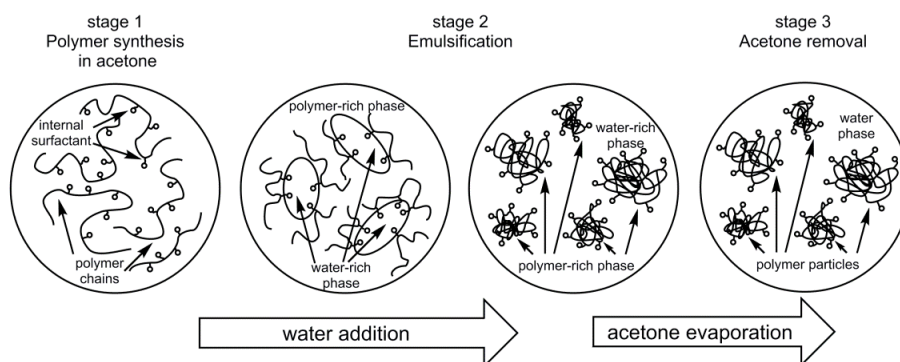
Scheme 1.3 *Waterborne polyurethane synthesis steps by means of the "acetone process".*

In the first step, the polyurethane is synthesized in a low boiling point solvent, usually acetone. During the polymerization, hydrophilic groups are incorporated

into the polymer backbone. These groups act as "internal emulsifiers", being responsible for the further polymer dispersion in water. The chemical nature of these hydrophilic groups can be both ionic and non-ionic, even though the ionic option is the most common one [67,68]. In the second step, water is added to the polymer acetone solution and finally, in the third step, the acetone is removed to obtain waterborne polyurethane with either very low or no volatile organic compounds in the final formulation.

This method is particularly appealing as it makes it possible to perform many modifications in the polymer. Nevertheless, the synthetic conditions and dispersion parameters (emulsifier content, neutralization degree, evaporation temperature and others) are very important to control in order to obtain stable WPU dispersions [69–71].

1.2.7.2 Healable polyurethanes

The specific characteristics of polyurethanes make them excellent candidates to develop healable materials. The easiness to functionalize the polymer structure as well as the possibility to adjust the physical properties of the final product almost on demand has attracted researchers' attention. Although they have been used as vessels to incorporate healing elements in extrinsic approaches, polyurethanes have been mainly employed in the development of intrinsic healable materials, incorporating a wide variety of healing monomers in the polymer backbone [72,73].

Among them, the incorporation of alkoxyamines, aromatic disulfides as well as ureidopyrimidinone and metallosupramolecular moieties led to autonomic healable polyurethanes [33,74–77]. In contrast, non-autonomic healable polyurethanes have been developed by introducing active monomers capable to respond to very diverse stimuli. The most successful attempts involve the incorporation of thiuram and coumarin moieties for optically healable polyurethanes or thermoreversible healing processes based on Diels-Alder reactions [78–81].

Apart from the incorporation of healing monomers, polyurethanes provide additional features to healable materials. Owing to the presence of urethane groups, polyurethanes are able to form strong Hydrogen-bonds between polymer chains. Furthermore, groups such as urea or acid groups, commonly presented in polyurethane chemistry, can also lead to non-covalent interactions. These non-covalent interactions not only give rise to phase separated morphologies but also facilitate the surface rearrangement and the interaction of the healing elements after the fracture [15,60,74,82].

1.3 Objective

Waterborne polyurethanes have been extensively used as sealants, adhesives, elastomers and coatings [58,62]. Among them, waterborne polyurethanes coatings have attracted the attention of the industry as they lead to suitable coatings for flexible and rigid substrates, such as leather, metal, plastic and paper. As a consequence, they have been applied in automotive, textile and decorative pant industry.

Although many healable polymeric materials, including healable polyurethanes, have been developed, to the best of our knowledge, healing agents have not been introduced in waterborne polyurethanes. However, it is clear that the incorporation of these features can be interesting in the aforementioned industries.

The objective of this work was the development of different types of intrinsic healable waterborne polyurethanes with the capability of repair damages. In order to fulfill this objective the efforts were centered on the development of three different repairing strategies. These healing alternatives were selected taking into consideration the general classification of non-autonomic and autonomic healable materials, following the scheme described in Table 1.2.

Among the non-autonomic possibilities, a reversible reaction triggered by light was selected. Thus, the introduction of UV-responsiveness into polyurethanes by incorporating coumarin monomers was studied. Coumarin monomers are usually

bonded to polymer chains in order to modulate their crosslinking density or molecular weight in response to UV-light at some specific wavelengths [83,84].

Autonomic healable waterborne polyurethanes were developed taking into consideration two different approaches. First, an autonomic healing mechanism based on dynamic covalent reactions, specifically in chain exchange reactions, was proposed. Aromatic disulfide bridges have demonstrated their ability to autonomously exchange and recombine, providing autonomic healing attributes to crosslinked polyurethanes [74,85]. In order to extent this concept to other crosslinked polyurethanes, aromatic disulfide monomers were introduced in waterborne organic-inorganic hybrid polyurethanes.

Finally, the incorporation of healing abilities by means of supramolecular chemistry was proposed. In particular, the ureidopyrimidinone moieties were introduced as chain extenders in linear waterborne polyurethane backbones. These monomers are capable to form strong and highly directional hydrogen bonds, leading to autonomic healable materials [41,86,87].

Taking into account the objective mentioned above, and the characteristics of the proposed polymer structures, this manuscript presents the different aspects of the work divided into the following chapters.

- Chapter 2 discusses the synthesis and characterization different healable waterborne polyurethanes, attending to different aspects such as the synthesis of the healing agents, reaction conditions and water dispersion abilities of the obtained materials.

- Chapter 3 focuses on the characterization of the response of the coumarin based systems by means of different analytical techniques. In addition, the influence of different parameters in the photoinduced reaction kinetics as well as the evolution under the Sunlight is reported.

- Chapter 4 analyses the characteristics of the synthesized autonomic healable waterborne polyurethanes.

- Chapter 5 is centered on the healing properties of all systems (autonomic and non autonomic) obtained waterborne polyurethanes.

- Chapter 6 summarizes the most relevant results obtained in this study.

1.4 References

[1]   Mutsaers SE, Bishop JE, McGrouther G, Laurent GJ. Mechanisms of tissue repair: From wound healing to fibrosis. Int J Biochem Cell Biol 1997;29:5–17.

[2]   Youngblood JP, Sottos NR. Bioinspired Materials for Self-Cleaning and Self-Healing. MRS Bull 2008;33:732–41.

[3]   Urban MW. Handbook of Stimuli-Responsive Materials. Weinheim, Germany: Wiley-VCH Verlag GmbH & Co. KGaA; 2011.

[4]   Ghosh SK. Self-healing materials: Fundamentals, Design Strategies and Applications. Weinheim, Germany: Wiley-VCH Verlag GmbH & Co. KGaA; 2009.

[5]   van der Zwaag S, van Dijk NH, Jonkers HM, Mookhoek SD, Sloof WG. Self-healing behaviour in man-made engineering materials: bioinspired but taking into account their intrinsic character. Philos Trans A Math Phys Eng Sci 2009;367:1689–704.

[6]   Laha K, Kyono J, Sasaki T, Kishimoto S, Shinya N. Improved creep strength and creep ductility of type 347 austenitic stainless steel through the self-healing effect of boron for creep cavitation. Metall Mater Trans A 2005;36:399–409.

[7]   Allen NS, Edge M. Fundamentals of Polymer Degradation and Stabilisation. Essex, England: Elsevier Science Publisher LTD; 1992.

[8]   Baker A, Jones R, Callinan RJ. Damage tolerance of graphite/epoxy composites. Compos Struct 1985;4:15–44.

[9]   Blaiszik BJ, Kramer SLB, Olugebefola SC, Moore JS, Sottos NR, White SR. Self-Healing Polymers and Composites. Annu Rev Mater Res 2010;40:179–211.

[10]   Fischer H. Self-repairing material systems — a dream or a reality? Nat Sci 2010;2:873–901.

[11]   Wu DY, Meure S, Solomon D. Self-healing polymeric materials: A review of recent developments. Prog Polym Sci 2008;33:479–522.

[12]   Cantwell WJ, Morton J. The significance of damage and defects and their detection in composite materials: A review. J Strain Anal Eng Des 1992;27:29–42.

[13]   Wool RP, O'Connor KM. A theory of crack healing in polymers. J Appl Phys 1981;52:5953–63.

[14]   Kim YH, Wool RP. A theory of healing at a polymer-polymer interface. Macromolecules 1983;16:1115–20.

[15]   Yamaguchi M, Ono S, Terano M. Self-repairing property of polymer network with dangling chains. Mater Lett 2007;61:1396–9.

[16]   Ho C-T (Minnesota M& M. Reactive two-part polyurethane compositions and optionally self-healable and scratch-resistant coatings prepared therefrom. PCT/US1995/012812, 1996.

[17]   Yang Y, Urban MW. Self-healing polymeric materials. Chem Soc Rev 2013;42:7446.

[18]   Hager MD, Greil P, Leyens C, Van Der Zwaag S, Schubert US. Self-healing materials. Adv Mater 2010;22:5424–30.

[19]   Williams KA, Dreyer DR, Bielawski CW. The Underlying Chemistry of Self-Healing Materials. MRS Bull 2008;33:759–65.

[20]   Billiet S, Hillewaere XKD, Teixeira RF a, Du Prez FE. Chemistry of crosslinking processes for self-healing polymers. Macromol Rapid Commun 2013;34:290–309.

[21]   Yuan YC, Yin T, Rong MZ, Zhang MQ. Self healing in polymers and polymer composites. Concepts, realization and outlook: A review. Express Polym Lett 2008;2:238–50.

[22]   Syrett J, Becer CR, Haddleton DM. Self-healing and self-mendable polymers. Polym Chem 2010;1:978–87.

[23]   Michael P, Döhler D, Binder WH. Improving autonomous self healing via combined chemical/physical principles. Polymer 2015;69:216–27.

[24]   Pang JWC, Bond IP. A hollow fibre reinforced polymer composite encompassing self-healing and enhanced damage visibility. Compos Sci Technol 2005;65:1791–9.

[25]   Cho SH, Andersson HM, White SR, Sottos NR, Braun P V. Polydimethylsiloxane-based self-healing materials. Adv Mater 2006;18:997–1000.

[26]   Defize T, Riva R, Thomassin J-M, Jérôme C, Alexandre M. Thermo-Reversible Reactions for the Preparation of Smart Materials: Recyclable Covalently-Crosslinked Shape Memory Polymers. Macromol Symp 2011;309-310:154–61.

[27]   Kaur G, Johnston P, Saito K. Photo-reversible dimerisation reactions and their applications in polymeric systems. Polym Chem 2014;5:2171.

[28]   Bassani DM. The dimerization of cinnamic acid derivatives. In: Horspool, William; Lenci F, editor. CRC Handb. Org. Photochem. Photobiol. 2nd Ed., CRC Press LLC Boca Raton, Fla; 2004, p. 20/1–20/20.

[29]   Mauldin T., Kessler M. Self-healing polymers and composites. Int Mater Rev 2010;55:317–46.

[30]   Bergman SD, Wudl F. Mendable polymers. J Mater Chem 2008;18:41.

[31]   Yoon JA, Kamada J, Koynov K, Mohin J, Nicolaÿ R, Zhang Y, et al. Self-healing polymer films based on thiol-disulfide exchange reactions and self-healing kinetics measured using atomic force microscopy. Macromolecules 2012;45:142–9.

[32]   Fenoli CR, Bowman CN. Synthesis of novel trithiocarbonate and allyl sulfide containing monomers. Polym Chem 2014;5:62.

[33]   Yuan C, Rong MZ, Zhang MQ. Self-healing polyurethane elastomer with thermally reversible alkoxyamines as crosslinkages. Polymer 2014;55:1782–91.

[34]   Brunsveld L, Folmer BJ, Meijer EW, Sijbesma RP. Supramolecular polymers. Chem Rev 2001;101:4071–98.

[35]   de Espinosa LM, Fiore GL, Weder C, Johan Foster E, Simon YC. Healable supramolecular polymer solids. Prog Polym Sci 2015.

[36]   Varley RJ, van der Zwaag S. Towards an understanding of thermally activated self-healing of an ionomer system during ballistic penetration. Acta Mater 2008;56:5737–50.

[37]   Appel WPJ, Portale G, Wisse E, Dankers PYW, Meijer EW. Aggregation of Ureido-Pyrimidinone Supramolecular Thermoplastic Elastomers into Nanofibers: A Kinetic Analysis. Macromolecules 2011;44:6776–84.

[38]   Burnworth M, Tang L, Kumpfer JR, Duncan AJ, Beyer FL, Fiore GL, et al. Optically healable supramolecular polymers. Nature 2011;472:334–7.

[39]   Yang X, Yu H, Wang L, Tong R, Akram M. Soft Matter macrocycle-based host – guest interactions. Soft Matter 2015;00:1–11.

[40]   Eisenberg A, Rinaudo M. Polyelectrolytes and ionomers. Polym Bull 1990;24:671.

[41]   van Gemert GML, Peeters JW, Söntjens SHM, Janssen HM, Bosman AW. Self-Healing Supramolecular Polymers In Action. Macromol Chem Phys 2012;213:234–42.

[42]   Folmer BJB, Sijbesma RP, Versteegen RM, van der Rijt J a. J, Meijer EW. Supramolecular Polymer Materials: Chain Extension of Telechelic Polymers Using a Reactive Hydrogen-Bonding Synthon. Adv Mater 2000;12:874–8.

[43]   Coulibaly S, Roulin A, Balog S, Biyani M V., Foster EJ, Rowan SJ, et al. Reinforcement of Optically Healable Supramolecular Polymers with Cellulose Nanocrystals. Macromolecules 2014;47:152–60.

[44]   Lee BP, Dalsin JL, Messersmith PB. Synthesis and gelation of DOPA-modified poly(ethylene glycol) hydrogels. Biomacromolecules 2002;3:1038–47.

[45]   Schmatloch S, González MF, Schubert US. Metallo-supramolecular diethylene glycol: Water-soluble reversible polymers. Macromol Rapid Commun 2002;23:957–61.

[46]   Yang X, Yu H, Wang L, Tong R, Akram M, Chen Y, et al. Self-healing polymer materials constructed by macrocycle-based host–guest interactions. Soft Matter 2015;11:1242–52.

[47]   Wang Y-F, Zhang D-L, Zhou T, Zhang H-S, Zhang W-Z, Luo L, et al. A reversible functional supramolecular material formed by host–guest inclusion. Polym Chem 2014;5:2922.

[48]   Liu D, Wang D, Wang M, Zheng Y, Koynov K, Auernhammer GK, et al. Supramolecular organogel based on crown ether and secondary ammoniumion functionalized glycidyl triazole polymers. Macromolecules 2013;46:4617–25.

[49]   Biyani M, Foster E, Weder C. Light-Healable Supramolecular Nanocomposites Based on Modified Cellulose Nanocrystals. ACS Macro Lett 2013;2:236–40.

[50]   Biyani M V., Weder C, Foster EJ. Photoswitchable nanocomposites made from coumarin-functionalized cellulose nanocrystals. Polym Chem 2014;5:5501–8.

[51]   McKee JR, Appel E a., Seitsonen J, Kontturi E, Scherman O a., Ikkala O. Healable, Stable and Stiff Hydrogels: Combining Conflicting Properties Using Dynamic and Selective Three-Component Recognition with Reinforcing Cellulose Nanorods. Adv Funct Mater 2014;24:2706–13.

[52]   Fiore GL, Rowan SJ, Weder C. Optically healable polymers. Chem Soc Rev 2013;42:7278–88.

[53]   Caruso MM, Davis D a., Shen Q, Odom S a., Sottos NR, White SR, et al. Mechanically-induced chemical changes in polymeric materials. Chem Rev 2009;109:5755–98.

[54]   Piermattei A, Karthikeyan S, Sijbesma RP. Activating catalysts with mechanical force. Nat Chem 2009;1:133–7.

[55]   Zhang Z, Hu Y, Liu Z, Guo T. Synthesis and evaluation of a moisture-promoted healing copolymer. Polym (United Kingdom) 2012;53:2979–90.

[56]   Yin X, Liu Z, Wang D, Pei X, Yu B, Zhou F. Bioinspired Self-Healing Organic Materials□: Chemical Mechanisms and Fabrications. J Bionic Engeniering 2015;12:1–16.

[57]   Zhong N, Post W. Composites: Part A Self-repair of structural and functional composites with intrinsically self-healing polymer matrices□: A review. Compos Part a 2015;69:226–39.

[58]   Engels HW, Pirkl HG, Albers R, Albach RW, Krause J, Hoffmann A, et al. Polyurethanes: Versatile materials and sustainable problem solvers for today's challenges. Angew Chemie - Int Ed 2013;52:9422–41.

[59]   Cherng JY, Hou TY, Shih MF, Talsma H, Hennink WE. Polyurethane-based drug delivery systems. Int J Pharm 2013;450:145–62.

[60]   He Y, Xie D, Zhang X. The structure, microphase-separated morphology, and property of polyurethanes and polyureas. J Mater Sci 2014;49:7339–52.

[61]   Król P. Synthesis methods, chemical structures and phase structures of linear polyurethanes. Properties and applications of linear polyurethanes in polyurethane elastomers, copolymers and ionomers. Prog Mater Sci 2007;52:915–1015.

[62]   Chattopadhyay DK, Raju KVSN. Structural engineering of polyurethane coatings for high performance applications. Prog Polym Sci 2007;32:352–418.

[63]   Barrère M, Landfester K. High molecular weight polyurethane and polymer hybrid particles in aqueous miniemulsion. Macromolecules 2003;36:5119–25.

[64]   Barni A, Levi M. Aqueous polyurethane dispersions: A comparative study of polymerization processes. J Appl Polym Sci 2003;88:716–23.

[65]   Vogt-Birnbrich B. Novel synthesis of low VOC polymeric dispersions and their application in waterborne coatings. Prog Org Coatings 1996;29:31–8.

[66]   Sardon H, Irusta L, Fernández-Berridi MJ, Lansalot M, Bourgeat-Lami E. Synthesis of room temperature self-curable waterborne hybrid polyurethanes functionalized with (3-aminopropyl)triethoxysilane (APTES). Polymer 2010;51:5051–7.

[67]   Jaudouin O, Robin J-J, Lopez-Cuesta J-M, Perrin D, Imbert C. Ionomer-based polyurethanes: a comparative study of properties and applications. Polym Int 2012;61:495–510.

[68]   Yen M-S, Chen P-Y, Tsai H-C. Synthesis, properties, and dyeing application of nonionic waterborne polyurethanes with different chain length of ethyldiamines as the chain extender. J Appl Polym Sci 2003;90:2824–33.

[69]   Nanda AK, Wicks D a. The influence of the ionic concentration, concentration of the polymer, degree of neutralization and chain extension on aqueous polyurethane dispersions prepared by the acetone process. Polymer 2006;47:1805–11.

[70]   Sardon H, Irusta L, Fernández-Berridi MJ, Luna J, Lansalot M, Bourgeat-Lami E. Waterborne Polyurethane Dispersions Obtained by the Acetone Process: A Study of Colloidal Features. J Appl Polym Sci 2011;120:2054–62.

[71]   Chinwanitcharoen C, Kanoh S, Yamada T, Hayashi S, Sugano S. Preparation of aqueous dispersible polyurethane: Effect of acetone on the particle size and storage stability of polyurethane emulsion. J Appl Polym Sci 2004;91:3455–61.

[72]   Tatiya PD, Hedaoo RK, Mahulikar PP, Gite V V. Novel polyurea microcapsules using dendritic functional monomer: Synthesis, characterization, and its use in self-healing and anticorrosive polyurethane coatings. Ind Eng Chem Res 2013;52:1562–70.

[73]   Sondari D, Septevani AA, Randy A, Triwulandari E. Polyurethane microcapsule with glycerol as the polyol component for encapsulated self healing agent. Int J Eng Technol 2010;2:466–71.

[74]   Rekondo A, Martin R, Ruiz de Luzuriaga A, Cabañero G, Grande HJ, Odriozola I. Catalyst-free room-temperature self-healing elastomers based on aromatic disulfide metathesis. Mater Horizons 2014:237–40.

[75]   Feldman KE, Kade MJ, Meijer EW, Hawker CJ, Kramer EJ. Model transient networks from strongly hydrogen-bonded polymers. Macromolecules 2009;42:9072–81.

[76]   Lin Y, Li G. An intermolecular quadruple hydrogen-bonding strategy to fabricate self-healing and highly deformable polyurethane hydrogels. J Mater Chem B 2014;2:6878–85.

34

[77]   Yuan J, Fang X, Zhang L, Hong G, Lin Y, Zheng Q, et al. Multi-responsive self-healing metallo-supramolecular gels based on "click" ligand. J Mater Chem 2012;22:11515.

[78]   Amamoto Y, Otsuka H, Takahara A, Matyjaszewski K. Self-healing of covalently cross-linked polymers by reshuffling thiuram disulfide moieties in air under visible light. Adv Mater 2012;24:3975–80.

[79]   Ling J, Rong MZ, Zhang MQ. Coumarin imparts repeated photochemical remendability to polyurethane. J Mater Chem 2011;21:18373–80.

[80]   Ling J, Rong MZ, Zhang MQ. Photo-stimulated self-healing polyurethane containing dihydroxyl coumarin derivatives. Polymer 2012;53:2691–8.

[81]   Du P, Liu X, Zheng Z, Wang X, Joncheray T, Zhang Y. Synthesis and characterization of linear self-healing polyurethane based on thermally reversible Diels–Alder reaction. RSC Adv 2013;3:15475–82.

[82]   Kim YJ, Huh PH, Kim BK. Synthesis of self-healing polyurethane urea-based supramolecular materials. J Polym Sci Part B Polym Phys 2015;53:468–74.

[83]   Trenor SR, Shultz AR, Love BJ, Long TE. Coumarins in polymers: from light harvesting to photo-cross-linkable tissue scaffolds. Chem Rev 2004;104:3059–77.

[84]   López-Vilanova L, Martinez I, Corrales T, Catalina F. Photoreversible crosslinking of poly-(ethylene-butyl-acrylate) copolymers functionalized with coumarin chromophores using microwave methodology. React Funct Polym 2014;85:28–35.

[85]   Martin R, Rekondo A, Ruiz de Luzuriaga A, Cabañero G, Grande HJ, Odriozola I. The processability of a poly(urea-urethane) elastomer reversibly crosslinked with aromatic disulfide bridges. J Mater Chem A 2014;2:5710.

[86]   Nobuhiro Oya TI and NY. A crystalline supramolecular polymer with self-healing capability at room temperature. Polym J 2013;45:955–61.

[87]   Wei M, Zhan M, Yu D, Xie H, He M, Yang K, et al. Novel Poly(tetramethylene ether)glycol and Poly(ε-caprolactone) Based Dynamic Network via Quadruple Hydrogen Bonding with Triple-Shape Effect and Self-Healing Capacity. ACS Appl Mater Interfaces 2015;7:2585–96.

CHAPTER 2

Synthesis and Characterization of Healable Waterborne Polyurethanes

2.1 Chapter Overview

In this section, the synthesis of three different healable waterborne polyurethanes is described. First, a non-autonomic healable polyurethane structure incorporating coumarin monomers is proposed. This light-responsive monomer was introduced in two different ways; as an end-capper in both polyurethane chain-ends and as a chain extender in the middle of the polymer structure. Second, aromatic disulfide monomers were introduced in order to develop autonomic healable polyurethanes. These monomers are capable of chain exchanging according to the disulfide metathesis reaction. Finally, autonomic healable polyurethanes based on supramolecular chemistry were developed. In this case, ureidopyrimidinone motifs were introduced in the polyurethane structure in order to provide the desired healing abilities.

Additionally, the chemical characterization of the obtained products as well as the determination of their water dispersion abilities was carried out. Thus, in order to characterize the obtained polymer structures, Fourier-Transform-Infrared spectroscopy (FTIR) and proton- nuclear magnetic resonance (^{1}H-NMR) were utilized. In the same manner, Dynamic Light Scattering (DLS) measurements were carried out to determine the polymer particle size in water.

2.2 Introduction

Polyurethanes are polymers that can be easily modified introducing different monomer structures. In addition, their physical properties can be tailored to those required in the final product. Hence, they have been widely used in the development of intrinsic healable materials [1–3].

As explained in the introduction, the intrinsic healing strategy is based on the incorporation of healing active elements in polymer backbones so the chemical nature of these elements determines the autonomic or non-autonomic nature of the healing process.

However, the introduction of active monomers into the polymer structure is not easy. On the one hand, these elements should be capable of reacting with isocyanate groups. Therefore, the selected active monomers should have hydrogen-containing nucleophiles in their structure. On the other hand, if a successful healing process is desired, there should be a sufficient amount of active elements on the surface of the damage without compromising the physical properties of the polyurethane. Hence, it is necessary to reach a compromise between the healing abilities and the desired physical properties of the final product.

2.2.1 Waterborne polyurethanes based on coumarin

Coumarin and its derivatives present properties such as anticoagulant, sweet odor, fluorescence and so forth [4–6], which enables them to be used in fields as diverse as medicine, cosmetics, laser dyes or polymer industry [7–10]. In addition, they have attracted researchers' attention in the field of stimuli-responsive materials due to their ability to interact with light.

Figure 2.1 shows the reversible photoinduced $[2\pi+2\pi]$ cycloaddition reaction that coumarin monomers can undergo [7,11].
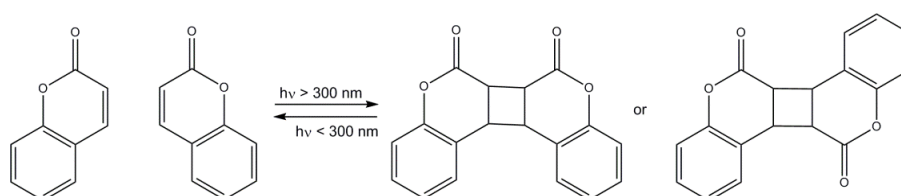
Figure 2.1 *Reversible photoinduced [2π+2π] cycloaddition reaction of coumarin monomers.*

This reaction enables the coumarin molecules to join or separate in a controlled way, selecting the appropriate irradiation conditions. Thus, it is possible to reversibly increase their molecular weight or crosslink samples by introducing coumarin molecules in polymer structures [12,13].

Taking advantage of this process, the possibility of introducing coumarin monomers in waterborne polyurethanes was explored in order to provide non-autonomic healing abilities. Thus, the polymer structures shown in Scheme 2.1 were synthesized.
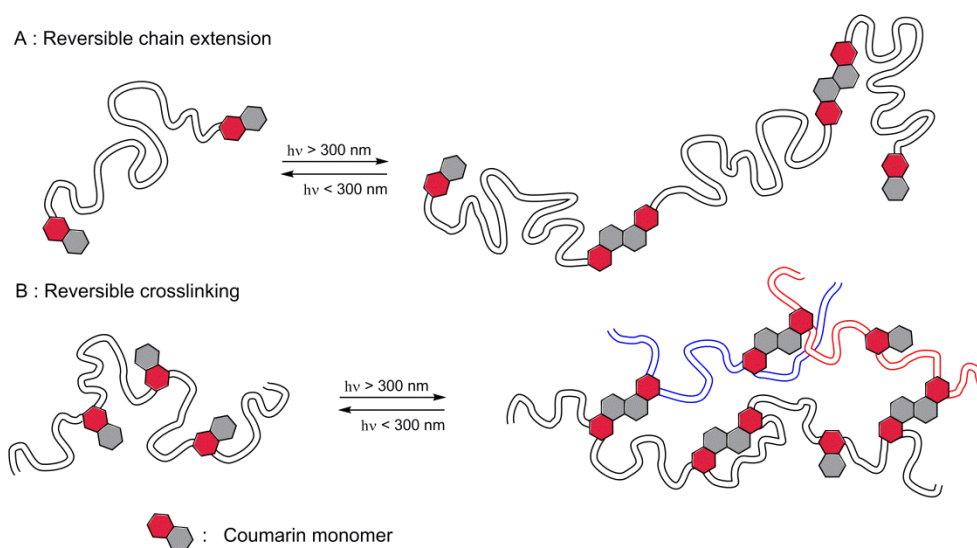

Scheme 2.1 *Schematic representation of proposed waterborne polyurethane structures: Coumarin end-capped (a) and coumarin chain-extended polyurethanes (b).*

In the first case, both polyurethane chain-ends are modified with coumarin monomers and the cycloaddition reaction leads to a reversible chain extension. In the second case, coumarin monomers are incorporated in the polyurethane structure as chain extenders and therefore, the polymer presents reversible crosslinking abilities.

2.2.2 Waterborne polyurethanes based on aromatic disulfide units

Disulfide bonds are dynamic covalent bonds which can be easily cleaved and formed under redox, light or mechanical force conditions [14,15]. The most important dynamic reactions involving disulfide bonds are the thiol-disulfide interchange and the metathesis, as represented in Scheme 2.2.
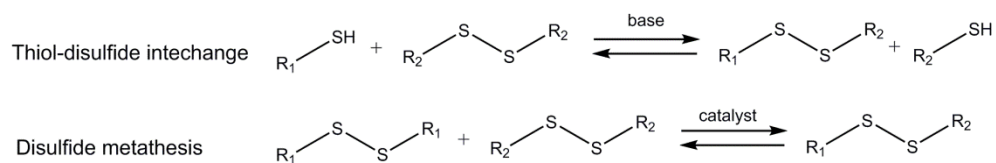
Scheme 2.2 *Dynamic reactions involving disulfide bonds.*

As a result of both reactions, the interchange of side groups of the disulfide bond occurs in a dynamic equilibrium, although they proceed in different experimental conditions. While the thiol-disulfide interchange occurs as a consequence of a nucleophilic attack of the thiol group under basic conditions, the metathesis reaction is promoted by an external catalyst and/or stimulus *via* ionic or free radical rearrangement [16–18]. These reactions occur not only in low molecular weight species but also in the disulfides forming part of polymers.

The dynamic nature of this bond has been used in order to incorporate healing characteristics to crosslinked polymer. Thus, sulfur containing polymers have presented non-autonomic healing abilities in different polymer structures under heat or light stimulation [19–21]. In addition, the incorporation of a catalyst to disulfide containing polymers has led to autonomic healable materials based in disulfide exchanges[22].

Recently, it has been shown that aromatic disulfide monomers undergo disulfide metathesis and provide autonomic healable characteristics to crosslinked polyurethanes without the incorporation of a catalyst [3,23].

In order to extent this concept to other crosslinked polyurethane structures, we have explored the possibility of incorporating these aromatic disulfides into organic-inorganic hybrid waterborne polyurethanes. The proposed polyurethane structure is represented in Scheme 2.3.
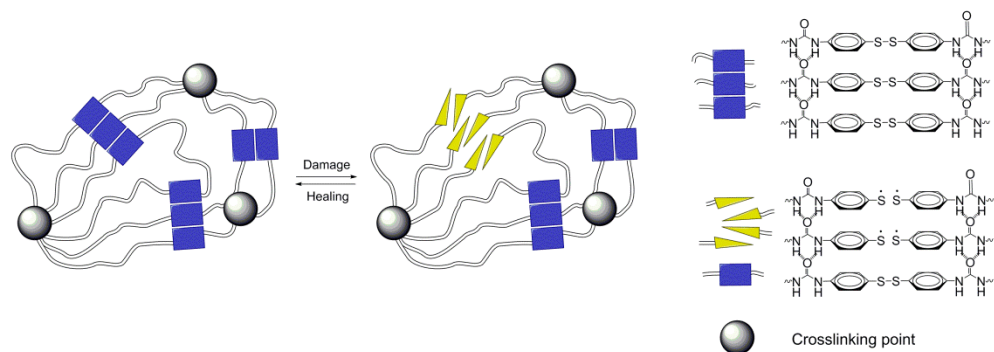
Scheme 2.3 *Representation of aromatic disulfide containing organic-inorganic hybrid polyurethane.*

These materials incorporate the disulfide bonds in form of chain extenders. In addition, their chain-ends are modified with inorganic precursors that, after the curing process, crosslink the sample by means of inorganic domains.
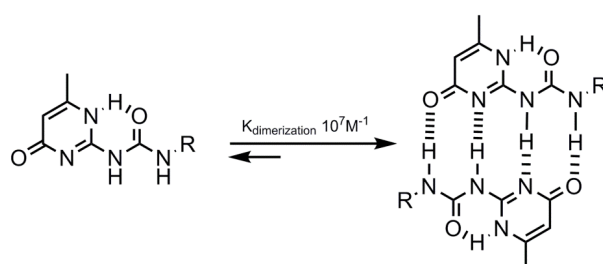
2.2.3 Waterborne polyurethanes based on ureidopyrimidinone units

In contrast to coumarin monomers where covalent bonds are formed between the healing agents, other successful attempts in the field of healable materials are based on supramolecular chemistry. These materials make use of highly directional noncovalent interactions of low molecular weight building blocks to generate the material structure [24].

As these blocks possess low viscosity, they provide the necessary molecular mobility. In addition, they generate reversible joins by means of noncovalent interactions. These joins act as structural reinforcement and lead to the recovery of the original physical properties of the material after the healing process.

Among all noncovalent interactions, hydrogen bonds are one of the most common in many biological supramolecular systems [25]. Despite not being strong noncovalent interactions, the combination of multiple hydrogen bonds can enhance both their strength and specificity.

This is the case of Ureidopyrimidinone (Upy) units, which have acquired significant importance in the field of supramolecular healable polymers. This structure, shown in Figure 2.2, presents a particular H-bond donor and acceptor arrangement that confers strong dimerization behavior ($K_{dimerization} \sim 10^7$ M^{-1}) [26,27]. Thus, many works have incorporated Upy units to different polymers in order to provide healing abilities [28–31].

Figure 2.2 *The equilibrium of ureidopyrimidinone monomer and dimer.*

In this work, the incorporation of ureidopyrimidinone motifs into waterborne polyurethanes was studied. To fulfill this objective, the following was proposed (Scheme 2.4).
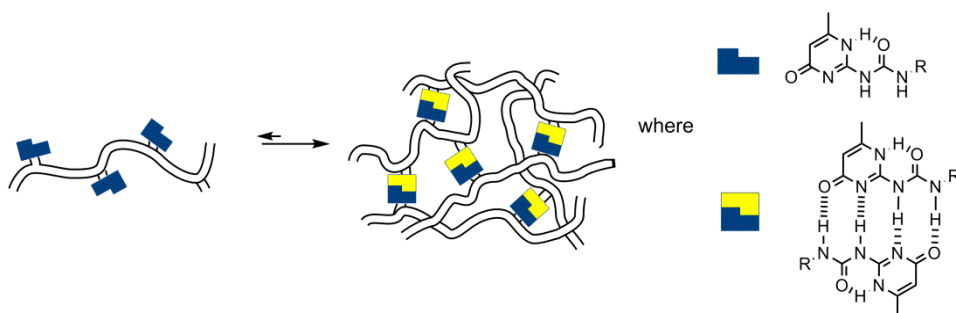
Scheme 2.4 *The proposed ureidopyrimidinone based waterborne polyurethane structure.*

The first approach proposes the incorporation of Upy units in linear waterborne polyurethanes as chain extenders. In this way, these supramolecular interactions lead to crosslinked polymers.

2.3 Experimental part

2.3.1 Materials

2.3.1.1 Materials for the synthesis of waterborne polyurethanes

The selection of the monomers for the synthesis of healable polyurethanes is crucial as they should possess the appropriate physical properties to enable the surface rearrangement after the damage without interfering in the healing process. This fact is particularly important for coumarin based formulations as none of the selected monomers should absorb in the UV region where the coumarin monomer does.

All the reagents used during the synthesis of waterborne polyurethanes were purchased from Sigma-Aldrich and characterized by FTIR, UV spectroscopy and ^{1}H-NMR. The FTIR, UV and ^{1}H-NMR spectra of the products are shown in the Appendix.

   a) Diisocyanate

Aromatic isocyanates are much more reactive and used than aliphatic ones. However, they were discarded because they absorb the UV light [32]. Thus, from commercially available diisocyanates, isophorone diisocyanate (IPDI) was selected for this work. This cycloaliphatic diisocyanate presents good oxidative and ultraviolet stabilities and does not absorb in the UV region of stimulation [32,33]. Furthermore, IPDI has been extensively used as the diisocyanate in the synthesis of waterborne polyurethanes [34–37].
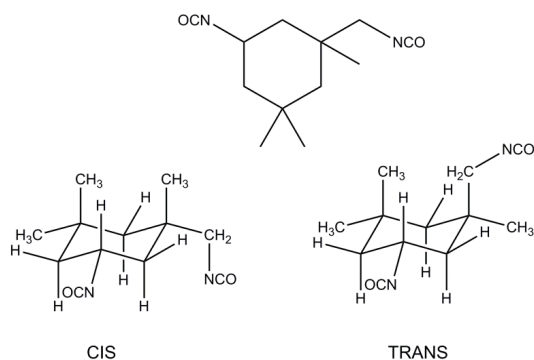
Figure 2.3 *The chemical structure of isophorone diisocyanate and both cis and trans isomers structure.*

As observed in Figure 2.3, the structure of IPDI possesses two different isocyanate groups; a secondary NCO directly attached to the cycle and a primary NCO group bonded to a primary carbon, so they present differences in reactivity [34]. It should be noted that the commercially available monomer consists of a mixture of both *cis* and *trans* isomers with a proportion of 72% of *cis* isomer [38].

b) Macrodiol

The selection of the macrodiol was not arbitrary as macrodiols possessing a low glass transition temperature (T_g) are required for the synthesis of healable materials. Hence, in this work, polypropylene glycol (PPG) with a molecular weight M_n=1000 g/mol and a T_g about -70 ºC was selected.

The chemical structure of PPG is shown in Figure 2.4.
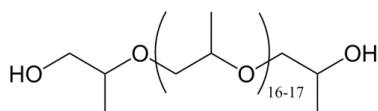
Figure 2.4 *The structure of polypropylene glycol.*

c) Chain extenders

Chain extenders are usually short chain diols or diamines that join different isocyanate functionalized chains together. They allow us to modify different properties and/or incorporate functionality to polyurethanes.

By them, hydrophilic groups, both ionic and non ionic, can be inserted in WPU backbones [39–42]. The inserted groups are responsible for the dispersion abilities of these polymers by acting as internal surfactant.
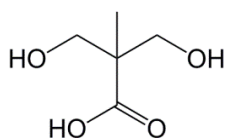
Figure 2.5 *Chemical structure of 2,2-dimethylolpropionic acid.*

In this work, polyurethanes were obtained using the anionic internal surfactant 2,2-dimethylolpropionic acid (DMPA). This chain extender, presented in Figure 2.5, allows us to insert acid groups in the polyurethane structure. However, the acid groups of DMPA should be partially or totally neutralized in the form of carboxylates in order for them to act as an internal emulsifier. For this reason, triethylamine (TEA), a neutralizing agent, was used in the formulation in molar excess to ensure the total neutralization of the acid groups.

Apart from DMPA, 1,4-butanodiol (Figure 2.6) was used as a non-functionalized chain extender. This molecule was added in order to modulate the chemical structure of the final polymer without introducing additional functionalities.
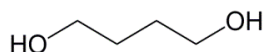
Figure 2.6 *The structure of 1,4-butanodiol.*

d) Catalyst

As presented in Table 2.1, isophorone diisocyanate presents a low reactivity compared to other commercially available diisocyanates [43,44]. Therefore, the introduction of catalysts is essential to promote the polymerization reaction.

Table 2.1 *Relative reactivity for some commercial uncatalysed diisocyanates at 25 ºC.*

Isocyanate	k1	k2
2,4-Toluene diisocianate (TDI)	400	33
4,4'-Diphenylmethane diisocianate (MDI)	320	110
Hexamethylene diisocyanate (HDI)	1	0.5
Isophorone diisocyanate (IPDI)	0.62	0.23
4,4'-dicyclohexylmethane diisocyanate (H12-MDI)	0.57	0.4

Nowadays, organocatalysts are currently available. However, the most widely used catalysts in polyurethane synthesis are the organometallic, mainly stannous salts [45]. The most accepted catalytic mechanism of these salts involves the polarization of the isocyanate group by the formation of the metal complex followed by a nucleophilic attack of the hydroxyl group [46–48].

In addition, the polymerization reaction can be catalyzed by tertiary amines which act as Lewis bases, enhancing the nucleophilic effect of hydroxyl groups [49–52].
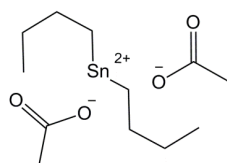
Figure 2.7 *Dibutyltin diacetate (DBTDA), the stannous catalyst used in the polymerization reaction.*

In our case, dibutyltin diacetate (DBTDA) (Figure 2.7), was selected as a stannous catalyst for the polymerization reaction. Additionally, the incorporation

of triethylamine (a tertiary amine) could provide an additional enhancement of the reaction rate.

2.3.1.2 Coumarin monomers

Owing to their intrinsic abilities to interact with UV light, significant efforts have been directed towards the incorporation of coumarin monomers in polymer backbones [7]. Hence, different coumarin derivatives with reactive groups in aromatic positions have been synthesized in order to facilitate this incorporation [53,54]. Coumarin monomers with aromatic hydroxyl groups for instance, can be easily synthesized and many of them are commercially available.

However, phenols are not appropriate candidates to be introduced in polyurethanes due to the low nucleophilic character of the phenolic hydroxyls [43]. Furthermore, the incorporation of coumarin groups is hindered owing to the low reactivity of IPDI (Table 2.1).

Therefore, coumarin derivatives with aliphatic hydroxyl groups in their structure are desirable in the polyurethane synthesis, as they present higher reactivity to isocyanates. As these monomers are less common, coumarin derivatives with aliphatic hydroxyl groups were expressly synthesized in this work.

Two coumarin derivatives were synthesized for the coumarin end-capped polyurethanes and coumarin chain extender polyurethanes; 7-hydroxyethoxy-4-methylcoumarin (HEMC) and 5,7-bis(2-hydroxyethoxy)-4-methylcoumarin (DHEMC) respectively.

HEMC was obtained by the modification of the commercial coumarin derivative methyl umbelliferone (7-hydroxyl-4-methylcoumarin). This monomer presents a phenolic hydroxyl group which was modified with bromoethanol, as shown in Figure 2.8.
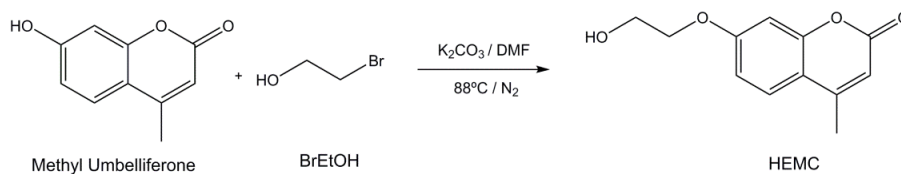
Figure 2.8 *Synthetic reaction of 7-hydroxyethoxy-4-methylcoumarin (HEMC) [55].*

The mechanism of this reaction is based on a nucleophilic substitution (S_N2) in basic medium. As depicted in Scheme 2.5, the substitution reaction occurs when the generated phenolate reacts with the electrophilic carbon directly attached to the bromine atom of bromoethanol.
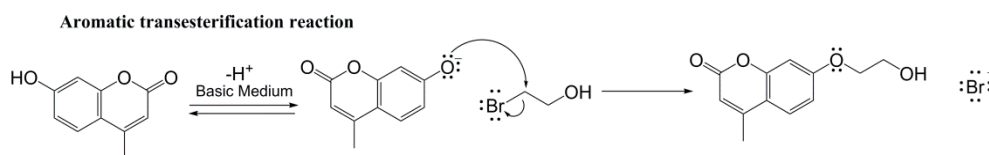
Scheme 2.5 *S_N2 reaction mechanism for HEMC formation.*

In this work, the formation of HEMC was performed following the experimental conditions described in the Appendix [55] and its structure was characterized by means of different spectroscopic techniques, such as UV, FTIR and ^{1}H-NMR.

The obtained ^{1}H-NMR signal assignment is shown in Figure 2.9 whereas the relative integral values are presented in Table 2.2.
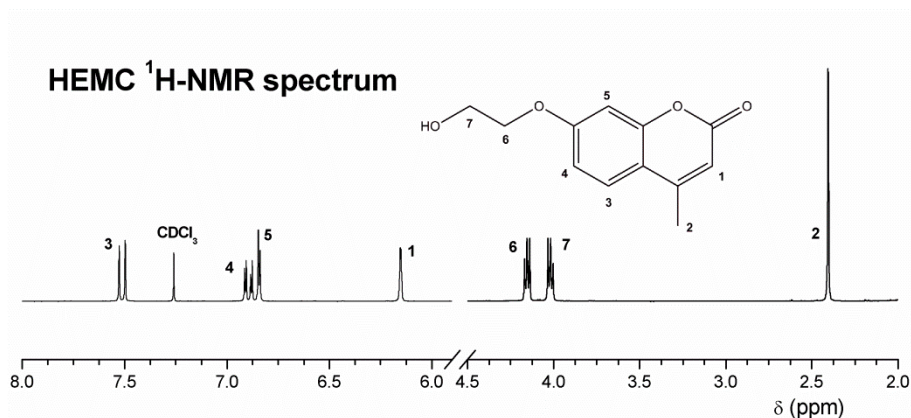
Figure 2.9 *^{1}H-NMR spectrum of 7-hydroxyethoxy-4-methylcoumarin (HEMC) in CDCl*$_3$*.*

As observed, the assignments corresponded to the proposed structure of the coumarin monomer.

Table 2.2 *Band assignment and integral values for HEMC ^{1}H-NMR spectrum.*

Proton assignment	[1]H-chemical shifts	Integral	Multiplicity
H-1	6.15	1H	singlet
H-2	2.40	3H	singlet
H-3	7.50-7.53	1H	doublet
H-4	6.91-6.89	1H	double-doublet
H-5	6.85	1H	doublet
H-6	4.15	2H	triplet
H-7	4.02	2H	triplet

In contrast to HEMC, the synthesis of DHEMC involved two separate reactions (Figure 2.10). In the first one, 5,7-dihydroxy-4-methylcoumarin (DHMC) was obtained, a coumarin derivative with two phenolic groups in its structure. Afterwards, these phenolic groups were reacted with bromoethanol, like in the case of the HEMC monomer [56,57].
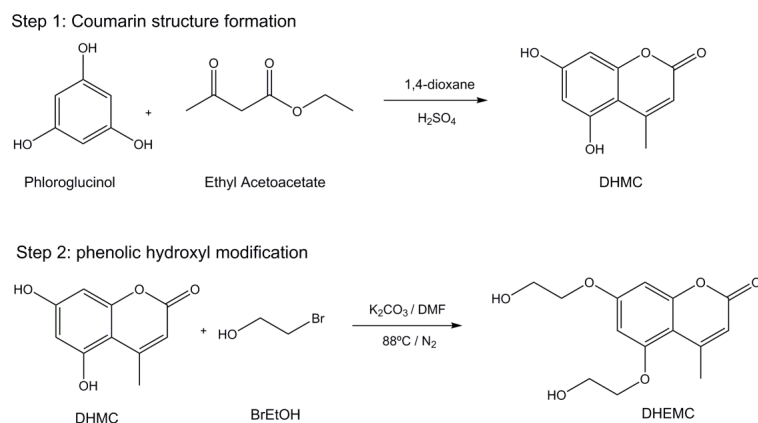
Figure 2.10 *Synthetic pathway of 5,7-bis(2-hydroxyethoxy)-4-methylcoumarin (DHEMC)* [56,57]*.*

The mechanism by which DHMC is obtained is based on the Pechmann condensation [53,58]. As observed in Scheme 2.6, this mechanism includes consecutive transesterification, Michael addition and elimination reactions under acid conditions.
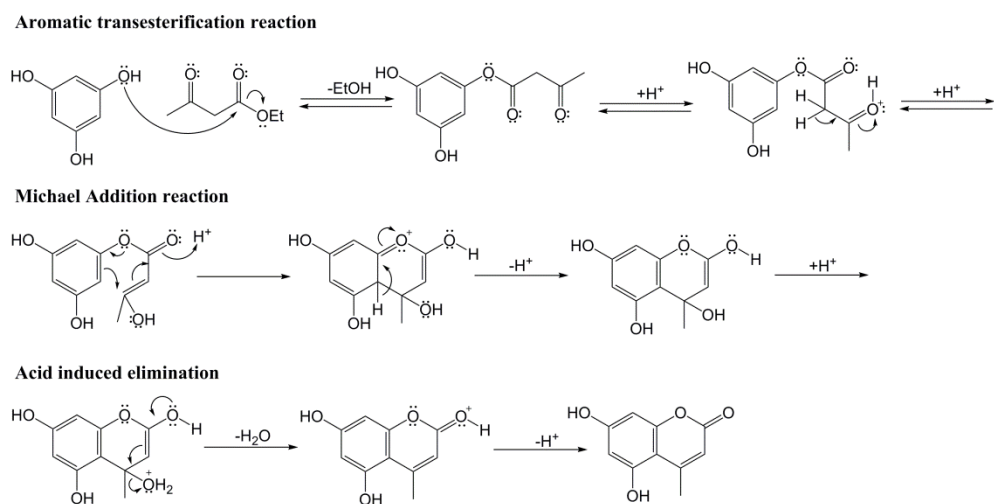
Scheme 2.6 *Pechmann condensation mechanism for the synthesis of DHMC monomer* [53,58]*.*

The modification of the phenolic hydroxyl groups in the second step occurred following the same mechanism described in Scheme 2.5.

The ^{1}H-NMR spectra of both DHMC and DHEMC monomers are presented in Figure 2.11 and their line assignment summarized in Table 2.3. As observed, ^{1}H-NMR spectra allowed us to confirm the chemical structure of both DHMC and DHEMC monomers. Additionally, no signals corresponding to reactants or byproducts appeared in the spectra.
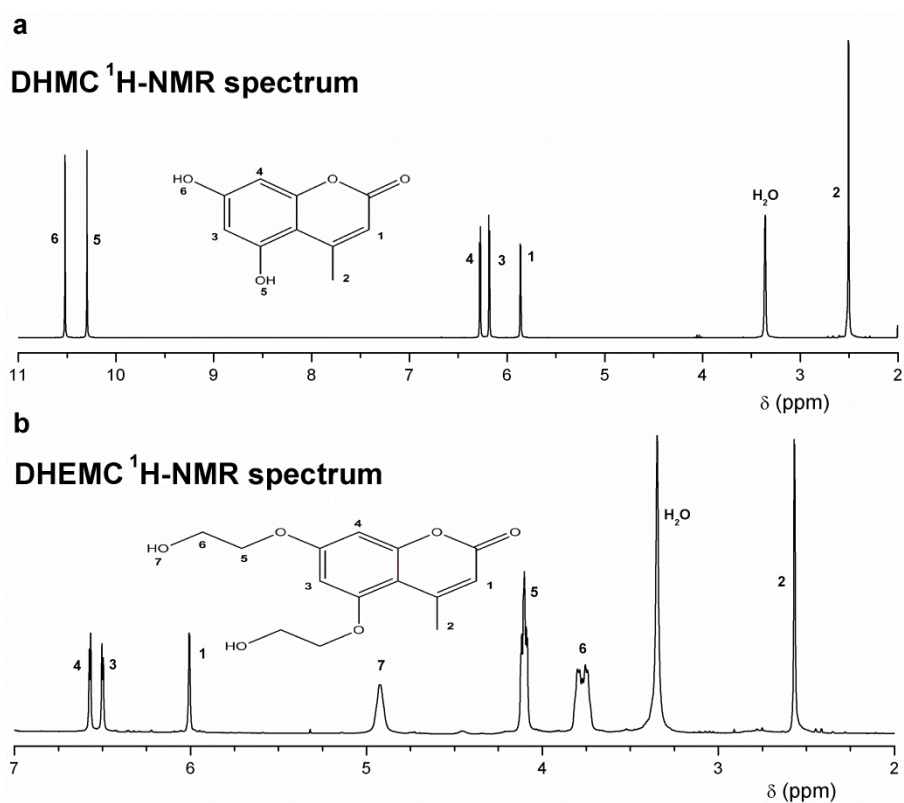
Figure 2.11 *^{1}H-NMR spectrum of 5,7-dihydroxy-4-methylcoumarin (DHMC) (a) and 5,7-bis(2-hydroxyethoxy)-4-methylcoumarin (DHEMC) (b) in d_6-DMSO.*

Table 2.3 *Proton assignment for DHMC and DHEMC ^{1}H-NMR spectra.*

Sample	Proton assignment	^{1}H-chemical shifts	Integral	Multiplicity
DHMC	H-1	5.85	1H	singlet
	H-2	2.51	3H	singlet
	H-3	6.18	1H	doublet
	H-4	6.28	1H	doublet
	H-5	10.29	1H	singlet
	H-6	10.52	1H	singlet
DHEMC	H-1	6.01	1H	singlet
	H-2	2.57	3H	singlet
	H-3	6.49	1H	doublet
	H-4	6.57	1H	doublet
	H-5	4.10	4H	triplet
	H-6	3.75	4H	multiplet
	H-7	4.92	2H	singlet

2.3.1.3 Aromatic disulfide monomers

The dynamic chemistry involving sulfur atoms has demonstrated to be a successful alternative to develop stimuli-responsive and healable materials. Disulfide bonds are able to break and reform in mild conditions leading to chain exchange reactions. In contrast to their aliphatic counterparts, the sulfur metathesis occurs at ambient temperature without catalyst for aromatic disulfides [59,60]. This characteristic has led to autonomic healable polyurethanes [3,23].
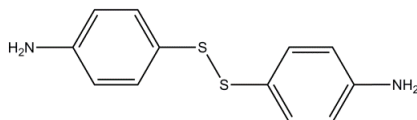
Figure 2.12 *4-Aminophenyl disulfide (APDS) monomer structure.*

For this work the commercially available 4-aminophenyl disulfide (APDS) was selected as aromatic disulfide derivative (Figure 2.12). This monomer presents

two aromatic amine groups which permits its incorporation as a chain extender in the polymer backbone.

As mentioned, aromatic disulfides can provide healing properties to crosslinked polymers. However, their incorporation limits the number of alternatives that can be used to obtain crosslinked structures. Thus, one of the most commercially used crosslinking alternatives for polyurethanes is the incorporation of acrylic derivatives in the polymer backbone. These systems crosslink as a consequence of free radical polymerizations initiated by heat or light [37,61]. Nevertheless, sulfur containing molecules are well known to act as chain transfer agents in free radical polymerization. Therefore, it is not possible to crosslink the polyurethanes by means of this reaction.

In this work, the incorporation of an inorganic precursor, the N-(n-butyl)-3-Aminopropyl trimethoxysilane (N-bAPTMS), Figure 2.13, into the polymer matrix was analyzed.
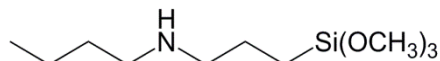
Figure 2.13 *N-(n-butyl)-3-Aminopropyl trimethoxysilane (N-bAPTMS) structure.*

This monomer presents a secondary amine in its structure that can give rise to substituted ureas after the reaction with IPDI. In addition, this monomer allows us to incorporate alkoxysilane functionalities in the polymer backbone. In contrast to the acrylic containing polyurethanes, where the crosslinking process occurs *via* free radical polymerization, the methoxysilane groups of N-bAPTMS are capable to condense by means of the sol-gel process [62]. For these systems, this crosslinking alternative was selected due to the presence of disulfide bonds do not interfere in the crosslinking process.
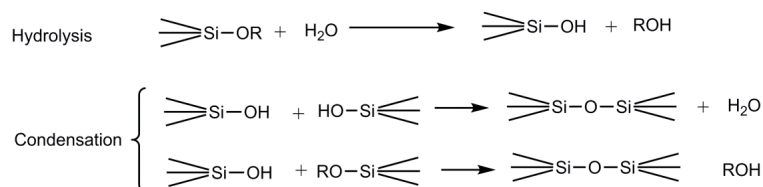
Figure 2.14 *Reactions taking place during the Sol-Gel process of alkoxysilane groups.*

According to the sol-gel process depicted in Figure 2.14, the alkoxysilane groups condensed to form silicon-oxygen networks. This process occurs in two separated reactions, the hydrolysis and the condensation reactions. During the hydrolysis reaction, silanol groups are obtained by reaction of alkoxysilanes with water. Afterwards, these silanol groups react with other silanol or alkoxysilanes, condense and form the Si-O-Si network [62–64]. This process is known to be catalyzed by acids, bases or organometallic compounds. Depending on the catalytic mechanisms either hydrolysis or the condensation is favored.

2.3.1.4 Ureidopyrimidinone monomers

The most common method to obtain Ureidopyrimidinone structures is by the reaction of isocytosine derivatives. In this work, 2-Amino-4-hydroxy-6-methylpyrimidine was used as isocytosine derivative. This monomer presents two tautomeric forms, as represented in Figure 2.15.
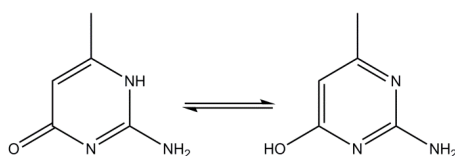
Figure 2.15 *Tautomeric forms of 2-Amino-4hydroxyl-6-pyrimidine*

The primary amine group of this monomer is susceptible to react with isocyanates at high temperatures [65–67]. However, it is also possible to form ureidopyrimidinone units by means of indirect methods [68–71]. Figure 2.16 shows the synthetic pathway to form ureidopyrimidinone derivatives by reaction

with 1,1'-carbonyldiimidazol (CDI). This strategy is based on two reactions. In the first one, the amine group of 2-Amino-4-hydroxy-6-methylpyrimidine reacts with CDI to form the corresponding carbamoylimidazol, 2-(Imidazolylcarbonylamino)-6-methyl-4[1H]-pyrimidinone (ICAmpy) [68]. These activated spices react with pimary amines in a very selective reaction, which can lead to different Ureidopyrimidinone derivatives formation or polymer modification [70–73].
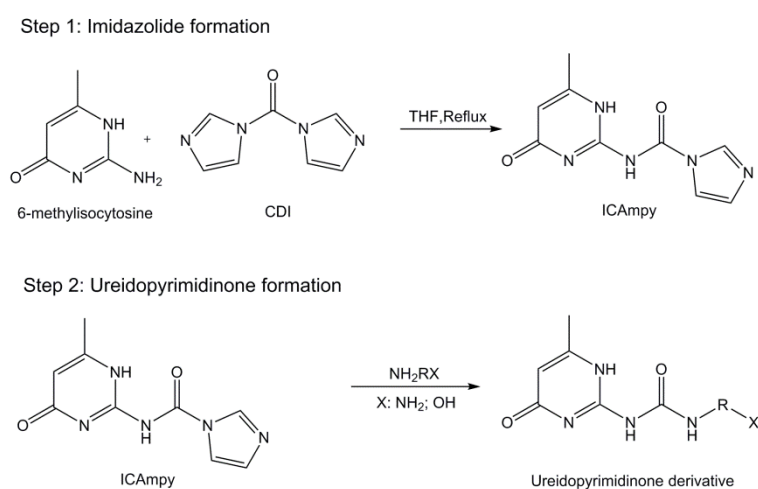
Figure 2.16 *Indirect synthetic method based on carbonyldiimidazol reaction to form Ureidopyrimidinone derivatives.*

The ICAmpy monomer formation implies an amidation reaction in the carbonyl group of the CDI monomer, following the mechanism represented in Scheme 2.7 [74,75].
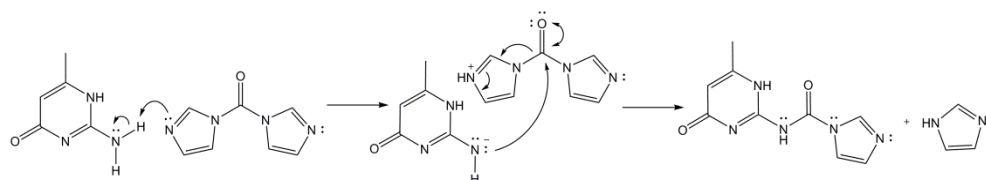
Scheme 2.7 *ICAmpy monomer formation mechanism.*

Owing to the extremely low solubility of this monomer, it was not possible to characterize its structure by ^{1}H-NMR. Consequently, the structure was confirmed from its FTIR spectrum (Figure 2.17) [73].
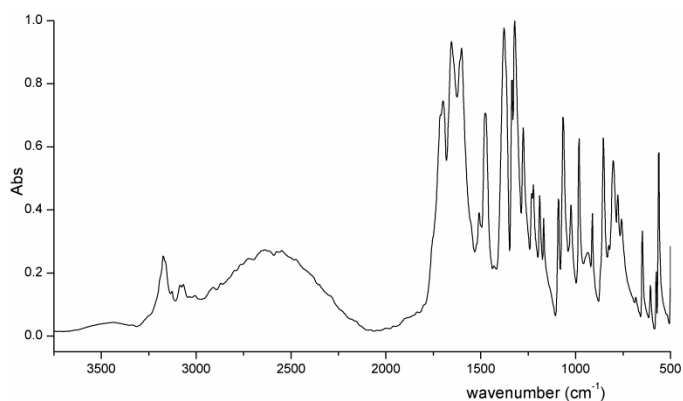
Figure 2.17 *FTIR spectrum of 2-(Imidazolylcarbonylamino)-6-methyl-4[1H]-pyrimidinone (ICAmpy).*

Following this strategy, an Ureidopyrimidinone derivative capable of acting as a chain extender was synthesized. The carbamoylimidazol obtained in the previous reaction was reacted with 2-Amino-2-methyl-1,3-propanediol, following the reaction shown in Figure 2.18. As a consequence of the amidation reaction, a Upy derivative with two aliphatic hydroxyl groups in its structure is formed. This reaction progresses following a similar reaction mechanism shown in Scheme 2.7.
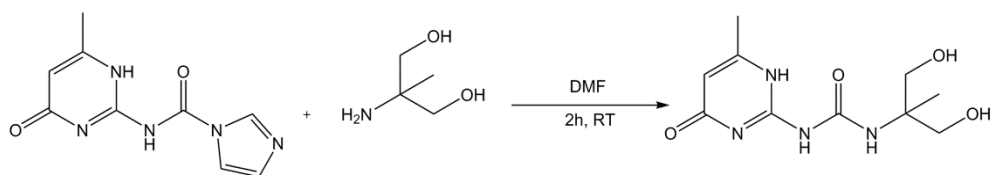
Figure 2.18 *Synthetic pathway of 1-(1,3-dihydroxy-2-methylpropan-2-yl)-3-(6-methyl-4-oxo-1,4-dihydropyrimidin-2-yl)urea (DHUpy).*

The obtained dihydroxyl ureidopyrimidinone derivative, 1-(1,3-dihydroxy-2-methylpropan-2-yl)-3-(6-methyl-4-oxo-1,4-dihydropyrimidin-2-yl)urea (DHUpy), is soluble in dimethyl formamide (DMF) and dimethyl sulfoxide (DMSO) although its solubility in THF, chloroform and acetone is low. However, it was possible to characterize this monomer by ^{1}H-NMR in d_6-DMSO. The obtained spectrum and the signal assignment is presented in Figure 2.19 and Table 2.4.
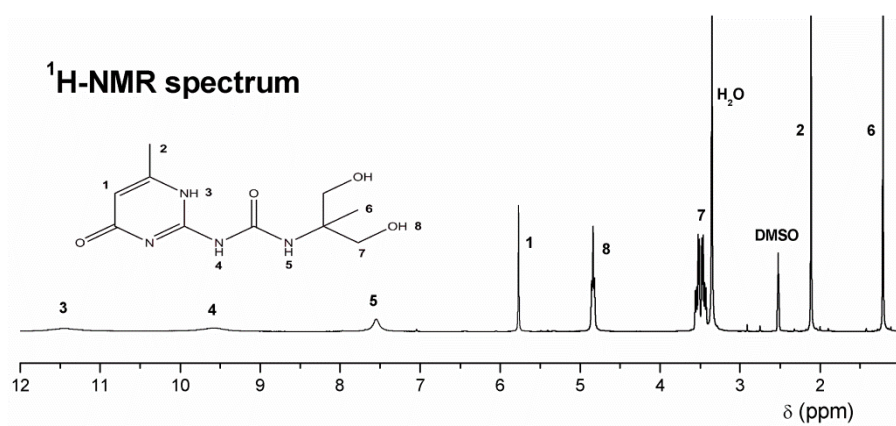
Figure 2.19 *^{1}H-NMR spectrum of 1-(1,3-dihydroxy-2-methylpropan-2-yl)-3-(6-methyl-4-oxo-1,4-dihydropyrimidin-2-yl)urea (DHUpy).*

Table 2.4 *Proton assignment for DHUpy ^{1}H-NMR spectrum.*

Proton assignment	[1]H-chemical shifts	Integral	Multiplicity
H-1	5.77	1H	singlet
H-2	2.11	3H	singlet
H-3	11.45	1H	broad
H-4	9.58	1H	broad
H-5	7.55	1H	singlet
H-6	1.21	3H	singlet
H-7	3.56-3.35	4H	double-quartet
H-8	4.84	2H	triplet

As occurred in the case of coumarin monomers, the line assignment and position confirmed the Upy derivative formation.

2.3.2   Waterborne polyurethanes synthesis and characterization

Waterborne polyurethanes were obtained in two different steps: The polymerization reaction and the polymer dispersion in water.

2.3.2.1 Polymerization reaction

Polymerization reactions were carried out in a jacketed glass reactor equipped with mechanical stirring, glass stirred gland, septum and refrigerator, as can be seen in Figure 2.20. This reaction equipment minimized the evaporation of solvent and reactants, not only during the reaction but also during the monomer addition, as they were injected through a septum.
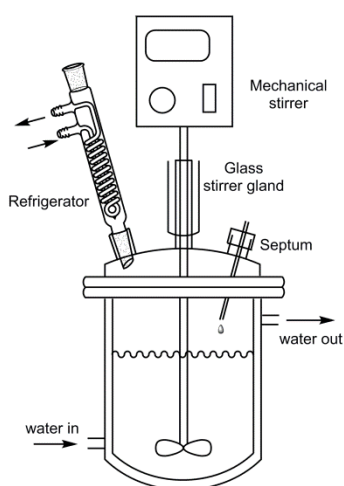
Figure 2.20 *Schematic representation of the used reaction equipment.*

The polymerization reaction of coumarin based waterborne polyurethanes is presented in Scheme 2.8. The reaction can be separated in three different steps: prepolymer synthesis, chain extension and coumarin monomer addition. This last step differs depending on the type of coumarin monomer. While the addition of the HEMC monomer gives rise to the capping of the polyurethane chain-ends (A), DHEMC leads to the incorporation of the coumarin monomers in the middle of polyurethane chain structures (B).

1st Step: Prepolymer synthesis

2nd Step: Chain Extention

3th Step A: Coumarin end-capping

3th Step B: Coumarin addition
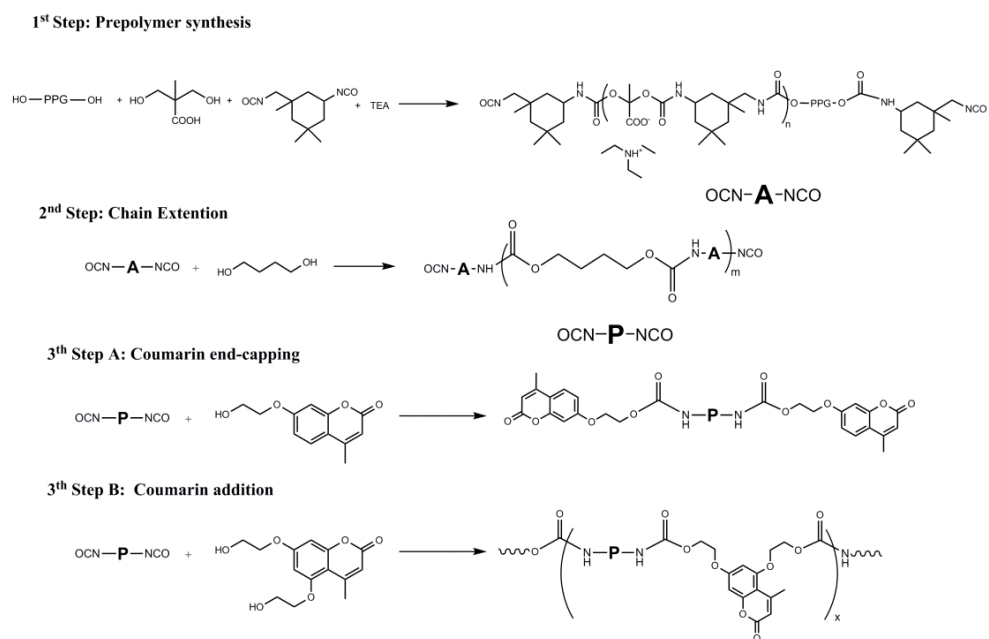
Scheme 2.8 *Synthetic pathway to obtain coumarin end-capped (a) and coumarin chain extended (b) waterborne polyurethanes.*

The reactions were performed as follows [76]. Polyol (PPG), internal emulsifier (DMPA) and neutralizing agent (TEA) were poured together with the catalyst (DBTDA, 800 ppm) and acetone into a flask reactor. When the reaction temperature reached 56 °C, the diisocyanate (IPDI) was added and the reaction was maintained for 3 h. In a further step, the polymer chains were extended using the appropriate BD amount, leaving some free isocyanate groups. This reaction was carried out for one additional hour. Afterwards, the coumarin monomer (HEMC in the case of coumarin end-capped polyurethanes and DHEMC in the case of coumarin chain-extended polyurethanes) was added to the reaction mixture with a stoichiometric ratio of NCO and OH groups.

The synthetic pathway for aromatic disulfides containing waterborne polyurethanes is represented in Scheme 2.9. Although the first step of the polymerization reaction is similar to the previous reaction, both in the chain extension and end-capping reactions forms linkages in the polyurethane

structure. As the amine groups are more reactive than hydroxyl groups towards isocyanates, the reaction was carried out in milder conditions.
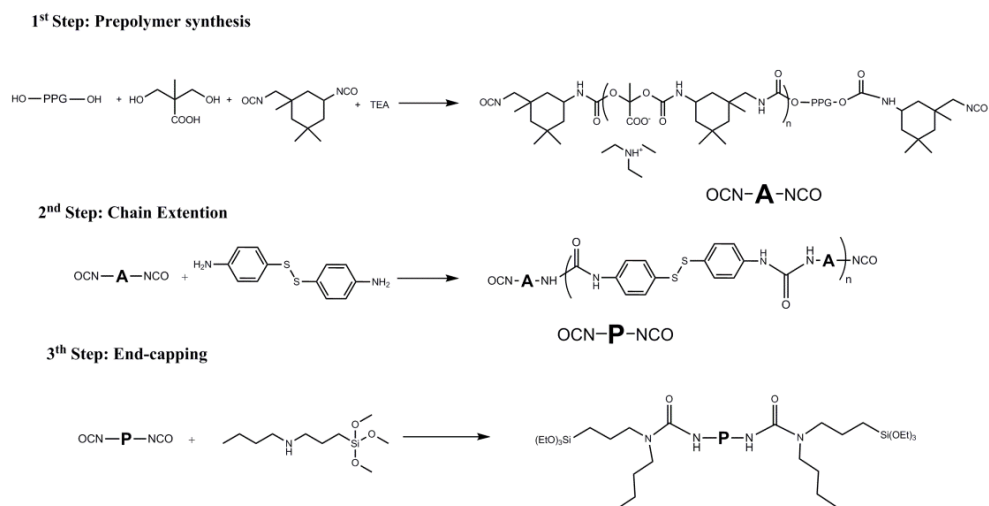
Scheme 2.9 *Synthetic pathway to obtain aromatic disulfide based waterborne organic-inorganic polyurethane hybrids.*

Thus, after the prepolymer synthesis, which was carried out in the conditions previously mentioned, the reaction was cooled down to room temperature and the appropriate amount of APDS was added to the reaction. This reaction was performed for two hours and afterwards, stoichiometric amounts of N-bAPTMS were incorporated in order to react with the remaining isocyanate groups, leading to the end-capping of the polyurethane.

The synthesis of ureidopyrimidinone based waterborne polyurethanes required different experimental conditions owing to solubility and reactivity problems DHUpy monomer presents. For this reason, tetrahydrofuran (THF) was selected as solvent for the polymerization reaction. This solvent presents a higher boiling point than acetone and therefore it is possible to carry out the polymerization reaction at 65ºC. Additionally, another important difference was made in the synthetic pathway, represented in Scheme 2.10.
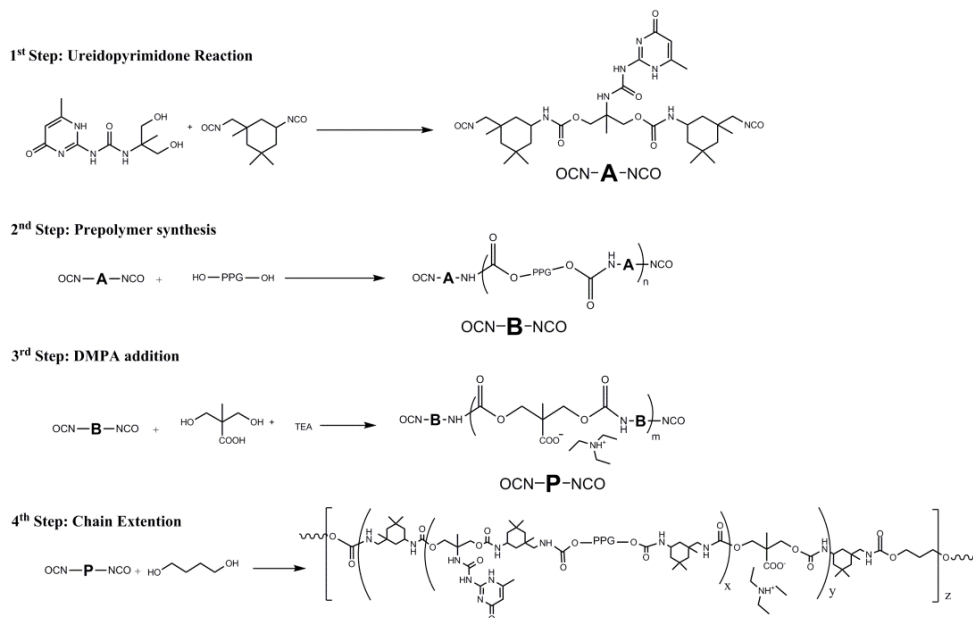
Scheme 2.10 *Synthetic pathway to obtain ureidopyrimidinone based waterborne polyurethanes.*

In order to ensure the incorporation of the DHUpy monomer into the polymer backbone, this monomer was introduced together with IPDI in the first step of the polymerization reaction. In this manner, the most reactive isocyanates (secondary isocyanates) as well as the isocyanate concentration favors the urethane formation. Once this reaction occurs, the following polyols were added in successive steps to form the polymer structure. As occurred in the case of coumarin based WPUs, the NCO:OH ratio was maintained 1:1.

2.3.2.2 Dispersion

The emulsification process is highly dependent on experimental parameters, such as polymer concentration, emulsification temperature, water addition rate, solvent evaporation temperature and so on [40]. In order to investigate the influence of different healing groups on the polyurethane water dispersion abilities, polymer dispersions in water were prepared under similar conditions for both coumarin based and ureidopyrimidinone based polyurethanes.

Dispersions were carried out in a flask reactor equipped with mechanical stirrer and addition pump, which is responsible for the water incorporation in a controlled way (Figure 2.21).
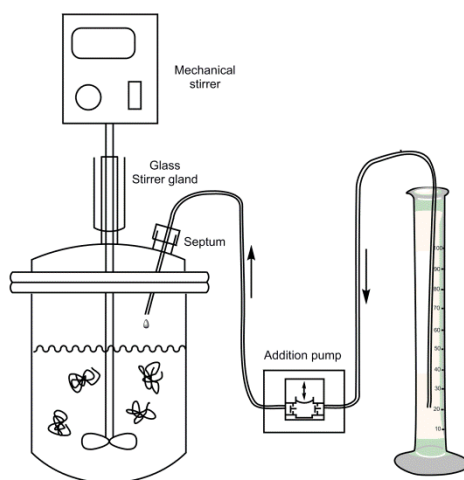
Figure 2.21 *Schematic representation of equipment used during the dispersion process.*

Before starting the water addition, the polymer concentration was adjusted to 60 wt%. The emulsification process was carried out at room temperature under mechanical stirring (400 rpm) to help the dispersion process. 25 g of the reaction mixture was incorporated into the reactor and water (60 g) was added drop-wise at 1 mL min^{-1}. After the water addition, the stirring was kept at the same rate for additional 30 min. Finally, the solvent was removed using distillation equipment at 30 °C under vacuum. The solid content of the resulting dispersion was 20 wt%.

2.3.2.3 Nomenclature

In this work, different polymer structures have been proposed for both coumarin based and ureidopyrimidinone based waterborne polyurethanes. In the case of coumarin based WPUs, different amounts of healing monomers (from 1 to 20 wt %) were introduced in the polymer structure. These polyurethanes were formulated following two different criteria.

On the one hand, the soft/hard segment ratio was maintained constant for all formulations. This implies that the molar amount of all coumarin monomers, DMPA, BD and IPDI is constant in all cases. On the other hand, the DMPA amount was maintained constant in order to analyze the influence of the incorporation of coumarin monomers in the water dispersability of WPUs. As a consequence, the increase of the coumarin monomer amount reduces BD concentration in the final formulation. Table 2.5 summarizes the reagent amounts used in the synthesis of different coumarin based WPU formulations.

Table 2.5 *Amount of reagents used in the synthesis of different coumarin based waterborne polyurethanes.*

Sample	Polyol	DMPA	IPDI	TEA	BD	Coumarin monomer		
	(mmol)					(mmol)	(mol %)	(wt %)
PPG1HEMC	22.5	11	56.5	15	22.0	2	1.75	1.13
PPG5HEMC	22.5	11	56.5	15	18.5	9	7.65	4.93
PPG10HEMC	22.5	11	56.5	15	13.5	19	15.51	9.97
PPG15HEMC	22.5	11	56.5	15	8.0	30	23.43	15.06
PPG20HEMC	22.5	11	56.5	15	2.5	41	30.71	19.71
PPG1DHEMC	22.5	11	56.5	15	21.5	1.5	1.32	1.08
PPG5DHEMC	22.5	11	56.5	15	14.5	8.5	7.52	5.91
PPG10DHEMC	22.5	11	56.5	15	6	17	15.04	11.38
PPG15DHEMC	22.5	11	56.5	15	0	23	20.35	14.98

The nomenclature used for these samples is based on the following aspects: the three first letters correspond to the polyol used in the synthesis, which is always PPG, and the following digits and letters express the quantity and the coumarin monomer type.

Using the same criteria, aminophenil disulfide and ureidopyrimidinone based waterborne polyurethane formulations are summarized in Table 2.6 and Table 2.7. For the case of aromatic disulfide containing samples, the increase in the APDS concentration was adjusted varying the amount of N-bAPTMS in the sample. As the sol-gel precursor is introduced in the chain-end, high amounts of the healing agents imply low concentrations of the crosslinking agent.

Table 2.6 *Formulations of waterborne polyurethanes based in aromatic disulfide units.*

| Sample | Polyol | DMPA | IPDI | TEA | APDS | | N-bAPTMS | |
		(mmol)			(mmol)	(wt %)	(mmol)	(wt %)
PPG2APDS	22.5	11	56.5	15	3	2.18	40	20.14
PPG5APDS	22.5	11	56.5	15	7	5.23	32	16.43
PPG10APDS	22.5	11	56.5	15	23	10.12	20	10.58
PPG15APDS	22.5	11	56.5	15	18.5	14.97	9	4.89

Table 2.7 *Amount of reagents used in the synthesis of different ureidopyrimidinone based waterborne polyurethanes.*

| Sample | Polyol | DMPA | IPDI | TEA | BD | DHUpy monomer | | |
		(mmol)				(mmol)	(mol %)	(wt %)
PPG1DHUpy	22.5	11	56.5	15	21.5	1.5	1.32	0.99
PPG5DHUpy	22.5	11	56.5	15	14.5	8.5	7.52	5.44
PPG10DHUpy	22.5	11	56.5	15	6	17	15.04	10.51
PPG15DHUpy	22.5	11	56.5	15	0	23	20.35	13.89

The nomenclature used for these samples is based on the following aspects: the three first letters correspond to the polyol used in the synthesis, which is always PPG, and the following digits and letters express the quantity and the monomer type. Thus, for coumarin containing samples, HEMC correspond to coumarin end-capped linear polyurethanes and DHEMC designates coumarin chain-extended systems. Both aromatic disulfide and ureidopyrimidinone containing samples are named by the corresponding name of the monomers, APDS and DHUpy.

2.3.3 Structural characterization

Both the evolution of the polymerization reaction and the chemical structure of the final products were characterized by FTIR spectroscopy. This technique is particularly appropriate to fulfill this aim, as polyurethanes present very distinctive spectral features not only in the final product but also during the polymerization reaction. The spectra corresponding to different reaction steps for PPGHEMC and PPGDHEMC samples are presented in Figure 2.22.
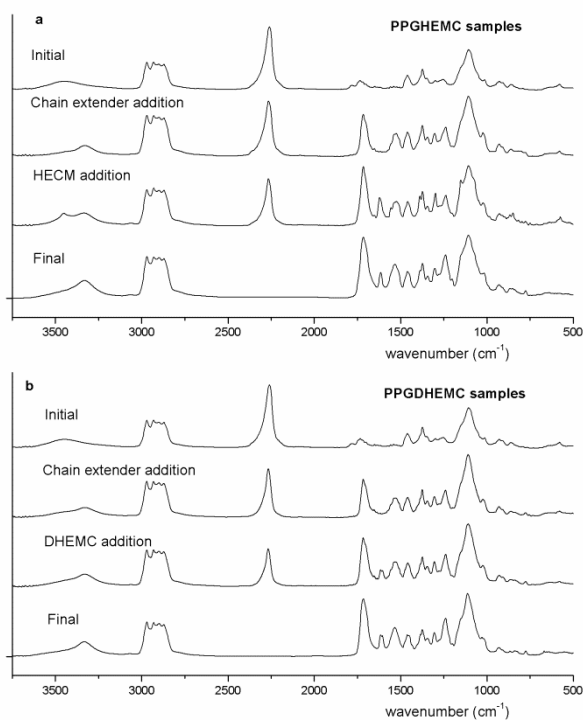
Figure 2.22 *FTIR spectra at different reaction steps of PPGHEMC samples (a) and PPGDHEMC samples (b).*

The initial spectrum, which corresponds to the time when IPDI was added to the reaction mixture, is characterized by the strong band at 2260 cm^{-1} due to the stretching vibration of isocyanate groups. As the reaction progresses, this band decreases and the bands due to Amide I and Amide II of the urethane groups at 1735 cm^{-1} and 1550 cm^{-1} appear, together with the N-H stretching vibration (3330 cm^{-1}). No additional spectral characteristics can be observed when butanodiol is incorporated. However, when the coumarin monomers are added, a band centered at 1635 cm^{-1} attributable to the stretching vibration of coumarin C=C bond (with the contribution of the aromatic ring of the coumarin) appears. Additionally, another band at 3450 cm^{-1} can be observed in Figure 2.22 a, associated to the OH stretching of the HEMC monomer. The FTIR spectra of the final products do not present either the isocyanate or the OH vibration bands, which means that the polymerization reaction was performed successfully.

67

Although FTIR spectroscopy allowed us to follow the reaction, ^{1}H NMR was used to characterize the structure of final products. ^{1}H NMR spectra of PPG10HEMC and PPG10DHEMC samples as well as the line assignment is shown in Figure 2. 23 and Figure 2. 24 respectively.
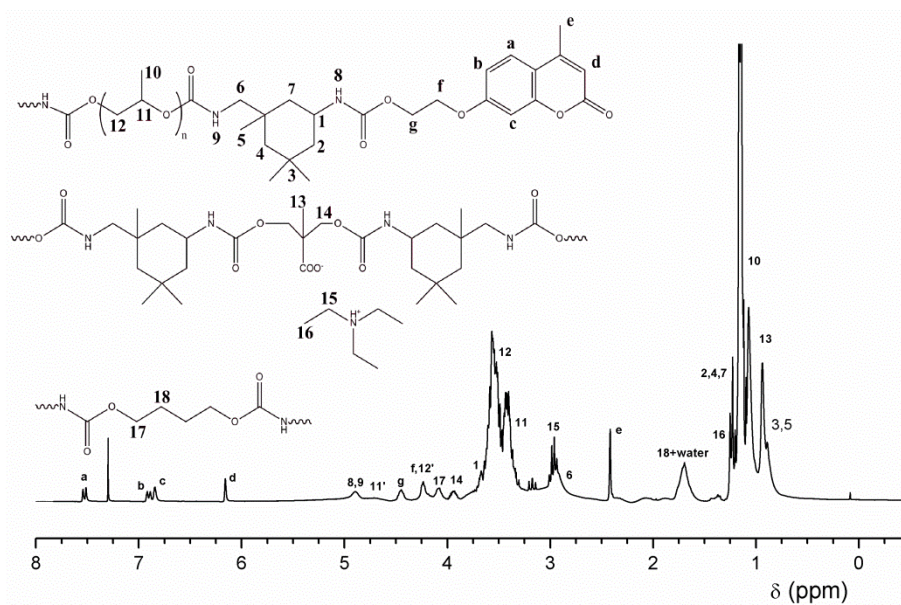
Figure 2. 23 *^{1}H NMR spectrum of PPG10HEMC and its signal assignment.*
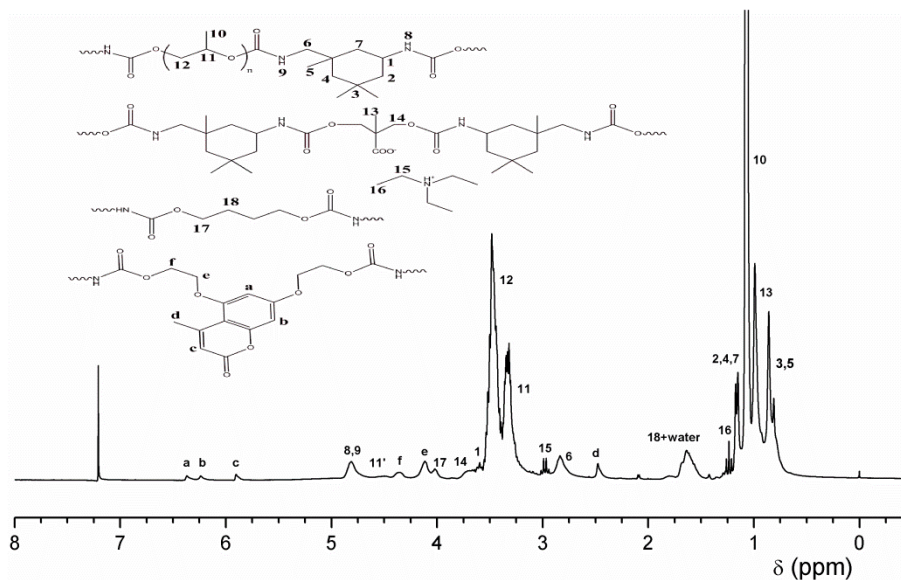
Figure 2. 24 *¹H NMR spectrum and line assignment for PPG10DHEMC sample.*

The signals were successfully assigned to both polymer structures. In the case of PPGHEMC samples, the signals between 7.5-6.8 ppm correspond to the aromatic protons, while that at 6.3 ppm is assigned to olefinic protons. In the case of PPGDHEMC samples, the lines corresponding to aromatic and olefinic protons appear at lower chemical shifts (6.3-5.9 ppm).

The region between 3.5 and 4.5 is particularly significant as it is the region where CH_2 protons directly attached to urethane bonds appear. Thus, the presence of f and g lines (PPGHEMC samples) and e and f (PPGDHEMC samples) confirms the incorporation of the coumarin monomers in the polymer structure.

As occurred in the case of coumarin based WPUs, the polymerization reaction of APDS based WPUs was followed by FTIR spectroscopy as presented in Figure 2.25.
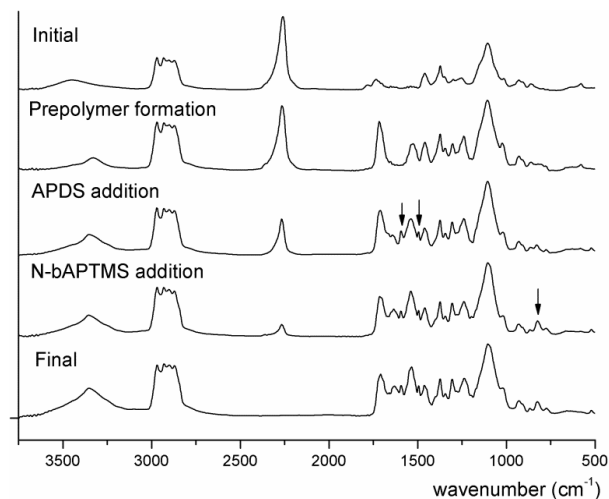
Figure 2.25 *Evolution of FTIR spectra during the reaction of PPGAPDS samples.*

The initial two spectra correspond to the first reaction step. As occurred for coumarin based samples, the main spectral features correspond to the isocyanate (stretching vibration at 2260 cm^{-1}) and urethane groups (Amide I Amide II bands at 1735 cm^{-1} and 1550 cm^{-1} as well as N-H stretching vibration at 3330 cm^{-1}). When the APDS is added into the reaction the bands corresponding to the C=C stretching vibration of aromatic rings (1595-1495 cm^{-1}) appears. Additionally, the Amide I band corresponding to urea bonds can be observed at 1635 cm^{-1}. Finally, the N-bAPTMS addition increases the absorbance of urea bond and a band corresponding to the Si-O bending vibration at 825 cm^{-1} appears. In the final spectrum the isocyanate stretching vibration is not detectable and maintains the aforementioned spectral characteristics.

The structural characterization of the final product was carried out by ^{1}H-NMR spectroscopy. The ^{1}H-NMR spectrum and the line assignment for PPG10APDS sample is shown in Figure 2.26.
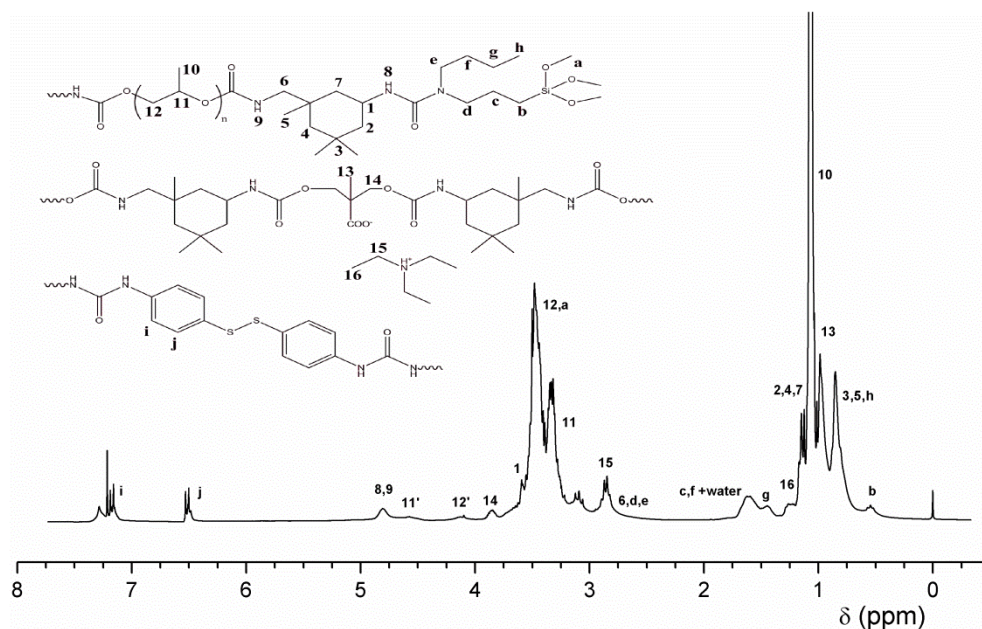
Figure 2.26 *1H NMR spectrum and line assignment for PPG10APDS sample.*

In contrast to coumarin based systems, where the region between 3.5 and 4.5 ppm allowed us to identify the urethane linkages, the most interesting line for PPGAPDS samples is the 2.8 ppm line, which corresponds to the urea linkages. Thus, according to the proposed line assignment, the incorporation of both APDS and N-bAPTMS monomers into the polymer structure could be confirmed.

The evolution of FTIR spectra during the reaction of PPGDHUpy is shown in Figure 2.27. Taking into account the proposed synthetic pathway represented in Scheme 2.10, the differences occurring between the initial and the second spectrum are particularly important. The band corresponding to the isocyanate stretching vibration decreases while new absorption bands appear. These bands correspond to Amide I and Amide II of the urethane groups (1745 - 1715 cm^{-1} and 1550 cm^{-1}) as well as to the N-H stretching band at 3320 cm^{-1}. These bands confirm the diisocyanate-ureidopyrimidone compound formation. This reaction produces significant changes in the polymerization reaction appearance; while the DHUpy monomer is present in the mixture, the reaction performs in

suspension. However, the mixture becomes homogeneous when the diisocyanate dimer is formed.
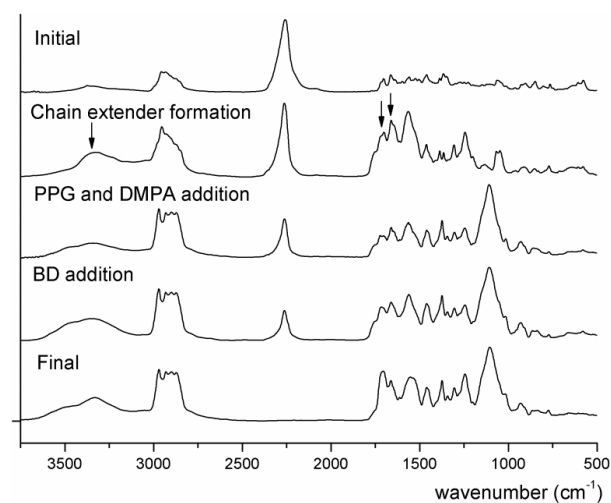
Figure 2.27 *Evolution of FTIR spectra for PPGDHUpy samples*

Once the dimer was formed, the rest of the monomers were added into the reactor in consecutive steps. The corresponding FTIR spectra showed an increase of the band intensity of the urethane group and a decrease in the isocyanate band. In addition, the band due to the ether C-O-C stretching vibration of PPG (1100 cm^{-1}) was observed.

The final product structure was analyzed by ^{1}H-NMR and the spectrum is depicted in Figure 2.28.
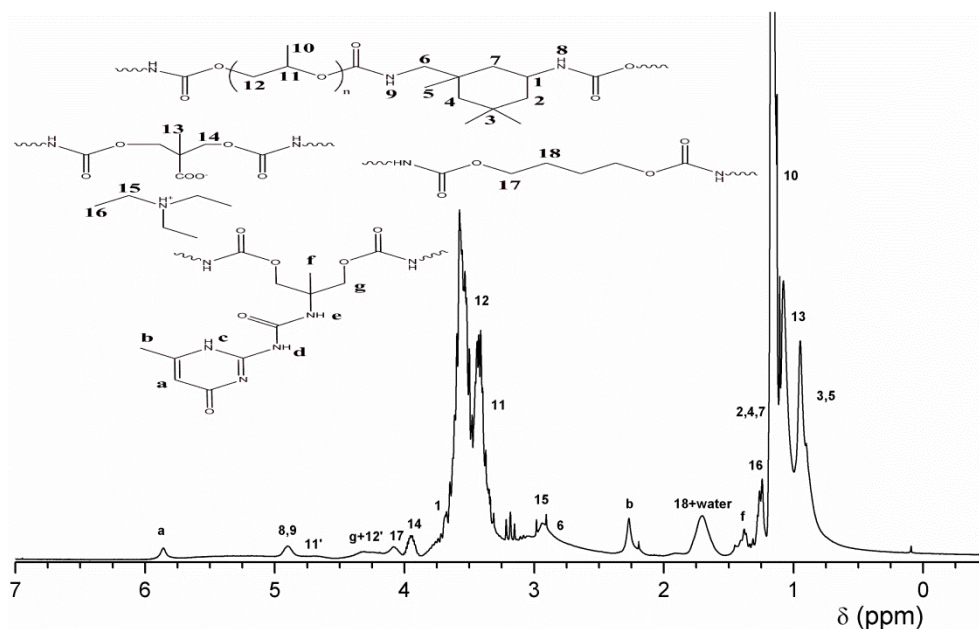
Figure 2.28 ^{1}*H-NMR spectrum for PPGDHUpy samples.*

The line assignment of PPGDHUpy samples was successfully carried out, confirming the proposed polymer structure. Nevertheless, the signals corresponding to NH bonds of the ureidopyrimidinone unit (c, d and e protons) were not detected. This could be related both to the amount of DHUpy in the sample and the presence of strong H-bond interactions in the polymer structure, which broaden their lines.

The proposed reaction scheme allowed us to synthesize PPGDHUpy samples containing 1, 5 and 10 wt% of DHUpy monomer. However, owing to the low reactivity of this monomer, it was not possible to obtain samples with higher amounts of the ureidopyrimidinone monomer.

2.3.4   Waterborne polyurethane dispersion stability

One of the main parameters in relation to the dispersion stability of waterborne polyurethanes is the polymer particle size in water. In order to determine the

particle size, waterborne polyurethane dispersions were analyzed by Dynamic Light Scattering measurements (DLS).

Generally, small particle sizes give rise to stable dispersions whereas an increase in the particle size produces polymer precipitation. As mentioned, several parameters influence particle size. On the one hand, the monomer nature, internal emulsifier concentration or the neutralization degree affect polymer particle size. Thus, interactions between healing agents could disturb polymer stability in water.

However, the dispersion stability is highly dependent on experimental conditions such as solvent evaporation temperature, polymer concentration in acetone or stirring velocity [40]. In order to avoid these effects, in this work, these parameters were maintained constant and the influence of the incorporation of the healing agents in the dispersion stability was determined.
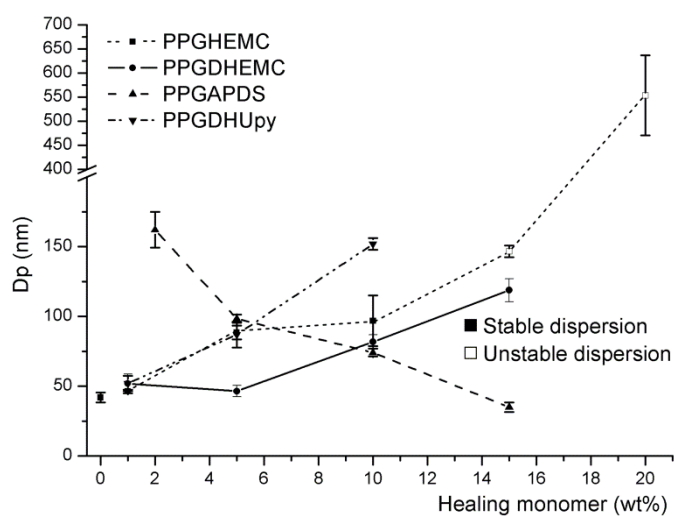
Figure 2.29 *Particle size variation as a function of the healing monomer concentration.*

As observed in Figure 2.29, not only does the amount of healing agent affect the polymer particle size but also the relative position in the polymer backbone, as chain extender or end-capper.

For coumarin containing samples, regardless of the monomer nature, the higher the coumarin monomer concentration the higher the polymer particle size, indicating that noncovalent interactions among coumarin moieties influence the particle size in water [77,78].

This effect is particularly relevant in the case of HEMC monomers. In fact, it was not possible to stabilize PU dispersions with coumarin amounts higher than 15 wt%. In contrast, PPGDHEMC samples presented smaller particle sizes than the corresponding coumarin concentrations in PPGHEMC samples. This difference in their behavior could be related to molecular weight differences among these types of samples and their effect on chain-end interactions. In PPGHEMC samples, as the monomer is monofunctional, higher amounts of coumarin imply lower molecular weights, and therefore more chain mobility. Additionally, the higher chain-end concentration in PPGHEMC samples also facilitates the interactions between coumarin groups, making them less effective in the case of PPGDHEMC samples owing to the difunctionality of coumarin monomer.

Similar results were obtained for PPGDHUpy samples, where the presence of ureidopyrimidinone units strongly increased the polymer particle size. As occurred in coumarin containing samples, the presence of strong hydrogen bonds in ureidopyrimidinone units, could be related to this behavior [26,73].

In contrast to the aforementioned systems, the introduction of the healing agent in PPGAPDS systems led to a decrease in the polymer particle size of the waterborne polyurethanes. In order to accurately analyze these results, the intrinsic characteristics of these systems should be taken into consideration. Aromatic disulfide bridges were introduced as chain-extenders in the polymer structure. Unlike PPGDHEMC or PPGDHUpy samples, the molecular weight was not maintained constant. As the APDS concentration increased, the amount of N-

bAPTMS end-capper decreased and, consequently, the molecular weight of the polymer was higher. Although, APDS moieties have the ability to interact via hydrogen bonding of urea groups, according to the results, it seems that the interaction of alkoxysilane groups located in the polymer chain ends was predominant [3,77,79].

2.4 Conclusions

This chapter focused on the synthesis and chemical characterization of healable waterborne polyurethanes as well as on the water dispersion abilities that they presented. From this work the following conclusions can be drawn:

- Both the coumarin and ureidopyrimidinone monomers were successfully modified and characterized making it possible for them to be introduced into polyurethane backbones.

- The synthesis of healable waterborne polyurethanes can be directly carried out by means of the acetone process, except for ureidopyrimidinone based systems.

- In ureidopyrimidinone based systems, the procedure should be modified owing to the low reactivity and solubility of the DHUpy monomer. Thus, it was necessary to perform the reaction at 65 ºC in THF, introducing the healing monomer in the first reaction step.

- Healable waterborne polyurethanes give rise to stable waterborne dispersions, regardless of the incorporated healing monomer.

- The inclusion of healing agents increases the polymer particle size coumarin and ureidopyrimidinone dispersions. Under these conditions, it is not possible to obtain stable dispersions above 10 wt% for PPGHEMC samples.

- In contrast, the effect of chain end interactions in the particle size is more significant than the healing monomer interactions for APDS based systems.

2.5 References

[1]   Heo Y, Sodano H a. Self-Healing Polyurethanes with Shape Recovery. Adv Funct Mater 2014;24:5261–8.

[2]   Du P, Liu X, Zheng Z, Wang X, Joncheray T, Zhang Y. Synthesis and characterization of linear self-healing polyurethane based on thermally reversible Diels–Alder reaction. RSC Adv 2013;3:15475–82.

[3]   Rekondo A, Martin R, Ruiz de Luzuriaga A, Cabañero G, Grande HJ, Odriozola I. Catalyst-free room-temperature self-healing elastomers based on aromatic disulfide metathesis. Mater Horizons 2014:237–40.

[4]   Sibbing D, Von Beckerath N, Morath T, Stegherr J, Mehilli J, Sarafoff N, et al. Oral anticoagulation with coumarin derivatives and antiplatelet effects of clopidogrel. Eur Heart J 2010;31:1205–11.

[5]   Bettero A, Benassi CA. Determination of coumarin and 6-methylcoumarin in cosmetics by high-performance liquid chromatography. J Pharm Biomed Anal 1983;1:229–33.

[6]   Winters BH. Photochemical products in coumarin laser dyes. Appl Phys Lett 1974;25:723.

[7]   Trenor SR, Shultz AR, Love BJ, Long TE. Coumarins in polymers: from light harvesting to photo-cross-linkable tissue scaffolds. Chem Rev 2004;104:3059–77.

[8]   Wang M, Kim J-C. Microgels of poly(hydroxyethyl acrylate-co-coumaryl acrylate-co-octadecyl acrylate): photo-responsive release. Colloid Polym Sci 2013;291:2319–27.

[9]   Ma Q, Xi H, Ma H, Meng X, Wang Z, Bai H, et al. Simultaneous Separation and Determination of 22 Coumarin Derivatives in Cosmetics by UPLC-MS/MS. Chromatographia 2015;78:241–9.

[10]   Lin H, Wan X, Li Z, Jiang X, Wang Q, Yin J. Photoreversible Resists for UV Nanoimprint Lithography (UV-NIL). ACS Appl Mater Interfaces 2010;2:2076–82.

[11]   Kaur G, Johnston P, Saito K. Photo-reversible dimerisation reactions and their applications in polymeric systems. Polym Chem 2014;5:2171.

[12]   Trenor SR, Long TE, Love BJ. Photoreversible Chain Extension of Poly(ethylene glycol). Macromol Chem Phys 2004;205:715–23.

[13]   López-Vilanova L, Martinez I, Corrales T, Catalina F. Photoreversible crosslinking of poly-(ethylene-butyl-acrylate) copolymers functionalized with coumarin chromophores using microwave methodology. React Funct Polym 2014;85:28–35.

[14]   Bang E-K, Lista M, Sforazzini G, Sakai N, Matile S. Poly(disulfide)s. Chem Sci 2012;3:1752.

[15]   Gyarmati B, Némethy Á, Szilágyi A. Reversible disulfide formation in polymer networks: A versatile functional group from synthesis to applications. Eur Polym J 2013;49:1268–86.

[16]   Caraballo R. Dynamic Sulfur Chemistry□: Screening , Evaluation and Catalysis. Royal Institute of Technology, Stockholm, 2010.

[17]   Li L, Song C, Jennings M, Thayumanavan S. Photoinduced heterodisulfide metathesis for reagent-free synthesis of polymer nanoparticles. Chem Commun 2015;51:1425–8.

[18]   Otsuka H, Nagano S, Kobashi Y, Maeda T, Takahara A. A dynamic covalent polymer driven by disulfide metathesis under photoirradiation. Chem Commun (Camb) 2010;46:1150–2.

[19]   AbdolahZadeh M, C. Esteves a. C, van der Zwaag S, Garcia SJ. Healable dual organic-inorganic crosslinked sol-gel based polymers: Crosslinking density and tetrasulfide content effect. J Polym Sci Part A Polym Chem 2014;52:1953–61.

[20]   Amamoto Y, Otsuka H, Takahara A, Matyjaszewski K. Self-healing of covalently cross-linked polymers by reshuffling thiuram disulfide moieties in air under visible light. Adv Mater 2012;24:3975–80.

[21]   Amamoto Y, Kamada J, Otsuka H, Takahara A, Matyjaszewski K. Repeatable photoinduced self-healing of covalently cross-linked polymers through reshuffling of trithiocarbonate units. Angew Chem Int Ed Engl 2011;50:1660–3.

[22]   Lei Z, Xiang H, Yuan Y. Room-Temperature Self-Healable and Remoldable Cross-linked Polymer Based on the Dynamic Exchange of Disulfide Bonds. Chem … 2014.

[23]   Martin R, Rekondo A, Ruiz de Luzuriaga A, Cabañero G, Grande HJ, Odriozola I. The processability of a poly(urea-urethane) elastomer reversibly crosslinked with aromatic disulfide bridges. J Mater Chem A 2014;2:5710.

[24]   Brunsveld L, Folmer BJ, Meijer EW, Sijbesma RP. Supramolecular polymers. Chem Rev 2001;101:4071–98.

[25]   Jeffrey GA, Saenger W. Hydrogen bonding in biological structures. Berlin: Springer Science & Business Media; 1994.

[26]   Beijer FH, Sijbesma RP, Kooijman H, Spek AL, Meijer EW. Strong dimerization of ureidopyrimidones via quadruple hydrogen bonding. J Am Chem Soc 1998;120:6761–9.

[27]   Söntjens SHM, Sijbesma RP, van Genderen MHP, Meijer EW. Stability and Lifetime of Quadruply Hydrogen Bonded 2-Ureido-4[1 H]-pyrimidinone Dimers. J Am Chem Soc 2000;122:7487–93.

[28]   de Espinosa LM, Fiore GL, Weder C, Johan Foster E, Simon YC. Healable supramolecular polymer solids. Prog Polym Sci 2015.

[29]   Chirila T V., Lee HH, Oddon M, Nieuwenhuizen MML, Blakey I, Nicholson TM. Hydrogen-bonded supramolecular polymers as self-healing hydrogels: Effect of a bulky adamantyl substituent in the ureido-pyrimidinone monomer. J Appl Polym Sci 2014;131:1–12.

[30]   Hentschel J, Kushner AM, Ziller J, Guan Z. Self-healing supramolecular block copolymers. Angew Chemie - Int Ed 2012;51:10561–5.

[31]   Nobuhiro Oya TI and NY. A crystalline supramolecular polymer with self-healing capability at room temperature. Polym J 2013;45:955–61.

[32]   Frisch K, Saunders J. Polyurethanes; Chemistry and Technology. New Jersey: Intersicience; 1962.

[33]   Chattopadhyay DK, Webster DC. Thermal stability and flame retardancy of polyurethanes. Prog Polym Sci 2009;34:1068–133.

[34]   Sardon H, Irusta L, Fernández-Berridi MJ. Synthesis of isophorone diisocyanate (IPDI) based waterborne polyurethanes: Comparison between zirconium and tin catalysts in the polymerization process. Prog Org Coatings 2009;66:291–5.

[35]   Asif A, Shi W, Shen X, Nie K. Physical and thermal properties of UV curable waterborne polyurethane dispersions incorporating hyperbranched aliphatic polyester of varying generation number. Polymer (Guildf) 2005;46:11066–78.

[36]   Chen R, Zhang C, Kessler MR. Anionic Waterborne Polyurethane Dispersion from Bio-based Ionic Segment. RSC Adv 2014;4:35476–83.

[37]   Hwang H-D, Park C-H, Moon J-I, Kim H-J, Masubuchi T. UV-curing behavior and physical properties of waterborne UV-curable polycarbonate-based polyurethane dispersion. Prog Org Coatings 2011;72:663–75.

[38]   Prabhakar a., Chattopadhyay DK, Jagadeesh B, Raju KVSN. Structural investigations of polypropylene glycol (PPG) and isophorone diisocyanate (IPDI)-based polyurethane prepolymer by 1D and 2D NMR spectroscopy. J Polym Sci Part A Polym Chem 2005;43:1196–209.

[39]   Jaudouin O, Robin J-J, Lopez-Cuesta J-M, Perrin D, Imbert C. Ionomer-based polyurethanes: a comparative study of properties and applications. Polym Int 2012;61:495–510.

[40]   Sardon H, Irusta L, Fernández-Berridi MJ, Luna J, Lansalot M, Bourgeat-Lami E. Waterborne Polyurethane Dispersions Obtained by the Acetone Process: A Study of Colloidal Features. J Appl Polym Sci 2011;120:2054–62.

[41]   Li B, Peng D, Zhao N, Mu Q, Li J. The physical properties of nonionic waterborne polyurethane with a polyether as side chain. J Appl Polym Sci 2012;127:1848–52.

[42]   Tsai H, Hong P, Yen M. Preparation and Physical Properties of Nonionic Aqueous Polyurethane Coatings Containing Different Side Chain PEGME lenght. J Appl Polym Sci 2008.

[43]   Szycher M. Szycher's Handbook of Polyurethanes, First Edition. 1999.

[44]   Ionescu M. Chemistry and Technology of Polyols for Polyurethanes. Shawbury, UK: iSmithers Rapra Publishing; 2005.

[45]   Sardon H, Pascual A, Mecerreyes D, Taton D, Cramail H, Hedrick JL. Synthesis of Polyurethanes Using Organocatalysis: A Perspective. Macromolecules 2015:150506135150009.

[46]   Delebecq E, Pascault JP, Boutevin B, Ganachaud F. On the versatility of urethane/urea bonds: Reversibility, blocked isocyanate, and non-isocyanate polyurethane. Chem Rev 2013;113:80–118.

[47]   Houghton RP, Mulvaney AW. Mechanism of tin(IV)-catalysed urethane formation. J Organomet Chem 1996;518:21–7.

[48]   Lipatova TE, Bakalo LA, Sirotinskaya AL, Lopatina VS. Mechanism of polyurethane formation with tin dibutyl-laurate. Polym Sci USSR 1970;12:1036–42.

[49]   Silva AL, Bordado JC. Recent Developments in Polyurethane Catalysis: Catalytic Mechanisms Review. Catal Rev 2004;46:31–51.

[50]   Chang M-C, Chen S-A. Kinetics and mechanism of urethane reactions: Phenyl isocyanate–alcohol systems. J Polym Sci Part A Polym Chem 1987;25:2543–59.

[51]   Baker JW, Holdsworth JB. The mechanism of aromatic side-chain reactions with special reference to the polar effects of substituents. Part XIII. Kinetic examination of the reaction of aryl isocyanates with methyl alcohol. J Chem Soc 1947:713–26.

[52]   Alsarraf J, Robert F, Cramail H, Landais Y. Latent catalysts based on guanidine templates for polyurethane synthesis. Polym Chem 2013;4:904.

[53]   De SK, Gibbs RA. An Efficient and Practical Procedure for the Synthesis of 4-Substituted Coumarins. Synthesis (Stuttg) 2005;8:1231–3.

[54]   Valizadeh H, Shockravi A. An efficient procedure for the synthesis of coumarin derivatives using TiCl4 as catalyst under solvent-free conditions. Tetrahedron Lett 2005;46:3501–3.

[55]   Ling J, Rong MZ, Zhang MQ. Coumarin imparts repeated photochemical remendability to polyurethane. J Mater Chem 2011;21:18373–80.

[56]   Jiang X, Wang R, Ren Y, Yin J. Responsive polymer nanoparticles formed by poly(ether amine) containing coumarin units and a poly(ethylene oxide) short chain. Langmuir 2009;25:9629–32.

[57]   Ling J, Rong MZ, Zhang MQ. Photo-stimulated self-healing polyurethane containing dihydroxyl coumarin derivatives. Polymer (Guildf) 2012;53:2691–8.

[58]   Potdar MK, Mohile SS, Salunkhe MM. Coumarin syntheses via Pechmann condensation in Lewis acidic chloroaluminate ionic liquid. Tetrahedron Lett 2001;42:9285–7.

[59]   Belenguer AM, Friščić T, Day GM, Sanders JKM. Solid-state dynamic combinatorial chemistry: reversibility and thermodynamic product selection in covalent mechanosynthesis 2011:696–700.

[60]   Sarma RJ, Otto S, Nitschke JR. Disulfides, imines, and metal coordination within a single system: Interplay between three dynamic equilibria. Chem - A Eur J 2007;13:9542–6.

[61]   Chattopadhyay DK, Raju KVSN. Structural engineering of polyurethane coatings for high performance applications. Prog Polym Sci 2007;32:352–418.

[62]   Brinker CJ, Scherer GW. Sol-Gel Science: the physics and chemistry of sol-gel processing. San Diego: Academic Press, Inc; 1990.

[63]   Sardon H, Irusta L, Aguirresarobe RH, Fernández-Berridi MJ. Polymer/silica nanohybrids by means of tetraethoxysilane sol-gel condensation onto waterborne polyurethane particles. Prog Org Coatings 2014;77:1436–42.

[64]   Rekondo a., Fernández-Berridi MJ, Irusta L. Synthesis of silanized polyether urethane hybrid systems. Study of the curing process through hydrogen bonding interactions. Eur Polym J 2006;42:2069–80.

[65]   Wei M, Zhan M, Yu D, Xie H, He M, Yang K, et al. Novel Poly(tetramethylene ether)glycol and Poly(ε-caprolactone) Based Dynamic Network via Quadruple Hydrogen Bonding with Triple-Shape Effect and Self-Healing Capacity. ACS Appl Mater Interfaces 2015;7:2585–96.

[66]   Aydin M, Uyar T, Tasdelen MA, Yagci Y. Polymer/clay nanocomposites through multiple hydrogen-bonding interactions. J Polym Sci Part A Polym Chem 2015;53:650–8.

[67]   Dankers PYW, Zhang Z, Wisse E, Grijpma DW, Sijbesma RP, Feijen J, et al. Oligo (trimethylene carbonate) -Based Supramolecular Biomaterials. Synthesis (Stuttg) 2006;39:8763–71.

[68]   Wong CH, Chow HF, Hui SK, Sze KH. Generation-independent dimerization behavior of quadruple hydrogen-bond-containing oligoether dendrons. Org Lett 2006;8:1811–4.

[69]   Keizer HM, Sijbesma RP, Meijer EW. The convenient synthesis of hydrogen-bonded ureidopyrimidinones. European J Org Chem 2004:2553–5.

[70]   Zhu B, Zhicheng F, Zheng Z, Xilnling W. Thermoreversible supramolecular polyurethanes with sel-complementary quadrypole hydrogen-bonded end groups. J Appl Polym Sci 2012;123:1755–63.

[71]   Feldman KE, Kade MJ, Meijer EW, Hawker CJ, Kramer EJ. Model transient networks from strongly hydrogen-bonded polymers. Macromolecules 2009;42:9072–81.

[72]   Feldman KE, Kade MJ, De Greef TF a, Meijer EW, Kramer EJ, Hawker CJ. Polymers with multiple hydrogen-bonded end groups and their blends. Macromolecules 2008;41:4694–700.

[73]   Meijer EW. Mechanically Induced Gelation of a Kinetically Trapped Supramolecular Polymer. Macromolecules 2014;47:8429–36.

[74]   Grzyb J a., Shen M, Yoshina-Ishii C, Chi W, Brown RS, Batey R a. Carbamoylimidazolium and thiocarbamoylimidazolium salts: Novel reagents for the synthesis of ureas, thioureas, carbamates, thiocarbamates and amides. Tetrahedron 2005;61:7153–75.

[75]   Montalbetti C a GN, Falque V. Amide bond formation and peptide coupling. Tetrahedron 2005;61:10827–52.

[76]   Aguirresarobe RH, Irusta L, Fernández-Berridi MJ. UV-light responsive waterborne polyurethane based on coumarin: synthesis and kinetics of reversible chain extension. J Polym Res 2014;21:505.

[77]   Sardon H, Irusta L, Fernández-Berridi MJ, Lansalot M, Bourgeat-Lami E. Synthesis of room temperature self-curable waterborne hybrid polyurethanes functionalized with (3-aminopropyl)triethoxysilane (APTES). Polymer (Guildf) 2010;51:5051–7.

[78]   Seth SK, Sarkar D, Jana AD, Kar T. On the Possibility of Tuning Molecular Edges To Direct Supramolecular Self-Assembly in Coumarin Derivatives through Cooperative Weak Forces: Crystallographic and Hirshfeld Surface Analyses. Cryst Growth Des 2011;11:4837–49.

[79]   Wang L, Shen Y, Lai X, Li Z, Liu M. Synthesis and properties of crosslinked waterborne polyurethane. J Polym Res 2010;18:469–76.

CHAPTER **3**

Light-Responsive Characteristics of Coumarin Based Waterborne Polyurethanes

3.1 Chapter Overview

This chapter focuses on the characterization of the photochemical reactions of coumarin based waterborne polyurethanes as well as the changes in the physical properties derived from these reactions. Given that the non-autonomic healing properties that these materials can present depend on their ability to interact with UV-light, a specific analysis of their light-responsive properties was conducted.

Thus, the structural changes produced as a consequence of the exposure at UV different wavelengths were determined using a variety of spectroscopic techniques (UV spectroscopy, FTIR, ^{1}H-NMR).

In addition, the evolution of the physical properties, such as material viscosity and gel content, as a function of the irradiation conditions was analyzed. As these variations depend on the coumarin disposition in the polymer backbone, different analyses were performed specifically for each system.

Finally, taking into account the healing requirements, the influence of different parameters in the reaction kinetics and reversibility of the process was investigated. Additionally, the light-responsive behavior that these systems can present under sunlight was reported.

3.2 Introduction

Light has been increasingly utilized in polymer chemistry as an energy source as reactions can be conducted at room temperature, often in solid-state, and do not leave residues [1–4]. Hence, light represents a green alternative for many industrial applications such as coating curing processes, lithography, biomedical applications and so forth [5–7].

In the case of stimuli-responsive materials, light has been used to provoke significant physicochemical responses incorporating photoreactive components to their structure [2,8]. Thus, by selecting the appropriate components, it is possible to synthesize optically healable materials that present the ability to

temporarily increase or reduce the chain mobility "on demand". Upon irradiation, these materials are able to refill damages and to form new linkages in the crack surfaces afterwards.

In addition, optically healable materials present several advantages over other non-autonomic healable ones. Owing to the intrinsic features of light, the stimulus can be applied locally from long distances, which permits the healing mechanism to be activated remotely. This characteristic potentially opens up the possibility of healing the material under load, selecting specific areas of the sample, while the undamaged areas remain intact. Furthermore, it is possible not only to stimulate specific components of the material structure, tailoring the wavelength of the used light, but also to halt and resume the healing process by turning the excitation light off or on.

Despite presenting several benefits to other healing alternatives, light-responsive materials also present some drawbacks. The main problem is that the light has to reach the damaged area in order to interact with the healing elements. This restricts its use to superficial damage, thin films or coatings and transparent materials.

3.2.1 Photo-reversible dimerization reactions

Optically healable materials incorporate photoreactive components in the material structure. The nature of these components determines the photochemical reactions and the healing mechanism [9–11]. Among different alternatives, photo-reversible dimerization reactions are particularly attractive as they are considered an appropriate method to modulate the crosslink density or molecular weight of photoreactive polymers [3,12,13]. Compared to other monomers, coumarin derivatives undergo these types of reactions leading to photoproducts under weak conditions [12,14].

The irradiation of coumarin derivatives with a 365 nm light provokes a $[2\pi+2\pi]$ cycloaddition reaction, which generates a cyclobutane ring between two coumarin molecules. In contrast, when irradiated at 254 nm, these coumarin dimers undergo a photocleavage reaction that leads to the original structures.

Taking advantage of the characteristics of coumarin, as explained in chapter 2, two different light-responsive waterborne polyurethanes based on the addition of coumarin monomers were synthesized. These polymers differ in the location of the coumarin monomer in the polymer chains and as a result, in their response to the applied stimulus.

In the first case, the coumarin monomers were located at both chain-ends of a linear waterborne polyurethane structure (Figure 3.1 a). The application of a 365 nm UV light provokes the dimerization of the coumarin moieties, increasing the molecular weight of the polymer (Figure 3.1 b). In contrast, this process reverses when the material is irradiated at 254 nm.

a   PPGHEMC polymer structure
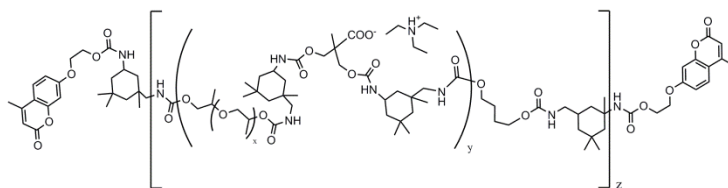
b   PPGHEMC light responsive behavior
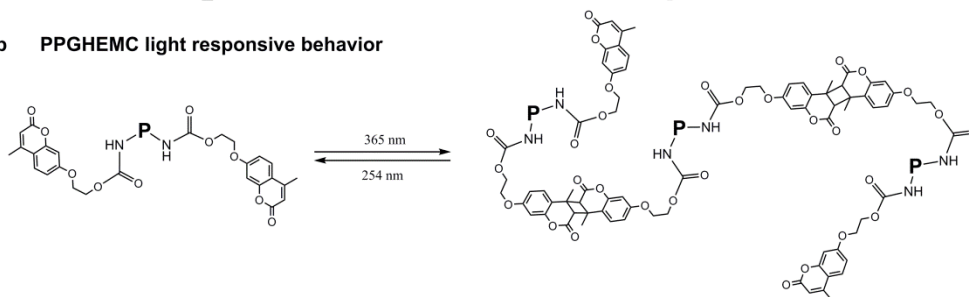
Figure 3.1 *Synthesized coumarin end-capped waterborne polyurethane structure (a) and its light-responsive behavior (b).*

In the case of the synthesized waterborne polyurethanes containing coumarin monomers in the middle of the polymer backbone (Figure 3.2 a), the interaction of coumarin monomers under different irradiation conditions leads to the material crosslinking or decrosslinking (Figure 3.2 b).

a PPGDHEMC polymer structure

b PPGDHEMC light responsive behavior
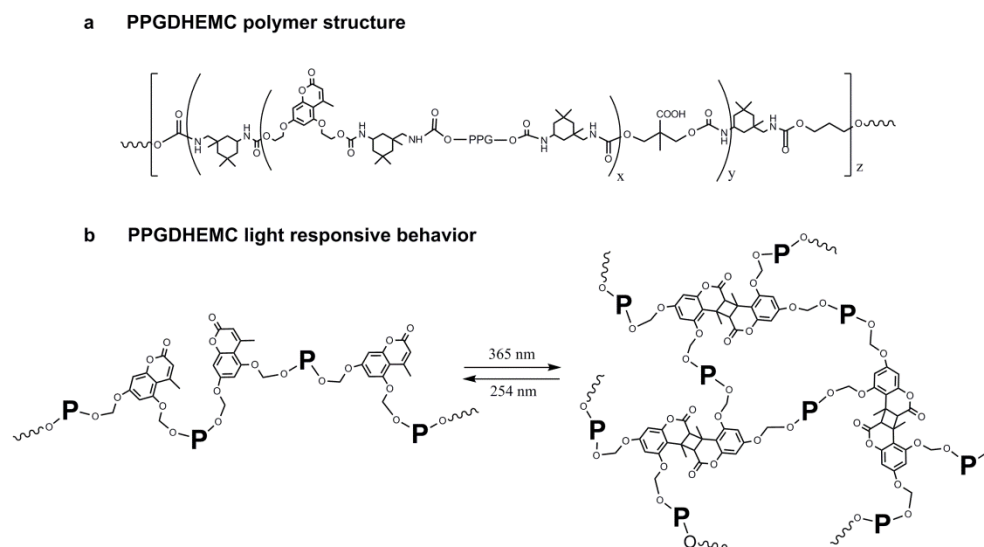
Figure 3.2 *Synthesized coumarin chain extended waterborne polyurethane structure (a) and its light-responsive behavior (b).*

3.3 Irradiation conditions and sample preparation

Apart from the nature of the photoreactive monomer and polymer structure, the response of the material strongly depends on experimental parameters. Among them the sample irradiation conditions and its preparation play an important role in the response of optically healable materials.

Thus, the response of coumarin based materials depends not only on the irradiation wavelength, which determines the photoinduced process, but also on the light intensity that reaches the material surface. Therefore, the control of both parameters should be precise as they determine the magnitude of the occurring physicochemical processes.

With reference to the light intensity, it depends both on the energy of the source and the distance from the sample to it, as shown by the inverse-square law in equation (1) [15,16].

$$\text{Intensity} \propto \frac{1}{dis\tan ce^{\,2}} \quad \textbf{(1)}$$

Hence, in order to control the irradiation conditions of all the experiments, an irradiation box was designed specifically for this work (Figure 3.3) equipped with a Vilber-Lourmat VL-6LC light source capable of irradiating at 365 nm and 254 nm. The light intensity in each wavelength was measured with a radiometer (Sglux UV Touch radiometer with UV-A and UV-C sensors) and controlled by adjusting the distance to the light source.
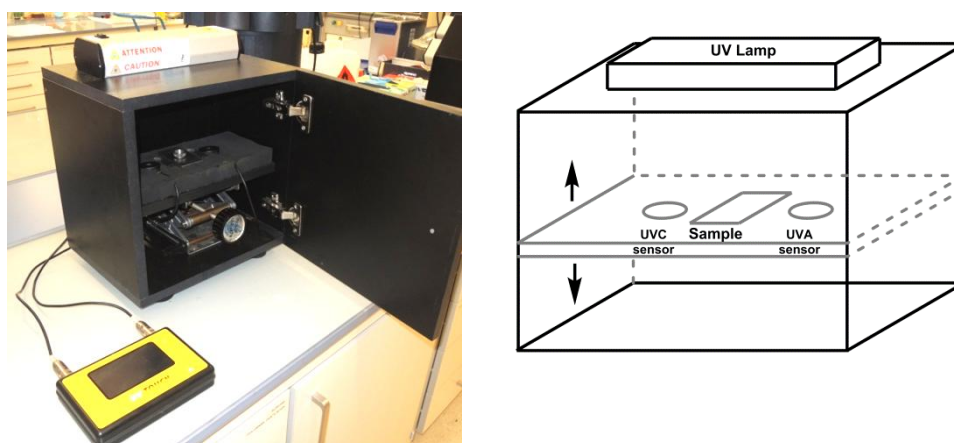
Figure 3.3 *Designed irradiation box.*

For this work, the irradiation intensity at 365 nm was maintained at 0.8 mW/ cm^2 whereas the intensity at 254 nm was kept at 0.16 mW/cm^2. These conditions were comparatively lower than those reported in literature (Table A.1 in Appendix).

Another important aspect that affects the response of these materials is the sample preparation. The reversible cycloaddition reaction occurs preferably in solid state as the sample orientation and geometry favor the photoinduced reactions [12]. Furthermore, the sample thickness is another factor that must be taken into account. Whereas the light easily interacts with the coumarin groups

located on the material surface, the photochemical reactions are hindered in the material bulk. Therefore, as the sample thickness increases, so does the irradiation time necessary to obtain significant responses in the whole sample. Accordingly, for an accurate analysis of the cycloaddition reaction, the measurements must be carried out in solid state, preferably in thin films.

Owing to the difficulties to obtain thin films directly from the water dispersions, the formulations were dried and redisolved in acetone. Depending on the analysis type, the films were obtained by casting or spin coating.

3.4 Spectroscopic characterization of coumarin dimerization reaction

As a consequence of UV irradiation, coumarin monomers undergo a series of photochemical processes that alter their molecular structure. Taking advantage of the changes in the spectroscopic features of the samples, the evolution of the photochemical reactions can successfully be analyzed by means of different techniques. In addition, although these techniques are not equally sensitive in the detection of the occurred transformations, their combination provides additional information and allows us to corroborate the obtained results.

3.4.1   Ultraviolet spectroscopy

Among different spectroscopic techniques, UV spectroscopy is specially powerful in monitoring the evolution of the cycloaddition reaction as it significantly alteres the UV spectra of coumarin containing samples.

Coumarin moieties present two different absorption bands in the UV region. The first one, centered at 320 nm, corresponds to pyrone n-π^* transition. The second one, corresponding to the π-π^* transition, appears at higher energies (between 240 and 310 nm) [17,18]. The band centered at 320 nm is particularly sensitive to structural changes occurring in the coumarin monomer. Hence it has been extensively used to analyze the photochemical processes of coumarin based systems [14,19–24].

In order to follow the photochemical reaction, films were prepared by casting on the outside wall of a quartz cell and their UV spectra were recorded at different irradiation times. Figure 3.4 shows the obtained spectra for the PPG10HEMC sample.
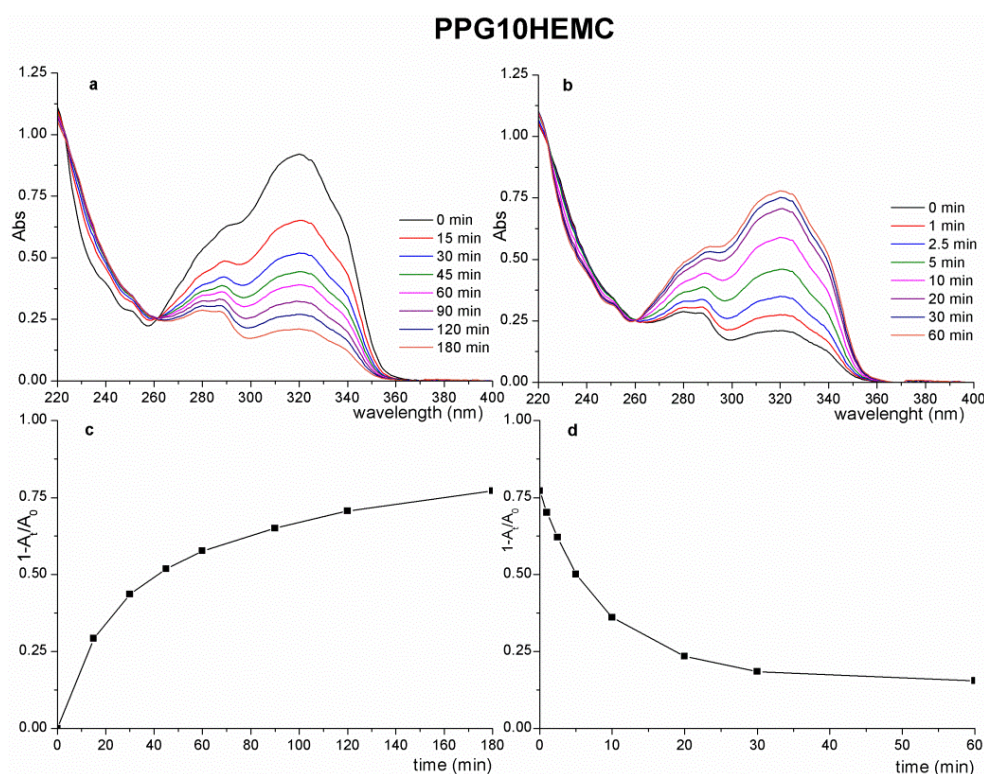
Figure 3.4 *UV-Vis spectra as a function of the irradiation time at 365 nm (a) and 254 nm (b). Conversion degree as a function of time at 365 nm (c) and 254 nm (d) for PPG10HEMC.*

As observed in Figure 3.4 a, the absorbance of the band centered at 320 nm decreases with the exposure time at 365 nm. This reduction in the absorbance is directly related to the dimerization process as the conjugation disappears when the cyclobutane structure is formed between two coumarin molecules. After being irradiated for 180 min at 365 nm, the samples were exposed at 254 nm, Figure 3.4 b. The absorbance of the band increases and tends to recover the

original intensity, indicating that photocleavage of the cyclobutane rings took place.

Given that the cycloaddition reaction extent is directly proportional to the decrease of the 320 nm absorption band, the dimerization degree can be estimated from equation (2) [25–27]:

$$p = 1 - \frac{A_t}{A_0}$$ (2)

Where p is the dimerization degree, A_t corresponds to the absorbance at 320 nm at time t and A_0 the original absorbance at 320 nm before irradiation at 365 nm.

According to this estimation, the dimerization of coumarin groups reached a conversion of 77% (Figure 3.4 c) when the sample was irradiated at 365 nm for 3 hours. However, when the sample was exposed to 254 nm, the coumarin moieties recovered the original structure and the absorbance increased accordingly (Figure 3.4 d). This photocleavage reaction occured more rapidly than the cycloaddition one, especially if we take into account that the radiation intensity at 254 nm was lower than that at 365 nm [25,28,29].

However, even after 60 min of exposure at 254 nm, the complete recovery of the original absorption was not reached. This effect is generally attributed to the dynamic equilibrium between the photodimerization and photocleavage processes occurring simultaneously at 254 nm [30].

PPGDHEMC samples were analyzed using the same method and Figure 3.5 shows the obtained UV spectra and the dimerization degree under different irradiation conditions for PPG10DHEMC.
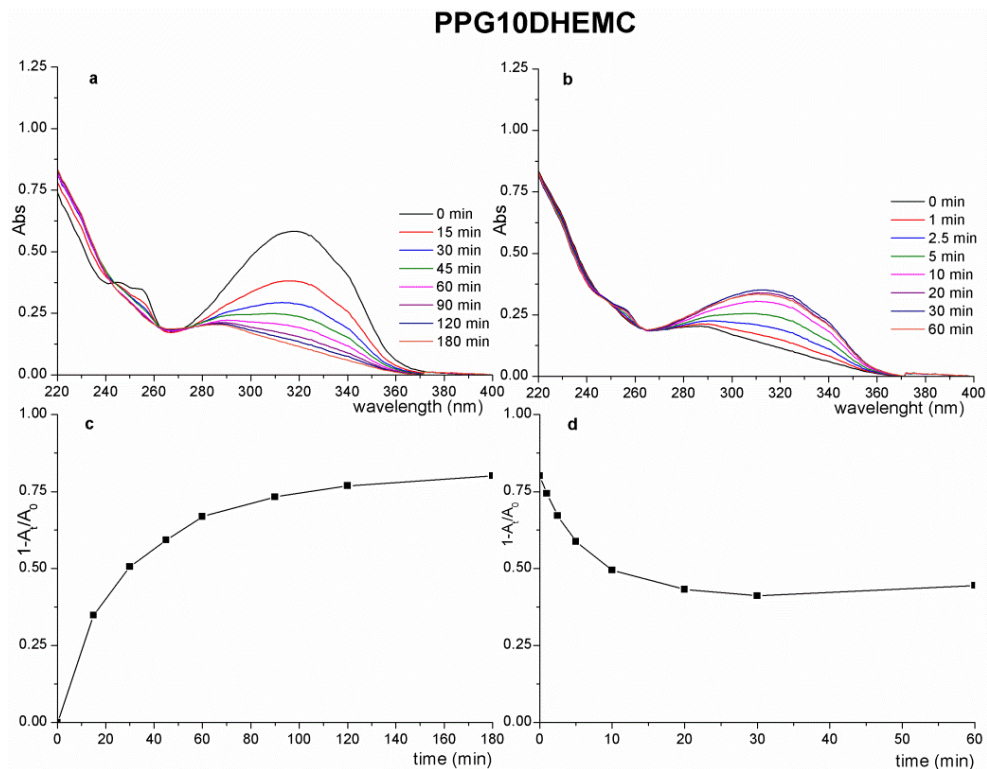
Figure 3.5 *UV-Vis spectra as a function of the irradiation time at 365 nm (a) and 254 nm (b). Conversion degree as a function of time at 365 nm (c) and 254 nm (d) for PPG10DHEMC.*

The photochemical behavior of PPGDHEMC samples was similar to that of PPGHEMC. During the irradiation at 365 nm, the band centered at 320 nm decreased as a consequence of the cycloaddition reaction and the calculated conversion reached 80 %.

However, slight differences could be perceived during the photocleavage reaction, Figure 3.5 b and d. At irradiation times below 30 minutes, an increase in the absorbance of the band at 320 nm occurred, indicating the photocleavage process progressed. Conversely, the absorbance of this band decreased slightly during the last 30 minutes.

95

Apart from the dynamic equilibrium in PPGHEMC samples, this could be related to assymetric bond scissions of the cyclobutane ring produced during the photocleavage process [30,31]. Consequently, reasonable irradiation times at 254 nm are necessary in order to obtain photoreversible properties and remendability as prolonged irradiation times at 254 nm could give rise to irreversible crosslinked structures [26].

3.4.2 Infrared spectroscopy

The cyclobutane ring formation and rupture occurring during the photochemical reactions altere the vibration frequencies not only of the functional groups involved in the reaction but also of those present in the coumarin structure. Accordingly, the photochemical processes can also be monitored using FTIR spectroscopy.

This analysis was carried out in thin films obtained by spin coating on the surface of KBr pellets and irradiated at different times. Figure 3.6 shows the FTIR spectra as a function of the irradiation time for both PPG10HEMC and PPG10DHEMC samples.
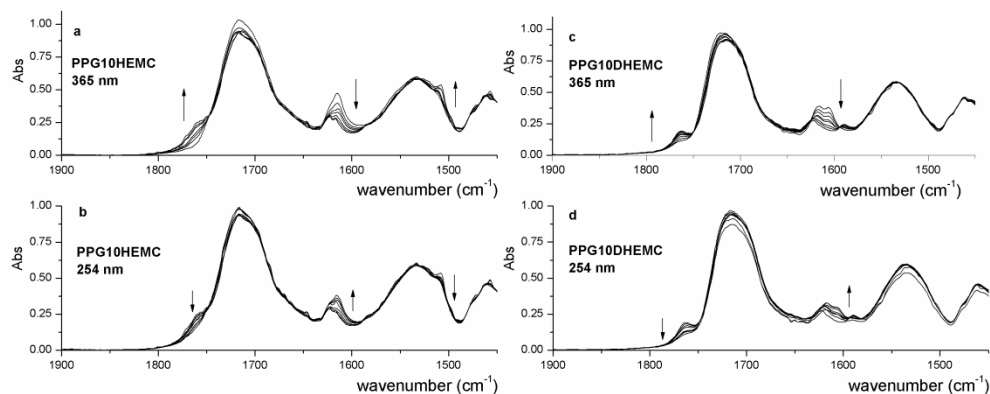
Figure 3.6 *Evolution of FTIR spectra for PPG10HEMC (a and b) and PPG10DHEMC (c and d) samples during the photochemical process.*

When the samples were exposed to irradiation at 365 nm, Figure 3.6 a and c, the intensity of the band due to the C=C stretching vibration (1635 cm^{-1}) decreased,

and a small shoulder in the carbonyl region at about 1760 cm^{-1} appeared. These spectral changes can be attributed to the disappearance of coumarin double bond and the absorption of the newly formed non-conjugated carbonyl group respectively [32–35]. In addition, a small band at 1500 cm^{-1} can also be observed in the case of PPG10HEMC, which can be assigned to the stretching vibration of the aromatic ring.

During the photocleavage reaction, Figure 3.6 b and d, when the samples were illuminated with a 254 nm light, the initial main spectral characteristics were recovered [36,37]. However, this recovery was not complete, in a similar way to what was observed in the UV spectra.

3.4.3 1H-NMR spectroscopy

The characterization of the the photoinduced [2+2] cycloaddition by ^{1}H-NMR in solution presents several difficulties over other spectroscopic techniques. On the one hand, the use of this technique is limited to soluble samples. Therefore, this analysis was performed for PPGHEMC samples as they are linear structures in all of the stages of the photochemical process. Conversely, PPGDHEMC samples crosslinked after the irradiation at 365 nm, which impeded their characterization by this technique. On the other hand, the ^{1}H-NMR assignment of the lines corresponding to thre resulting photoproducts was difficult due to their complexity. For this reason, the analysis was restricted to the regions where the lines corresponding to the coumarin moeties appeared. Even so, this technique is specially useful to detect possible side reactions or byproducts in the photochemical process.

The experiment was performed subjecting thin films to different irradiation conditions and the ^{1}H-NMR spectra were obtained from the solution of these films in CDCl$_3$. Figure 3.7 shows the evolution of the ^{1}H-NMR spectra at different irradiation times for 365 nm as well as the line assignment for PPG10HEMC sample.
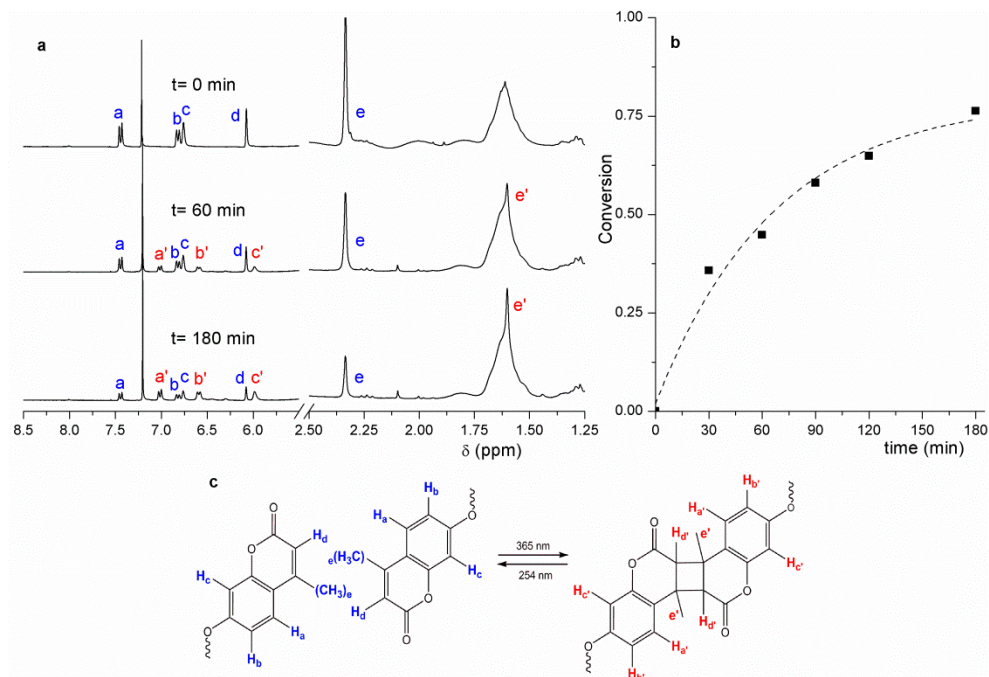
Figure 3.7 *¹H-NMR evolution at different irradiation times at 365nm (a), the calculated conversion (b) and structural assignment for PPG10HEMC sample.*

As can be seen in Figure 3.7 a, the intensity of the signals corresponding to coumarin protons (a, b, c, d and e) decreased as the cycloaddition reaction took place, and new signals assignable to coumarin dimer structure (a', b', c' and e') appeared. These new lines were at lower chemical shifts than those of coumarin, as a consequence of the new chemical environment generated after the cleavage of the coumarin double bond [38–41].

These spectral changes allowed us to perform a quantitative analysis of the photoinduced [2+2] cycloaddition reaction. Thus, the olefinic proton signal at 6.1 ppm in the NMR spectra was used to calculate the reaction conversion, according to equation (3).

$$p = 1 - \frac{X_t}{X_0} \qquad (3)$$

Where p is the dimerization degree, X_t is the ratio between the signal at 6.1 ppm and the signal at 4.8 ppm at time t, whereas X_0 corresponds to the value of this ratio before irradiation.

As can be observed in Figure 3.7 b, 76 % conversion was reached in 3 hours, in good agreement with UV spectroscopic results. However, the conversion at intermediate times obtained by this technique was lower than that calculated using equation (2).

The photocleavage process was also characterized by ^{1}H-NMR, and Figure 3.8 shows the spectra and the calculated conversion for each irradiation time.
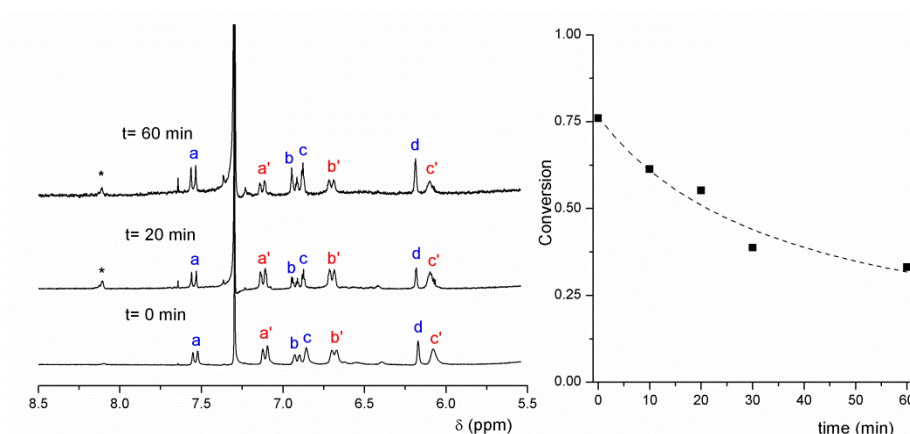
Figure 3.8 *^{1}H-NMR evolution at different irradiation times at 254 nm (a) and the calculated conversion (b) for PPG10HEMC sample.*

As a consequence of the irradiation at 254 nm, the signals corresponding to the coumarin dimer decreased in intensity while the lines of the coumarin monomer increased.

Similarly to the cycloaddition reaction, the dimerization degree was calculated, using equation (3). The conversion reached a 33 % value when the samples where irradiated during 60 min. Although the conversion value is higher than the one calculated using equation (2), the behavior of the sample was similar to that observed in the UV analysis.

Apart from these lines, a small peak at 8.1 ppm appeared. Although it was not possible to assign this line to an specific structure, it could be related to the presence of byproducts produced in asymmetric bond scissions [31].

3.5 Physical response characterization

Regardless their disposition in the polymer backbone, coumarin moieties undergo reversible [2+2] photoinduced cycloaddition reaction as confirmed in section 3.4. However, this disposition determines the polymer morphology after the photochemical reaction occurs and, consequently, the response of the material. Accordingly, the evaluation of the physical properties of both systems has to take into consideration the polymer morphology and the foreseen response.

3.5.1 PPGHEMC systems

In the case of coumarin end-capped polyurethanes, the cycloaddition reaction of the coumarin moieties joins linear polymer chains together, which gives rise to an increment of the polymer chain length. In contrast, the photocleavage process of the already formed coumarin dimers reverses this situation, separating previously attached chains.

Regarding the physical properties, the material viscosity is clearly affected by these changes in the polymer chain length. In fact, the rheological behavior has been studied in multiple light-responsive systems owing to their potential applications [42–46].

The rheological characterization of PPGHEMC samples was studied by means of oscillatory measurements using parallel-plates geometry. PPG10HEMC sample was used as a model and its viscosity as a function of different irradiation conditions was measured. Thus, both the viscosity changes produced by the cycloaddition reaction and the photocleavage reaction can be seen in Figure 3.9.
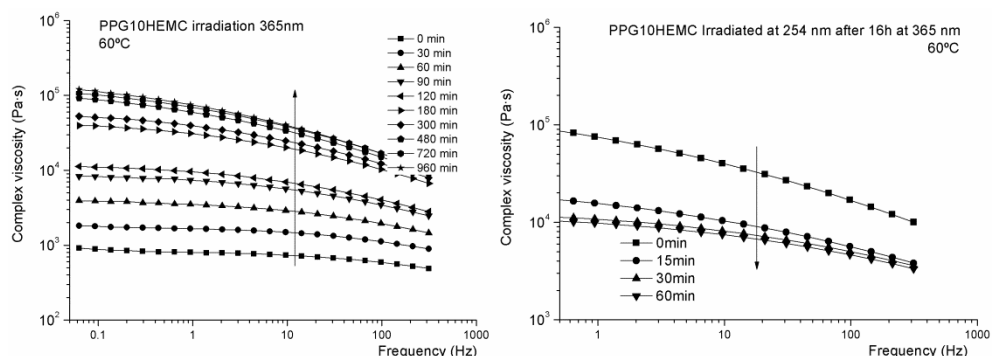
Figure 3.9 *Complex viscosity as a function of frequency for samples irradiated at 365 nm (left) and 254 nm (right).*

The photoinduced [2+2] cycloaddition reaction provoked an increment in the viscosity of the system about two orders of magnitude after 16h of irradiation. It is to note that the irradiation time necessary to obtain significant viscosity changes was higher than that measured in spectroscopic analysis. This behavior can be explained by two different effects. On the one hand, the chain extension reaction can be considered a step polymerization reaction, where coumarin end-capped polymer chains act as macromonomers. Hence, high conversion values are needed to obtain high molecular weights and therefore high viscosities [47–50]. On the other hand, given that the necessary mass to perform these experiments is high, the irradiated film thickness was higher compared to those used in spectroscopic measurements, which implies larger times in order for light to penetrate in the sample.

However, when the samples are irradiated at 254 nm, the effect reversed and tended to recover the original values. This behavior clearly indicated that the photocleavage of coumarin monomer leaded to polymer chain scissions.

In order to obtain a more accurate overview of the rheological response of the material to the irradiation, the viscosity values at one specific frequency (1 Hz) were represented as a function of the irradiation time for both irradiation conditions (Figure 3.10).
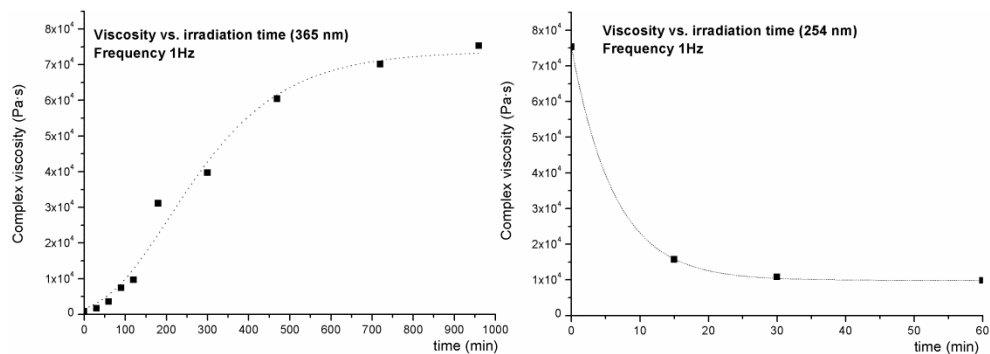
Figure 3.10 *The evolution of the complex viscosity at 1 Hz as a function of the irradiation time for 365 nm and 254 nm.*

These representations clearly depict the effect of the irradiation conditions on the material viscosity. On the one hand, the cycloaddition reaction at 365 nm gave rise to a strong increase in the material viscosity. This increase presented a sigmoid dependence with the irradiation time and it reached a plateau at about 7.5×10^4 Pa·s [47].

In contrast, the viscosity decayed when the sample was irradiated at 254 nm. Owing to the coumarin dimers did not completely reverse during the photocleavage process, the viscosity value remained about one order of magnitude higher than the viscosity of the non-irradiated material.

The molecular weight changes occurred in coumarin end-capped WPUs were also characterized by Size Exclusion Chromatography (SEC). By means of this technique, it is possible to obtain the molecular weight distribution of polymeric samples. Furthermore, it allowed us to calculate different molecular weight averages, the number and weight average molecular weight (M_n and M_w) referred to polystyrene standards, as well as the polydispersity index of the distribution obtained as the ratio of the previous values. Hence, it seems to be a powerful tool in the physical characterization of the photochemical process.

Thus, in order to obtain the molecular weight distribution of PPGHEMC samples, thin films were casted in Petri dishes from a 0.1 wt% polymer solution. After

being irradiated at different times, these films were dissolved in anhydrous THF. Table 3.1 summarizes the calculated values for different irradiation conditions for PPG10HEMC sample.

Table 3.1 *Evolution of the molecular weight and polydispersity as a function of the irradiation time for PPG10HEMC sample.*

	Irradiation time (h)	M_n	M_w	Polydispersity
		10^3 (g/mol)		
365 nm	0	4646	5710	1.21
	1	4702	5910	1.26
	3	4919	6660	1.35
	5	4853	6800	1.40
	16	5111	7369	1.44
254 nm	0.25	4953	7043	1.42
	0.5	4770	7077	1.48
	1	4695	6370	1.36

The obtained molecular weight values for non irradiated samples are in good agreement with the theoretical value calculated taking into account the end-capping degree of the polymer ($M_{n\ theoretical}$= 4414 g mol^{-1}). As the irradiation time 365 nm increased, the molecular weight of the sample increased. This effect was more noticeable in M_w values, and therefore, the polydispersity of the samples increased. As occurred for rheological measurements, high irradiation times were needed in order to obtain significant molecular weight changes. In contrast, when the samples were exposed to 254 nm light, the molecular weight of the sample decreased, indicating that the photocleavage process provokes the excision of the polymer chains.

In spite of presenting the expected behavior, PPG10HEMC samples presented low molecular weights, before and after the irradiation. It is to note that the cycloaddition reaction provokes chemical changes in the polymer structure. Therefore, not only the hydrodynamic volume of the polymers but also the interactions between the polymer and the column can be altered.

3.5.2 PPGDHEMC systems

The physical characterization of coumarin chain extended samples, PPGDHEMC samples, presents several difficulties owing to their intrinsic photoinduced response. The cycloaddition reaction gives rise to crosslinked structures, which limits the amount of analytical techniques that can be used in the determination of the response.

In this sense, the determination of the crosslinked fraction of the sample is especially important due to these samples crosslinked and decrosslinked in response of the irradiation conditions. The evolution of this parameter as a function of different irradiation conditions reflects the abilities of these systems to form tridimensional networks and it could determine the further healing abilities of these materials.

Thus, this fraction was estimated by measuring the gel content [51–54]. For this purpose, samples were extracted in a soxhlet extractor using THF as a solvent and the gel content was calculated as the ratio between the mass of the insoluble part of the sample and its total mass before starting the extraction. Figure 3.11 shows the evolution of the gel content of the samples during the cycloaddition reaction and the photocleavage.
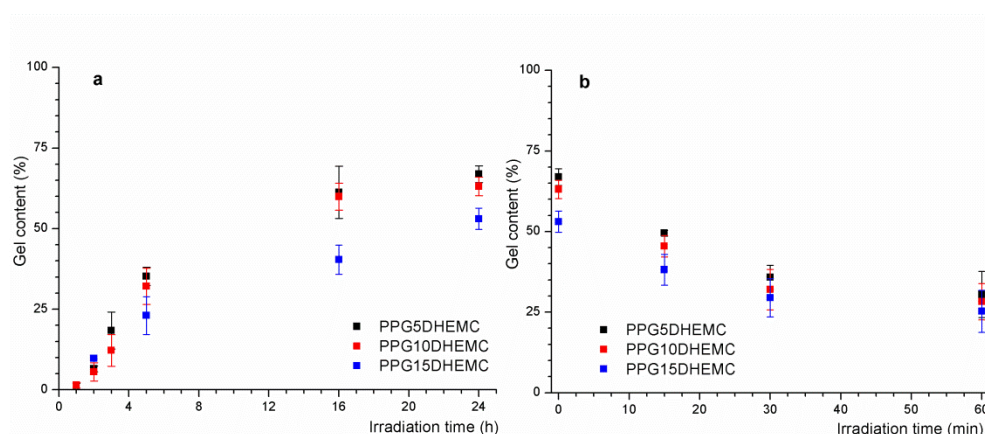
Figure 3.11 *Evolution of the gel content of PPGDHEMC samples during the irradiation at 365 nm (a) and 254 nm (b).*

As the irradiation time at 365 nm increased, Figure 3.11 a, the cycloaddition reaction of the coumarin moieties took place and the gel content of the samples increased accordingly. Similarly to the rheological behavior of PPGHEMC samples, large times were necessary to obtain significant gel content values. Furthermore, the gel content presented a sigmoid dependence with the irradiation time.

After being subjected to 365 nm light for 24 hours, these films were exposed to 254 nm light and the evolution of the gel content was measured, Figure 3.11 b. The insoluble part of the material decreased until reaching a plateau when the irradiation time increased, confirming the reversibility of the material response.

The coumarin monomer concentration affected the magnitude of the response, especially for the cycloaddition process. Although this effect was not significant in the first stages, the insoluble fraction decreased as the coumarin concentration in the samples increased. However, the photocleavage process presented less dependence to the coumarin concentration. In spite of starting at different crosslinking values, all the formulations reached similar gel contents after the irradiation at 254 nm.

In contrast to the rest of samples, PPG1DHEMC sample was totally soluble and did not present insoluble fraction, even at times as high as 24 hours of irradiation. It seems that the amount of coumarin in the formulation (1 wt%) was not enough to form a tridimensional network.

3.6 [2+2] Cycloaddition reaction characteristics

The incorporation of coumarin monomers provided light-responsive characteristics to waterborne polyurethanes through reversible photoinduced [2+2] cycloaddition reactions. As explained, these reactions were detected both from their spectral features and physical properties. However, among the healing requirements, factors such as the reversibility of the process or the reaction kinetics, can limit their application as optically healable materials.

For this reason, taking advantage of the conversion vs. time plots obtained by UV spectroscopy, the influence of different parameters on these characteristics was

analyzed. Additionally, the ageing process occurring outdoors and the light-responsive properties of these systems under the irradiation of Sunlight were investigated.

3.6.1 Reversibility and efficiency of the process

One of the most important characteristics of intrinsic healable materials is that they can present repeated healing events. In the case of non-autonomic healing materials, these healing events occur as a consequence of reversible interactions triggered by external stimuli. Hence, the ability of the active monomers to recover their original structure is a fundamental factor to achieve a successful healable material as it determines the efficiency of the process. For coumarin based systems, the reversibility is based on the [2+2] cycloaddition reaction occurring at 365 nm, which reverses when the samples are irradiated at 254 nm.

Thus, in order to verify the photoreversibility of the process, samples were subjected to alternate irradiations with light at 365 and 254 nm. This experiment was performed for both PPGHEMC and PPGDHEMC samples and Figure 3.12 shows the obtained results.
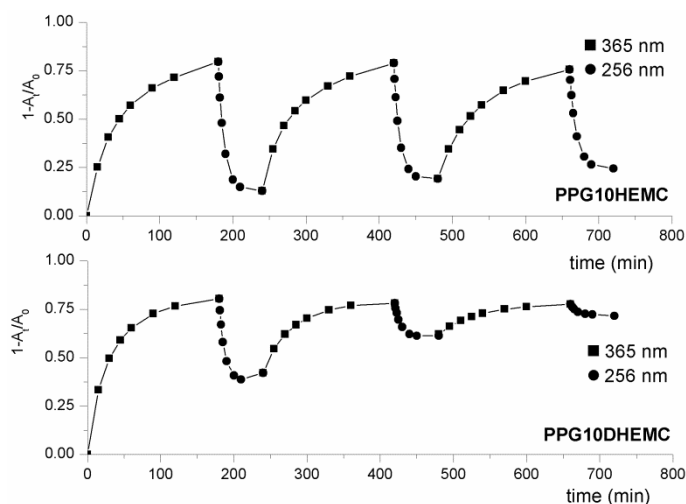
Figure 3.12 *Cycloaddition and photocleavage reaction conversion for different 365/254 nm irradiation cycles for PPPG10HEMC and PPG10DHEMC samples.*

According to Figure 3.12, the reversivility of the photochemical process seems to depend not only on the irradiation conditions but also on the sample morphology. Thus, during the irradiation at 365 nm, the maximum value reached for both types of systems decreased albeit insignificantly. In constrast, the photocleavage reactions occurring upon 254 nm light exposure had more influence. As the number of irradiation cycles increased the recovery of the process was reduced.

However, the coumarin monomer disposition seems to have a stronger impact on the photoreversiblity of the process. Thus, for PPG10HEMC, the efficiency could be estimated around 75 % whereas in the case of PPGDHEMC, only 30% of the coumarin dimers reverse to their original structure after three irradiation cyles. Undoubtedly, this behavior limits the efficiency of these systems as light-responsive and optically healable materials.

The loss of efficiency has been extensivebly reported on in relation to light-responsive systems based on coumarin [17,25,30,35,52]. As explained, this effect has been attributed to the photochemical equilibrium occurring at 254 nm and asymmetric photocleavage reactions [27,31,35,55].

3.6.2   [2+2] Cycloaddition reaction kinetics

In general terms, a successful healing process requires high concentrations of healing agents as it magnifies the response of the material to the external stimuli. In addition, the role of the response kinetics is also relevant, as it permits accurate control of the process as well as determining its time efficiency.

Thus, the effect of different parameters on the cycloaddition reaction rate, such as the coumarin based polymer, the monomer concentration and the irradiation cycle, was investigated. Figure 3.13 shows the dimerization degree, calculated by UV spectroscopy, as a function of time for different concentrations of coumarin monomers for the first irradiation cycle both for PPGHEMC and PPGDHEMC samples.
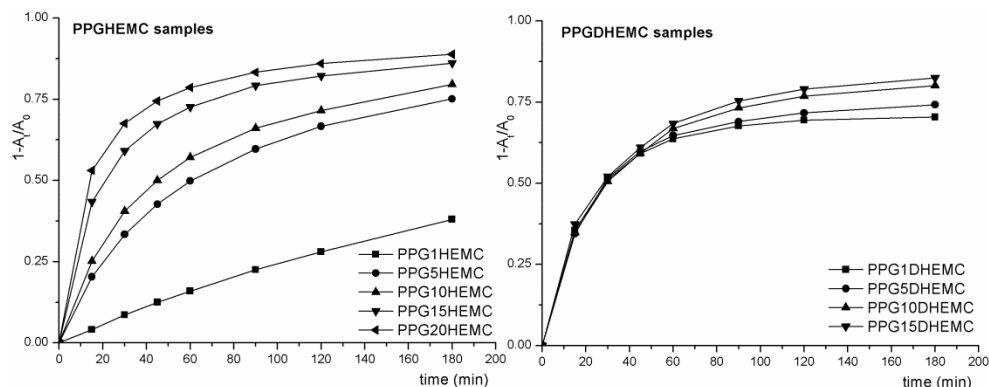
Figure 3.13 *First cycle kinetics plots at different amounts of coumarin for PPGHEMC and PPGDHEMC samples.*

As can be seen in Figure 3.13, PPGHEMC and PPGDHEMC show contrasting behavior. In the case of PPGHEMC samples, the reaction rate increased as the coumarin amount attached to the main chain increased. This effect was more important between 1 and 5 wt% of coumarin containing samples. However, in PPGDHEMC samples, the cycloaddition rate was independent of the coumarin monomer concentration up to 45 minutes. Afterwards, the reaction rate increased as the coumarin concentration increased. In addition, PPGDHEMC samples presented higher conversion values than the corresponding samples of the PPGHEMC system.

This different behavior could be directly related to the phase separated morphology of coumarin based polyurethanes. As a consequence of the interactions of the hard segments, these systems tend to form separated microdomains, especially when the number and strength of the interactions is high.

For coumarin based polyurethanes, Hydrogen bonds of urethane groups and the π−π interactions of coumarin moieties are responsible for the formation of these domains, as represented in Figure 3.14 [56,57]. Although these interactions are present in both systems, PPGDHEMC samples have a higher amount of urethane groups, which favors their phase separation.
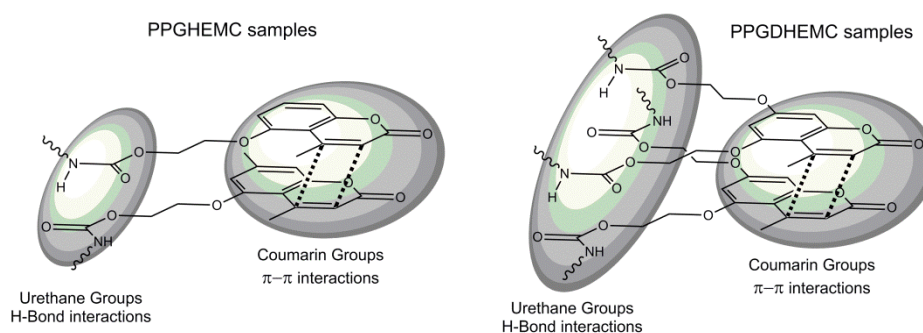
Figure 3.14 *Hydrogen bonds of urethane groups and $\pi-\pi$ interactions of coumarin moieties for different coumarin containing systems.*

In order to corroborate this theory, the polymer morphology was characterized by Atomic Force Microscopy (AFM) in tapping mode. AFM is considered a suitable technique to analyze the phase separated morphology of segmented polyurethanes [58–60].

Apart from analyzing the sample topography, AFM measurements allow us to indentify stiffness variations on the local surface by means of the phase imaging. Phase imaging relies on vibration changes in the tip as a consequence of interactions between it and the surface. Accordingly, the higher the modulus of the material is the higher the phase offset and the lighter it appears in contrast to a softer phase.

Figure 3.15 shows the phase images of different coumarin containing samples before being exposed to 365 nm UV light.
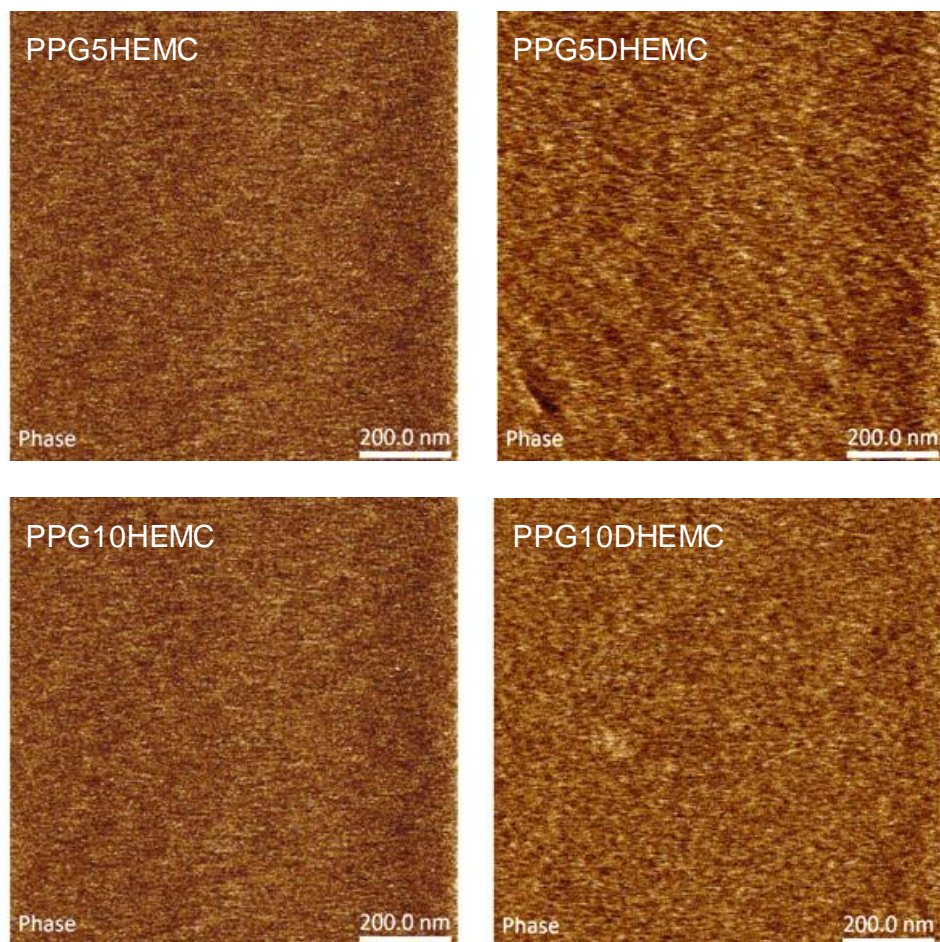
Figure 3.15 *AFM phase images for PPG5HEMC (top left), PPG10HEMC (bottom left), PPG5DHEMC (top right) and PPG10DHEMC (bottom right) samples.*

As can be seen, PPGHEMC samples present a more homogeneous morphology, which indicates a less phase separation. In contrast, the phase images of PPGDHEMC samples show brighter and darker regions, which can be respectively attributed to harder and softer domains.

In our opinion, the photochemical process for PPGDHEMC samples occurs preferably in these domains, as the coumarin mobility is reduced [12,14]. If we assume that the coumarin concentration in these domains is similar in all cases,

the coumarin amount in the sample would not affect the cycloaddition reaction rate in the first stages of the reaction.

Additionally the dimerization of the coumarin outside these domains would take place, and its effect would be more significant as the overall concentration in the samples increases.

In contrast, in PPGHEMC samples, the reaction seems to occur homogeneously in the polymer matrix, indicating a less phase separated morphology. This behavior would respond to the fact that the number and strength of their interactions is lower in comparison to those of PPGDHEMC (Figure 3.14).

In order to better understand the influence of the coumarin concentration, a quantitative analysis of the reaction kinetics was performed. Thus, the cycloaddition reaction kinetics was adjusted to n^{th}-order model [61–63]. According to this model, the conversion rate is proportional to the concentration of unreacted coumarin monomer according to the following equation (4).

$$\frac{dp}{dt} = k(1 - p)^n \qquad \textbf{(4)}$$

Where n parameter is related to the reaction order and k is the value of the rate constant. Regarding the n value, the conversion vs. time data were adjusted to first, second and third order kinetics and the fitting plots are shown in the Appendix.

Coumarin end-capped polyurethanes showed a pseudo-second order kinetics and the data fitted equation (5) appropriately [17,64].

$$\frac{1}{(1 - p)} = kt + C \qquad \textbf{(5)}$$

The 1/(1-p) vs. time plots represented in Figure 3.16 show linear fitting for all PPGHEMC formulations in the first 90 minutes of irradiation at 365 nm.
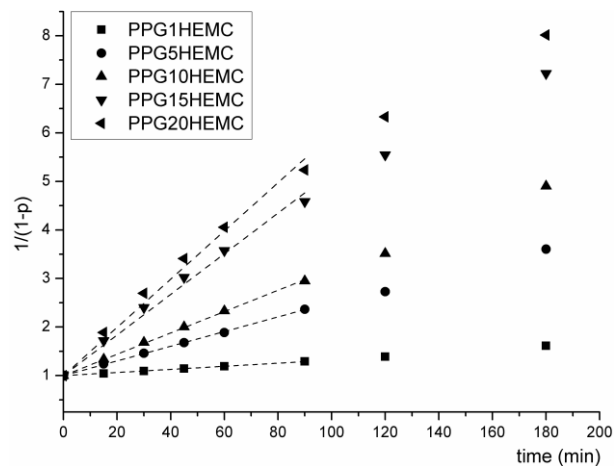
Figure 3.16 *Second order modeling and fitting curves for different amounts of coumarin for the first irradiation cycle kinetics for PPGHEMC samples.*

This fitting for the cycloaddition reaction data implies a bimolecular process between the coumarin monomers. A second order process involves the approach and interaction of two coumarin monomers to produce the cycloaddition reaction [65].

According to a second order kinetics, the rate constant for each sample was calculated from the slope of the fitting curves for three different cycles, and Table 3.2 summarizes these results.

Table 3.2 *Rate constant of cycloaddition reaction at 365 nm for different amounts of coumarin and number of irradiation cycles for PPGHEMC samples.*

Rate constant (second order) (10^{-3} min^{-1})

Sample	First cycle	Second cycle	Third cycle
PPG1HEMC	3.45 ± 0.7	3.55 ± 0.1	3.25 ± 0.1
PPG5HEMC	15.6 ± 1.7	11.7 ± 0.9	9.45 ± 0.6
PPG10HEMC	21.1 ± 0.5	15.9 ± 0.9	12.5 ± 0.6
PPG15HEMC	34.5 ± 0.3	23.9 ± 0.3	20.3 ± 0.6
PPG20HEMC	41.3 ± 3.5	26.1 ± 0.6	21.3 ± 0.3

As can be seen both in Figure 3.16 and Table 3.2, the rate constant increased as the amount of coumarin in the polymer increased. Furthermore, the reaction kinetics were also affected by the irradiation cycle. The reaction rate decreased when the number of cycles increased. This effect is directly related to the efficiency loss in the recovery process.

It is important to mention that the rate constant for sample PPG1HEMC remained constant for the first two cycles and slightly decreased in the third one. In our opinion, the low dimerization degree and the low rate constant that this system presents could be related to the difference between the theoretical molecular weight of this sample compared with those of the rest of the systems.

In contrast to PPGHEMC systems, coumarin chain extended polyurethanes did not appropriatelly fit any simple kinetic laws. However, whether we asume a phase separated morphology for PPGDHEMC samples, it is possible to estimate a rate constant for the process. Thus, the conversion data of PPGDHEMC samples are represented using equation (5) and Figure 3.17 shows the obtained plot.
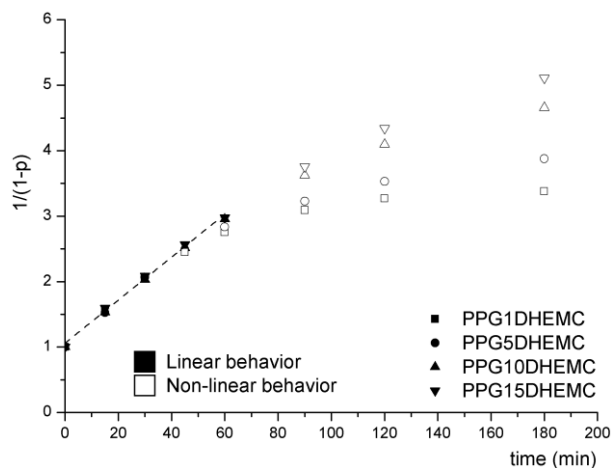
Figure 3.17 *Second order modeling and fitting curves for different amounts of coumarin for the first irradiation cycle kinetics for PPGDHEMC samples.*

This plot clearly depicted two different kind of behavior, one in the first stages of the reaction and another one at longer irradiation times. In addition, the data

appropriately fitted a pseudo second order kinetics during the first stages of the reaction, with similar rate values, regardless of coumarin concentration. However, as represented, the linearity deviation took place at longer reaction times when increasing the coumarin concentration. This effect can be attributed to the different amount and/or size of the hard domains in PPGDHEMC systems.

It was assumed that the molecular mobility of coumarin moieties in the hard domains is similar in all systems, and consequently, the data were fitted in the linear region of each system and the rate constant was calculated. The rate constants for different coumarin concentrations and irradiation cycles are shown in Table 3.3.

Table 3.3 *Initial rate constants for PPGDHEMC samples as a function of the amount of coumarin and number of irradiation cycles.*

Rate constant (second order) (10^{-3} min^{-1})			
Sample	**First cycle**	**Second cycle**	**Third cycle**
PPG1DHEMC	32.4 ± 0.2	23.1 ± 0.7	11.1 ± 1.7
PPG5DHEMC	33.8 ± 0.3	27.4 ± 3.5	16.2 ± 3.9
PPG10DHEMC	33.2 ± 1.1	30.1 ± 0.5	18.4 ± 0.2
PPG15DHEMC	35.3 ± 1.0	31.5 ± 0.8	17.5 ± 1.4

The obtained values for the initial rate constant did not significantly change for different formulations, indicating that the molecular mobility in the hard domains is almost constant in all the samples. However, the rate constant values, decreased with the number of irradiation cycles.

If we compare the contant values to those corresponding to PPGHEMC samples, the rate constant presented higher values, in good agreement with the proposed phase separated behavior. The relative coumarin concentration in the coumarin domains is higher compared to the corresponding PPGHEMC sample and therefore, the rate constant is also higher. However, as the total coumarin concentration is similar for both types of systems, the final rate constant is comparatively lower.

3.6.3   Evolution under Sunlight

The Earth is continuously being irradiated by the light coming from the Sun. This light supplies energy to multiple photochemical and biological processes. Although the most energetic wavelengths do not reach the Earth's surface due to oxygen photolysis and ozone formation in the atmosphere, a large number of processes occur by direct irradiation under sunlight [66–68]. Coumarin and its derivatives are well known to be able to evolve under the sunlight [69–71]. Owing to its irradiation characteristics, the cycloaddition reaction of the coumarin monomers is favored. On the contrary, the photocleavage process of the coumarin dimers is strongly hindered.

It is important to take into consideration that the sunlight irradiation conditions are highly dependent on the season and weather conditions, as can be seen in the Appendix. The irradiation intensity reached values up to 0.6 mW/cm^2 in March while it surpassed 3 mW/cm^2 in July. Consequently, the photoinduced cycloaddition reaction kinetics of coumarin will depend accordingly.
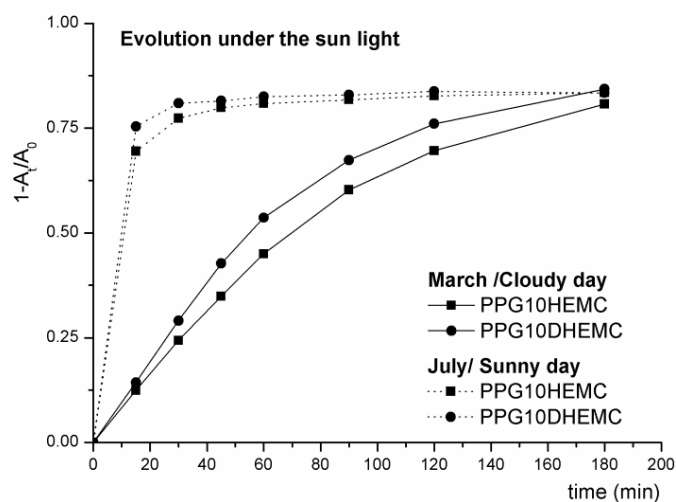
Figure 3.18 *Cycloaddition reaction kinetics plots for two different weather conditions and coumarin systems, PPG10HEMC and PPG10DHEMC.*

In order to better understand this process, PPG10HEMC and PPG10DHEMC samples were directly exposed to sunlight in two different weather conditions and seasons, a cloudy day in March and a sunny day in July. The evolution of the cycloaddition reaction was followed by UV spectroscopy and Figure 3.18 shows the reaction kinetics plots for both systems and irradiation conditions.

Regardless of the polymeric system, the dimerization process presents similar behavior. The cycloaddition reaction in March occurred slowly and 3 hours were necessary to obtain a conversion of approaching 80 per cent. In contrast, the maximum photochemical process progressed more rapidly in July and the reaction conversion was reached in the first 30 minutes. This fact is directly related to the UV-A light intensity measured in both experiments (shown in the Appendix) as this intensity is more than three times higher in July than in March. Surprisingly, no extra conversion was obtained in comparison to the experiments performed in March.

When both systems, PPGHEMC and PPGDHEMC, are compared, slight differences can be observed in their reaction kinetics. For both weather conditions, PPG10DHEMC sample presented slightly higher conversion values than the PPG10HEMC sample. This difference was more remarkable in the March experiment, probably because the reaction kinetics was slower.

This behavior offers the opportunity of synthesizing optically healable materials that can be autonomically healed under sunlight. However, as previously explained, it is necessary to irradiate the samples at 254 nm to provoke the dimer photocleavage, which leads to an increased chain mobility and promotes the surface rearrangement after damage.

3.7 Conclusions

This chapter analyzed the photochemical response involving different coumarin based waterborne polyurethanes. Thus, samples were irradiated using a UV light source emitting at different wavelengths (365 and 254 nm) and the response of

the material was characterized by means of different analytical techniques. According to the obtained results we can extract the following conclusions:

- The irradiation of the coumarin based polyurethanes at 365 nm gives rise to the cycloaddition reaction of the coumarin moieties, reaching high conversion values. However, during the photocleavage process, the reaction conversion does not reach the original values after one hour of irradiation. Additionally, longer irradiation times do not increase, but even decrease, the photocleavage conversion. Therefore, reasonable irradiation times at 254 nm are necessary in order to obtain photoreversible properties.

- The reversible cycloaddition reaction of coumarin monomers directly affects the physical properties of the polyurethanes. Thus, the irradiation of PPGHEMC samples at 365 nm increases their molecular weight and consequently, their viscosity, whereas PPGDHEMC samples crosslink. In both cases, large coumarin amounts are necessary to obtain significant responses. However, neither PPGHEMC nor PPGDHEMC samples recover the physical properties of non irradiated samples after being exposed to a 254 nm light.

- The reversible reaction loses efficiency as the number of 365/254 nm irradiation cycles increases. This effect is more significant for the case of PPGDHEMC samples.

- The reaction rate presents contrasting behavior for different systems. While the reaction rate increases with the coumarin concentration for PPGHEMC samples, it is independent of the coumarin amount in PPGDHEMC ones. These differences are attributed to the phase separated morphology these samples present. However, the reaction rate decreases as the number of 365/254 nm irradiation cycles increases.

- The reaction rate fits a pseudo-second order kinetics law for PPGHEMC samples. In contrast, PPGDHEMC samples do not fit any simple kinetics

law appropriately. However, if we assume a phase separated morphology, a pseudo-second order rate constant can be calculated in both domains.

- Coumarin containing systems are able to undergo the cycloaddition reaction under the irradiation of sunlight. However, the weather conditions influence the reaction rate of the process. While the reaction takes place in three hours on a cloudy spring day, the reaction reaches its maximum conversion in 30 minutes in the summer.

3.8 References

[1]   Chatani S, Kloxin CJ, Bowman CN. The power of light in polymer science: photochemical processes to manipulate polymer formation, structure, and properties. Polym Chem 2014;5:2187.

[2]   Habault D, Zhang H, Zhao Y. Light-triggered self-healing and shape-memory polymers. Chem Soc Rev 2013;42:7244–56.

[3]   Kaur G, Johnston P, Saito K. Photo-reversible dimerisation reactions and their applications in polymeric systems. Polym Chem 2014;5:2171.

[4]   Anastas P, Warner J. Green Chemistry: Theory and practice. London: Oxford University Press; 1998.

[5]   Schwalm R. UV Coatings: Basics, Recent Developments and New Applications. Elsevier Science; 2006.

[6]   Pimpin A, Srituravanich W. Reviews on micro- and nanolithography techniques and their applications. Eng J 2012;16:37–55.

[7]   Ferreira P, Coelho JFJ, Almeida JF, Gil MH. Photocrosslinkable Polymers for Biomedical Applications. In: Fazel-Rezai R, editor. Biomed. Eng. - Front. Challenges, InTech; 2009, p. 55–74.

[8]   Urban MW. Handbook of Stimuli-Responsive Materials. Weinheim, Germany: Wiley-VCH Verlag GmbH & Co. KGaA; 2011.

[9]   Fiore GL, Rowan SJ, Weder C. Optically healable polymers. Chem Soc Rev 2013;42:7278–88.

[10]   Burnworth M, Tang L, Kumpfer JR, Duncan AJ, Beyer FL, Fiore GL, et al. Optically healable supramolecular polymers. Nature 2011;472:334–7.

[11]   Fenoli CR, Bowman CN. Synthesis of novel trithiocarbonate and allyl sulfide containing monomers. Polym Chem 2014;5:62.

[12]   Bassani DM. The dimerization of cinnamic acid derivatives. In: Horspool, William; Lenci F, editor. CRC Handb. Org. Photochem. Photobiol. (2nd Ed., CRC Press LLC Boca Raton, Fla; 2004, p. 20/1–20/20.

[13]   Yang Y, Urban MW. Self-healing polymeric materials. Chem Soc Rev 2013;42:7446.

[14]   Trenor SR, Shultz AR, Love BJ, Long TE. Coumarins in polymers: from light harvesting to photo-cross-linkable tissue scaffolds. Chem Rev 2004;104:3059–77.

[15]   Al-Azzawi A. Light and Optics: Principles and Practices. Boca Raton, FL: CRC Press LLC Boca Raton, Fla; 2006.

[16]   Ryer. AD. Light measurement handbook. Newburyport: International Light Inc.; 1998.

[17]   Kehrloesser D, Baumann R-P, Kim H-C, Hampp N. Photochemistry of coumarin-functionalized SiO2 nanoparticles. Langmuir 2011;27:4149–55.

[18]   Moore TA, Harter ML, Song P-S. Ultraviolet spectra of coumarins and psoralens. J Mol Spectrosc 1971;40:144–57.

[19]   Mohamed MG, Hsu K-C, Kuo S-W. Bifunctional polybenzoxazine nanocomposites containing photo-crosslinkable coumarin units and pyrene units capable of dispersing single-walled carbon nanotubes. Polym Chem 2015;6:2423–33.

[20]   Lin H, Wan X, Li Z, Jiang X, Wang Q, Yin J. Photoreversible Resists for UV Nanoimprint Lithography (UV-NIL). ACS Appl Mater Interfaces 2010;2:2076–82.

[21]   Jin Q, Liu X, Liu G, Ji J. Fabrication of core or shell reversibly photo cross-linked micelles and nanogels from double responsive water-soluble block copolymers. Polymer (Guildf) 2010;51:1311–9.

[22]   Nasu S, Tsuchiya A, Kuroda K. Preparation of lamellar inorganic–organic hybrids from tetraethoxysilane and a coumarin derivative containing a triethoxysilyl group and photodimerization of the interlayer coumarin groups. J Mater Chem 2010;20:6688–95.

[23]   Maddipatla MVSN, Wehrung D, Tang C, Fan W, Oyewumi MO, Miyoshi T, et al. Photoresponsive Coumarin Polyesters That Exhibit Cross-Linking and Chain Scission Properties. Macromolecules 2013;46:5133–40.

[24]   Biyani M V., Weder C, Foster EJ. Photoswitchable nanocomposites made from coumarin-functionalized cellulose nanocrystals. Polym Chem 2014;5:5501–8.

[25]   Fu Q, Cheng L, Zhang Y, Shi W. Preparation and reversible photo-crosslinking/photo-cleavage behavior of 4-methylcoumarin functionalized hyperbranched polyester. Polymer (Guildf) 2008;49:4981–8.

[26]   Ling J, Rong MZ, Zhang MQ. Coumarin imparts repeated photochemical remendability to polyurethane. J Mater Chem 2011;21:18373–80.

[27]   Ling J, Rong MZ, Zhang MQ. Photo-stimulated self-healing polyurethane containing dihydroxyl coumarin derivatives. Polymer (Guildf) 2012;53:2691–8.

[28]   Saigo K, Shiwaku T, Hayashi K, Fujioka K, Sukegawa M, Chen Y, et al. Optically active polyamides consisting of anti head-to-head coumarin dimer and α,ι-alkanediamine. Odd-even discrimination in chiral recognition ability depending on the number of the diamine component and correlation between the ability and crystallizabil. Macromolecules 1990;23:2830–6.

[29]   Saigo K, Nakamura M, Suzuki Y, Fang L, Hasegawa M. Synthesis and properties of polyamides having anti head-to-head umbelliferone dimer as a component. Macromolecules 1990;23:3722–9.

[30]   Chen YUN, Jean C. Polyethers Containing Coumarin Dimer Components in the Main Chain. II. Reversible Photocleavage and Photopolymerization. J Appl Polym Sci 1997;64:1759–68.

[31]   Yonezawa N, Yoshida T, Hasegawa M. Symmetric and Asymmetric Photocleavage of the Cyclobutane Rings in Head-to-head Coumarin Dimers and Their Lactone-opened Derivatives. J Chem Soc Perkin Trans 1 1983;1:1083–6.

[32]   Obi M, Morino S, Ichimura K. Factors affecting photoalignment of liquid crystals induced by polymethacrylates with coumarin side chains. Chem Mater 1999;11:656–64.

[33]   Li W, Lynch V, Thompson H, Fox M. Self-assembled monolayers of 7-(10-thiodecoxy) coumarin on gold: Synthesis, characterization, and photodimerization. J Am Chem Soc 1997;7863:7211–7.

[34]   Jackson PO, O'Neill M, Duffy WL, Hindmarsh P, Kelly SM, Owen GJ. An Investigation of the Role of Cross-Linking and Photodegradation of Side-Chain Coumarin Polymers in the Photoalignment of Liquid Crystals. Chem Mater 2001;13:694–703.

[35]   Trenor SR, Long TE, Love BJ. Photoreversible Chain Extension of Poly(ethylene glycol). Macromol Chem Phys 2004;205:715–23.

[36]   Guo Z, Jiao T, Liu M. Effect of substituent position in coumarin derivatives on the interfacial assembly: Reversible photodimerization and supramolecular chirality. Langmuir 2007;23:1824–9.

[37]   Li W, Lynch V, Thompson H, Fox MA. Self-assembled monolayers of 7-(10-thiodecoxy)coumarin on gold: Synthesis, characterization, and photodimerization. J Am Chem Soc 1997;119:7211–7.

[38]   Chen YUN. Synthesis and Reversible Photocleavage of Novel Polyurethane Containing Coumarin Dimer Components. J Polym Sci Part A Polym Chem 1997;35:613–24.

[39]   Zhao L, Vaupel M, Loy D a., Shea KJ. Photoresponsive Hybrid Materials: Synthesis and Characterization of Coumarin-Dimer-Bridged Polysilsesquioxanes. Chem Mater 2008;20:1870–6.

[40]   Kiskan B, Yagci Y. Thermally curable benzoxazine monomer with a photodimerizable coumarin group. J Polym Sci Part A Polym Chem 2007;45:1670–6.

[41]   Yu X, Scheller D, Rademacher O, Wolff T. Selectivity in the photodimerization of 6-alkylcoumarins. J Org Chem 2003;68:7386–99.

[42]   Paulusse JMJ, Sijbesma RP. Molecule-based rheology switching. Angew Chemie - Int Ed 2006;45:2334–7.

[43]   Ketner AM, Kumar R, Davies TS, Elder PW, Raghavan SR. A simple class of photorheological fluids: Surfactant solutions with viscosity tunable by light. J Am Chem Soc 2007;129:1553–9.

[44]   Lee HY, Diehn KK, Sun K, Chen T, Raghavan SR. Reversible photorheological fluids based on spiropyran-doped reverse micelles. J Am Chem Soc 2011;133:8461–3.

[45]   Avó J, Cidade MT, Rodriguez V, Lima JC, Parola a. J. Photorheological Ionic Liquids. J Phys Chem B 2015:150521110722000.

[46]   Draper E, McDonald TO, Adams DJ. Photodimerisation of a Coumarin-Dipeptide Gelator. Chem Commun 2015;51:12827–30.

[47]   Chen Y, Hong R. Photopolymerization of 7,7'-coumarinyl Polymethylene Dicarboxylates: Fluorescence and Kinetic Study. J Polym Sci Part A Polym Chem 1997;35:2999–3008.

[48]   Flory PJ. Fundamental Principles of Condensation Polymerization. Chem Rev 1946;39:137–97.

[49]   Odian G. Principles of Polymerization. 4th ed. Hoboken, New Jersey: John Wiley & Sons; 2004.

[50]   Brandt J, Oehlenschlaeger KK, Schmidt FG, Barner-Kowollik C, Lederer A. State-of-the-Art Analytical Methods for Assessing Dynamic Bonding Soft Matter Materials. Adv Mater 2014;26:5758–85.

[51]   Huyck RH, Trenor SR, Love BJ, Long TE. Photodimerization of Coumarin Functionalized Poly(alkyl Acrylate) and Poly(alkyl Methacrylate) Random Copolymers: Influence of Copolymer Composition on Photocrosslinking. J Macromol Sci Part A 2007;45:9–15.

[52]   Nagata M, Yamamoto YU. Synthesis and Characterization of Photocrosslinked Poly (e -caprolactone) s Showing Shape-Memory Properties. J Polym Sci Part A Polym Chem 2009;47:2422–33.

[53]   Nagata M, Inaki K. Synthesis and characterization of photocrosslinkable poly(l-lactide)s with a pendent cinnamate group. Eur Polym J 2009;45:1111–7.

[54]   Nagata M, Yamamoto Y. Photocurable Shape-Memory Copolymers of ε-Caprolactone and L-Lactide. Macromol Chem Phys 2010;211:1826–35.

[55]   Chen Y, Geh J-L. Copolymers derived from 7-acryloyloxy-4-methylcoumarin and acrylates: 2. Reversible photocrosslinking and photocleavage. Polymer (Guildf) 1996;37:4481–6.

[56]   He Y, Xie D, Zhang X. The structure, microphase-separated morphology, and property of polyurethanes and polyureas. J Mater Sci 2014;49:7339–52.

[57]   Seth SK, Sarkar D, Jana AD, Kar T. On the Possibility of Tuning Molecular Edges To Direct Supramolecular Self-Assembly in Coumarin Derivatives through Cooperative Weak Forces: Crystallographic and Hirshfeld Surface Analyses. Cryst Growth Des 2011;11:4837–49.

[58]   Frommer J. Scanning Tunneling Microscopy and Atomic Force Microscopy in Organic Chemistry. Angew Chemie Int Ed English 1992;31:1298–328.

[59]   McLean RS, Sauer BB. Tapping-mode AFM studies using phase detection for resolution of nanophases in segmented polyurethanes and other block copolymers. Macromolecules 1997;30:8314–7.

[60]   Lan Q, Haugstad G. Characterization of polymer morphology in polyurethane foams using atomic force microscopy. J Appl Polym Sci 2011;121:2644–51.

[61]   Khawam A, Flanagan DR. Solid-state kinetic models: Basics and mathematical fundamentals. J Phys Chem B 2006;110:17315–28.

[62]   House JE. Principles of Chemical Kinetics. 2nd ed. London: Academic Press; 2007.

[63]   Aguirresarobe RH, Irusta L, Fernández-Berridi MJ. UV-light responsive waterborne polyurethane based on coumarin: synthesis and kinetics of reversible chain extension. J Polym Res 2014;21:505.

[64]   Tong U, Chen W, Ritchie C, Wang X, Song Y-F. Reversible light-driven polymerization of polyoxometalate tethered with coumarin molecules. Chemistry 2014;20:1500–4.

[65]   Moore JW, Pearson RG. Kinetics and Mechanism. 3rd ed. Hoboken, New Jersey: John Wiley & Sons; 1981.

[66]   Boule P. Environmental Photochemistry. In: Hutzinger O, editor. Handb. Environ. Chem., BerlinHeidelberg: Springer-Verlag; 1999, p. 367.

[67]   Matsumi Y, Kawasaki M. Photolysis of Atmospheric Ozone in the Ultraviolet Region. Chem Rev 2003;103:4767–81.

[68]   Caldwell MM, Flint SD. Stratosferic Ozone Reduction, Solar UV-B Radiation and Terrestrial Ecosystems. Clim Change 1994;28:375–94.

[69]   Mustafa A. Dimerization Reactions in Sunlight. Chem Rev 1952;51:1–23.

[70]   Mustafa A, Kamel M, Allam M ali. Dimerization Reactions in Sunlight. V: Photodimerization of Substituted Coumarins. J Org Chem 1957;22:888–91.

[71]   Kiliç H. Sunlight-exposure photodimerization behavior of some 7,8-ethylenedioxycoumarins: Experimental and theoretical evidence of photodimerization. J Mol Liq 2014;200:238–45.

CHAPTER 4

Characterization of Autonomic Healable Waterborne Polyurethanes

4.1 Chapter Overview

This chapter focuses on the characterization of the properties of the synthesized autonomic healable systems. As the characteristics of the proposed systems were very diverse, this study was carried out taking into consideration the polymer structure as well as the corresponding healing process.

Thus, in the first section, the film forming properties of the different systems are described as well as their morphology, determined by Atomic Force Microscopy in the solid state.

The second section is centered on the influence of the introduction of dynamic reactions such as disulfide metathesis and hydrogen bond interactions, on different properties. These aspects are analyzed from the spectroscopic, rheological and processability points of view.

4.2 Introduction

The autonomic healing approach implies the restoration of the material functionality without any external intervention. Hence, the generation of damage in the material should be responsible for the activation of the healing mechanism [1–3]. Generally, during such a process, active species are generated in the newly formed surface, such as free radicals, hydroxyl, amine, acid or thiol groups [4,5]. Ideally, the recombination of these active groups should lead to the material reparation. However, due to their low concentration and/or reduced lifetime, autonomic healing alternatives additionally incorporate dynamic structures able to recombine at room temperature in order to enhance the reparation possibilities.

These structures are capable of breaking and reforming linkages in the material, both by a dynamic equilibrium or in response to the generated active species, increasing the chain mobility, even in highly crosslinked structures. Therefore, these materials act as solid polymers during their lifetime but they can flow under certain circumstances, promoting material healing [1,2,5].

127

According to the general classification presented in Chapter 1 (Scheme 1.1), dynamic reactions can mainly be separated into dynamic covalent reactions and supramolecular interactions. This work explores the possibility of introducing different healing monomers corresponding to both types of healing alternatives into waterborne polyurethane structures.

The selected dynamic covalent reaction was disulfide metathesis. This reaction is known to provoke the exchange of the side groups of disulfide bridges in the presence of initiators, catalysts, high temperatures or light [6,7]. Taking advantage of this process, several non-autonomic reparable polymers were synthesized based on aliphatic disulfide units and even produced autonomic healable features by the addition of catalysts [8–11].

Recently, the capability of aromatic disulfide moieties to chain exchange under mild conditions, even at room temperature, without catalyst has been used to develop autonomic healable polyurethanes, opening new alternatives in the field of self-healing materials [12–14]. The concept has been applied to crosslinked polyurethane structures, where the metathesis of disulfide linkages permits the reparation of fractured elastomers.

As explained in Chapter 2, the polymer structure was based on the introduction of aromatic disulfide moieties into waterborne organic-inorganic polyurethane hybrids in order to provide autonomic healing characteristics. The synthesized polymer structure and the corresponding healing mechanism are presented in Figure 4.1.

a   **PPGAPDS polymer structure**

b   **PPGAPDS disulfide metathesis**
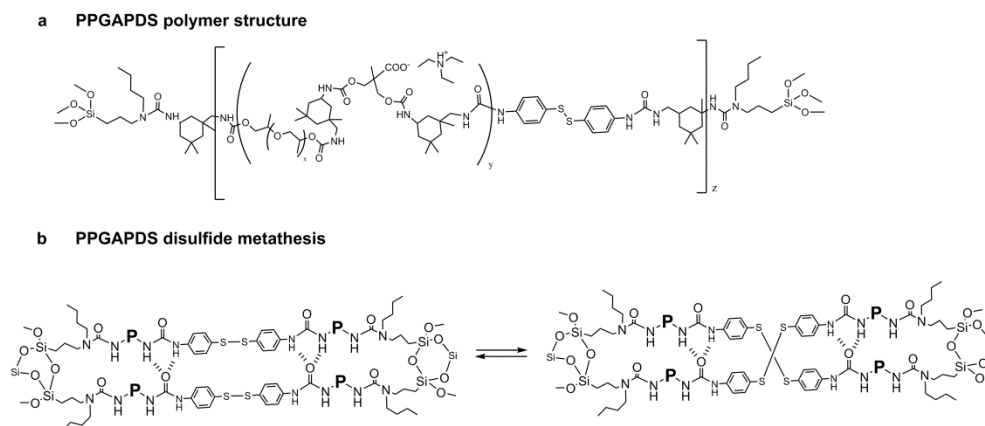
Figure 4.1 *PPGAPDS polymer structure (a) and the proposed healing mechanism by means of aromatic disulfide metathesis (b).*

The proposed polymer structure was defined by different characteristics. On the one hand, these systems crosslinked by means of silicon-oxygen networks formed as a consequence of the condensation of N-bAPTMS moieties. On the other hand, aromatic disulfide moieties were incorporated as chain extenders in the polyurethane backbone. Dynamic chain exchange reactions of such disulfide bonds would enable the recovery of the structural integrity of the material after being damaged.

In contrast to the previous systems, the supramolecular healing approach takes advantage of non covalent interactions [15,16]. Although their strength is comparatively lower than that of covalent bonds, these interactions can act at longer distances, facilitating surface rearrangement [2].

Several non covalent interactions have been applied in healable polymers, including ionic interactions, coordination bonds, π-π stacking, host-guest interactions and so on [17–20]. In this work, H-bond interactions of ureidopyrimidinone units (Upy) were selected to develop WPUs based on supramolecular chemistry.

As explained, the specific hydrogen-bond donor/acceptor configuration (DDAA) of Upy monomer structure enhances the strength of the interaction. As a

consequence, these Upy moieties generally appear in the form of dimers [16,21,22]. Figure 4.2 depicts the synthesized polymer structure as well as the dimerization process of PPGDHUpy samples.

a   PPGDHUpy polymer structure

b   PPGDHUpy dimerization
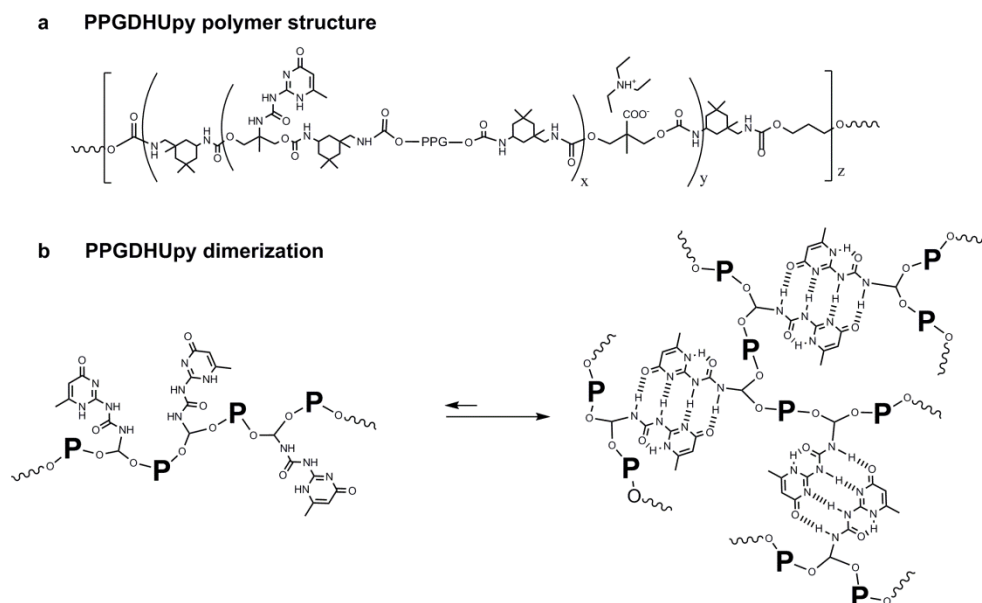
Figure 4.2 *Synthesized PPGDHUpy polymer structure (a) and polymer network formation by strong hydrogen bonding (b).*

As presented in Figure 4.2 a, ureidopyrimidinone units were introduced into the middle of waterborne polyurethane backbones. As a result, the dimerization of these moieties leads to the material crosslinking via non covalent interactions (Figure 4.2 b).

The healing abilities of these systems are based on the assumption that the crack propagates by rupturing the weakest bonds in the structure (H-Bonds). Therefore, the recombination of these H-bonds would provoke material healing.

As explained, the generation of mobile phases after damage is on the basis of autonomic healable approaches. However, such generation should not compromise the structural integrity of the materials during their lifetime. Hence,

an accurate characterization of the material response should take into consideration both aspects. In addition, this response is highly dependent not only on the structural characteristics of the proposed materials but also on external factors, such as temperature or time.

This chapter analyzes different structural characteristics affecting the film formation and the material behavior in the solid state, such as crosslinking reactions or material morphology. In addition, the influence of H-bonds on the material behavior as well as their capability of generating mobile phases was also studied under different experimental conditions. Although these aspects do not determine directly the healing abilities of these materials, they provide significant information about the healing conditions of each system.

4.3 Film features and morphology

The film formation processes for the proposed autonomic healable materials were significantly different. Aromatic disulfide based WPUs acquired their structural integrity as a result of the condensation of the alkoxysilane groups, which crosslinked the samples. In contrast, ureidopyrimidinone based systems formed films as a consequence of water evaporation.

For PPGAPDS samples, not only the reaction conditions but also the amount of N-bAPTMS monomer in the sample influenced the physical properties of the final materials [23–25]. In order to determine the influence of such factors in the crosslinking capabilities of these materials, polymer films for different formulations were obtained by crosslinking the samples at room temperature for at least one week and their gel content was calculated by soxhlet extraction in THF.
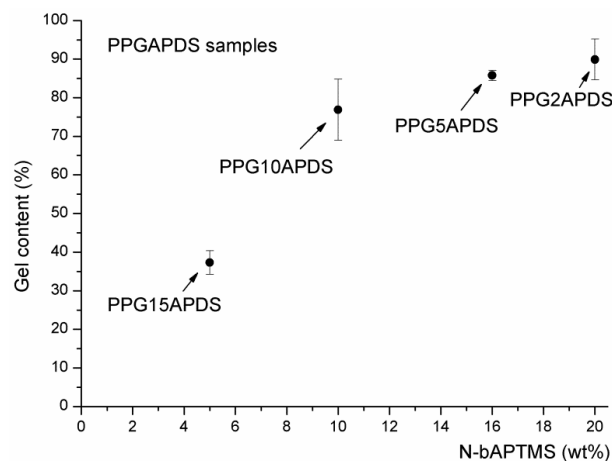
Figure 4.3 *Gel content values for PPGAPDS samples containing different amounts of N-bAPTMS.*

As can be observed in Figure 4.3, the gel fraction increased as the amount of alkoxysilane in the sample increased, reaching values higher than 75% for samples containing more than 10 wt% of N-bAPTMS. In addition, it should be mentioned that the crosslinking degree also influenced the healing characteristics of these materials. According to the formulation presented in Chapter 2 for PPGAPDS samples, the higher the amount of N-bAPTMS in the sample, the lower the aromatic disulfide concentration. Therefore, a compromise between the crosslinking degree and the amount of the healing agent should be reached.

The crosslinking behavior of these samples was also analyzed by solid state ^{29}Si-NMR spectroscopy. Owing to the different chemical environments, the lines corresponding to silicon atoms appeared at different chemical shifts in the NMR spectra depending not only on the number of oxygen atoms directly attached to them but also on their condensation degree. According to the nomenclature proposed by Lippmaa and coworkers, silicon atoms of N-bAPTMS moieties can be classified as T species (those directly attached to three oxygen atoms) [26,27]. In addition, the condensation degree of alkoxysilane groups also influenced the chemical shifts. Thus, the condensation of N-bAPTMS moieties leads to T_1, T_2 and

T_3 depending on the number of Si-O-Si bonds, as presented in Figure A.18 in the Appendix.
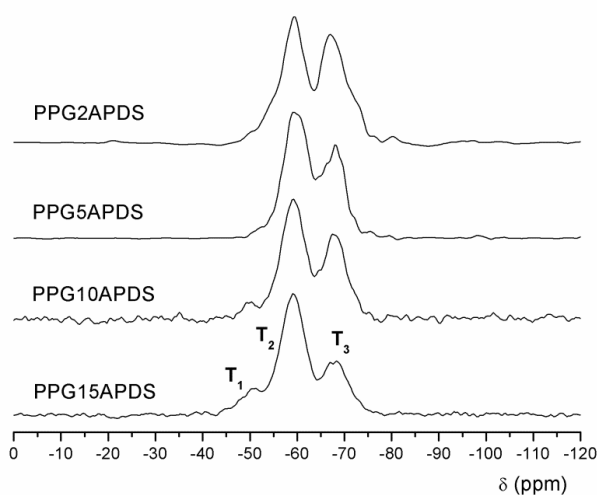
Figure 4.4 [29]*Si-NMR spectra of different PPGAPDS samples.*

The obtained spectra (Figure 4.4) depicted the influence of N-bAPTMS concentration on the sample condensation degree. Although all samples presented lines corresponding to T_2 and T_3 condensed species, additional signals corresponding to T_1 structures appeared in the spectra of PPG15APDS and PPG10APDS samples. However, the intensity of this line decreased as N-bAPTMS concentration in the sample increased while the intensity of more condensed species (T_2 and T_3) increased.

These results are in good agreement with the corresponding gel content values for these samples. Samples containing higher amounts of N-bAPTMS presented signals attributable to highly condensed structures in their ^{29}Si-NMR spectra and also high gel fractions. In contrast, the presence of T_1 species in PPG15APDS indicated the higher amount of uncondensed alkoxysilane species, which were responsible for the low gel fraction values.

The formation of silica networks by alkoxysilane condensation is reflected in the morphology that these materials presented. As a consequence of the intrinsic

incompatibility between hard and soft segments as well as the different chemical nature of the organic and inorganic moieties, these materials tended to form separated domains, as presented in the AFM images of Figure 4.5.
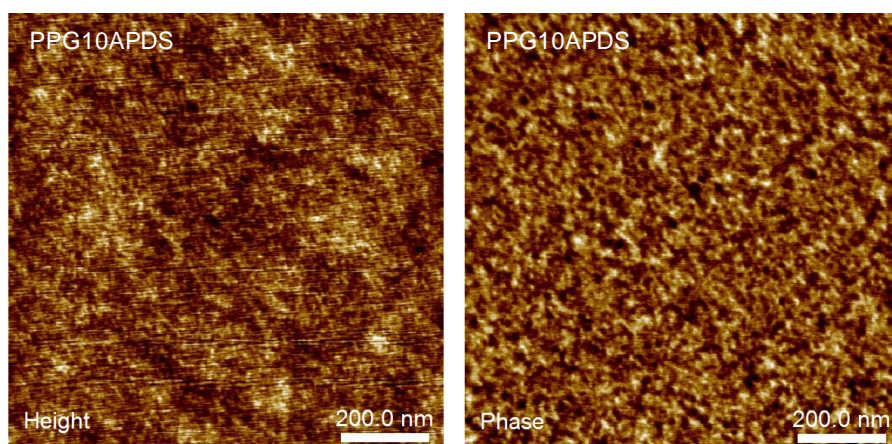
Figure 4.5 *Height (left) and phase (right) AFM images for PPG10APDS samples.*

PPGAPDS samples showed highly separated morphologies, characterized by brighter and darker areas both in the height and phase images, which affected the material roughness [28]. This specific morphology can be related to the inorganic domains formed by condensation of the alkoxysilane precursors, which are known to affect the material morphology [29–31]. However, both the aromatic nature and the presence of hydrogen bond interactions between urea groups also lead to the phase separation of aromatic disulfide moieties [32,33].

However, from the phase image it was not possible to differentiate the hard segments formed by silicon-oxygen networks from those corresponding to the aromatic disulfide moieties. Nevertheless, taking into consideration the difference in nature between silica domains and the polyurethane structure, it seems more reasonable to associate these regions to silicon-oxygen domains. Even so, the phase separation of aromatic disulfide moieties cannot be discarded.

In contrast to PPGAPDS systems, non covalent interactions were responsible for the physical properties of ureidopyrimidinone based waterborne polyurethanes in

the solid state. Therefore, these materials acquired their final structural integrity after water removal. In order to ensure the evaporation, waterborne polyurethane dispersions were dried for at least one week at room temperature.

As occurred both for coumarin and aromatic disulfide containing systems, the presence of ureidopyrimidinone moieties in the polymer backbone altered the polymer morphology. The specificity of hydrogen bonds between ureidopyrimidinone units as well as their ability to self-assemble have led to the formation of different phase separated structures [34,35]. For PPGDHUpy, the phase separated morphology was characterized by AFM and a representative image is shown in Figure 4.6.
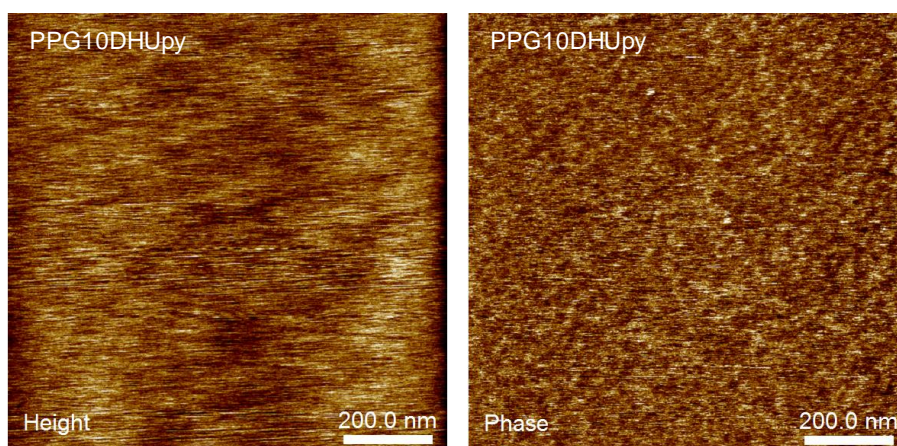
Figure 4.6 *Height (left) and phase (right) AFM images for PPG10DHUpy samples.*

According to these images, PPG10DHUpy displayed smaller domains than its PPGAPDS counterpart, and their influence on the material roughness was almost negligible. On the contrary, the morphology resembled the one of coumarin chain extended polyurethanes. This fact could be related to the similar nature of non covalent interactions, hydrogen bonds, responsible for the phase separated behavior.

4.4 Characterization of dynamic reactions

4.4.1 Spectroscopic characterization

As a result of H-bond interactions, the healing agents of both autonomic healable systems tended to form separated domains. This specific morphology would promote the healing process as it would permit the healing agents in the hard domains to interact and allow the dynamic interaction to take place effectively. Nevertheless, these healing agents should have enough mobility to interact with groups of different domains in order to promote a successful surface rearrangement after damage. The partial or total disconnection of H-bonds, as a consequence of temperature or damage, is on the basis of the generation of chain mobility, as represented in Scheme 4.1.
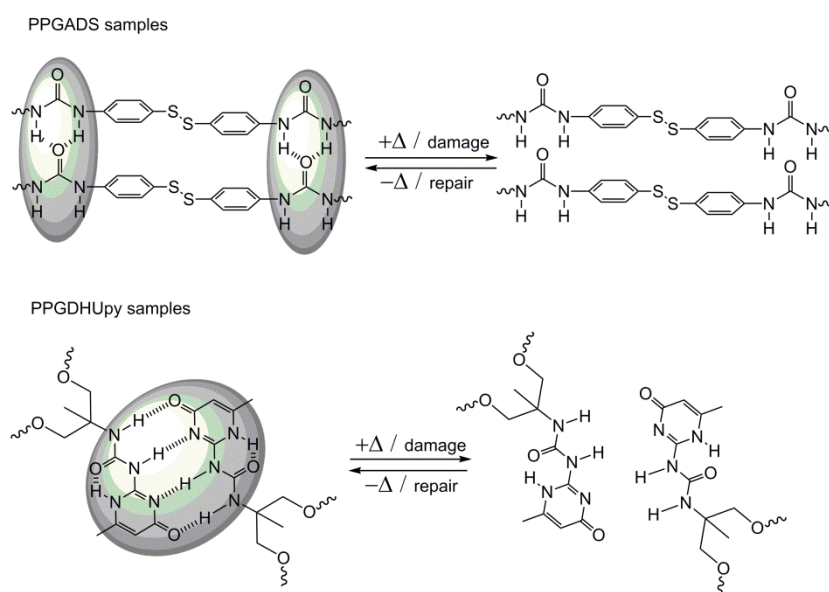
Scheme 4.1 *H-bond disconnection of urea bonds in aromatic disulfide moieties (top) and ureidopyrimidinone dimers (bottom).*

However, the systems showed different behavior due to the disruption or weakening of the H-bonds between healable moieties. While such a disconnection

provoked the flow of PPGDHUpy samples, PPGAPDS systems required the disulfide metathesis reaction to take place also.

FTIR spectroscopy is particularly appropriate when evaluating the strength of H-bonds. The presence of such interactions influences the vibrations of the participating functional groups and consequently, the corresponding absorption bands experiment a variation of both their intensity and position.

Owing to their complex chain structure, which includes different functionalities, the proposed WPUs combined several groups susceptible to forming hydrogen bonds. Urethane groups of polyurethane backbones, for instance, are known to form strong H-bonds [36,37]. Furthermore, the strength of such interactions depends on the chemical nature of the participating groups as well as the chemical environment. Hence, the strength of urethane groups formed by the reaction of different chain extenders, PPG, BD and DMPA, would be different.

In addition, the proposed autonomic healable WPUs incorporated additional functionalities corresponding to active monomers. Thus, PPGAPDS samples presented urea groups of different nature, as a consequence of the reaction of APDS monomer and N-bAPTMS addition. It is known that urea groups of APDS moieties can self-associate [13,14]. Nevertheless, although their ability to interact with other groups was hindered due to their nature and proximity to the condensed silica domains, the substituted urea groups of the polymer chain ends were still susceptible forming H-bonds [38,39].

Ureidopyrimidinone units introduced several groups capable of forming H-bonds, such as urea, amine and amide groups. Due to their specific donor-acceptor configuration, these moieties tended to self-associate in form of dimers. However, the possibility of H-bond interactions with other groups cannot be ruled out.

Given the special sensitivity of the stretching vibration of carbonyl bands to the presence of H-bonds, the evaluation of the temperature dependence was centered in the carbonyl region. These bands comprised vibrations of urethane and urea bonds of different nature. In addition, each group was susceptible of

generating H-bonds and therefore both types of bonds appeared in their "associated" and "free" form depending on the temperature.

The study of the H-bond interactions was centered in the 1900-1300 cm^{-1} region of the FTIR spectra. In this region, the bands associated to urethane carbonyl groups (urethane Amide I band), urea carbonyl groups (urea Amide I band) as well as the Amide II band (corresponding to both urethane and urea groups) appear. The strength of the H-bond interactions was studied at different temperatures and the evolution of these bands was monitored for both PPG10APDS and PPG10DHUpy samples, as represented in Figure 4.7.
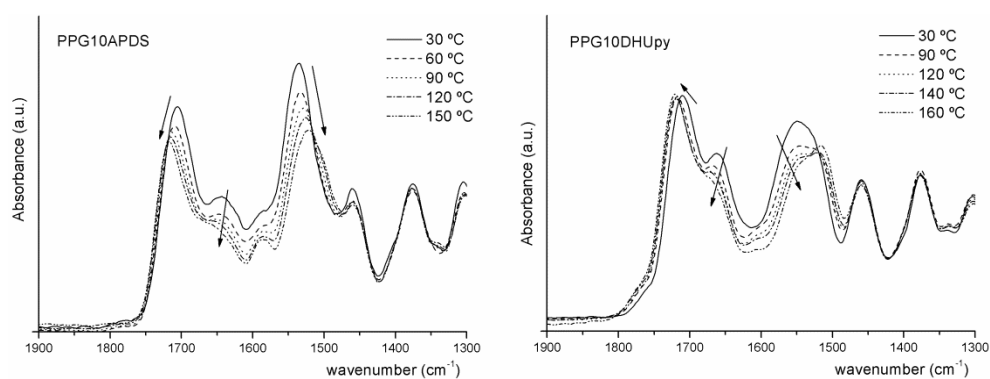
Figure 4.7 *Evolution of the FTIR spectra at different temperatures for PPG10APDS (left) and PPG10DHUpy (right).*

PPGAPDS samples (Figure 4.7, left) presented variations both in the bands attributable to urethane (1715 cm^{-1}) and urea (1635 cm^{-1}) carbonyl groups. These bands decreased their relative intensity with temperature and shifted to higher wavenumber values, as corresponds to the appearance of non associated carbonyl moieties [40]. Conversely, the position of the Amide II band (1550 cm^{-1}) varied to lower wavenumber values, corroborating the progressive weakening of the of H-bonds interactions.

Similarly, the H-bonds of PPGDHUpy systems showed a temperature dependence, which indicated the weakening of the H-bond interactions. In addition to this, it should be mentioned that the intensity of the urethane

carbonyl band (1715 cm^{-1}) increased with the temperature. In order to explain these results the contribution of carbonyl bands corresponding to non associated Upy amide groups should be considered.

Taking advantage of Peak Resolve models included in the Omnic software, the spectral resolution of these bands was performed [41,42]. This technique permits the separation of the spectral bands into individual contributions, according to prefixed parameters [43–45]. In our case, two separate contributions were assigned to describe the region, corresponding to "associated" urethane and urea carbonyl bonds respectively. According to the parameters presented in Table A.2 in the Appendix, the spectral resolution of carbonyl bands was conducted both for aromatic disulfide and ureidopyrimidinone based systems as shown in Figure 4.8.
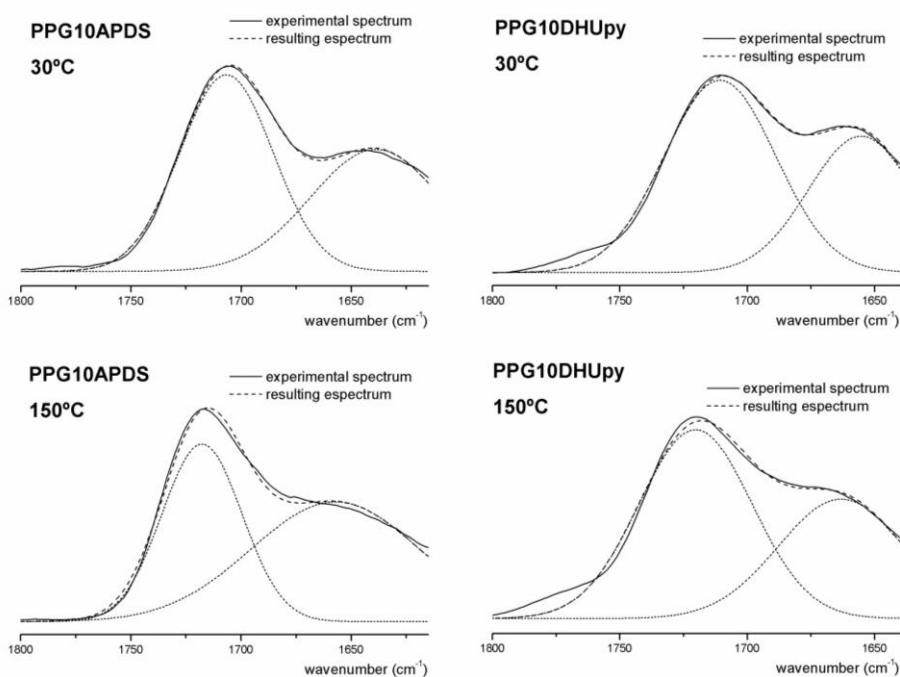
Figure 4.8 *Spectral resolution of the carbonyl region for PPG10APDS and PPG10DHUpy at different temperatures.*

This mathematical approximation provided a general overview of the contribution of different vibrations, due to urethane and urea bonds, in the experimental infrared band. However, the information was qualitative as this approximation did not consider the complexity of the systems. Thus, the entire carbonyl band, corresponding to urea and urethane bonds of different nature, was described using only two contributions. Even so, it permitted the analysis of the strength and temperature dependence of the H-bonds corresponding to both urethane and urea groups.

As mentioned, the position of the carbonyl bands shifted to higher wavenumbers as the temperature increased. Thus, the evolution of the urethane band wavenumber as a function of temperature both for PPG10APDS and PPG10DHUpy is represented in Figure 4.9.
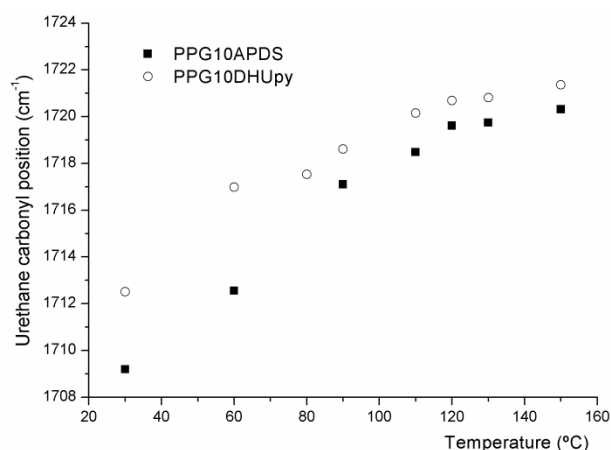
Figure 4.9 *Evolution of the position of the urethane carbonyl band as a function of temperature for PPG10APDS and PPG10DHUpy.*

As shown, the position of the urethane band varied from 1709 to 1721 cm^{-1} depending on the "free" / "associated" fraction [40,44,45]. Taking into account that the vibration of "free" carbonyl groups appears at higher wavenumber values, the shift of the carbonyl band was taken as a significant parameter involving the strength of H-bond interactions. Thus, the fraction of

"free" urethane carbonyl groups increased almost linearly from 30 to 110ºC for both systems. From that point on, the evolution seemed to be slower.

Similarly, the urea carbonyl band position was obtained by spectral resolution analysis and it was plotted versus temperature for both materials, as presented in Figure 4.10.
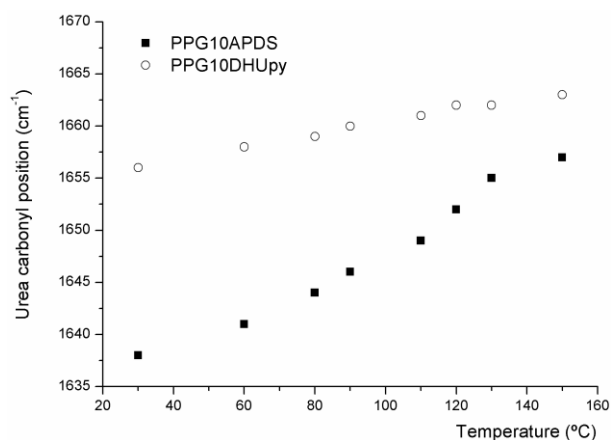
Figure 4.10 *Urea carbonyl band position as a function of temperature for PPG10APDS and PPG10DHUpy.*

As occurred for urethane bonds, the increase in the wavenumber of the urea carbonyl band relied on the weakening of H-bonds interactions [40]. For PPGAPDS systems, the position increased linearly in the analyzed region, indicating the weakening or partial disconnection of the H-bonds of urea groups. This process started at room temperature, although similar systems showed this weakening starting at temperatures of nearly 60ºC [14,46]. This behavior in the low temperature region could be related to the disconnection of weak H-bonds associated to urea bonds corresponding to N-bAPTMS moieties.

In contrast, PPG10DUpy sample showed lower temperature dependence of the urea carbonyl band position. This fact indicated higher strength for the urea H-bonds corresponding to Upy dimers than those for APDS moieties.

4.4.2 Rheological characterization

The rheological characterization is of special relevance in autonomic healable systems. In contrast to non-autonomic healable materials where the mobile phase is generated in response to a certain stimulus, autonomic healable materials act autonomously after damage generation. Therefore, a precise rheological analysis can serve not only to demonstrate the physical properties of the material but also to determine the temperature and time intervals where the materials are capable of flowing (and healing damage just in case).

As mentioned, the introduction of dynamic structures, able to break and reform bonds, would be responsible for the generation of mobile phases inside the polymer networks. Therefore, intrinsic characteristics of these structures, such as the proposed dynamic reaction and its kinetics, temperature dependence and so on, would influence the rheological behavior of autonomic healable waterborne polyurethanes. Furthermore, additional factors such as H-bond interactions or the incorporation of inorganic moieties into the WPU structure, would also influence the flow conditions of the materials.

The rheological behavior can be characterized under different experimental conditions. Taking into consideration the specific characteristics of the dynamic structures, the research focused on viscoelastic experiments: small-amplitude oscillatory shear experiments and Creep and stress relaxation tests.

Small-amplitude oscillatory shear experiments are widely used in the characterization of the viscoelastic properties of polymer materials as they can serve to determine their predominant response in steady flow conditions [47]. Essentially, small deformations allow the properties of the sample to be measured without altering the internal structure of materials. Thus, the prevalence of the elastic or viscous behavior can be established by the comparison of the corresponding storage modulus (G') or loss modulus (G'') [48,49].

The evaluation of the prevalent behavior of the material can be analyzed as a function of different parameters. Generally, the influence of temperature and

time (frequency) on the rheological response is studied. Both experiments were conducted using parallel plate geometry.

Temperature sweep experiments permitted us to obtain a general overview of the material behavior over a wide temperature range. These experiments consisted of establishing constant oscillation conditions, corresponding to the linear viscoelastic region, and recording the material response at different temperatures. In our case, strain and frequency were fixed at 1% and 1 Hz respectively.

As represented in Figure 4.11, the rheological behavior was evaluated by determining the storage and loss moduli as a function of temperature for PPG10APDS. Different behavior was observed not only at different temperatures but also when two consecutive experiments were carried out.
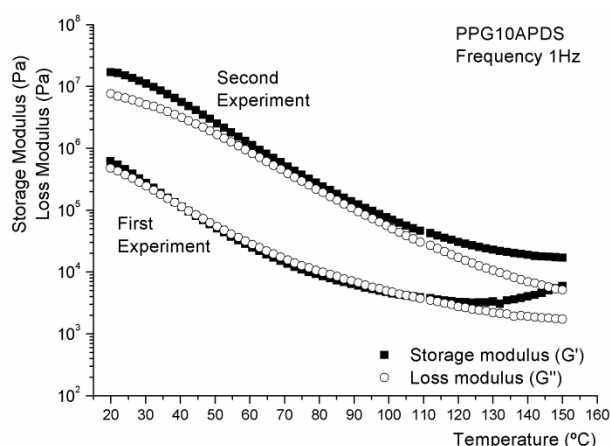
Figure 4.11 *Storage Modulus (G') and Loss Modulus (G'') vs. temperature of PPG10APDS sample.*

For the first experiment, at temperatures close to room temperature, the material presented an elastomeric behavior, characterized by G'>G''. Although the temperature was above the T_g of the soft segment of the polyurethane, the silica networks, which crosslinked the sample as well as presented non covalent interactions, conferred elastic behavior to the material. As the temperature

increased, the loss modulus surpassed the storage modulus indicating the prevalence of the viscous character. This fact can be related to the partial disconnection or weakening of the H-bonds as well as to the increase of the kinetics of the disulfide metathesis process [50]. However, at temperatures ranging from 100 to 150ºC, a significant increase on the storage modulus occurred and the elastic behavior became predominant. This behavior change can be associated to condensation reactions of the alkoxysilane groups occurring at high temperatures [51–54].

As mentioned, the condensation of the alkoxysilane groups gave rise to highly crosslinked structures. However, according to the ^{29}Si-NMR spectra (Figure 4.4), the condensation process was not complete and some alkoxysilane groups were still available. During the heating process, the condensation of these groups took place and the physical properties were modified accordingly [55–57].

The second experiment, which was run immediately after the first one, clearly depicted such alteration of the physical properties. Instead of recovering the original values, both storage and loss moduli increased after the first heating [58]. Additionally, the rheological behavior at higher temperatures was also affected. In contrast to the first experiment, the material presented an elastic character over the whole temperature range and the crossover of G' and G'' was no longer observed. However, at high temperatures, changes presumably produced due to the alkoxysilane condensation were still observed.

Following the same procedure, the rheological properties of ureidopyrimidinone based WPUs were evaluated. Unlike PPGAPDS samples, the tridimensional network, which provided the structural integrity to these systems, was based on supramolecular interactions, more specifically on hydrogen bonds. It is well known that these interactions are highly dependent on temperature [59–61]. Therefore, the potential applications of these materials required a precise rheological characterization as a function of temperature, which is presented in Figure 4.12 for PPG10DHUpy.
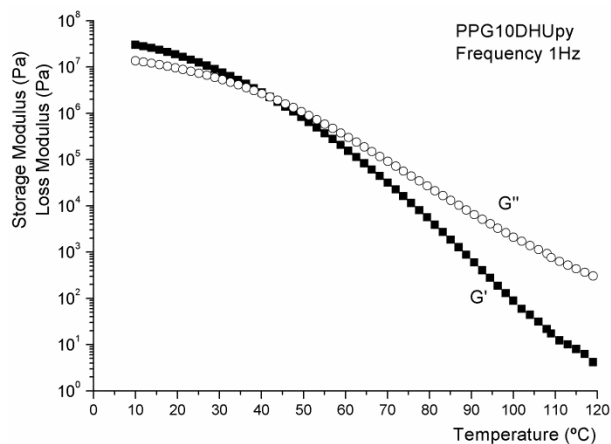
Figure 4.12 *Evolution of the Storage Modulus (G') and Loss Modulus (G'') as a function of temperature for PPG10DHUpy.*

As occurred for PPGAPDS samples, an elastomeric region was observed at temperatures below 40ºC, where the storage modulus presented higher values than the loss modulus [62]. At that temperature (40ºC) the material changed its character, represented by a moduli crossover. From that point on, the viscous modulus (G'') was predominant with respect to the elastic modulus. This fact does not imply the total loss of the tridimensional network at 40ºC, but it demonstrates the capability of the material to flow, even though this flow is hindered. In addition, this material recovered the original moduli values when temperature was decreased, proving the reversible generation of the H-bonds.

In addition to the evolution of the rheological behavior of materials, frequency sweep experiments in linear viscoelastic conditions were conducted at different temperatures. The representation of G' and G'' vs. frequency provided information about the internal structure of materials in steady state [49,63,64]. It is commonly accepted as a rheological criterion that for gels with a permanent character, both G' and G'' moduli show little dependence on frequency, while gels where the bonds have a temporary character (e.g. reversible bonds) G' and G'' present a crossover [65,66]. As both systems differed on the polymer network structure, these experiments allowed us to clarify the nature of the interactions present in such structures. The corresponding results of frequency sweep

experiments for both PPG10APDS and PPG10DHUpy are represented in Figure 4.13.
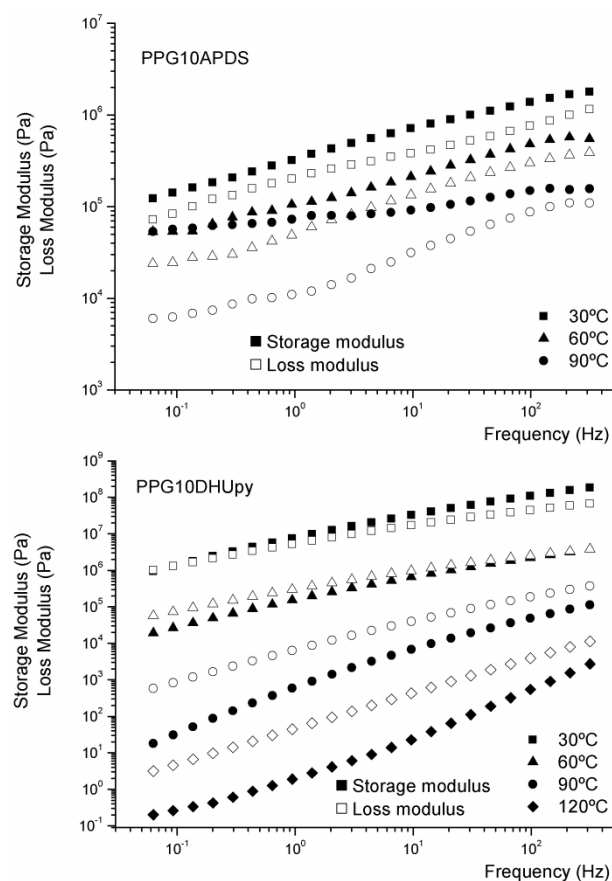
Figure 4.13 *Storage and Loss Modulus (G' and G'') as a function of frequency at different temperatures for PPG10APDS (top) and PPG10DHUpy (bottom).*

Regarding the influence of temperature, the values of both storage and loss moduli for PPGAPDS and PPGDHUpy samples decreased as the temperature increased, similar to the results obtained in temperature sweep experiments. In contrast to PPGAPDS systems, where the elastic character was predominant, the rheological behavior of PPGDHUpy strongly depended on time, especially at low temperatures. While the sample behaved as an elastic material at high

frequencies (G'>G''), the rheological response was inverted at low frequencies and a moduli crossover was observed [62].

Additionally, the terminal zone of both samples, which corresponds to low frequencies, was altered. This region for non structured materials is characterized by -2 and -1 slopes for G' and G'' in the logarithmic representation and corresponds to a flow regime. However, alterations of this behavior indicated the formation of structured polymer networks, in our case both by silica domains or supramolecular interactions, which hindered the material from flowing [48,67–69]. This effect was more noticeable in PPGAPDS, where G' values were almost independent of frequency at all temperatures, indicating the formation of a strong polymer network by covalent bonds.

Although the temperature and frequency dependence of G' and G'' could be established by small amplitude oscillatory measurements, prevalence of the elastic behavior of the material did not exclude the material from flowing [49,64]. Therefore, these experiments did not demonstrate the generation of dynamic mobile phases at different temperatures, which is the basis of autonomic healable abilities.

Viscoelastic behavior of autonomic healable systems is directly related to polymer nature and the incorporation of dynamic structures. Taking into account the dynamic structures, the viscoleastic characterization of these materials was carried out by creep and stress relaxation measurements. These experiments can be considered complementary for analyzing the viscoelastic properties of materials. Thus, while Creep experiments consist of the application of a constant stress to the sample and the registration of the produced deformation as a function of time, the stress relaxation measurements rely on analyzing the necessary stress to maintain a constant deformation in the material.

Creep experiments were performed using a stress control rheometer (parallel plate geometry and D = 25 mm) and applying a 50 Pa stress to the samples. Additionally, the recovery of the material was also monitored after the stress

removal. Figure 4.14 represents the evolution of the generated strain as a function of time for both systems.
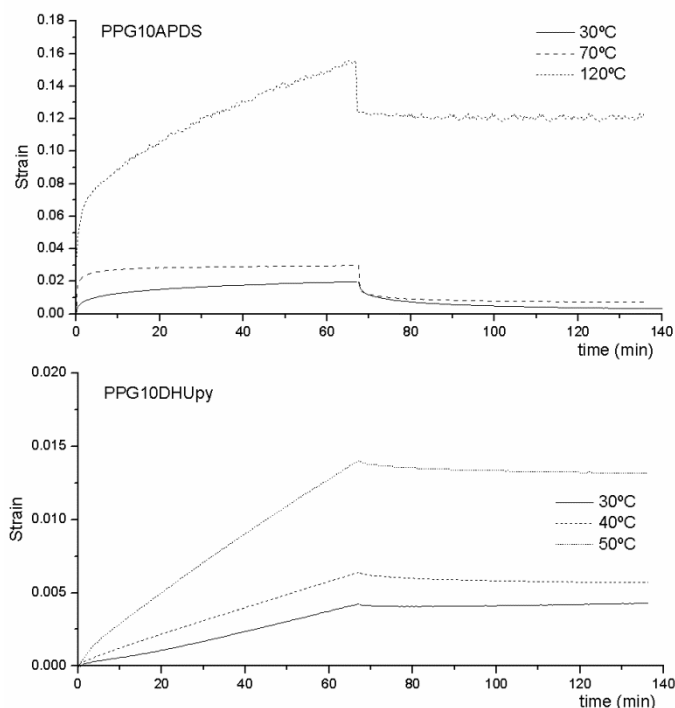
Figure 4.14 *Creep experiments at different temperatures for PPG10APDS (top) and PPG10DHUpy samples (bottom) applying a stress of 50 Pa. The normal force was kept at 1 N in all cases.*

The behavior greatly differed not only between both materials but also depending on the temperature. At temperatures below 70ºC, PPGAPDS samples presented a predominantly elastic response with a slight increase in the strain at long experiment times. In contrast, the material deformed more and faster at higher temperatures, as a consequence of rearrangements provoked by disulfide metathesis reactions [70,71]. After the stress removal, the strain was partially recovered in all cases, being less pronounced in the case of 120ºC. This phenomenon indicated the ability of this system to rearrange and flow at high temperatures.

In contrast to previous results, PPG10DHUpy behaved as a very viscous liquid, even at low temperatures. The application of the stress initially generated lower deformations compared to PPGAPDS samples. However, the provoked strain increased almost linearly, which resembled the viscous behaviour [49,72]. In order to complete the viscoelastic information, stress relaxation experiments were performed for both systems. The representative parameter of these experiments is the relaxation modulus, G(t), calculated as the ratio of the measured stress and the applied constant deformation as a function of time. Using parallel plates geometry, samples were deformed 10% and the relaxation modulus, G(t) was plotted versus time Figure 4.15.
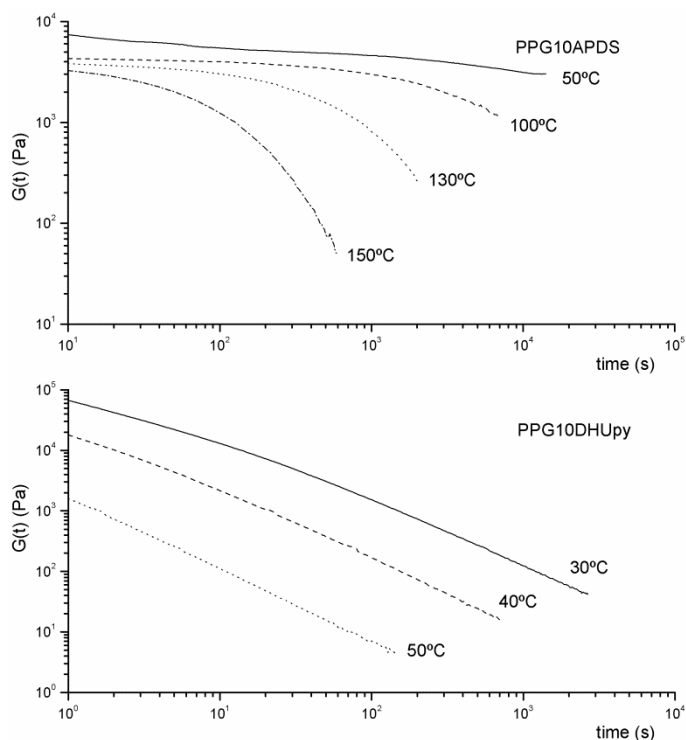
Figure 4.15 *Stress relaxation experiments at different temperatures for PPG10APDS (top) and PPG10DHUpy samples (bottom). The normal force was kept at 1N in all cases.*

The possibility of rearrangement at 50ºC of PPGAPDS samples was hindered. As a result, they showed a mostly flat curve, attributable to elastic materials, and only at long times did the material start to relax slightly. As the temperature increased, the relaxation process took place at shorter times. Apart from the aromatic disulfide metathesis, these results suggested the presence of strong H-bond interactions, which prevent the material from relaxing the stress at temperatures below 100ºC [14].

In contrast, ureidopyrimidinone based systems exhibited a substantial stress relaxation at temperatures as low as 30ºC and no elastic behavior was observed. This material behaved both in creep and stress relaxation experiments as linear unentangled polymers above their T_g [73,74]. Therefore, the results suggested that ureidopyrimidinone moieties were unable to form a real polymer network or its strength was not high enough to impede the material flow.

4.4.3 Processability

Apart from healing properties, the introduction of dynamic structures can provide additional features to crosslinked polymer structures. Among them, the possibility of designing reprocessable and recyclable thermosets has become particularly relevant [75–78]. These structures, also called covalent adaptable networks or CANs, incorporate dynamically exchangeable structures, based on dynamic covalent reactions and/or supramolecular interactions, which permit material rearrangements at molecular scale.

This process is kinetically controlled by the dynamic reaction. Thus, when the bond rupture and reforming is slow compared to the time of an applied stress, materials present elastic behavior. In contrast, when the dynamic exchange of bonds is sufficiently rapid (at one specific temperature), the polymer network becomes viscoelastic.

Different dynamic structures have been introduced in polymer chains in order to provide reprocessable characteristics [70,79–81]. This work proposed the incorporation of two different dynamic structures, aromatic disulfide structures and ureidopyrimidinone units, to waterborne polyurethanes and their

reprocessing characteristics were directly related to the polymer network structure and the nature of the dynamic reaction.

The tridimensional network occurring in PPGDHUpy samples was formed as a consequence of supramolecular interactions of the ureidopyrimidinone units. The disconnection of these interactions, both by increasing the temperature or by the addition of solvents, allowed PPGDHUpy to flow and they consequently showed the reprocessing and recycling characteristics of thermoplastic polymers [82,83].

In contrast, the reprocessing of aromatic disulfide containing samples was not so evident. The polymer structure was formed by polyurethane chains covalently attached to silica networks. However, the presence of aromatic disulfide dynamic structures permitted certain chain mobility and reconnection [13,14,71]. In fact, creep and stress relaxation experiments suggested such behavior.

Taking into consideration the results obtained in both experiments, the material was reprocessed by compression molding. After applying pressure and temperature (30 minutes at 10 bar and 130ºC), PPGAPDS fragments were able to form 1 mm thick homogeneous films, as shown in Figure 4.16.

Figure 4.16 *PPG10APDS sample before (left) and after being reprocess (right) by compression molding.*

The material reprocessing was performed for samples with different aromatic disulfide content (ranging from 2 to 10 wt% of APDS) and homogeneous films

were obtained in all cases. However, the application of high temperatures provoked the condensation of alkoxysilane groups and altered the physical properties of reprocessed materials, as concluded from the rheological characterization (Figure 4.11). The influence of the sample reprocessing was also studied by stress-strain tests and it will be discussed in Chapter 5.

4.5 Conclusions

Chapter 4 was centered on the characterization of autonomic healable waterborne polyurethanes. Taking into consideration the intrinsic features of proposed autonomic healable systems, the analysis was divided into the determination of the crosslinking abilities, the analysis of the rheological behavior and the morphological characterization. The following points can be concluded from the obtained results:

- The film formation of PPGAPDS samples occurred by condensation of terminal alkoxysilane groups. The amount of the alkoxysilane precursor in the aromatic disulfide containing samples influenced the crosslinking degree and therefore the gel content. In order to obtain significant gel contents, N-bAPTMS amounts higher than 10 wt% were required. In contrast, PPGDHUpy samples formed films after the water removal.

- Both polymers showed phase separated morphologies. For PPGAPDS samples, this morphology was attributed to the presence of silica domains although the phase separation of APDS moieties was not discarded. In contrast, the self-assembly of Upy moieties was responsible for the phase separated morphology in PPGDHUpy systems.

- The evolution of the strength of H-bonds at different temperatures was analyzed by FTIR spectral resolution in the carbonyl region. The results demonstrated the H-bond weakening or disconnection at high temperatures. This process started at room temperature for urethane and urea bonds of both systems, which also showed similar temperature dependence for urethane carbonyl bands. In contrast, urea bonds

showed different behavior for each system. Urea carbonyl bands corresponding to PPGDHUpy systems showed lower temperature dependence than their PPGAPDS counterpart, indicating higher strength of the H-bond interactions.

- The rheological behavior, characterized by small amplitude oscillatory experiments, allowed us to determine the temperature and frequency regions where the material presented a predominant viscous character.

- For aromatic disulfide containing samples this region was limited from 40 to 110ºC. However, as a consequence of residual alkoxysilane condensation, the material became more elastic after being heated in the overall temperature range. In contrast, ureidopyrimidinone based systems presented a crossover of G' and G'' at 40ºC from which the rheological response was predominantly viscous.

- In addition, the terminal zone of both materials was altered, indicating the presence of structured networks in the internal structure of materials. This phenomenon was more noticeable for aromatic disulfide based WPUs due to the covalent character of the networks.

- According to Creep and stress relaxation experiments both systems showed contrasting behavior. While PPGAPDS samples presented a viscoelastic response, PPGDHUpy behaved as viscous polymer liquids. However, the incorporation of dynamic structures provided flowing abilities to the aromatic disulfide systems at high temperatures. Both creep and stress relaxation results for PPGDHUpy samples suggested that ureidopyrimidinone moieties were unable to form tridimensional networks by means of hydrogen bonds.

- As a consequence of the incorporation of dynamic structures to WPUs, it was possible to reprocess aromatic disulfide containing samples by compression molding and homogeneous films were obtained.

153

4.6 References

[1]   Ghosh SK. Self-healing materials: Fundamentals, Design Strategies and Applications. Weinheim, Germany: Wiley-VCH Verlag GmbH & Co. KGaA; 2009.

[2]   Urban MW. Handbook of Stimuli-Responsive Materials. Weinheim, Germany: Wiley-VCH Verlag GmbH & Co. KGaA; 2011.

[3]   Bergman SD, Wudl F. Re-Mendable Polymers. Self Heal Mater An Altern Approach to 20 Centuries Mater Sci 2007:45–68.

[4]   Yang Y, Urban MW. Self-healing polymeric materials. Chem Soc Rev 2013;42:7446–67.

[5]   Yang Y, Ding X, Urban MW. Chemical and physical aspects of self-healing materials. Prog Polym Sci 2015;49-50:34–59.

[6]   Bang E-K, Lista M, Sforazzini G, Sakai N, Matile S. Poly(disulfide)s. Chem Sci 2012;3:1752.

[7]   Gyarmati B, Némethy Á, Szilágyi A. Reversible disulphide formation in polymer networks: A versatile functional group from synthesis to applications. Eur Polym J 2013;49:1268–86.

[8]   Li L, Song C, Jennings M, Thayumanavan S. Photoinduced heterodisulfide metathesis for reagent-free synthesis of polymer nanoparticles. Chem Commun 2015;51:1425–8.

[9]   Pepels M, Filot I, Klumperman B, Goossens H. Self-healing systems based on disulfide-thiol exchange reactions. Polym Chem 2013;4:4955–65.

[10]   Canadell J, Goossens H, Klumperman B. Self-Healing Materials Based on Disulfide Links. Macromolecules 2011;44:2536–41.

[11]   Lei ZQ, Xiang HP, Yuan YJ, Rong MZ, Zhang MQ. Room-temperature self-healable and remoldable cross-linked polymer based on the dynamic exchange of disulfide bonds. Chem Mater 2014;26:2038–46.

[12]   Rekondo A, Martin R, Ruiz de Luzuriaga A, Cabañero G, Grande HJ, Odriozola I. Catalyst-free room-temperature self-healing elastomers based on aromatic disulfide metathesis. Mater Horizons 2014:237–40.

[13]   Martin R, Rekondo A, Ruiz de Luzuriaga A, Santamaria A, Odriozola I. Mixing the immiscible: blends of dynamic polymer networks. RSC Adv 2015;5:17514–8.

[14]   Martin R, Rekondo A, Ruiz de Luzuriaga A, Cabañero G, Grande HJ, Odriozola I. The processability of a poly(urea-urethane) elastomer reversibly crosslinked with aromatic disulfide bridges. J Mater Chem A 2014;2:5710–5.

[15]   de Espinosa LM, Fiore GL, Weder C, Johan Foster E, Simon YC. Healable supramolecular polymer solids. Prog Polym Sci 2015;49-50:60–78.

[16]   Armstrong G, Buggy M. Hydrogen-bonded supramolecular polymers: A literature review. J Mater Sci 2005;40:547–59.

[17]   Varley RJ, van der Zwaag S. Towards an understanding of thermally activated self-healing of an ionomer system during ballistic penetration. Acta Mater 2008;56:5737–50.

[18]   Coulibaly S, Roulin A, Balog S, Biyani M V., Foster EJ, Rowan SJ, et al. Reinforcement of Optically Healable Supramolecular Polymers with Cellulose Nanocrystals. Macromolecules 2014;47:152–60.

[19]   Burnworth M, Tang L, Kumpfer JR, Duncan AJ, Beyer FL, Fiore GL, et al. Optically healable supramolecular polymers. Nature 2011;472:334–7.

[20]   Yang X, Yu H, Wang L, Tong R, Akram M, Chen Y, et al. Self-healing polymer materials constructed by macrocycle-based host–guest interactions. Soft Matter 2015;11:1242–52.

[21]   Beijer FH, Sijbesma RP, Kooijman H, Spek AL, Meijer EW. Strong dimerization of ureidopyrimidones via quadruple hydrogen bonding. J Am Chem Soc 1998;120:6761–9.

[22]   Creff G, Arrachart G, Hermet P, Wadepohl H, Almairac R, Maurin D, et al. Investigation on the vibrational and structural properties of a self-structured bridged silsesquioxane. Phys Chem Chem Phys 2012;14:5672–9.

[23]   Sardon H, Irusta L, Santamaría P, Fernández-Berridi MJ. Thermal and mechanical behaviour of self-curable waterborne hybrid polyurethanes functionalized with (3-aminopropyl)triethoxysilane (APTES). J Polym Res 2012;19:9956–65.

[24]   Lai X, Shen Y, Wang L. Preparation and properties of self-crosslinkable polyurethane/silane hybrid emulsion. J Polym Res 2011;18:2425–33.

[25]   Wang L, Shen Y, Lai X, Li Z, Liu M. Synthesis and properties of crosslinked waterborne polyurethane. J Polym Res 2010;18:469–76.

[26]   Lippmaa E, Maegi M, Samoson A, Engelhardt G, Grimmer AR. Structural studies of silicates by solid-state high-resolution silicon-29 NMR. J Am Chem Soc 1980;102:4889–93.

[27]   Magi M, Lippmaa E, Samoson A, Engelhardt G, Grimmer AR. Solid-state high-resolution silicon-29 chemical shifts in silicates. J Phys Chem 1984;88:1518–22.

[28]   Zhu F, Zhang G, Xu S, Hong X, Dong J. A novel alkoxysilane-modified high solids hydroxyl acrylic polyurethane: Preparation and surface properties. J Appl Polym Sci 2006;101:1866–71.

[29]   Metwalli E, Haines D, Becker O, Conzone S, Pantano CG. Surface characterizations of mono-, di-, and tri-aminosilane treated glass substrates. J Colloid Interface Sci 2006;298:825–31.

[30]   Guo SZ, Zhang C, Wang WZ, Liu TX. Preparation and characterization of organic-inorganic hybrid nanomaterials using polyurethane-b-poly[3-(trimethoxysilyl) propyl methacrylate] via RAFT polymerization. Express Polym Lett 2010;4:17–25.

[31]   Jo S, Park K. Surface modification using silanated poly(ethylene glycol)s. Biomaterials 2000;21:605–16.

[32]   Garrett JT, Siedlecki C a., Runt J. Microdomain morphology of poly(urethane urea) multiblock copolymers. Macromolecules 2001;34:7066–70.

[33]   McLean RS, Sauer BB. Tapping-mode AFM studies using phase detection for resolution of nanophases in segmented polyurethanes and other block copolymers. Macromolecules 1997;30:8314–7.

[34]   Appel WPJ, Portale G, Wisse E, Dankers PYW, Meijer EW. Aggregation of Ureido-Pyrimidinone Supramolecular Thermoplastic Elastomers into Nanofibers: A Kinetic Analysis. Macromolecules 2011;44:6776–84.

[35]   Kieltyka RE, Bastings MMC, van Almen GC, Besenius P, Kemps EWL, Dankers PYW. Modular synthesis of supramolecular ureidopyrimidinone–peptide conjugates using an oxime ligation strategy. Chem Commun 2012;48:1452–4.

[36]   He Y, Xie D, Zhang X. The structure, microphase-separated morphology, and property of polyurethanes and polyureas. J Mater Sci 2014;49:7339–52.

[37]   Król P. Synthesis methods, chemical structures and phase structures of linear polyurethanes. Properties and applications of linear polyurethanes in polyurethane elastomers, copolymers and ionomers. Prog Mater Sci 2007;52:915–1015.

156

[38]   Kolodziejski W, Wawer I, Wozniak K, Klinowski J. Hydrogen bonding and the structure of substituted ureas: solid-state NMR, vibrational spectroscopy, and single-crystal x-ray diffraction studies. J Phys Chem 1993;97:12147–52.

[39]   Golub AA, Zubenko AI, Zhmud B V. γ-APTES Modified Silica Gels: The Structure of the Surface Layer. J Colloid Interface Sci 1996;179:482–7.

[40]   Mattia J, Painter P. A Comparison of Hydrogen Bonding and Order in a Polyurethane and Poly(urethane−urea) and Their Blends with Poly(ethylene glycol). Macromolecules 2007;40:1546–54.

[41]   Griffiths PR, Pariente GL. Introduction to spectral deconvolution. TrAC Trends Anal Chem 1986;5:209–15.

[42]   Coleman MM, Painter PaC, Graf JF. Specific Interactions and the Miscibility of Polymer Blends. Lancaster, Pennsylvania: Technomic Publishing Company; 1991.

[43]   González a., Irusta L, Fernández-Berridi MJ, Iruin JJ, Sierra T, Oriol L. Determination of the self-association and inter-association equilibrium constants of a carboxylic acid and its mixtures with pyridine derivates. Vib Spectrosc 2006;41:21–7.

[44]   Irusta L, Iruin JJ, Fernández-Berridi MJ, Sobkowiak M, Painter PC, Coleman MM. Infrared spectroscopic studies of the self-association of ethyl urethane. Vib Spectrosc 2000;23:187–97.

[45]   Irusta L, L'Abee M, Iruin JJ, Fernández-Berridi MJ. Infrared spectroscopic studies of the urethane/ether inter-association. Vib Spectrosc 2001;27:183–91.

[46]   Wolinska-Grabczyk a., Jankowski B, Jankowski A. Investigations of hydrogen bonding in the poly (urethane-urea) -based membrane materials by using FTIR spectroscopy. Polish J Chem Technol 2008;10:53–6.

[47]   R. Byron Bird, Armstrong RC, Hassager O. Dynamics of Polymeric Liquids. 2nd ed. New York, NY: John Wiley & Sons; 1987.

[48]   Chirila T V., Lee HH, Oddon M, Nieuwenhuizen MML, Blakey I, Nicholson TM. Hydrogen-bonded supramolecular polymers as self-healing hydrogels: Effect of a bulky adamantyl substituent in the ureido-pyrimidinone monomer. J Appl Polym Sci 2014;131:39932–44.

[49]   Ferry JD. Viscoelastic Properties of Polymers. 3rd ed. New York, NY: Wiley-VCH Verlag GmbH & Co. KGaA; 1980.

[50]   Houton K a, Wilson AJ. Hydrogen-bonded supramolecular polyurethanes. Polym Int 2015;64:165–73.

[51]   Hofacker S, Mechtel M, Mager M, Kraus H. Sol–gel: a new tool for coatings chemistry. Prog Org Coatings 2002;45:159–64.

[52]   Hernández-Escolano M, Juan-Díaz M, Martínez-Ibáñez M, Jimenez-Morales A, Goñi I, Gurruchaga M, et al. The design and characterisation of sol–gel coatings for the controlled-release of active molecules. J Sol-Gel Sci Technol 2012;64:442–51.

[53]   Hernández-Escolano M, Juan-Díaz MJ, Martínez-Ibáñez M, Suay J, Goñi I, Gurruchaga M. Synthesis of hybrid sol-gel materials and their biological evaluation with human mesenchymal stem cells. J Mater Sci Mater Med 2013;24:1491–9.

[54]   Brinker CJ, Scherer GW. Sol-Gel Science: the physics and chemistry of sol-gel processing. San Diego: Academic Press, Inc; 1990.

[55]   Barghi N, Berry T, Chung K. Effects of timing and heat treatment of silanated porcelain on the bond strength. J Oral Rehabil 2000;27:407–12.

[56]   Subramanian V, van Ooij WJ. Effect of the Amine Functional Group on Corrosion Rate of Iron Coated with Films of Organofunctional Silanes. Corrosion 1998;54:204–15.

[57]   Li G, Wang X, Li A, Wang W, Zheng L. Fabrication and adhesive properties of thin organosilane films coated on low carbon steel substrates. Surf Coatings Technol 2007;201:9571–8.

[58]   Liu X, Zhao S. Measurement of the condensation temperature of nanosilica powder organically modified by a silane coupling agent and its effect evaluation. J Appl Polym Sci 2008;108:3038–45.

[59]   Brunsveld L, Folmer BJ, Meijer EW, Sijbesma RP. Supramolecular polymers. Chem Rev 2001;101:4071–98.

[60]   Feldman KE, Kade MJ, Meijer EW, Hawker CJ, Kramer EJ. Model transient networks from strongly hydrogen-bonded polymers. Macromolecules 2009;42:9072–81.

[61]   Folmer BJB, Sijbesma RP, Versteegen RM, van der Rijt JAJ, Meijer EW. Supramolecular Polymer Materials: Chain Extension of Telechelic Polymers Using a Reactive Hydrogen-Bonding Synthon. Adv Mater 2000;12:874–8.

[62]   Nobuhiro Oya TI and NY. A crystalline supramolecular polymer with self-healing capability at room temperature. Polym J 2013;45:955–61.

[63]   Vinckier I. Relationship between rheology and morphology of model blends in steady shear flow. J Rheol 1996;40:613.

[64]   Bousmina M, Muller R. Rheology / morphology / flow conditions relationships for polymethylmethacrylate / rubber blend. Rheol Acta 1996;35:369–81.

[65]   Ross-Murphy SB. Rheological characterization of polymer gels and networks. Polym Gels Networks 1994;2:229–37.

[66]   Kavanagh GM, Ross-Murphy SB. Rheological characterization of polymer gels. Prog Polym Sci 1998;23:533–62.

[67]   Fernandez I, Santamaría A, Muñoz ME, Castell P. A rheological analysis of interactions in phenoxy/organoclay nanocomposites. Eur Polym J 2007;43:3171–6.

[68]   Solomon MJ, Almusallam AS, Seefeldt KF, Somwangthanaroj A, Varadan P. Rheology of polypropylene/clay hybrid materials. Macromolecules 2001;34:1864–72.

[69]   Cassagnau P. Melt rheology of organoclay and fumed silica nanocomposites. Polymer (Guildf) 2008;49:2183–96.

[70]   Imbernon L, Oikonomou EK, Norvez S, Leibler L. Chemically crosslinked yet reprocessable epoxidized natural rubber via thermo-activated disulfide rearrangements. Polym Chem 2015;6:4271–8.

[71]   Xiang HP, Qian HJ, Lu ZY, Rong MZ, Zhang MQ. Crack healing and reclaiming of vulcanized rubber by triggering the rearrangement of inherent sulfur crosslinked networks. Green Chem 2015;17:4315–25.

[72]   Münstedt H. Viscoelasticity of polystyrene melts in tensile creep experiments. Rheol Acta 1975;1088:1077–88.

[73]   Tobolsky A V. Stress Relaxation Studies of the Viscoelastic Properties of Polymers. J Appl Phys 1956;27:673.

[74]   Osswald TA. Understanding Polymer Processing. Munich: Hanser Publishing; 2010.

[75]   Kloxin CJ, Scott TF, Adzima BJ, Bowman CN. Covalent Adaptable Networks (CANs): A Unique Paradigm in Crosslinked Polymers. Macromolecules 2010;43:2643–53.

[76]   Bowman CN, Kloxin CJ. Covalent adaptable networks: Reversible bond structures incorporated in polymer networks. Angew Chemie - Int Ed 2012;51:4272–4.

[77]   Yu K, Taynton P, Zhang W, Dunn ML, Qi HJ. Reprocessing and recycling of thermosetting polymers based on bond exchange reactions. RSC Adv 2014;4:10108.

[78]   Zhang Y, Broekhuis AA, Picchioni F. Thermally Self-Healing Polymeric Materials: The Next Step to Recycling Thermoset Polymers? Macromolecules 2009;42:1906–12.

[79]   Lei ZQ, Xie P, Rong MZ, Zhang MQ. Catalyst-free dynamic exchange of aromatic Schiff base bonds and its application to self-healing and remolding of crosslinked polymers. J Mater Chem A 2015;3:19662–8.

[80]   Cordier P, Tournilhac F, Soulié-Ziakovic C, Leibler L. Self-healing and thermoreversible rubber from supramolecular assembly. Nature 2008;451:977–80.

[81]   Defize T, Riva R, Thomassin J-M, Jérôme C, Alexandre M. Thermo-Reversible Reactions for the Preparation of Smart Materials: Recyclable Covalently-Crosslinked Shape Memory Polymers. Macromol Symp 2011;309-310:154–61.

[82]   Aida T, Meijer EW, Stupp SI. Functional Supramolecular Polymers. Science (80-) 2012;335:813–7.

[83]   Chino K. Thermoreversible crosslinking rubber using supramolecular hydrogen bonding networks. KGK Kautschuk Gummi Kunststoffe 2006;59:158–62.

CHAPTER 5

Healable Waterborne Polyurethanes:

Repairing Properties

5.1 Chapter Overview

This chapter discusses the healing characteristics of synthesized waterborne polyurethanes, centering attention on materials capable of repairing catastrophic damage, that is, damage which implies the total loss of functionality. Hence, the characterization of the healing abilities was performed taking into account this prerequisite.

In a first approach, the crack refilling process was studied by optical microscopy, which permitted the evaluation of the reparation abilities of different materials according to their intrinsic healing mechanism.

Additionally, a sequential method was conducted in order to evaluate the healing abilities of different materials. This method involved a qualitative analysis of the healing characteristics, the study of surface rearrangement by means of permeation measurements and the quantification of the healing efficiency by mechanical tests.

5.2 Introduction

The main objective of healable polymers is to restore the structural integrity and/or the performance of polymeric materials after being damaged [1]. As mentioned, this process occurs as a consequence of the activation of a healing mechanism that, taking advantage of the chemical reactions and physical properties of the polymer network, is able to refill the defect and restore the physical properties in the damaged area [1–3]. Therefore, provided a successful healing approach is desirable, both the physical properties of the polymer network and chemical reactions involved in the healing mechanism should be taken into consideration.

The restoration of the structural integrity of the material occurs in different stages, which vary depending on the specific healing mechanism. Accordingly, the evaluation of the healing process should involve not only the recovery of the

original physical properties after the appearance of the damage, but also the conditions in which the healing process occurs (time, temperature, irradiation intensity and so on). Therefore, the analysis of the healing properties can be described with respect to parameters corresponding to the healing mechanisms and the restoration of the physical properties of the material.

Regardless of the healing mechanism involved in the reparation, a successful surface rearrangement is required to obtain significant healing abilities. As presented in the diffusion model proposed by Wool et al., the recovery of the structural integrity of the damaged material occurs as a consequence of the randomization in the generated surfaces [4,5]. Therefore, the analysis of this step can establish different healing parameters, such as the healing time and temperature, for each specific system [6,7].

From a functional point of view, the effectiveness of a healing process is based on its ability to restore the physical properties of the damaged material above their limit of reliability [8]. The quality of the healing process is often referred to the healing efficiency (η) [9–12]. This parameter is defined as the ratio of a physical property for both the healed material and the undamaged one. It is often expressed as a percentage of recovery, according to equation (6):

$$\eta = \frac{p_{healed} - p_{damaged}}{p_{virgin} - p_{damaged}} \times 100 \tag{6}$$

Where P is the physical property of interest.

In the case of catastrophic damage, which involves the total failure of the system, equation (6) can be simplified as equation (7):

$$\eta = \frac{p_{healed}}{p_{virgin}} \times 100 \tag{7}$$

No specific healing test is currently available to determine healing efficiency and different testing procedures give rise to different results as the restoration of an individual physical property does not imply the recovery of the original internal

structure of the material [13]. As a consequence, the healing efficiency values of an individual healing experiment cannot be extrapolated to physical properties in general. Hence, healing efficiency must be limited to the physical property of interest, the analytical method used in its determination and the material application [8].

In addition, several factors can complicate the interpretation of the healing efficiency results [9]. The incorporation of healing elements, for instance, may alter the physical properties of polymer matrixes. As a consequence, the healing efficiency can increase or decrease not only because of the capability of healing agents to restore the material properties but also their influence on the physical properties of undamaged materials.

5.3 Crack refilling studies

In damaged materials, the appearance of defects generates new surfaces in the material structure. In order to avoid the associated degradation process and the failure of the material, healable polymers have to be able to refill the damage and promote the polymer randomization of both parts of the damage.

The ability of different materials to fill cracks has been studied by analytical techniques such as Atomic Force Microscopy (AFM) or optical microscopy [7,14–20]. In this study, the experiments were performed by scratching films, obtained by casting, with a razor and following the filling process by optical microscopy at varying temperatures.

As mentioned, the filling abilities depend not only on the healing conditions but also on the physical properties of the polymer network under study. Consequently, factors modifying the physical properties of the material, such as structure, irradiation conditions, crosslinking degree or strength of interactions, influence the filling characteristics of the synthesized healable materials.

For coumarin based waterborne polyurethanes, the photochemical processes as well as the synthesized polymer structure determined the refilling process. As they present linear structures before and after the cycloaddition reaction,

coumarin end-capped WPUs refilled scratches in all conditions. In contrast, the filling abilities of coumarin chain-extended WPU films depended on the irradiation conditions. Figure 5.1 shows the filling process for non irradiated, irradiated at 365 nm and 254 nm PPG10DHMC samples at 80ºC.
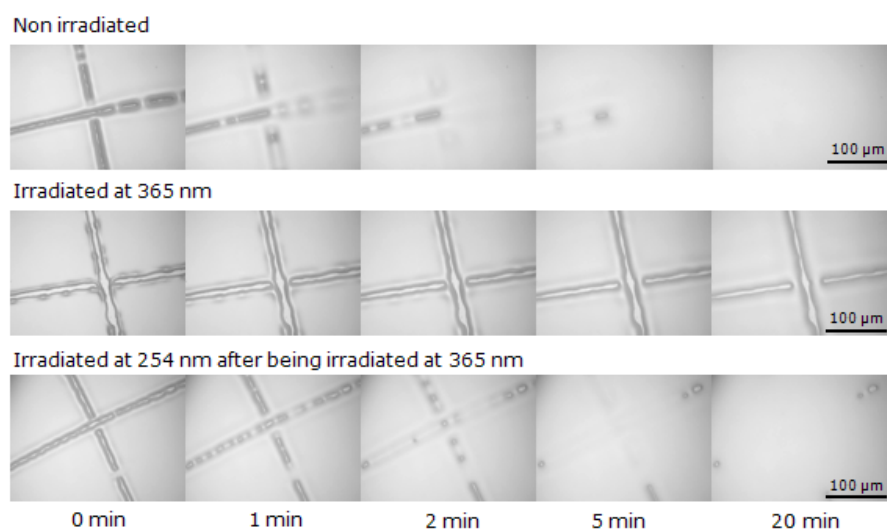
Figure 5.1 *Evolution of scratch refilling under different irradiation conditions for PPG10DHEMC at 80 ºC.*

The differences in the material behavior represented in Figure 5.1 are related to changes in the polymer structure provoked by the application of UV light. Thus, the linear structure of non irradiated samples promotes the scratch refilling when heated at 80ºC. After being exposed at 365 nm for three hours, the [2+2] cycloaddition reaction took place, crosslinking the sample. Although the generation of the scratch provokes the rupture of the polymer chains, increasing the chain mobility in the damage surroundings, the crosslinked network prevents surface rearrangement and damage refilling. However, when this sample was irradiated at 254 nm for one hour, the ability of refilling scratches was partially recovered due to the polymer network decrosslinking.

Regarding the healing behavior at different temperatures, no refilling was observed below 60ºC. At that temperature, the surface rearrangement took place

in 40 minutes. As the temperature increased, the filling process proceeded more rapidly, and less than ten minutes were needed to refill the damage in non-irradiated and decrosslinked samples at 80ºC.

Similarly, the evolution of the crack refilling for PPGAPDS samples containing different amounts of aromatic disulfide monomer in their structure was monitored and the obtained results are shown in Figure 5.2.
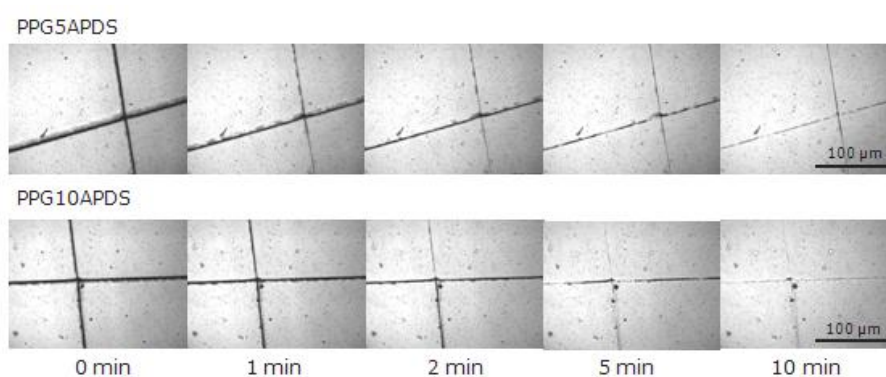
Figure 5.2 *Crack refilling abilities of PPGAPDS samples.*

Regardless of the aromatic disulfide content, the filling process at 80ºC occurred in 10 minutes. However, the damage refilling was not complete and the scratch was still perceptible, even at higher refilling temperatures. Furthermore, the process for these samples was influenced by the polymer structure and the intrinsic characteristics of the healing mechanism. As PPGAPDS samples were crosslinked by means of silicon-oxygen networks, the molecular mobility and the surface rearrangement was hindered. On the contrary, the disulfide metathesis increased the chain mobility, promoting crack refilling [21–23]. As observed in Figure 5.2a, the refilling process was slower and less efficient for the sample containing less APDS monomer concentration, which also implies higher crosslinking degrees.

Healable WPUs based on ureidopyrimidinone units presented contrasting behavior compared to that of the rest of the systems. As represented in Figure 5.3, PPG10DHUpy filling abilities strongly depended on temperature.
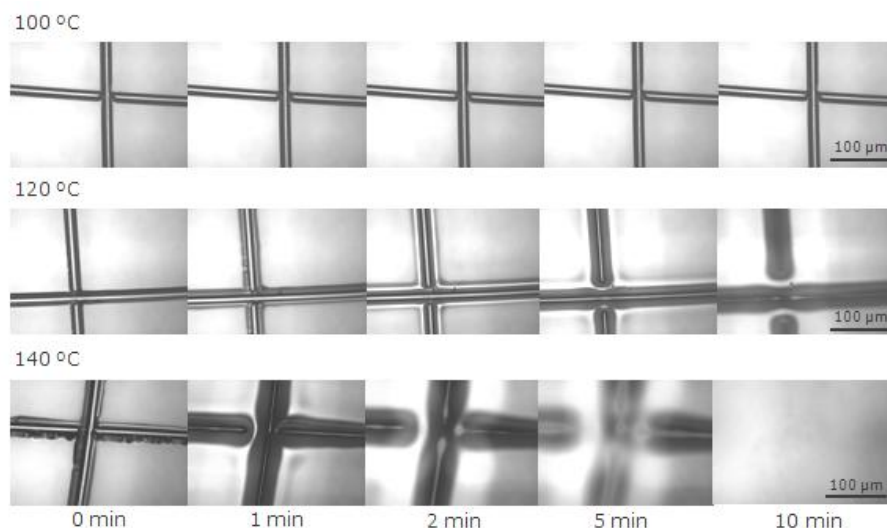
Figure 5.3 *Scratch refilling process at different temperatures for PPG10DHUpy.*

Below 100ºC, no refilling was observed and it was necessary to increase the temperature to 120ºC in order to start the refilling process. This behavior could be related to the strength of the H-bonds of the ureidopyrimidinone units [20]. Furthermore, no successful surface rearrangement was observed until 140ºC.

As observed in the rheological analysis of these samples presented in chapter 4, the tridimensional network formed by H-bond interactions of the ureidopyrimidinone units hindered the material flow even up to 120ºC, represented by the changes of G' in the flow zone (Figure 4.13).

5.4 Evaluation of the healing properties

The main objective of incorporating active monomers into the polymer backbones was to develop healable polymeric films capable of restoring their structural integrity after catastrophic damage, which implies the total loss of functionality.

In order to achieve this objective, the evaluation of the healing process was performed according to a sequential method involving the qualitative analysis of

the healing process, the recovery of the barrier properties and the restoration of the physical properties after the material repair.

5.4.1 Qualitative analysis

In order to prove the concept, the healing abilities of different polyurethane formulations were qualitatively analyzed regarding the aforementioned requisites for damage. Thus, in a first step, polymer films were obtained in solid state taking into account the intrinsic features of the proposed polymer structure. Secondly, polymer films were cut into two separate parts and finally the recovery of the structural integrity was promoted according to the healing mechanism of each system.

The overall healing process of coumarin based systems implied the response of the material to the application of UV light at different wavelengths. Thus, polymer films acquired their structural integrity by being irradiated for 24 hours (12 hours on each side of the film) with 365 nm light, which provoked coumarin dimerization and sample crosslinking.

Furthermore, the fracture reparation required irradiation of damaged films at 254 nm for one hour. Afterwards, both parts were put in close contact and the sample irradiated (365 nm) again for an additional 24 hours.

Figure 5.4 depicts the obtained results of the qualitative analysis for PPG10DHEMC. Successive cuts were healed after applying the 254/365 nm irradiation cycles, and the material was able to bend and to maintain an arbitrary load without breaking.

Figure 5.4 *Qualitative analysis of the healing abilities of PPGDHMC samples. Methylene blue was used for visibility.*

Similarly, the quantitative analysis was performed for autonomic healable polyurethanes. In this case, the film formation differed from PPGAPDS to PPGDHUpy systems. While PPGDHUpy films were directly obtained by drying the water dispersion, PPGAPDS samples crosslinked at room temperature in Teflon molds for one week.

Conversely to coumarin based WPUs, the healing process of such systems did not require external stimulation after the fracture. Damage was healed by putting both sides of the fracture in close contact. This procedure was performed immediately after the cut in order to avoid the passivation of the generated surface.

Figure 5.5 and Figure 5.6 show pictures corresponding to the different steps of the process for PPG10APDS and PPG10DHUpy samples.
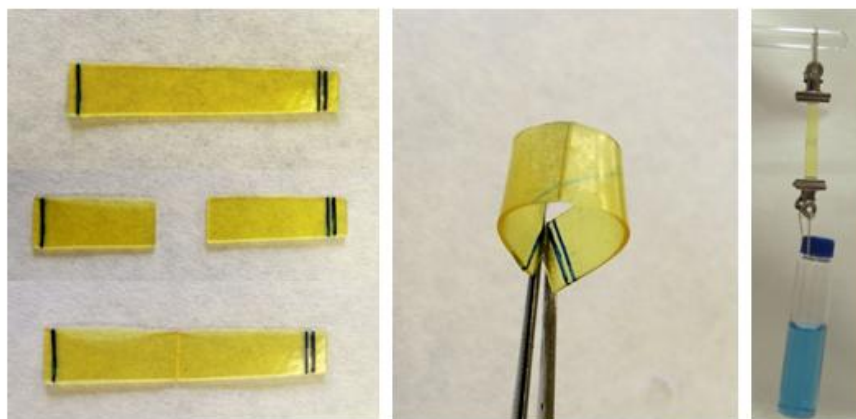
Figure 5.5 *Restoration of the structural integrity of PPG10APDS sample after the material fracture.*
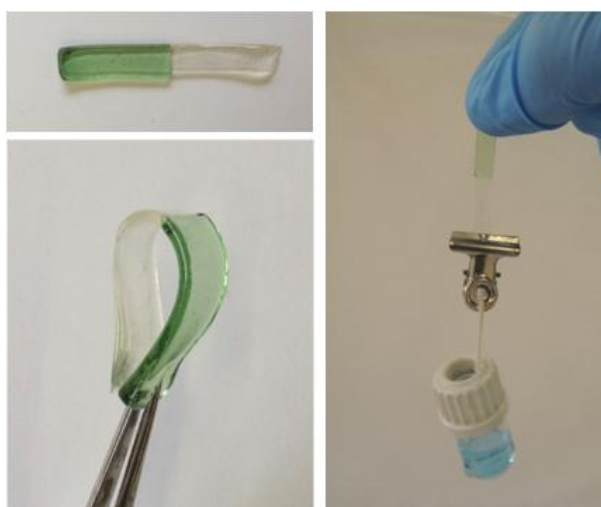
Figure 5.6 *Healing abilities of PPG10DHUpy sample. Bromocresol green was used for visibility.*

After a healing time of two hours, both systems were able to recover their structural integrity, proving their autonomic healing properties. However, due to their physical properties, the load that PPGDHUpy was able to maintain was

lower compared to the one maintained by other systems. This behavior will be discussed more extensively in section 5.4.3.

5.4.2   Recovery of the gas transport properties

Healable membranes capable of self-repair after puncture or tear have been a topic of interest for many applications, mainly focused on the storage of harmful liquids or gases, preventing the gas release in aerospace industry and ultrafiltration systems [24–27]. These systems have mainly been based on ionomers, space filling gels and self-inflatable structures [28–31].

Apart from that, the recovery of the barrier properties of polymer films after being damaged can provide additional information about the effectiveness of the surface rearrangement and the healing process.

When a pressure difference is established between the opposite side of polymer films, gas or vapor can go through the membrane. This permeation process is generally described as the "solution-diffusion" mechanism [32,33]. Although the mass transport occurs according to a complex process, the main events can be summarized as the solution of the gas at the exposed interface of the membrane (absorption), the molecular diffusion across the membrane (random walk) and finally the release of the gas at the opposite interface (desorption). Thus, the permeation describes the overall mass transport process whereas the term diffusion refers to the movement of the gas across the membrane [34].

The experiments were conducted measuring the barrier properties of different polymer films towards carbon dioxide before and after cutting the membrane in two separate parts according to Figure 5.7.
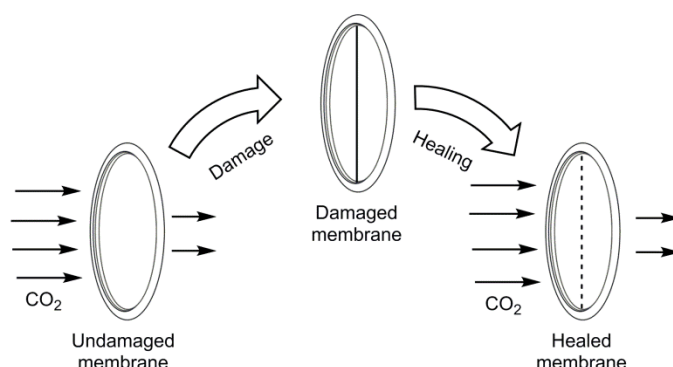
**Figure 5.7** *Scheme of gas permeation fracture-healing experiments.*

The experiments were carried out for coumarin and aromatic disulfide containing systems. Due to the poor physical properties of the PPGDHUpy membranes, it was not possible to measure the healing properties of these systems. The damage was repaired by applying the healing conditions for each system, previously mentioned in section 5.4.1.

Poorly healed crack surfaces provide preferential pathways for gas diffusion across the membrane, significantly increasing the permeability of the membrane. In contrast, successful healing processes recover the original permeability values [14,35,36].

Although there are many different alternatives to describe the mass transfer and the barrier properties across a polymeric membrane, material permeability to CO_2 was focused on, according to the barometric or constant volume method. Thus, as a consequence of a pressure difference, CO_2 transport occurred along the membrane and the process was described by an increment of the pressure on the low pressure zone. This experiment was conducted at 25ºC and 1 atmosphere (atm) in the high pressure zone. The obtained results for PPG10DHEMC and PPG10APDs samples are represented both in Table 5.1 and Figure 5.8.

Table 5.1 *Summary of the permeability values for virgin and healed specimens of PPG10DHEMC and PPG10APDS samples.*

Sample		Permeability	Increment	
		Barrer	Barrer	%
PPG10DHEMC	Virgin	22.3±0.6	1.2±0.9	5.4±4.0
	Healed	23.5±0.7		
PPG10APDS	Virgin	15.5±0.6	3.6±1.1	23.2±6.1
	Healed	19.1±0.9		
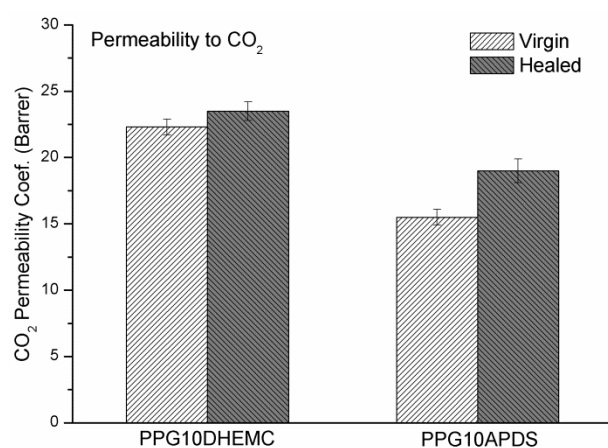
Figure 5.8 *CO_2 permeability values for virgin and healed PPG10DHEMC and PPG10APDS samples.*

According to these results, undamaged PPGDHEMC membranes presented higher permeability values than those of PPGAPDS systems. This behavior was attributed to the presence of inorganic domains in the aromatic disulfide containing samples. The presence of silica networks, which are considered impenetrable to gas molecules, hindered gas permeation through the membrane for materials with high compatibility [37,38].

After the application of the healing conditions, membranes recovered their structural integrity to such an extent as to withstand the high pressure conditions of the measurements. However, as a consequence of the fracture healing, the permeability values of both systems increased and this effect was more

significant for PPGAPDS than PPGDHEMC samples. These results are in good agreement with those of optical microscopy results shown in Figure 5.1 and Figure 5.2. While PPGDHEMC samples lead to successful surface rearrangements after the healing process, the scratch was still perceptible in healed PPGAPDS films. Consequently, the defects created preferential pathways, which made the permeability increase owing to the fact that the damaged area of the membrane was small. However, the permeability values of PPGAPDS samples did not surpassed those of coumarin containing membranes.

5.4.3 Restoration of the physical properties

The recovery of the structural integrity of healable waterborne polyurethanes was determined by the mechanical characterization measured by strain-stress tests. Given the elastomeric character of the samples and taking advantage of the aforementioned test, the healing efficiency of the process was evaluated using the elongation at break and the material toughness as the physical properties of interest. Test specimens were obtained by die-cutting about 0.5 mm thick polymer films in dumbbell-shape, according to the dimensions presented in Figure 5.9 a.
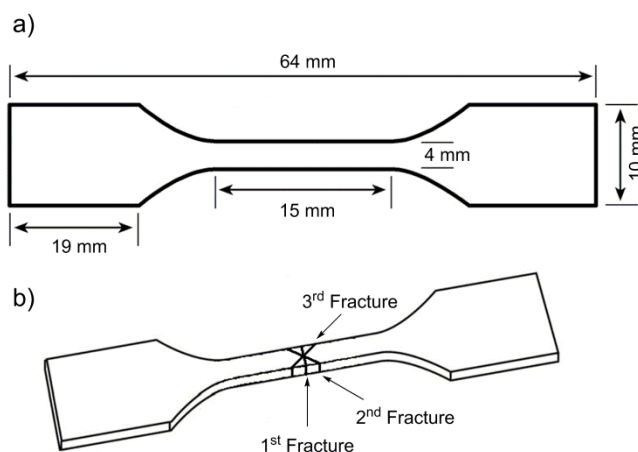

Figure 5.9 *Dumbbell-shape specimens (a) and generated fractures (b).*

The evaluation of the healing process was carried out for three independent healing events. As represented in Figure 5.9 b, specimens were initially cut perpendicularly whereas the subsequent fractures were cut at 45º with respect to the first. After each fracture, the specimens were repaired by applying the appropriate healing conditions. As such conditions depended on the proposed system, the healing abilities of the different formulations will be evaluated separately.

5.4.3.1 Coumarin based waterborne polyurethanes

Coumarin based WPUs present damage repairing ability due to the light-responsive behavior of coumarin monomers [14,16,39,40]. However, owing to the lack of specimen consistency, it was not possible to test PPGHEMC samples. Therefore, the analysis of the healing properties for coumarin based systems was centered on PPGDHEMC samples.

The evaluation of the physical properties of PPGDHEMC was carried out by irradiating die-cut samples at 365 nm for 24 hours, 12 hours on each side of the film, in order to maximize the crosslinking degree and to provide structural integrity to the polymer films. The crosslinked samples were tested and the obtained results are shown in Figure 5.10.
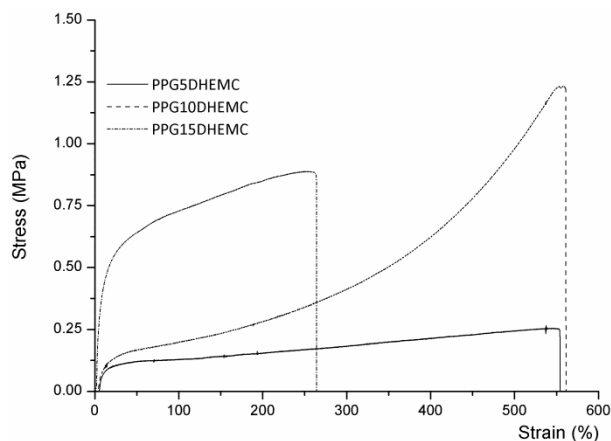
Figure 5.10 *Stress-strain curves for PPGDHEMC samples containing different amounts of coumarin.*

PPGDHEMC samples presented different physical properties depending on coumarin concentration. Thus, PPG5DHEMC shows a high elongation at break but a low tensile strength due to its low crosslinking density. On the contrary, PPG15DHEMC shows the opposite, low elongation at break but high tensile strength values. PPG10DHEMC formulation reaches a compromise between the physical properties of the other two.

In order to determine healing ability, fractures were made using a razor to die-cut samples according to Figure 5.9 b. The fractures were then healed by applying a 254/365 nm irradiation cycle. The healing experiments were performed for samples containing coumarin amounts from 5 to 15 wt%. PPG1DHEMC was not analyzed as it was not possible to obtain test specimens due to the gel consistency of the material. The obtained results for the rest of PPGDHEMC samples are summarized in Figure 5.11.
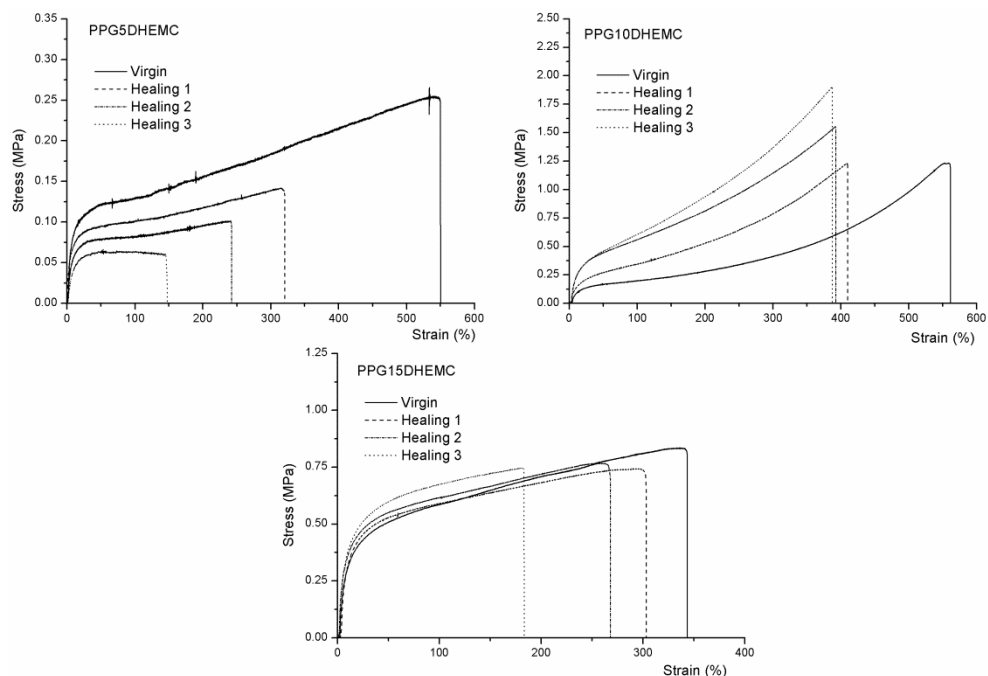
Figure 5.11 *Stress-strain plots for PPGDHEMC samples containing different amounts of coumarin monomers after different healing cycles.*

Although the systems behave differently depending on coumarin concentration, the integrity of the PPGDHEMC samples was high enough to be tested after suffering the damage, which implied a certain degree of recovery.

Regardless of coumarin concentration, the application of the healing events affected the elongation at break of the repaired material and this effect was more noticeable as the number of healing events increased. In contrast, the tensile strength at break depended on coumarin concentration. Thus, the increase of the healing event made the tensile strength for PPG5DHEMC samples decreased, but this increment had the opposite effect on samples containing 10 and 15 wt% of coumarin in the second and third events. Accordingly, the material toughness, calculated as the area under the stress-strain curve, vs. the healing event did not present a clear tendency.

As mentioned, the healing efficiency of the process for different coumarin concentrations was evaluated using the elongation at break and the material toughness as physical properties of interest. Taking into account that the generated damage was catastrophic fractures, which implied the total loss of functionality after the damage, the healing efficiency was calculated using equation (7) for each physical property. The obtained results are summarized in Table 5.2.

Table 5.2 *Physical properties and healing efficiency values for PPGDHEMC samples.*

Sample		Elongation at break		Toughness	
		(%)	Healing (%)	(MPa)	Healing (%)
PPG5DHEMC	Virgin	532±25	-	97.3±6.6	-
	1st cut	322±11	60.5±3.5	35.2±5.7	36.2±6.4
	2nd cut	237±18	44.5±3.7	20.7±4.4	21.3±4.4
	3rd cut	145±3	27.3±2.1	8.2±1.3	8.6±1.5
PPG10DHEMC	Virgin	556±9	´-	271±12	-
	1st cut	419±22	78.7±4.5	242±21	89.3±8.5
	2nd cut	397±12	74.5±4.7	374±12	136.0±14.3
	3rd cut	376±11	70.7±3.1	329±31	113.7±6.4
PPG15DHEMC	Virgin	349±9	-	223±25	-
	1st cut	302±9	56.6±2.2	186±45	83.4±22.1
	2nd cut	262±4	49.2±1.6	168±60	75.3±28.1
	3rd cut	192±18	36.1±3.4	114±25	51.1±12.5

As can be seen in Table 5.2, PPGDHEMC samples recovered more than 55 % of the elongation at break of the virgin material for the first healing event, reaching nearly 80 % for the case of PPG10DHEMC sample. This behavior can be related to the physical properties of the virgin material, which facilitated the wetting process of both parts of the crack together leading to a successful network formation by means of coumarin dimers [41–43]. However, the healing efficiency values decreased as the number of healing events increased.

However, the healing efficiency calculated from the material toughness results, gave both unexpected and different values to those obtained from the elongation

at break. Healed specimens of PPG10DHEMC presented a higher toughness than the virgin material for the second and third healing events and therefore, healing efficiency values higher than 100 %.

In order to evaluate these results appropriately, the influence of the sample preparation on the healing process should be taken into consideration. One of the main drawbacks of coumarin based systems is the difficulty of coumarin monomers in the material bulk to interact with the applied light. Therefore, it is necessary to irradiate the samples from both sides of the film for a long time [16,39]. However, although this methodology increased the crosslinking degree, coumarin monomers located on the inner parts of the sample remained still intact. When the temperature increased, as a consequence of the irradiation at 254 nm, the material was able to randomize and the coumarin moieties from the inner parts would reach the material surface. This effect increased the crosslinking density of the polymer network after the subsequent irradiation at 365 nm [39].

5.4.3.2 Waterborne polyurethanes based on aromatic disulfide units

In contrast to coumarin based systems, the healing mechanism involving aromatic disulfide units acted autonomously, without any external intervention. In addition, the structural integrity of the material did not depend on neither the healing nor the amount and strength of the healing moieties. In this case, the condensation of alkoxysilane groups was responsible for the material strength whereas the incorporation of aromatic disulfide units, provided the healing features.

Waterborne organic-inorganic hybrid polyurethanes showed superior physical properties compared to those of their waterborne counterparts owing to their ability to combine the strength and modulus of the inorganic moieties and the ductility of the polyurethane chains [44–46]. In addition, the physical properties of such materials can vary from very ductile to very hard depending on the formulation [44]. Therefore, by selecting the appropriate amount of the

alkoxysilane precursor, it is possible to control precisely the physical properties of the material.

In the present work, the amount of the alkoxysilane precursor (N-bAPTMS) ranged from 5 to 20 wt%. However, the specimens corresponding to the sample containing 5 wt% of N-bAPTMS (PPG15APDS sample) did not display sufficient integrity to be tested. Figure 5.12 presents the stress-strain plots of the rest of PPGAPDS samples.
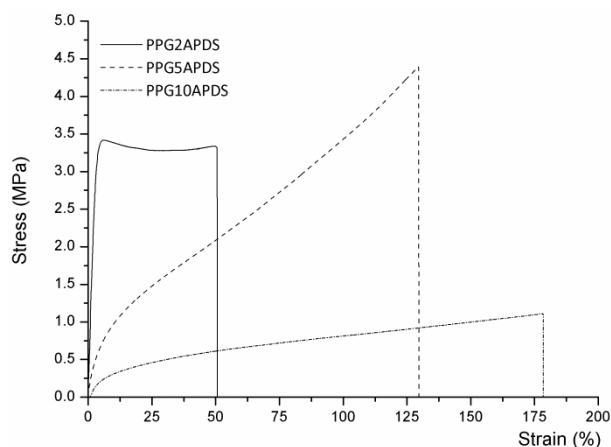
Figure 5.12 *Stress-strain curves for PPGAPDS samples containing different amounts of N-bAPTMS.*

The elongation at break and Young's modulus of the samples presented the opposite dependence to the N-bAPTMS concentration with respect to the others. As the N-bAPTMS amount in the sample increased, the elongation at break of the samples decreased while the Young's modulus increased.

Furthermore, systems containing 20 wt% of alkoxysilane groups (PPG2APDS) displayed non elastomeric behavior showing a Yield point at low deformation values. This fact, together with the low amount of APDS in these systems, can be responsible for the absence of reparation after the fracture of the material.

Thus, the healing abilities of the synthesized PPGAPDS systems were restricted to the samples containing 5 and 10 wt% of the healing monomer. In Figure 5.13 the obtained stress- strain for different healing events are represented.
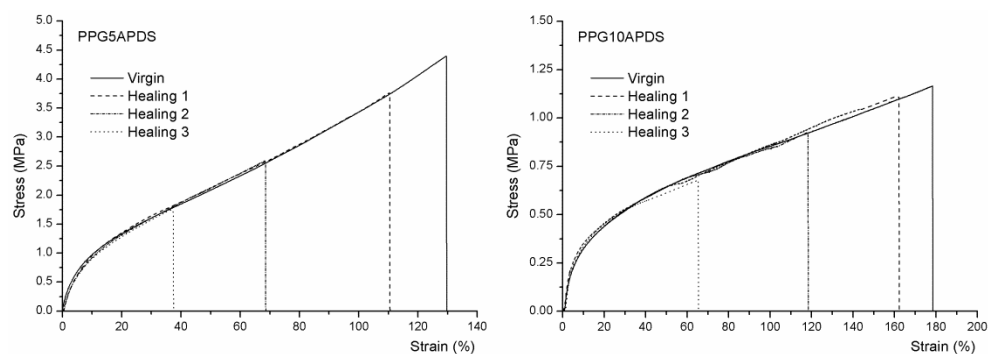
Figure 5.13 *Stress-strain curves corresponding to the subsequent healing events for PPG5APDS (left) and PPG10APDS (right) systems.*

The incorporation of PPGAPDS moieties to waterborne polyurethane hybrids provided repetitive healing characteristics. As shown, both samples containing 5 and 10% of APDS were able to repair the fracture for three independent healing events.

In contrast to coumarin containing samples, where the application of fracture healing processes varied the physical properties of the material, PPGAPDS samples presented similar physical characteristics to the virgin materials, except for the elongation at break. This property decreased as the number of fracture healing events increased, and consequently, the material toughness was also influenced. However, the fracture surfaces became the weakest part of the specimens. Thus, in contrast to coumarin based systems, the material failed by the reconnected surface after the different healing events.

The healing efficiency of the process was calculated in a similar way as proposed for coumarin based systems. Table 5.3 summarizes the obtained physical properties as well as the calculated healing efficiencies.

Table 5.3 *Summary of the physical properties and healing efficiency values for PPGAPDS samples.*

Sample		Elongation at break		Toughness	
		(%)	Healing (%)	(MPa)	Healing (%)
PPG5APDS	Virgin	128±3	-	313±13	-
	1st cut	113±6	88.6±3.9	258±17	82.4±7.7
	2nd cut	65±5	51.0±8.5	103±13	33.1±12.7
	3rd cut	36±2	28.6±4.7	42±2	13.6±5
PPG10APDS	Virgin	178±4	´-	140±4	-
	1st cut	162±5	90.7±3.8	122±3	88.0±3.8
	2nd cut	118±7	66.1±6.3	76±5	54.6±7.2
	3rd cut	65±3	36.4±5.1	32±1	23.0±4.2

The healing efficiency for PPGAPDS, both calculated as the recovery of the elongation at break and expressed by the material toughness, slightly increased with the aromatic disulfide concentration, mainly in the second and third healing events. Accordingly, despite the significant difference in the physical properties of both materials, the controlling factor in the healing process seemed to be the dynamic structure concentration [23,47,48].

In addition to the healing experiments, the physical properties of the reformed specimens were determined. The 1 mm thick polymer films were obtained by compression molding and their physical properties were determined by strain-stress tests, following the procedure described in section 4.4.3. The obtained results as well as the corresponding physical properties of the pristine materials are represented in Figure 5.14.
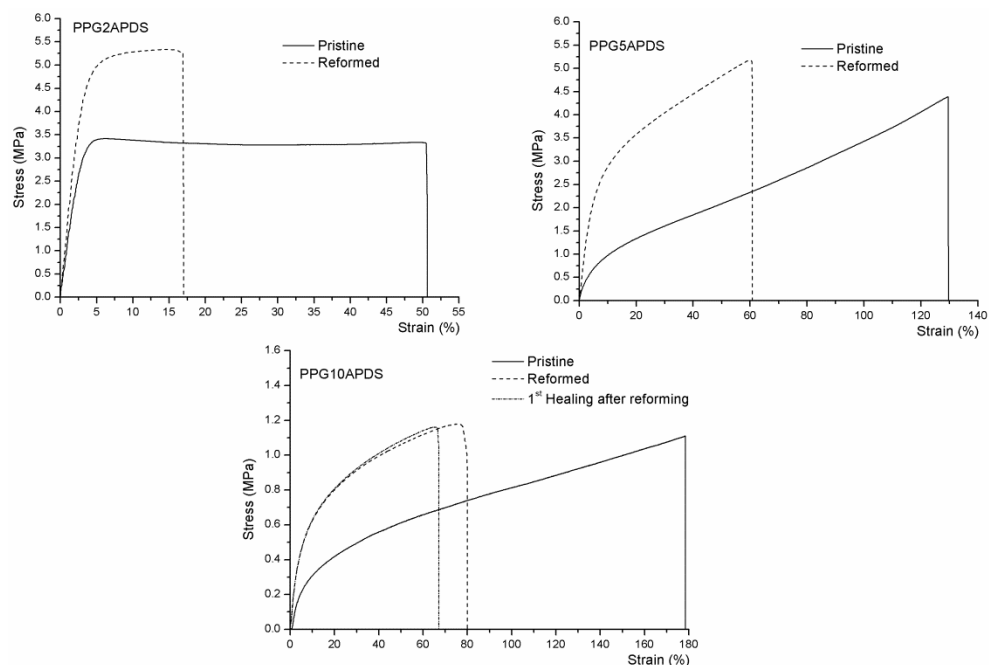
Figure 5.14 *Comparison of the physical properties of pristine and reformed PPGAPDS samples containing different amounts of aromatic disulfide moieties.*

PPGAPDS systems, including PPG2APDS, which did not present healing abilities, were able to form new materials from fragments. Under the appropriate conditions, the dynamic nature of the aromatic disulfide moieties imparted new reprocessable and recyclable features to crosslinked structures of PPGAPDS samples [49–53].

However, the reformation process gave rise to the disturbance of the physical properties of the material, as occurred in the rheological measurements. Reformed specimens presented higher modulus but lower elongation at break values than the corresponding pristine materials as a result of the reaction of uncondensed alkoxysilane groups [54,55].

In addition, PPG10APDS maintained its healing characteristics after fracture. Conversely, the PPG5APDS system lost its capability of restoration. This effect suggested that the healing abilities of these systems were restricted to a certain

crosslinking degree or physical properties, which permit the molecular diffusion between both parts of the sample [47].

### 5.4.3.3 Waterborne polyurethanes based on ureidopyrimidinone units

The physical properties of ureidopyrimidinone based WPUs depended on the strength of the interactions between different polymer chains. Despite being weaker than covalent bonds, supramolecular interactions provided healing characteristics owing to their ability to self-assembly even after fracture [56,57]. In our case, the ureidopyrimidinone dimerization by H-bond interactions was responsible for both the structural integrity of the material and the material reparation after damage.

In the same way as in the previous systems, the physical properties of PPGDHUpy systems were analyzed by strain-stress tests. Due to the material consistency, the analysis was carried out only for the samples containing 5 and 10 wt% of ureidopyrimidinone units. The obtained results are shown in Figure 5.15.
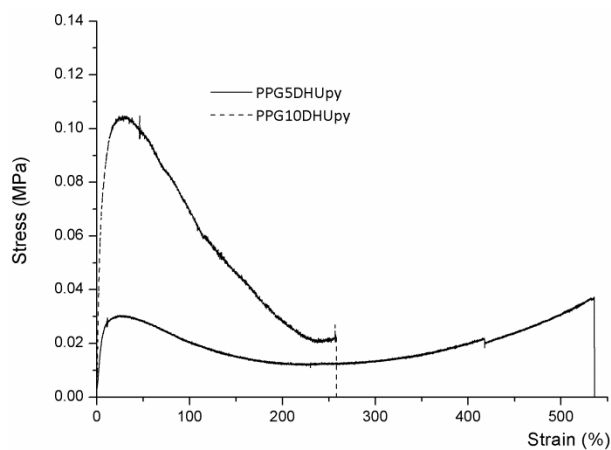
Figure 5.15 *Stress-strain plots corresponding to PPGDHUpy samples containing different amounts of ureidopyrimidinone units.*

Compared to PPGDHEMC and PPGAPDS systems, these materials showed significantly lower modulus and toughness values. Apart from the strength of the H-bond interactions, this effect suggested that a successful dimerization process of ureidopyrimidinone structures was not reached. However, these samples presented good healing properties after being cut, as depicted in Figure 5.16.
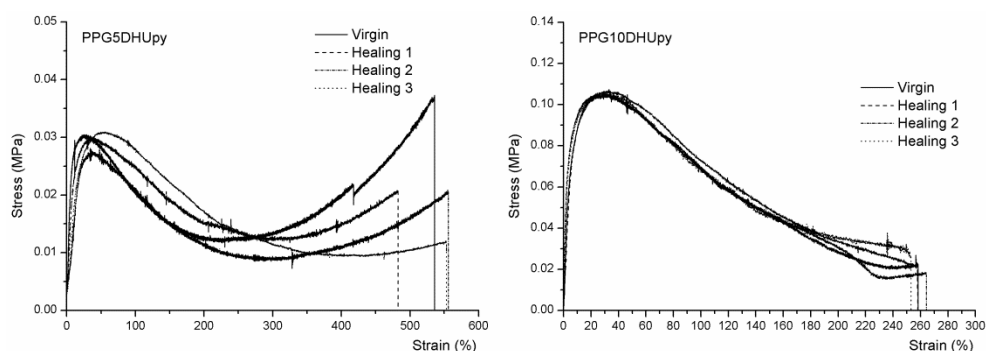
Figure 5.16 *Stress-strain curves of PPG5DHUpy (left) and PPG10DHUpy (right) of virgin and healed specimens.*

Thus, for PPG5DHUpy samples, the appearance of the obtained plot differed for the consecutive healing events. However, taking into consideration the physical properties of this material, these differences can be ignored as they fall within the error of the measurement. In contrast, the stress/strain curves of the healed PPG10DHUpy system maintained the same features as that of the virgin one, which implied a successful material rearrangement in the crack and the recovery of the interactions after the fracture.

However, after a yield point, the necessary stress to deform both materials decreased. The results implied the material flow, which was suggested by Creep experiments.

The healing efficiency values were calculated from the corresponding curves and the obtained results are summarized in Table 5.4.

Table 5.4 *Summary of the physical properties and healing abilities of PPGDHUpy samples.*

Sample		Elongation at break		Toughness	
		(%)	Healing (%)	(MPa)	Healing (%)
PPG5DHUpy	Virgin	530±48	-	9.64±0.92	-
	1st cut	503±27	94.9±10.5	8.54±0.41	83.1±10.7
	2nd cut	542±35	102.2±11.1	8.38±0.32	86.9±10.2
	3rd cut	544±51	103.6±13.0	8.01±0.38	88.6±10.7
PPG10DHUpy	Virgin	253±9	´-	15.41±0.34	-
	1st cut	245±12	96.8±6.1	15.32±0.25	99.4±2.7
	2nd cut	260±5	102.8±4.0	15.42±0.29	100.1±2.9
	3rd cut	249±8	98.4±4.8	15.33±0.42	99.5±3.5

The healing efficiency, calculated from the elongation at break and the material toughness, reached values up to 90% for both PPGDHUpy samples. These healing efficiency values are higher compared to ureidopyrimidinone containing systems reported in literature [58–60]. However, it must be mentioned that these systems present higher modulus and lower elongation at break values, so an accurate analysis should take into consideration the physical properties of the undamaged material.

In order to better understand these results, the healing efficiency values should be compared with those obtained for the rest of healable waterborne polyurethanes. This analysis will be discussed in the following section.

5.4.3.4 Comparison of the healing properties of all the systems studied

As mentioned in different sections of this chapter, several parameters affect the healing properties of the proposed materials. Aspects such as the nature and concentration of the healing agent, the physical properties of the polymer matrix, the physical property of interest among others should be taken into consideration in order to appropriately evaluate the effectiveness of the healing process [8,9,13]. In addition, the intrinsic characteristics of each healing process, such as

its autonomic or non autonomic nature or the healing time and temperature, should not be excluded from the analysis.

In this work, the healing efficiency was calculated taking into account two different physical properties of the materials, the elongation at break and toughness. Therefore, the comparison of the obtained healing efficiency values has to be referred necessarily to the physical property of interest specifically. For instance, the recovery of the elongation at break of the corresponding virgin material or its toughness.

Figure 5.17 summarizes the healing efficiency calculated as the restoration of the elongation at break of the three healable waterborne polyurethanes containing different amounts of the healing agents. As shown, ureidopyrimidinone based systems displayed a higher healing efficiency with respect to the corresponding coumarin or aromatic disulfide counterparts. Comparing these two systems, PPGAPDS showed a higher efficiency after the first healing event than PPGDHEMC systems with similar healing agent amounts (5 and 10 wt%). However, in contrast to coumarin containing systems, the healing efficiency sharply decreased as the number of healing events increased.
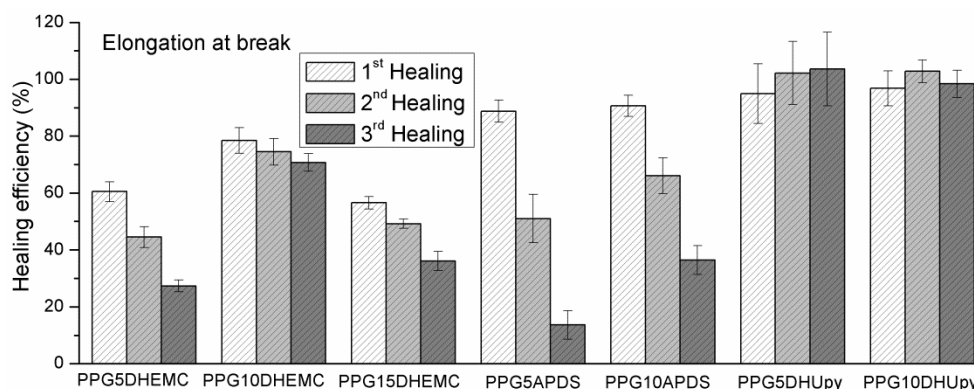
Figure 5.17 *Healing efficiency calculated as the recovery of the elongation at break for different formulations and healing events.*

Similar conclusions can be extracted from the analysis of the healing efficiency values represented in Figure 5.18. On the one hand, the recovery of the material toughness was more efficient in samples containing ureidopyrimidinone units. On the other hand, PPGAPDS samples presented significant results for the first healing event, although the reliability is seriously compromised as the number of healing events increased.
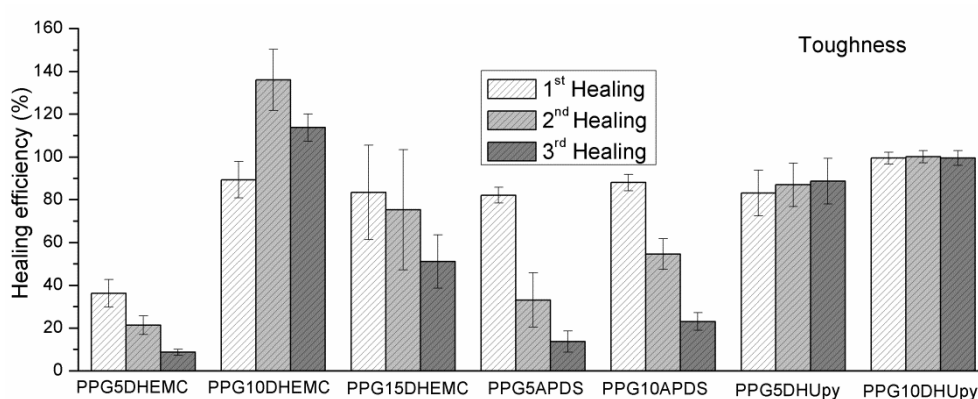

Figure 5.18 *Healing efficiency calculated as the recovery of the toughness for different formulations and healing events.*

As mentioned, the toughness of coumarin containing samples was influenced by the subsequent 365/254 nm irradiation cycles necessary for the material reparation. These variations in the physical properties of the undamaged material altered the healing efficiency, whose values widely surpassed 100% for the PPG10DHEMC system. Hence, this calculation method presented significant drawbacks when comparing the results with other systems.

Although the healing efficiency results were representative of the healing abilities of each system, an accurate analysis of the data should consider the physical properties of the obtained materials. The synthesized polymers presented very diverse physical properties with elongation at break values between 128 and 556% and toughness values ranging from 10 to 313MPa. In addition, the shape of the stress-strain curves also differed among the synthesized polymers, as shown in Figure A.18 of the Appendix. Therefore, the material application and

performance will be determined not only by the healing abilities but also by the physical properties of the pristine material.

Figure 5.19 presents an overview of the elongation at break and toughness values for all virgin and healed materials.
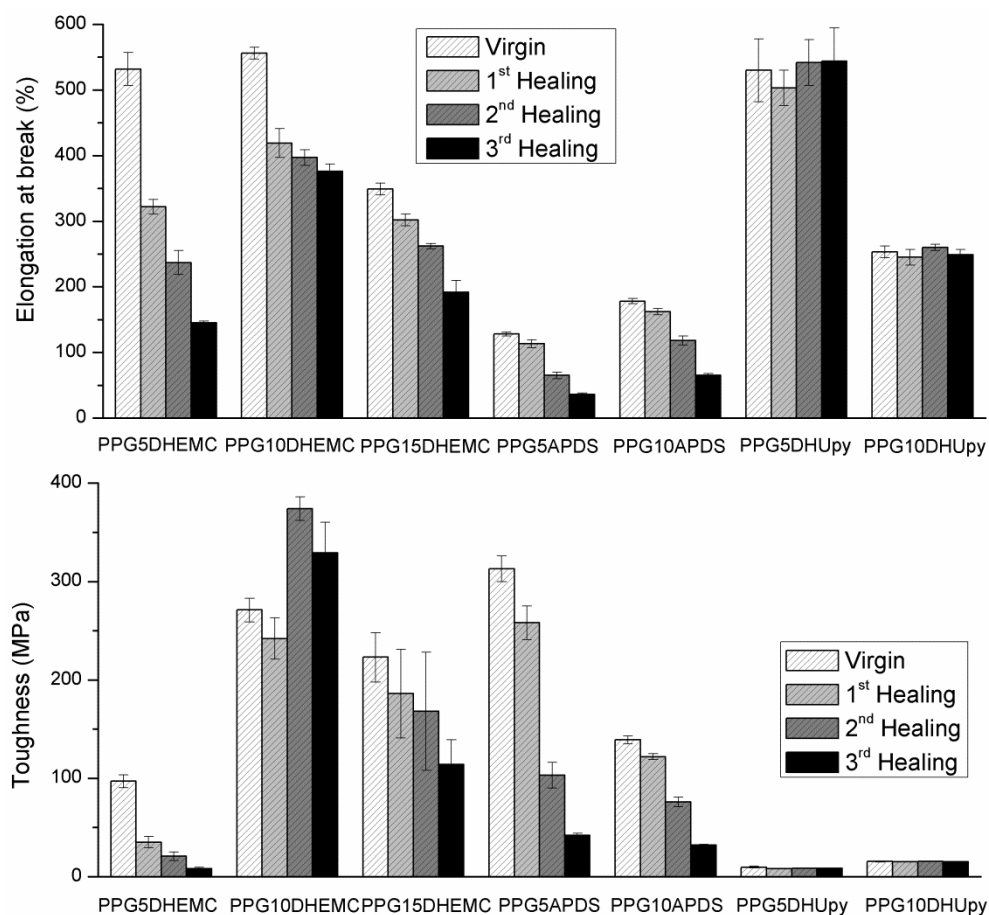
Figure 5.19 *Comparison of the physical properties*, elongation at break (top) and toughness (bottom), *for different formulation and healing events.*

In spite of presenting the best healing efficiency values, PPGDHUpy systems showed very poor physical properties with high elongation at break but low toughness values. This fact limits the number of possible applications for these

systems. In contrast, coumarin and aromatic disulfide based systems become particularly relevant as they possess a good balance between elongation at break and toughness.

Owing to the presence of inorganic domains, PPGAPDS systems presented lower elongation at break values but higher moduli in comparison to the samples crosslinked by means of coumarin dimers (Figure A.18 from the Appendix). As a result, no significant tendency was observed comparing the toughness values of different systems.

Despite this, both coumarin and aromatic disulfide systems presented potential applicability as healable materials. The selection of the most appropriate systems would be determined by the physical properties and the autonomic or non autonomic healing process required for the specific application.

5.5 Conclusions

This chapter focused on the characterization of the physical properties as well as on the determination of the healing abilities of synthesized healable waterborne polyurethanes. As mentioned, this characterization involved different physical properties and analytical methods. From the obtained results the following conclusions can be extracted:

- According to crack refilling studies, both the intrinsic features of the healing mechanism, such as the autonomic and non autonomic behavior, the physical properties of the polymer matrix and temperature were estimated the most important factors in obtaining successful damage fillings.

- Qualitative analysis demonstrated the capability of all synthesized materials to repair catastrophic damages. As a result, after applying the appropriate healing conditions, all systems recovered their structural integrity.

- The barrier properties of PPGDHEMC and PPGAPDS were determined in order to estimate the efficiency of the surface rearrangement after fracture. However, the structural integrity of PPGDHUpy membranes made it impossible to determine their barrier properties. After the healing process, the membranes presented little increments in their permeability, which suggested the generation of preferential pathways in the material structure. This effect was more noticeable for PPGAPDS samples, which are in good agreement with the crack refilling abilities shown in optical microscopy measurements.

- Proposed healable waterborne polyurethanes presented repetitive healing abilities. However, owing to the physical properties of certain formulations, the healing abilities were restricted to healing monomer amounts ranging from 5 to 15 wt%.

- The incorporation of the coumarin monomer varied the physical properties of polymer matrixes and consequently their healing abilities. PPG10DHEMC system reached a compromise between the wetting abilities and the successful network formation, which maximized the efficiency of the healing process.

- The healing efficiency calculated as the recovery of the material toughness seemed to be inappropriate to compare with other systems owing to the influence of the irradiation cycles on the physical properties of the coumarin based systems.

- Aromatic disulfide containing polyurethane networks presented both repetitive healing and reprocessing abilities. Although the healing process for pristine materials was slightly influenced by the crosslinking degree, the reprocessing event lead to the disappearance of the healing properties for PPG5APDS samples.

- The alteration of the physical properties and/or the presence of side reactions limited the healing abilities of PPGAPDS systems.

- The incorporation of ureidopyrimidinone moieties to polyurethane was unable to provide high modulus and toughness values to WPUs, although these systems showed excellent healing efficiency values.

- As a result of incorporating healing monomers into the WPU structure, material showed very diverse mechanical behavior. Therefore, the analysis of the healing capabilities of these materials should take into consideration different factors, such as the physical properties of the polymer matrix, the autonomic or non-autonomic character of the healing process and the healing conditions.

5.6 References

[1]   Fischer H. Self-repairing material systems — a dream or a reality□? Nat Sci 2010;2:873–901.

[2]   Yang Y, Urban MW. Self-healing polymeric materials. Chem Soc Rev 2013;42:7446–67.

[3]   van der Zwaag S, van Dijk NH, Jonkers HM, Mookhoek SD, Sloof WG. Self-healing behaviour in man-made engineering materials: bioinspired but taking into account their intrinsic character. Philos Trans A Math Phys Eng Sci 2009;367:1689–704.

[4]   Wool RP, O'Connor KM. A theory of crack healing in polymers. J Appl Phys 1981;52:5953–63.

[5]   Kim YH, Wool RP. A theory of healing at a polymer-polymer interface. Macromolecules 1983;16:1115–20.

[6]   Brandt J, Oehlenschlaeger KK, Schmidt FG, Barner-Kowollik C, Lederer A. State-of-the-Art Analytical Methods for Assessing Dynamic Bonding Soft Matter Materials. Adv Mater 2014;26:5758–85.

[7]   Yoon JA, Kamada J, Koynov K, Mohin J, Nicolaÿ R, Zhang Y, et al. Self-healing polymer films based on thiol-disulfide exchange reactions and self-healing kinetics measured using atomic force microscopy. Macromolecules 2012;45:142–9.

[8]   Garcia SJ, Fischer HR. Self-healing polymer systems: properties, synthesis and applications. Woodhead Publishing Limited; 2014.

[9]   Mauldin T, Kessler M. Self-healing polymers and composites. Int Mater Rev 2010;55:317–46.

[10]   Kessler MR. Self-healing: a new paradigm in materials design. Proc Inst Mech Eng Part G J Aerosp Eng 2007;221:479–95.

[11]   Blaiszik BJ, Kramer SLB, Olugebefola SC, Moore JS, Sottos NR, White SR. Self-Healing Polymers and Composites. Annu Rev Mater Res 2010;40:179–211.

[12]   Murphy EB, Wudl F. The world of smart healable materials. Prog Polym Sci 2010;35:223–51.

[13]   Yuan YC, Yin T, Rong MZ, Zhang MQ. Self healing in polymers and polymer composites. Concepts, realization and outlook: A review. Express Polym Lett 2008;2:238–50.

[14]   Banerjee S, Tripathy R, Cozzens D, Nagy T, Keki S, Zsuga M, et al. Photoinduced Smart, Self-Healing Polymer Sealant for Photovoltaics. ACS Appl Mater Interfaces 2015;7:2064–72.

[15]   Yuan C, Rong MZ, Zhang MQ. Self-healing polyurethane elastomer with thermally reversible alkoxyamines as crosslinkages. Polymer (Guildf) 2014;55:1782–91.

[16]   Ling J, Rong MZ, Zhang MQ. Coumarin imparts repeated photochemical remendability to polyurethane. J Mater Chem 2011;21:18373–80.

[17]   Michal BT, Jaye CA, Spencer EJ, Rowan SJ. Inherently Photohealable and Thermal Shape-Memory Polydisulfide Networks. ACS Macro Lett 2013;2:694–9.

[18]   Biyani M, Foster E, Weder C. Light-Healable Supramolecular Nanocomposites Based on Modified Cellulose Nanocrystals. ACS Macro Lett 2013;2:236–40.

[19]   Du P, Liu X, Zheng Z, Wang X, Joncheray T, Zhang Y. Synthesis and characterization of linear self-healing polyurethane based on thermally reversible Diels–Alder reaction. RSC Adv 2013;3:15475–82.

[20]   van Gemert GML, Peeters JW, Söntjens SHM, Janssen HM, Bosman AW. Self-Healing Supramolecular Polymers In Action. Macromol Chem Phys 2012;213:234–42.

[21]   An SY, Noh SM, Nam JH, Oh JK. Dual Sulfide-Disulfide Crosslinked Networks with Rapid and Room Temperature Self-Healability. Macromol Rapid Commun 2015;36:1255–60.

[22]   Yang WJ, Tao X, Zhao T, Weng L, Kang E-T, Wang L. Antifouling and antibacterial hydrogel coatings with self-healing properties based on a dynamic disulfide exchange reaction. Polym Chem 2015;6:7027–35.

[23]   Canadell J, Goossens H, Klumperman B. Self-Healing Materials Based on Disulfide Links. Macromolecules 2011;44:2536–41.

[24]   Ghosh SK. Self-healing materials: Fundamentals, Design Strategies and Applications. Weinheim, Germany: Wiley-VCH Verlag GmbH & Co. KGaA; 2009.

[25]   Kalista SJ, Pflug JR, Varley RJ. Effect of ionic content on ballistic self-healing in EMAA copolymers and ionomers. Polym Chem 2013;4:4910–26.

[26]   Cadogan D, Stein J, Grahne M. Inflatable composite habitat structures for lunar and mars exploration. Acta Astronaut 1999;44:399–406.

[27]   Zaribaf BH, Lee S, Kim J-H, Park P, Kim J. Toward in Situ Healing of Compromised Polymeric Membranes. Environ Sci Technol Lett 2014;1:113–6.

[28]   Kalista SJ, Ward TC, Oyetunji Z. Self-Healing of Poly(Ethylene-co-Methacrylic Acid) Copolymers Following Projectile Puncture. Mech Adv Mater Struct 2007;14:391–7.

[29]   Nagaya K, Ikai S, Chiba M, Chao X. Tire with Self-Repairing Mechanism. Trans Japan Soc Mech Eng Ser C 2005;71:2635–42.

[30]   Beiermann B a, Keller MW, Sottos NR. Self-healing flexible laminates for resealing of puncture damage. Smart Mater Struct 2009;18:085001.

[31]   Rampf M, Speck O, Speck T, Luchsinger RH. Self-repairing membranes for inflatable structures inspired by a rapid wound sealing process of climbing plants. J Bionic Eng 2011;8:242–50.

[32]   Hsieh KH, Tsai CC, Tseng SM. Vapor and gas permeability of polyurethane membranes. Part I. Structure-property relationship. J Memb Sci 1990;49:341–50.

[33]   Hsieh KH, Tsai CC, Chang DM. Vapor and gas permeability of polyurethane membranes. Part II. Effect of functional group. J Memb Sci 1991;56:279–87.

[34]   Geschke D. Physical Properties of Polymers Handbook. In: Marck JE, editor. Zeitschrift für Phys. Chemie, vol. 199, New York, NY: Springer Science & Business Media; 2007, p. 128–128.

[35]   Gugliuzza A. Smart Membrane Surfaces: Wettability Amplification and Self-Healing. Smart Membr. Sensors, Hoboken, NJ, USA: John Wiley & Sons, Inc.; 2014, p. 161–84.

[36]   Ulbricht M. Advanced functional polymer membranes. Polymer (Guildf) 2006;47:2217–62.

[37]   Lagaron JM, Catalá R, Gavara R. Structural characteristics defining high barrier properties in polymeric materials. Mater Sci Technol 2004;20:1–7.

[38]   Vladimirov V, Betchev C, Vassiliou a., Papageorgiou G, Bikiaris D. Dynamic mechanical and morphological studies of isotactic polypropylene/fumed silica nanocomposites with enhanced gas barrier properties. Compos Sci Technol 2006;66:2935–44.

[39]   Ling J, Rong MZ, Zhang MQ. Photo-stimulated self-healing polyurethane containing dihydroxyl coumarin derivatives. Polymer (Guildf) 2012;53:2691–8.

[40]   Ling J, Rong M, Zhang M. Effect of molecular weight of PEG soft segments on photo-stimulated self-healing performance of coumarin functionalized polyurethanes. Chinese J Polym Sci 2014;32:1286–97.

[41]   Yamaguchi M, Ono S, Terano M. Self-repairing property of polymer network with dangling chains. Mater Lett 2007;61:1396–9.

[42]   Yamaguchi M, Ono S, Okamoto K. Interdiffusion of dangling chains in weak gel and its application to self-repairing material. Mater Sci Eng B 2009;162:189–94.

[43]   Wool RP. Self-healing materials: a review. Soft Matter 2008;4:400–18.

[44]   Sardon H, Irusta L, Santamaría P, Fernández-Berridi MJ. Thermal and mechanical behaviour of self-curable waterborne hybrid polyurethanes functionalized with (3-aminopropyl)triethoxysilane (APTES). J Polym Res 2012;19:9956–65.

[45]   Chattopadhyay DK, Muehlberg AJ, Webster DC. Organic–inorganic hybrid coatings prepared from glycidyl carbamate resins and amino-functional silanes. Prog Org Coatings 2008;63:405–15.

[46]   Chattopadhyay DK, Raju KVSN. Structural engineering of polyurethane coatings for high performance applications. Prog Polym Sci 2007;32:352–418.

[47]   AbdolahZadeh M, C. Esteves a. C, van der Zwaag S, Garcia SJ. Healable dual organic-inorganic crosslinked sol-gel based polymers: Crosslinking density and tetrasulfide content effect. J Polym Sci Part A Polym Chem 2014;52:1953–61.

[48]   Pepels M, Filot I, Klumperman B, Goossens H. Self-healing systems based on disulfide-thiol exchange reactions. Polym Chem 2013;4:4955–65.

[49]   Martin R, Rekondo A, Ruiz de Luzuriaga A, Santamaria A, Odriozola I. Mixing the immiscible: blends of dynamic polymer networks. RSC Adv 2015;5:17514–8.

[50]   Martin R, Rekondo A, Ruiz de Luzuriaga A, Cabañero G, Grande HJ, Odriozola I. The processability of a poly(urea-urethane) elastomer reversibly crosslinked with aromatic disulfide bridges. J Mater Chem A 2014;2:5710–5.

[51]   Xiang HP, Qian HJ, Lu ZY, Rong MZ, Zhang MQ. Crack healing and reclaiming of vulcanized rubber by triggering the rearrangement of inherent sulfur crosslinked networks. Green Chem 2015;17:4315–25.

[52]   Bowman CN, Kloxin CJ. Covalent adaptable networks: Reversible bond structures incorporated in polymer networks. Angew Chemie - Int Ed 2012;51:4272–4.

[53]   Kloxin CJ, Scott TF, Adzima BJ, Bowman CN. Covalent Adaptable Networks (CANs): A Unique Paradigm in Crosslinked Polymers. Macromolecules 2010;43:2643–53.

[54]   Hofacker S, Mechtel M, Mager M, Kraus H. Sol–gel: a new tool for coatings chemistry. Prog Org Coatings 2002;45:159–64.

[55]   Hernández-Escolano M, Juan-Díaz M, Martínez-Ibáñez M, Jimenez-Morales A, Goñi I, Gurruchaga M, et al. The design and characterisation of sol–gel coatings for the controlled-release of active molecules. J Sol-Gel Sci Technol 2012;64:442–51.

[56]   Brunsveld L, Folmer BJ, Meijer EW, Sijbesma RP. Supramolecular polymers. Chem Rev 2001;101:4071–98.

[57]   de Espinosa LM, Fiore GL, Weder C, Johan Foster E, Simon YC. Healable supramolecular polymer solids. Prog Polym Sci 2015;49-50:60–78.

[58]   Wei M, Zhan M, Yu D, Xie H, He M, Yang K, et al. Novel Poly(tetramethylene ether)glycol and Poly(ε-caprolactone) Based Dynamic Network via Quadruple Hydrogen Bonding with Triple-Shape Effect and Self-Healing Capacity. ACS Appl Mater Interfaces 2015;7:2585–96.

[59]   Nobuhiro Oya TI and NY. A crystalline supramolecular polymer with self-healing capability at room temperature. Polym J 2013;45:955–61.

[60]   Hentschel J, Kushner AM, Ziller J, Guan Z. Self-healing supramolecular block copolymers. Angew Chemie - Int Ed 2012;51:10561–5.

CHAPTER 6

General Conclusions

The general objective of this thesis was the development of healable waterborne polyurethanes capable to repair catastrophic damages. Thus, different alternatives were selected according to the general classification of autonomic and non autonomic healable polymer materials. From the results obtained in this study and taking into consideration the general objectives proposed for this work, the following conclusions can be extracted:

- The methodology applied in this work has demonstrated to be a successful alternative to provide healing capacity to waterborne polyurethanes. The proposed modification for repairing monomer structures can be considered a feasible method to introduce such functionalities in the polymerization of commercial polyurethanes.

- The stability of healable waterborne polyurethane dispersions is influenced by the introduced healable monomer concentration. In this work, the selection of appropriate formulations and reaction conditions lead to stable waterborne polyurethane dispersions with significant amounts of healing moieties (up to 15 wt%).

- The physical properties of the materials can be tuned by incorporating coumarin moieties in their structures. Aspects such us the material viscosity or crosslinking degree can be controlled by selecting the appropriate irradiation conditions. However, the efficiency of the photochemical reversible reaction is reduced as the number of irradiation cycles increases, limiting the control of this process. In addition, the physical properties of coumarin based systems can change in outdoors applications, as the photochemical reaction progresses under Sunlight.

- The incorporation of aromatic disulfide dynamic structures generates crosslinked materials that present a predominantly elastic behavior at room temperature, but are able to flow and be reprocessed and recycled.

- The introduction of ureidopyrimidinone monomers gives rise to materials with an elastic behavior in steady conditions. However, their viscous character under flow conditions suggests that Upy moieties are unable to form a real tridimensional network by means of Hydrogen bonds. Hence, a further investigation about these materials would be required.

- The incorporation of different repairing monomers leads to highly efficient healable waterborne polyurethanes. However, these materials require a minimum amount of healing moieties to produce significant reparations, which was estimated around 5 wt%. Therefore, they can be considered a relevant alternative to develop healable materials.

- Apart from the incorporation of active elements in the polymeric structure, the physical properties of the polymer matrix plays a relevant role in the reparation process, as it determines the flux and rearrangement conditions of damaged materials. Therefore, in the development of healable materials the introduction of active species into a polymer matrix capable not only to fulfill the characteristics required in the application but also to permit a successful healing process should be considered.
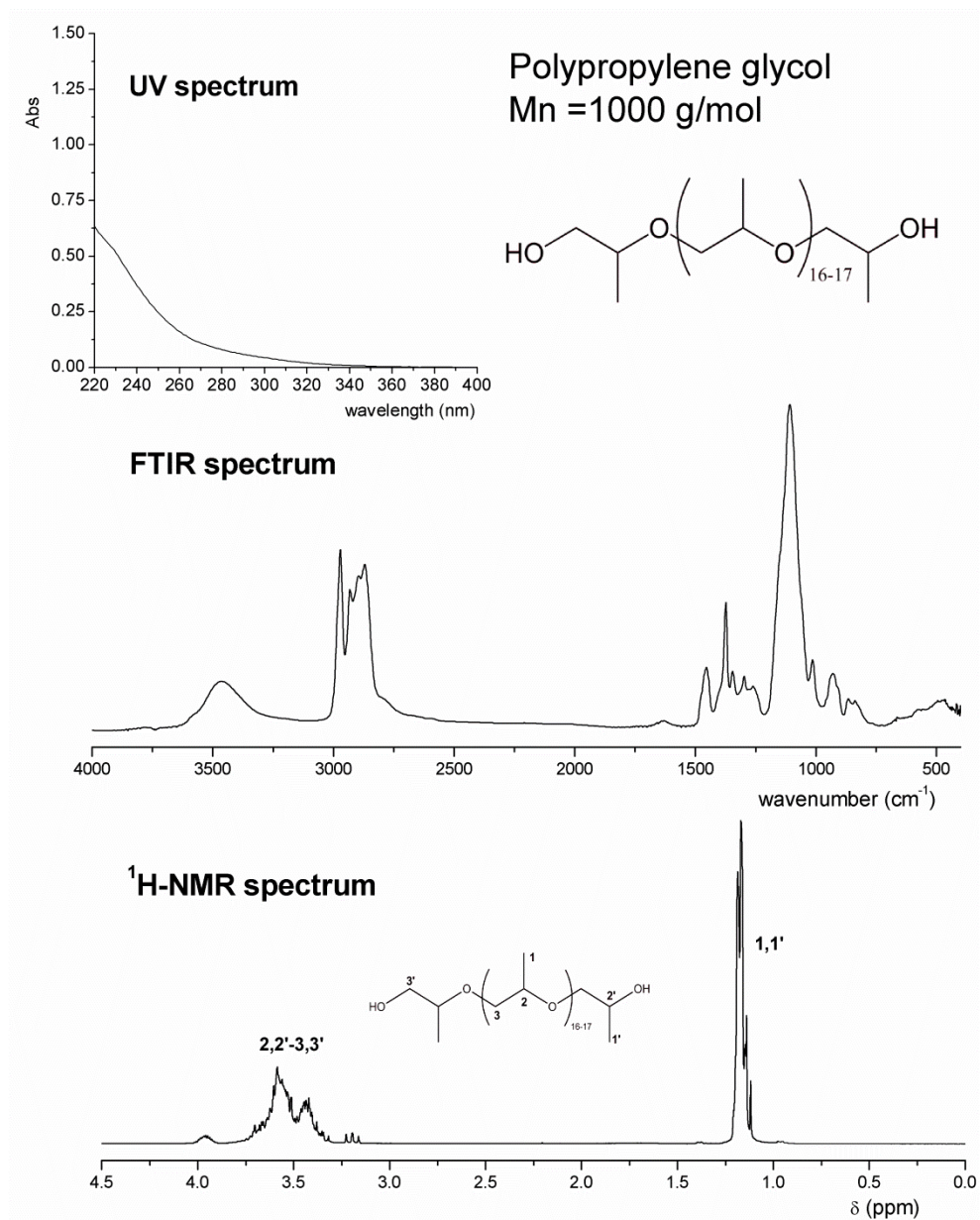
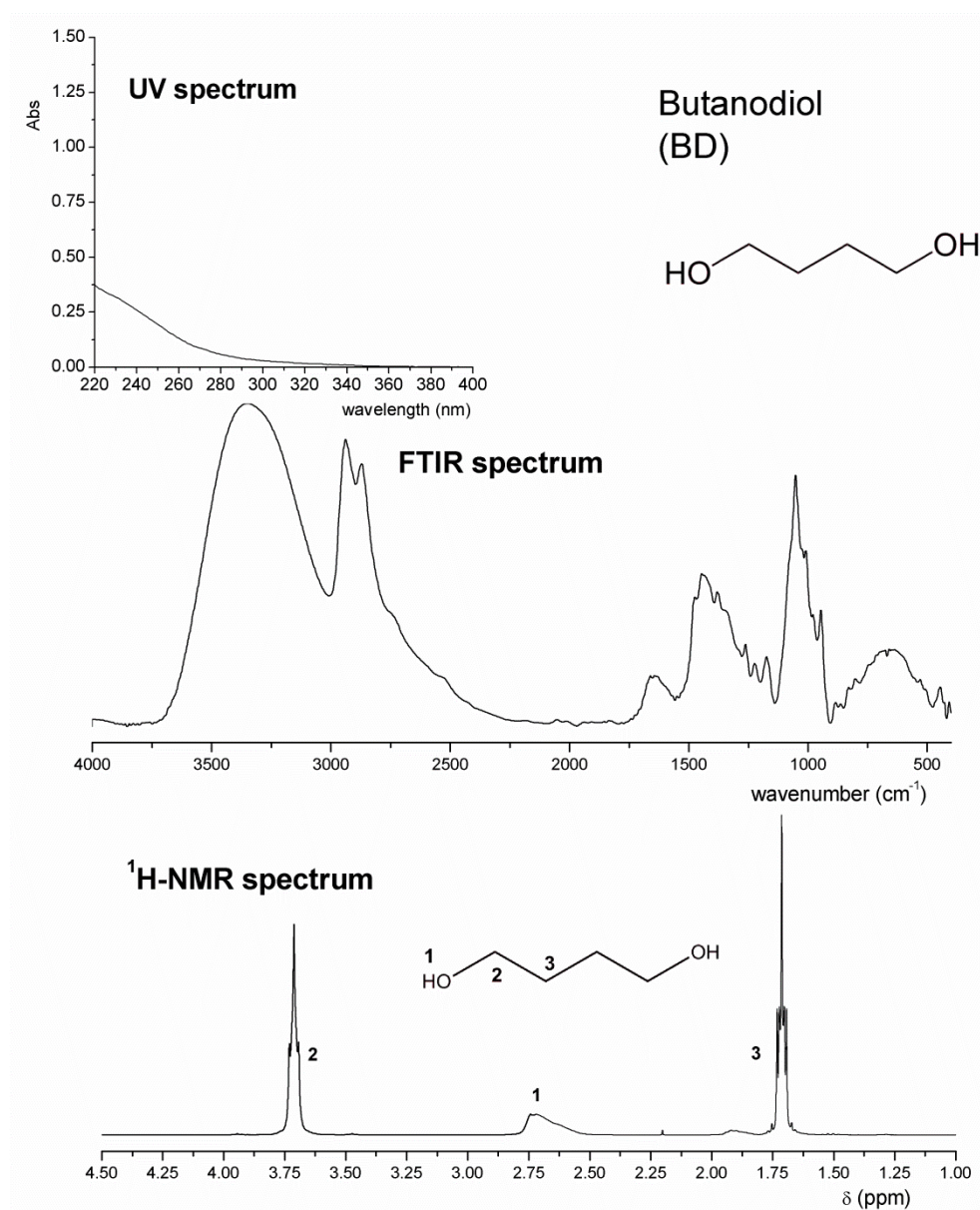# APPENDIX

A.1 Monomer spectral features
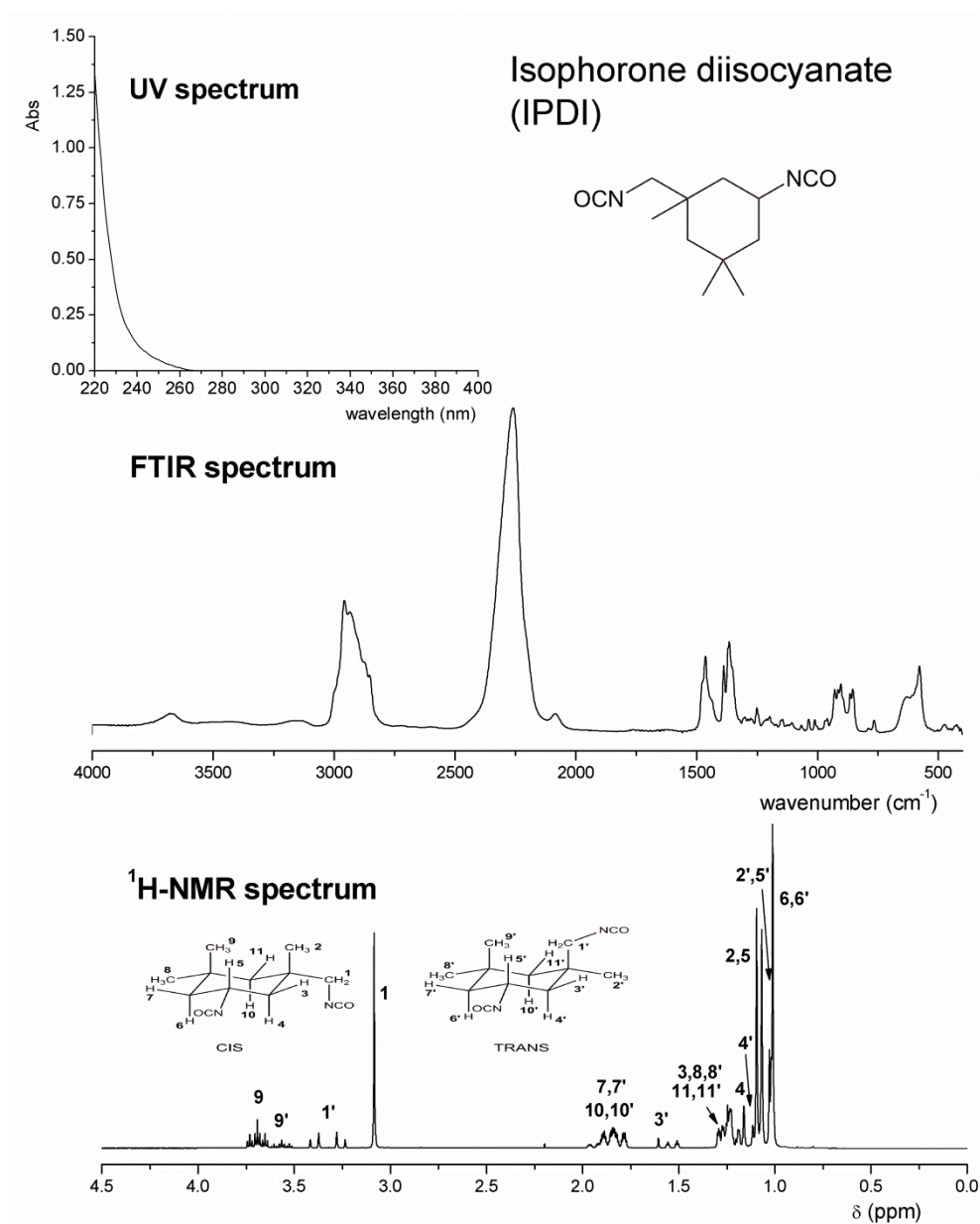
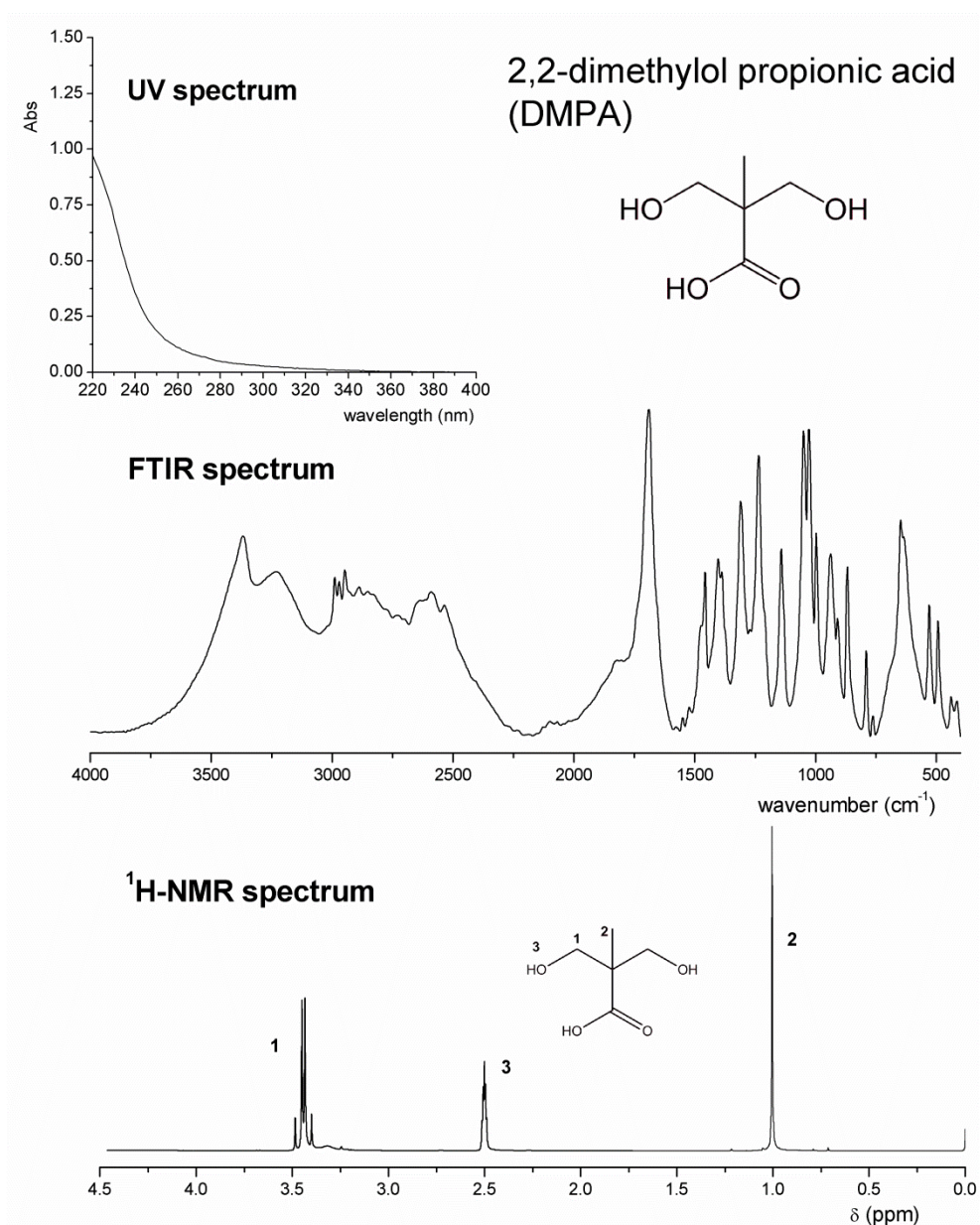**Figure A.1** *UV-vis, FTIR and 1H-NMR spectra of the Isophorone diisocianate monomer* [1]*.*

Figure A.2 *Spectral features corresponding to polypropylene glycol (Molecular weight 1000 g/mol).*
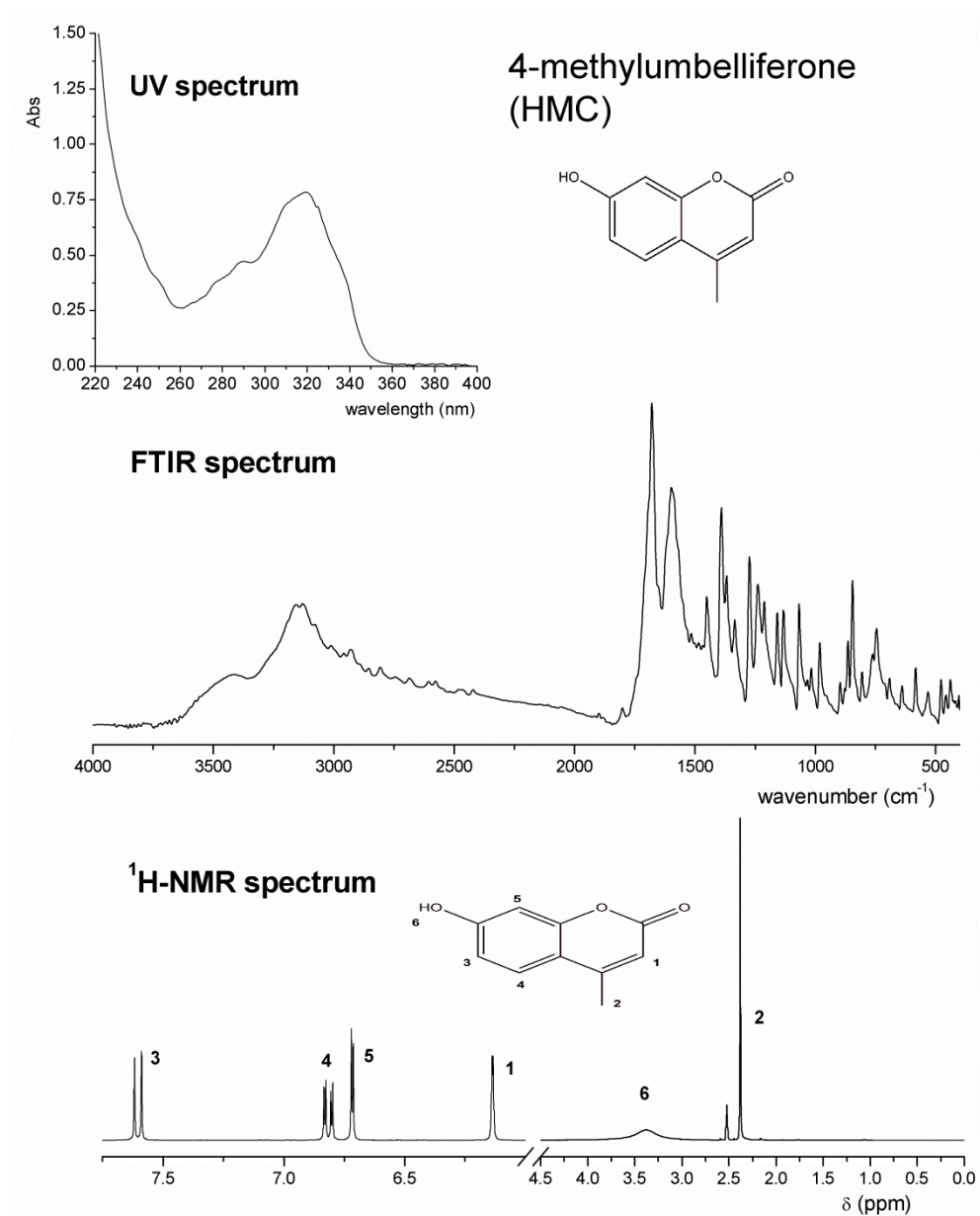
Figure A.3 *UV-Vis, FTIR, and ^{1}H-NMR spectra corresponding to butanediol monomer.*

Figure A.4 *Characteristic spectra of 2,2-dimethylol propionic acid (DMPA).*

Figure A.5 *UV-Vis, FTIR, and ^{1}H-NMR spectra of 4-methylumbelliferone (HMC).*
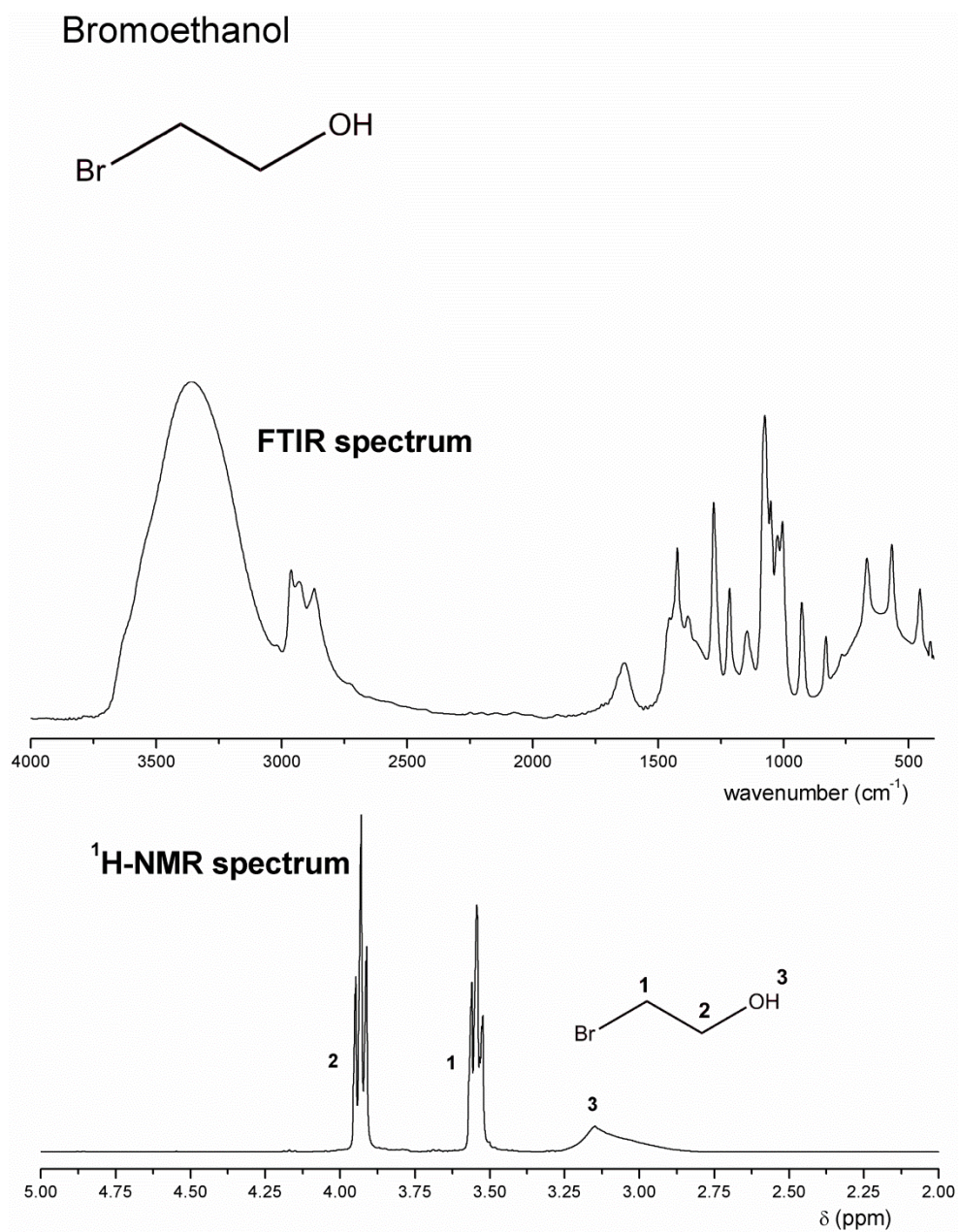
Figure A.6 *FTIR and ^{1}H-NMR spectra of Bromoethanol reagent.*

Ethyl Acetoacetate

FTIR spectrum

wavenumber (cm^{-1})

^{1}**H-NMR spectrum**

δ (ppm)
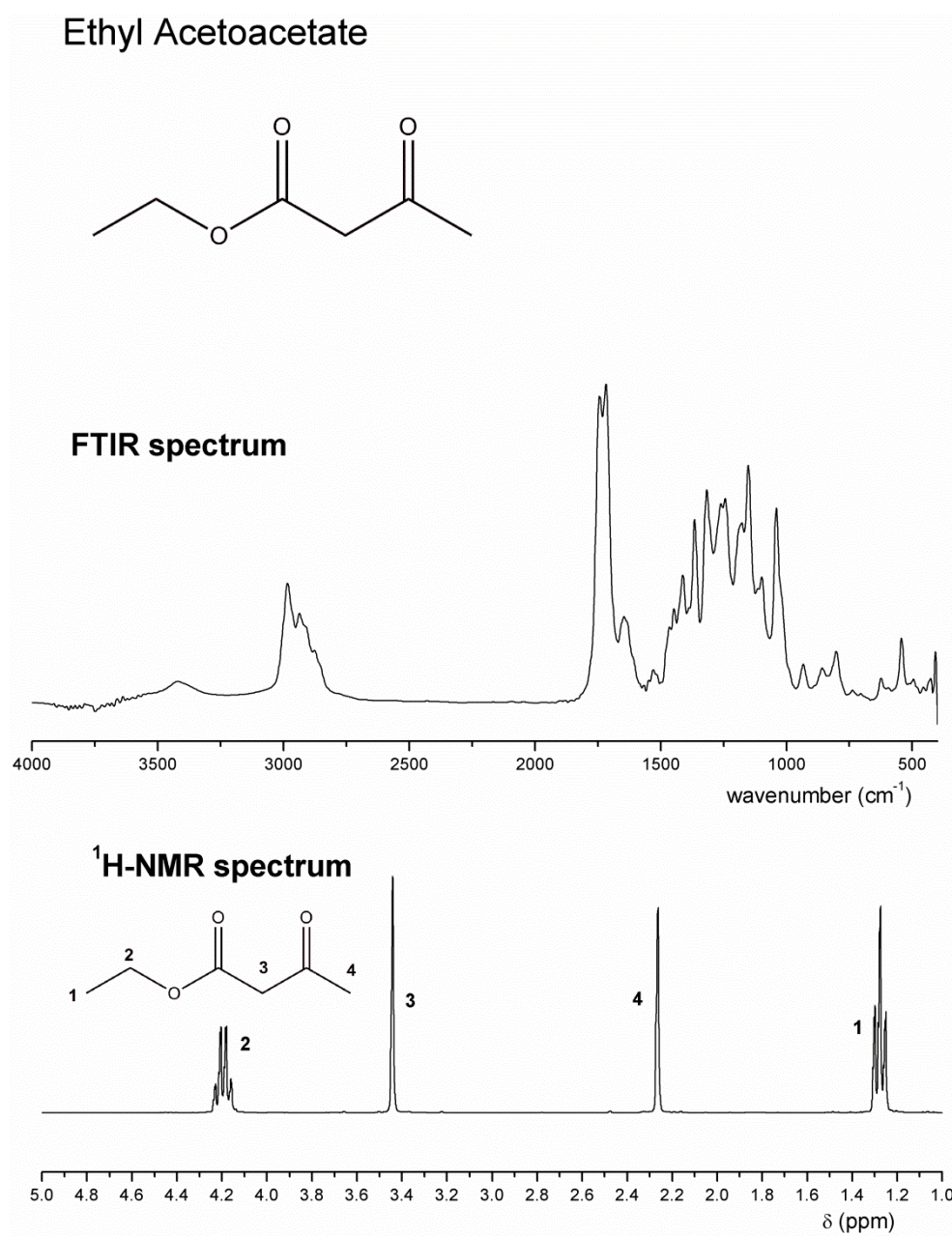
Figure A.7 *Spectral features (FTIR and ^{1}H-NMR) of Ethyl acetoacetate.*

1,3,5-trihydroxyl bencene (Phloroglucinol)

FTIR spectrum

wavenumber (cm^{-1})

^{1}**H-NMR spectrum**

δ (ppm)
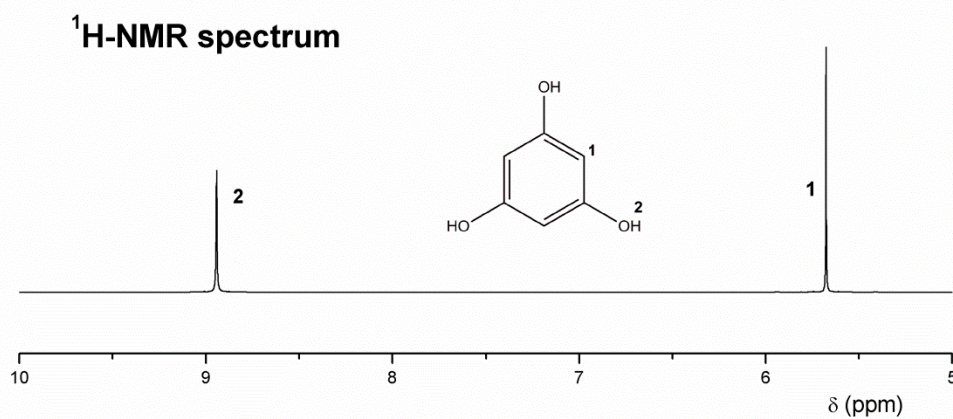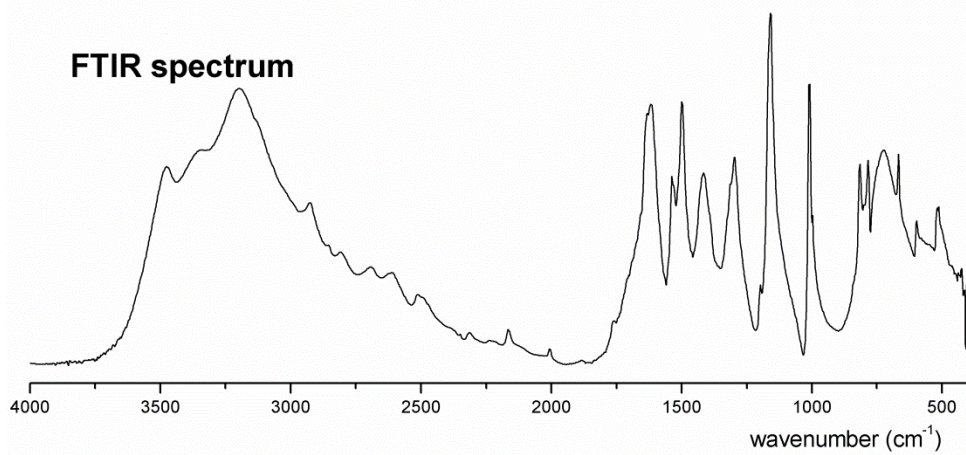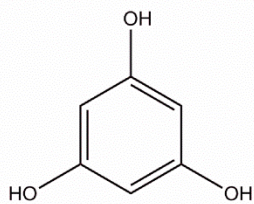
Figure A.8 *FTIR and ^{1}H-NMR corresponding to 1,3,5-trihydroxylbencene (Phloroglucinol).*

4-Aminophenil disulfide (APDS)
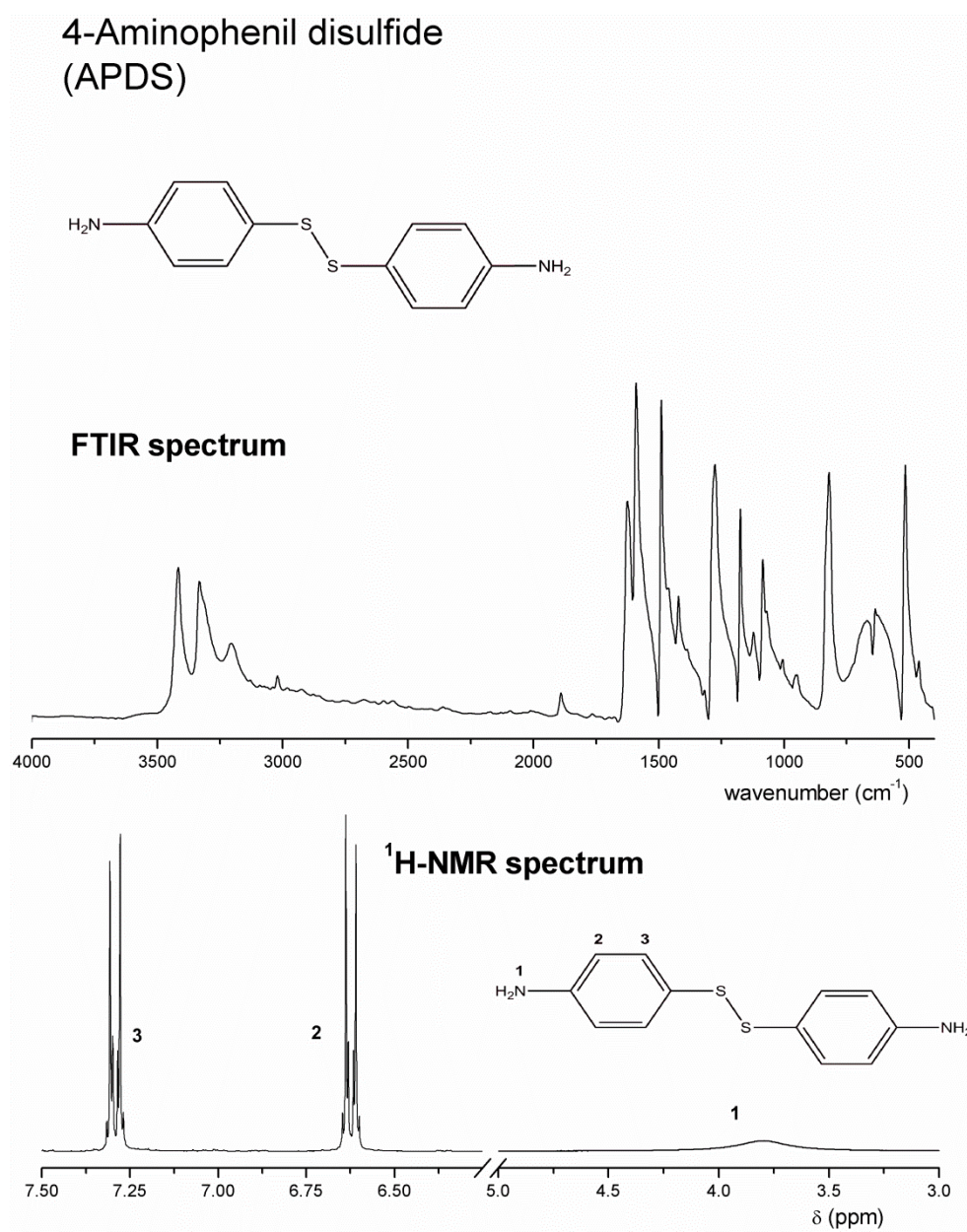
Figure A.9 *Spectral characteristics of 4-aminophenyl disulfide (APDS).*

N-(n-butyl)-3-Aminopropyl trimethoxysilane (N-bAPTMS)
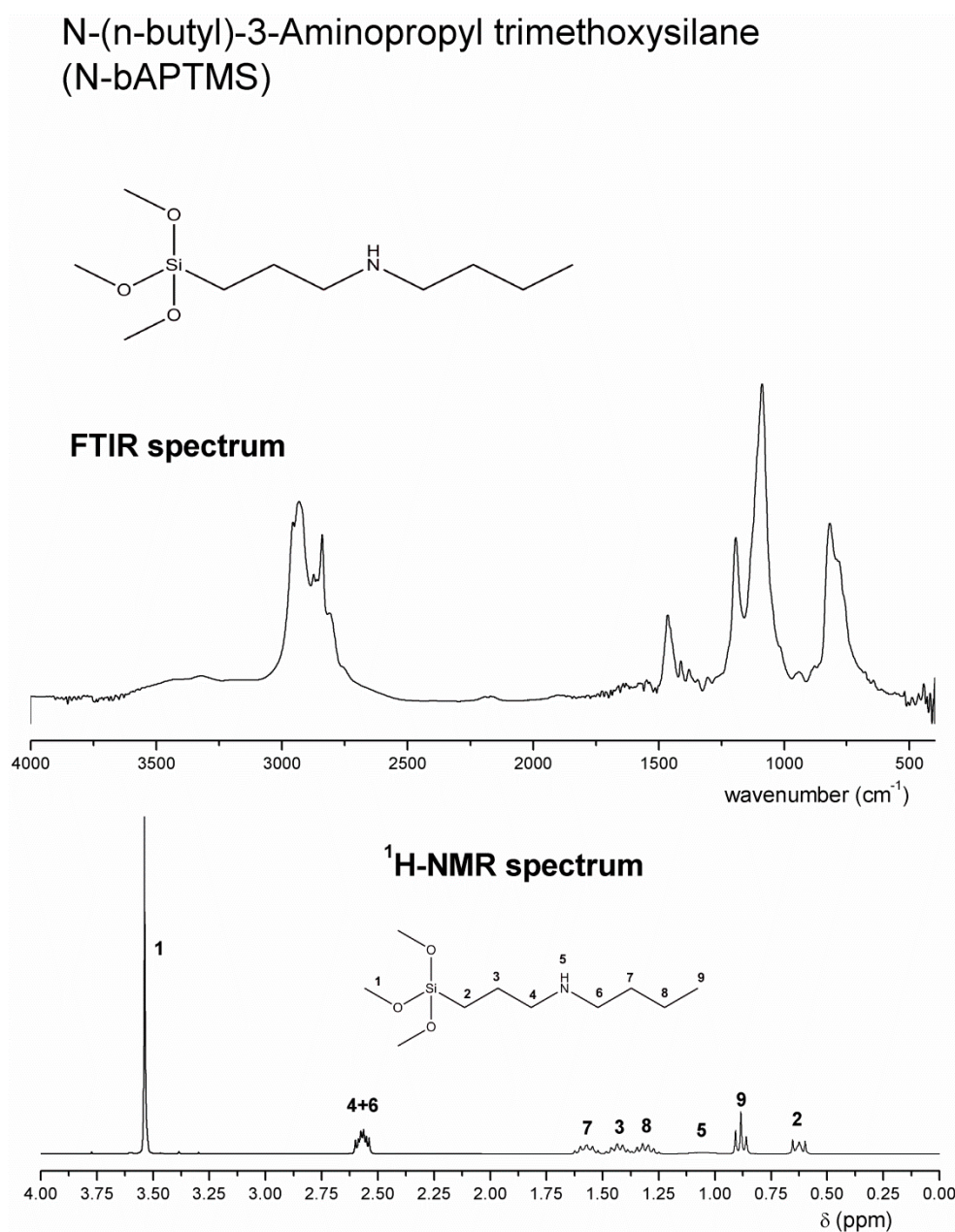
Figure A.10 *Spectral characterization of N-(n-butyl)-3-aminopropyl trimethoxysilane (N-bAPTMS).*

2-Amino-4-hydroxyl-6-methylpyrimidine (6-methylisocytosine)

Figure A.11 *FTIR and ^{1}H-NMR spectra of 2-Amino-4-methyl-6-methylpyrimidine.*

1,1'-carbonyldiimidazol (CDI)
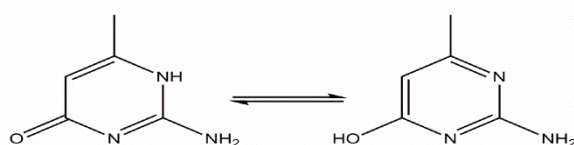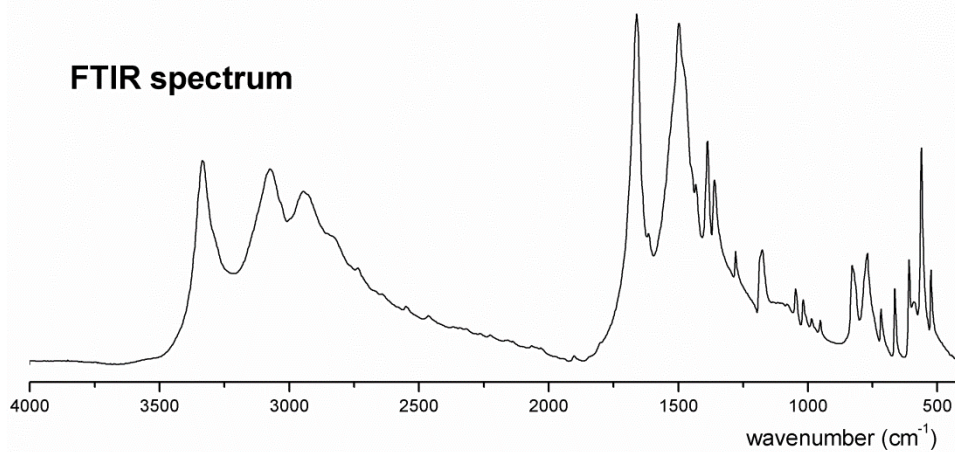
FTIR spectrum

¹H-NMR spectrum

Figure A.12 *Structural characterization of 1,1'-carbonyldiimidazol (CDI) by FTIR and ¹H-NMR spectra.*

2-amino-2-methyl-1,3-propanediol
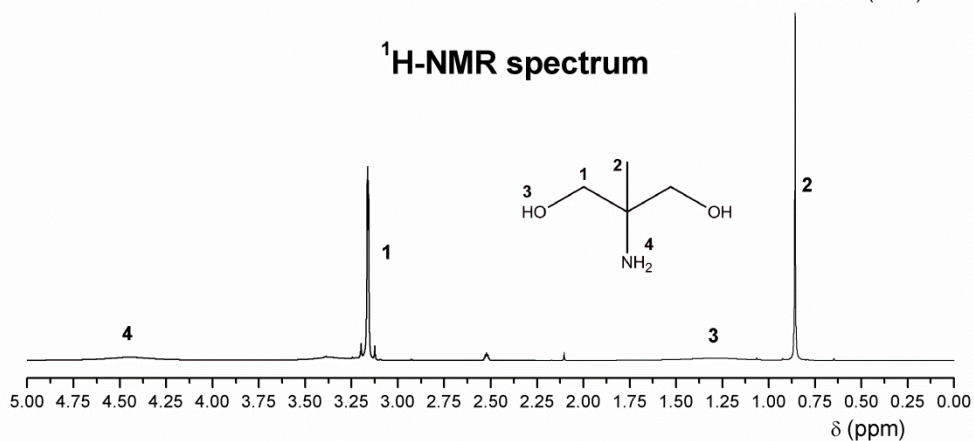
Figure A.13 *FTIR and ^{1}H-NMR spectra corresponding to 2-amino-2-methyl-1,3-propanediol.*

A.2 Experimental techniques

Fourier Transform Infrared Spectroscopy (FTIR)

Fourier Transform Infrared (FTIR) spectra of the synthesized polymers as well as the irradiated films for coumarin based systems were obtained using a Nicolet 6700 spectrometer (Thermo Scientific) at a resolution of 4 cm^{-1} and ten scans.

In contrast, the study of the hydrogen bonds at different temperatures was carried out in a Nicolet 560 spectrometer equipped with a heating cell (Harrick). In all cases, the spectra were obtained from films spin-coated onto KBr pellets by recording ten scans at a resolution of 4 cm^{-1}.

Nuclear Magnetic Resonance (NMR)

The structural characterization by means of ^{1}H liquid Nuclear Magnetic Resonance (NMR) was conducted in a Fourier Transform Bruker 300 MHz spectrometer (model Avance 300 DPX), using $CDCl_3$ or d_6-DMSO as solvents. Solid state NMR spectra were obtained in a Bruker Avance 400 spectrometer using cross polarization magic angle spinning methodology.
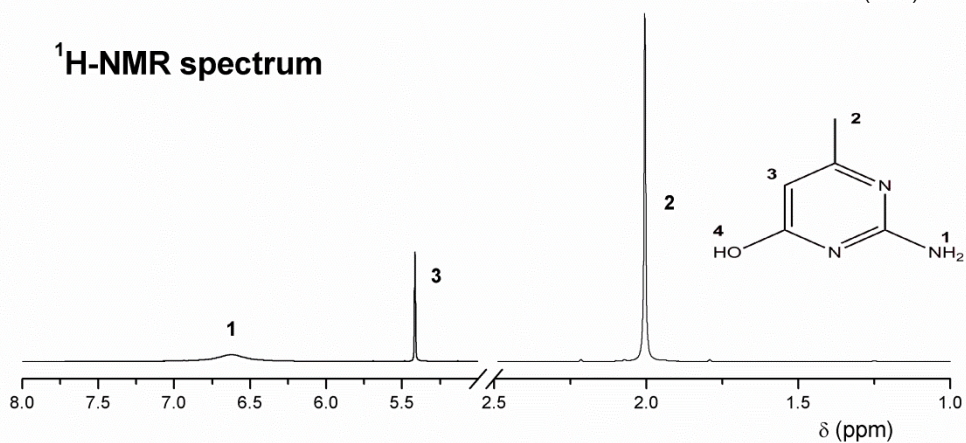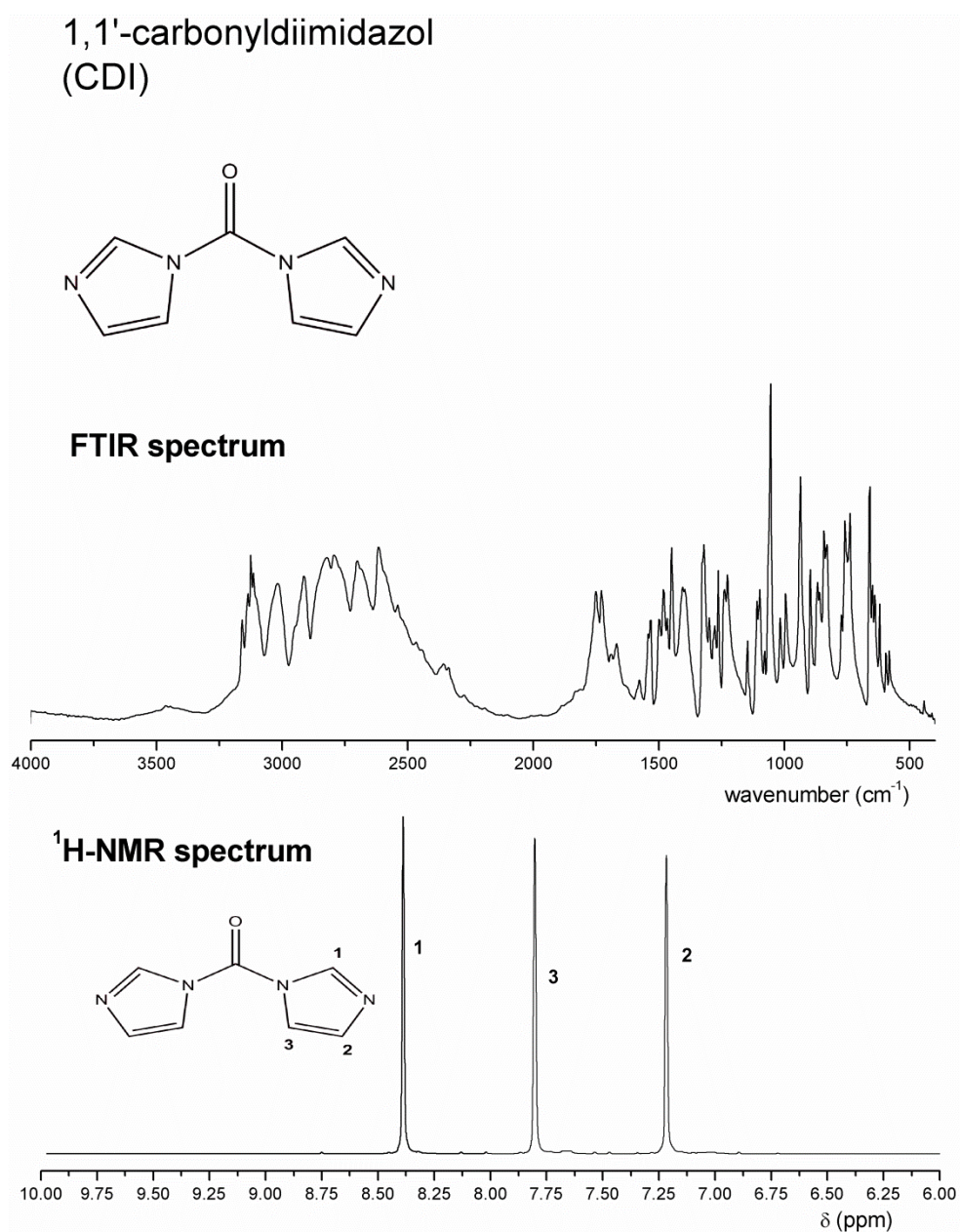
Ultraviolet-Visible Spectroscopy (UV-Vis)

The reversible photoreaction was monitored by UV-vis Spectromety in a Helios Omega UV-Vis spectrometer (Thermo Scientific).

Dynamic Light Scattering (DLS)

Dynamic Light Scattering (DLS) measurements were carried out using 90Plus (Brookhaven) Particle Size Analyzer in order to obtain the diameter of the particles, Dp, as an average of eight measurements.

Atomic Force Microscopy (AFM)

AFM images were obtained in a Dimension ICON Nanoscope V (Bruker) device using TESP-V2 tips (f=320 kHz, k=40 N/m), in 1 μm x 1 μm frames.

Optical Microscopy

The filling abilities of different healable systems were evaluated in a Nikon Eclipse E6000 optical microscope equipped with a temperature controller unit Mettler Toledo FP90.

Rheological measurements

The rheological measurements were carried out in two different equipments. Small-amplitude oscillatory experiments as well as Creep measurements were performed in an Anton Paar Physica MCR101 rheometer while the stress relaxation characteristics were analyzed using an AR-G2 equipment (TA instruments). Both devices present stress controller characteristics and the experiments were carried out using 25 mm parallel plate geometry.

Size Exclusion Chromatography (SEC)

The molecular weight distribution was obtained in an Ultimate 3000 (Thermo Scientific) SEC equipped with a refraction index detector, RefractoMax 520 RI. The selected columns were Phenomenex Phenogel with a detection range from 100 to 10^6 g·mol^{-1}.

Universal test

Tensile tests were carried out on a universal Instron 5569 tensile test machine. A load cell of 100 N was used and the initial distance between clamps was fixed at 30 mm and the experiments were perform using a crosshead-speed of 20 mm/min.

Manometric CO2 Permeation Cell

The CO_2 Permeation analysis was conducted at 25ºC and 1 atm pressure in a Manometric Permeation Cell which consisted in a dual-volume-type cell made of stainless steel connected to two pressure transducers (MKS Instruments model Baratron 672B in the downstream region, and a transducer model Baratron 740B

MKS Instruments in the upstream). The transducer was monitored in a PC with ad hoc software. A polymer sample with 1.8 cm^2 was used.

A.3 Monomer synthesis

HEMC

7-hydroxy-4-methylcoumarin (4 g, 0.0227 mol) was dissolved in 20 mL of DMF in a flask reactor and the temperature was raised up to 88 °C. Then, bromoethanol (4.3 g ,0.0344 mol) diluted in 10 mL of DMF and potassium carbonate (6.3 g, 0.0456 mol) were added under mechanical stirring. The reaction was carried out under N$_2$ atmosphere for 18h. Afterwards, the reaction mixture was cooled down to room temperature, poured into 70 mL ice water, and filtered to obtain the crude product, which was then recrystallized twice in ethyl acetate [2].

DHMC

DHMC was synthesized according to the route reported in literature [3,4]. Phloroglucinol (12.6 g, 0.1 mol) and ethyl acetoacetate (13.0 g 0.1 mol) were completely dissolved in 1,4-dioxane (60 mL). Afterwards, concentrated sulfuric acid (3 mL) was dropped into the mixture and the reaction was warmed up to 65 ºC for 1 hour. Then, the reaction was cooled down to room temperature and poured into icy water (300 mL) to obtain a yellowish precipitate. The crude product was recrystallized twice in ethyl acetate.

DHEMC

DHEMC was synthesized in a similar way as proposed elsewhere [4]. DHMC (0.86 g, 4.47 mmol) was dissolved in DMF (15 mL) under continuous stirring. Potassium carbonate (6.3 g, 0.0456 mol) was added to the mixture, and BrEtOH (1.67 g, 13.4 mmol) was added dropwise. The reaction was heated to 85 ºC and let 18 h under N$_2$ atmosphere. Finally, the reaction was cooled down and filtrated in order to remove the inorganic salt. The crude product was purified by chromatography on a silica gel column with EtOAc/EtOH solvent mixture.

N-MOPIC

A mixture of 6-methyllisocytosine (3.29 g, 0.026 mol) and 1,1'-carbonyldiimidazole (5.59 g, 0.034 mol) in dry THF (50 ml) was refluxed for 8 hours. The suspension was cooled to room temperature and filtrated. The solid was washed with acetone (2 x 20 mL) and dried *in vacuo* to obtain the final product as a white solid [5].

DHUpy

A suspension of N-MOPIC (20 g, 91.2 mmol) and 2-Amino-2-methyl-1,3-propanediol (14.6 g, 139 mmol) in dry DMF (450 mL) was reacted at room temperature under stirring. Once the reaction mixture became homogeneous (2-3 hours), the product was crystallized and washed with ethanol (3x20 mL) [6,7].

A.4 Additional information
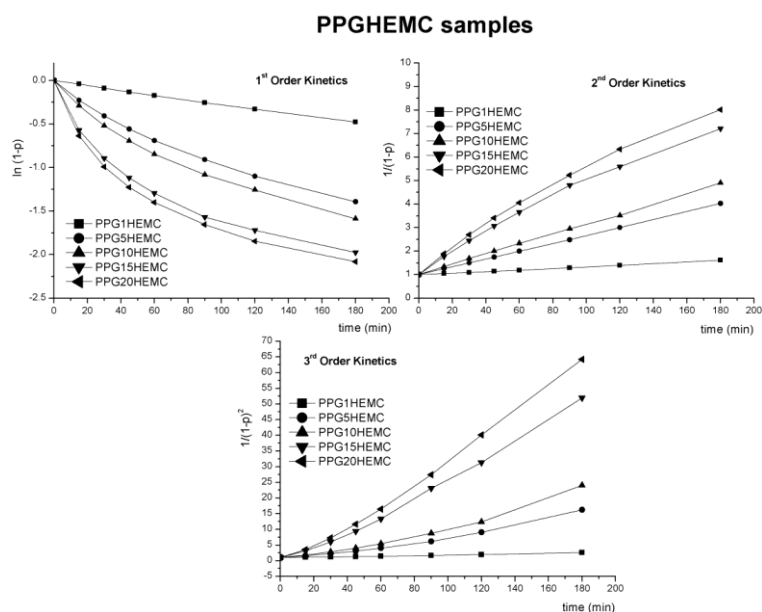
Figure A.14 *First, second and third order modeling curves for PPGHEMC.*
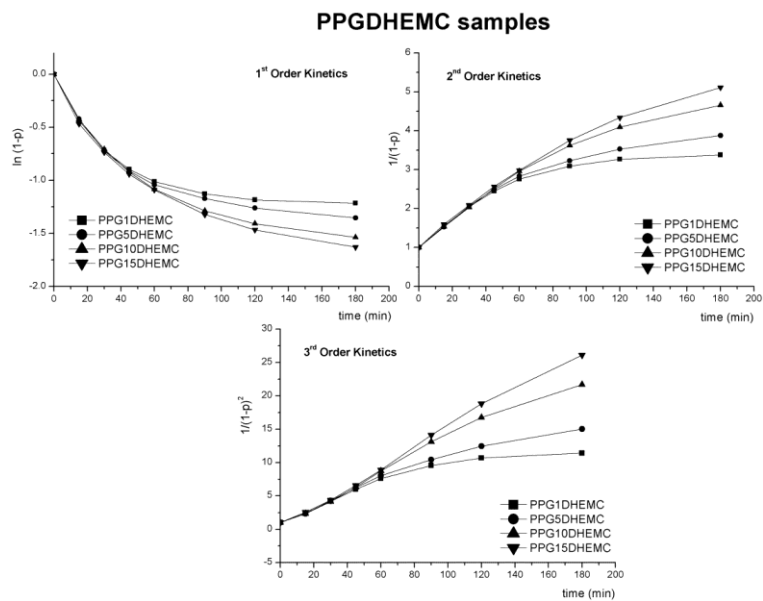
Figure A.15 *First, second and third order modeling curves for coumarin chain extended samples.*
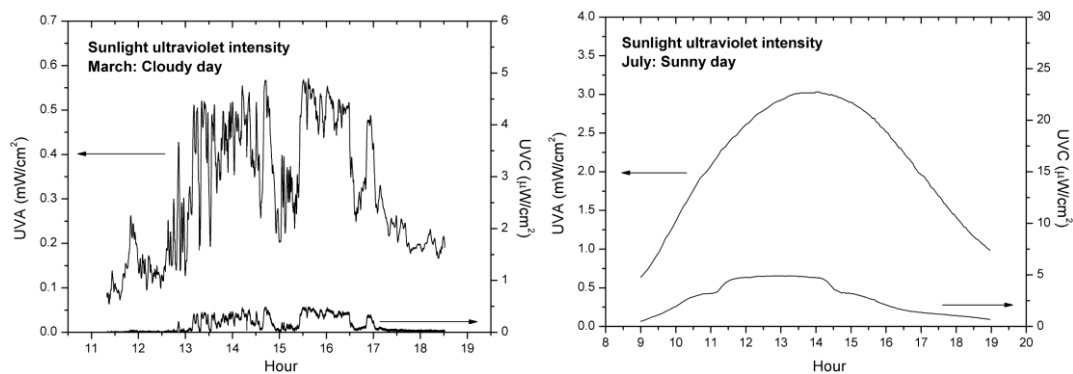
Figure A.16 *Sunlight intensity in Donostia-San Sebastián (43º19'N 1º59'O) in a cloudy day of March (top) and sunny day of July (bottom).*

System	Thickness	Intensity /Energy	Lamp	Comments	Ref
Cumarin based PU	3-200 μm	14.4-15.6 mW/cm^2	Rayonet RPR-100 16UV	Self-healing polymers	[2,4]
Cumarin-acrylate	0.03 μm	-	Moritex MUV-250U,250W 150W Xenon	-	[8]
Cumarin-silica	monolayer	87 mJ /cm^2	500W Oriel Mercury Lamp	Light responsive monolayers	[9]
Cumarina Low MW	17 μm	12 mW/cm^2	Argon Ion laser	liquid crystals	[10]
Coumarin endcapped PU	Thin films	6.17 mJ/cm^2	Rayonet RPR-100 16UV	Reversible chain extension	[11,12]
Monolayers	45.6 nm (particles)	1.41 J/cm^2	AVIA 355-7 laser (coherent)	Nanoparticles	[13]
Liquid crystals	80 nm	10 J/cm^2	Ushico USH-500D High Presure Hg lamp	Liquid crystals	[14]
Coumarin containing polymers	60 μm	14 mW/cm^2	Rayonet	Photoresist	[15]
Monolayers	-	-	200W mercury Xenon lamp	Light responsive monolayers	[16]
Cumarin acrylate	-	22 J/cm^2	F300s Fusion systems LC-6B (80W/cm)	Self-healing polymers	[17]
PEG-Cumarin	-	100 J/cm^2	Oriel UV reactor	Reversible chain extension	[18]
PLLA-Coumarin	100-200 μm	1.0 mW/cm^2	400W Hg lamp Sen Light Company	Shape-memory polymers	[19]
Hyperbranched polymers	Solution	9.2 mW/cm^2	EF-140 C UV systems Spectronics	Photoresponsive solutions	[20]
Micelles	-	-	200W lamp	Photoresponsive micelles	[21]
Coumarin Acrylates	300 nm	30-50 mW/cm^2	USHIO SP 9UV	Photoresist	[22]

Table A.1 *Summary of the irradiation conditions for coumarin containing samples presented in bibliography.*

223

```
     OR              OSi             OSi             OSi             OSi
      |               |               |               |               |
RO——Si——OR   RO——Si——OR   RO——Si——OR   RO——Si——OSi  SiO——Si——OSi
      |               |               |               |               |
     OR              OR              OSi             OSi             OSi
     Q0              Q1              Q2              Q3              Q4

     OR              OSi             OSi             OSi
      |               |               |               |
 R——Si——OR    R——Si——OR    R——Si——OR    R——Si——OSi
      |               |               |               |
     OR              OR              OSi             OSi
     T0              T1              T2              T3

     OR              OSi             OSi
      |               |               |
 R——Si——R     R——Si——R     R——Si——R
      |               |               |
     OR              OR              OSi
     D0              D1              D2

     OR              OSi
      |               |
 R——Si——R     R——Si——R
      |               |
      R               R
     M0              M1
```
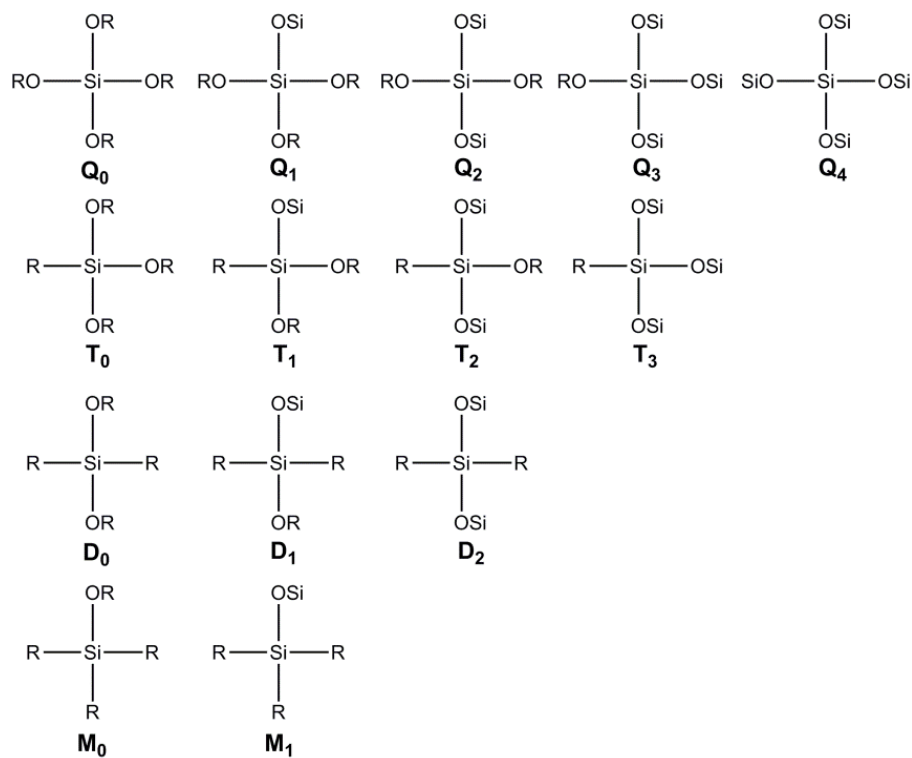
Figure A.17 *Structures coexisting in the Sol-Gel process, as called by Lippmaa et al. [23,24].*

Table A.2 *FTIR spectral deconvolution parameters.*

Sample	Contribution	FTIR region	Center	Height	FFWH
PPGAPDS	Associated urea	1800-1600	1610-1670	0-10	0-70
	Associated urethane		1750-1700		
PPGDHUpy	Associated urea	1800-1625	1625-1690	0-10	0-70
	Associated urethane		1750-1700		
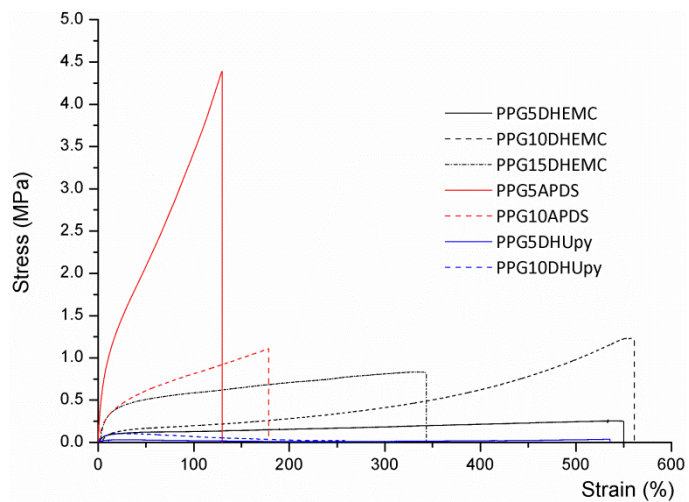
Figure A.18 *Strain-stress plots corresponding to waterborne polyurethane formulations with healable characteristics.*

A.5 Abbreviations

^{1}H-NMR: Proton - Nuclear magnetic resonance

AFM: Atomic Force Microscopy

CAN: Covalent Adaptable Networks

CDI: 1,1'-Carbonyldiimidazol

DA: Diels-Alder

DBTDA: Dibutyltin diacetate

DHEMC: 5,7-bis(2-hydroxyethoxy)-4-methylcoumarin

DHMC: 5,7-dihydroxy-4-methylcoumarin

DHUpy: 1-(1,3-dihydroxy-2-methylpropan-2-yl)-3-(6-methyl-4-oxo-1,4-dihydropyrimidin-2-yl)urea

DLS: Dynamic Light Scattering

DMF: Dimethyl formamide

DMPA: 2,2-Dimethylolpropionic acid

DMSO: Dimethyl sulfoxide

FTIR: Fourier-Transform-Infrared spectroscopy

H12-MDI: Diciclohexilmethane diisocyanate

HDI: Hexamethylene diisocyanate

HEMC: 7-hydroxyethoxy-4-methylcoumarin

ICAmpy: 2-(Imidazolylcarbonylamino)-6-methyl-4[1H]-pyrimidinone

IPDI: Isophorone diisocyanate

KBr: Potassium bromide

MDI: 4,4'-diphenylene diisocyanate

M_n: Number average molecular weight

M_w: Weight average molecular weight

PPG: Polypropylene glycol

PU: Polyurethane

SEC: Size Exclusion Chromatography

TDI: 2,4-Toluene diisocyanate

TEA: Triethylamine

T_g: Glass transition temperature

THF: Tetrahydrofuran

Upy: Ureidopyrimidinone

UV: Ultraviolet

UV-A: Ultraviolet A

UV-C: Ultraviolet C

WPU: Waterborne Polyurethane

A.6 References

[1]   Prabhakar a., Chattopadhyay DK, Jagadeesh B, Raju KVSN. Structural investigations of polypropylene glycol (PPG) and isophorone diisocyanate (IPDI)-based polyurethane prepolymer by 1D and 2D NMR spectroscopy. J Polym Sci Part A Polym Chem 2005;43:1196–209.

[2]   Ling J, Rong MZ, Zhang MQ. Coumarin imparts repeated photochemical remendability to polyurethane. J Mater Chem 2011;21:18373–80.

[3]   Jiang X, Wang R, Ren Y, Yin J. Responsive polymer nanoparticles formed by poly(ether amine) containing coumarin units and a poly(ethylene oxide) short chain. Langmuir 2009;25:9629–32.

[4]   Ling J, Rong MZ, Zhang MQ. Photo-stimulated self-healing polyurethane containing dihydroxyl coumarin derivatives. Polymer (Guildf) 2012;53:2691–8.

[5]   Wong CH, Chow HF, Hui SK, Sze KH. Generation-independent dimerization behavior of quadruple hydrogen-bond-containing oligoether dendrons. Org Lett 2006;8:1811–4.

[6]   Zhu B, Zhicheng F, Zheng Z, Xilnling W. Thermoreversible supramolecular polyurethanes with sel-complementary quadrypole hydrogen-bonded end groups. J Appl Polym Sci 2012;123:1755–63.

[7]   Feldman KE, Kade MJ, De Greef TF a, Meijer EW, Kramer EJ, Hawker CJ. Polymers with multiple hydrogen-bonded end groups and their blends. Macromolecules 2008;41:4694–700.

[8]   Sato E, Nagai S, Matsumoto A. Reversible thickness control of polymer thin films containing photoreactive coumarin derivative units. Prog Org Coatings 2013;76:1747–51.

[9]   Fang J, Whitaker C, Weslowski B, Chen M, Naciri J, Shashidhar R, et al. Synthesis and photodimerization in self-assembled monolayers of 7- (8-trimethoxysilyloctyloxy) coumarin 2001:3–6.

[10]   Jackson PO, O'Neill M, Duffy WL, Hindmarsh P, Kelly SM, Owen GJ. An Investigation of the Role of Cross-Linking and Photodegradation of Side-Chain Coumarin Polymers in the Photoalignment of Liquid Crystals. Chem Mater 2001;13:694–703.

[11]   Chen YUN, Jean C. Polyethers Containing Coumarin Dimer Components in the Main Chain. II. Reversible Photocleavage and Photopolymerization. J Appl Polym Sci 1997;64:1759–68.

[12]   Chen YUN. Synthesis and Reversible Photocleavage of Novel Polyurethane Containing Coumarin Dimer Components. J Polym Sci Part A Polym Chem 1997;35:613–24.

[13]   Kehrloesser D, Baumann R-P, Kim H-C, Hampp N. Photochemistry of coumarin-functionalized SiO2 nanoparticles. Langmuir 2011;27:4149–55.

[14]   Obi M, Morino S, Ichimura K. Factors affecting photoalignment of liquid crystals induced by polymethacrylates with coumarin side chains. Chem Mater 1999;11:656–64.

[15]   Maddipatla MVSN, Wehrung D, Tang C, Fan W, Oyewumi MO, Miyoshi T, et al. Photoresponsive Coumarin Polyesters That Exhibit Cross-Linking and Chain Scission Properties. Macromolecules 2013;46:5133–40.

[16]   Nasu S, Tsuchiya A, Kuroda K. Preparation of lamellar inorganic–organic hybrids from tetraethoxysilane and a coumarin derivative containing a triethoxysilyl group and photodimerization of the interlayer coumarin groups. J Mater Chem 2010;20:6688–95.

[17]   Huyck RH, Trenor SR, Love BJ, Long TE. Photodimerization of Coumarin Functionalized Poly(alkyl Acrylate) and Poly(alkyl Methacrylate) Random Copolymers: Influence of Copolymer Composition on Photocrosslinking. J Macromol Sci Part A 2007;45:9–15.

[18]   Trenor SR, Long TE, Love BJ. Photoreversible Chain Extension of Poly(ethylene glycol). Macromol Chem Phys 2004;205:715–23.

[19]   Nagata M, Yamamoto Y. Photocurable Shape-Memory Copolymers of ε-Caprolactone and L-Lactide. Macromol Chem Phys 2010;211:1826–35.

[20]   Fu Q, Cheng L, Zhang Y, Shi W. Preparation and reversible photo-crosslinking/photo-cleavage behavior of 4-methylcoumarin functionalized hyperbranched polyester. Polymer (Guildf) 2008;49:4981–8.

[21]   Jin Q, Liu X, Liu G, Ji J. Fabrication of core or shell reversibly photo cross-linked micelles and nanogels from double responsive water-soluble block copolymers. Polymer (Guildf) 2010;51:1311–9.

[22]   Lin H, Wan X, Li Z, Jiang X, Wang Q, Yin J. Photoreversible Resists for UV Nanoimprint Lithography (UV-NIL). ACS Appl Mater Interfaces 2010;2:2076–82.

[23]   Lippmaa E, Maegi M, Samoson A, Engelhardt G, Grimmer AR. Structural studies of silicates by solid-state high-resolution silicon-29 NMR. J Am Chem Soc 1980;102:4889–93.

[24]   Magi M, Lippmaa E, Samoson A, Engelhardt G, Grimmer AR. Solid-state high-resolution silicon-29 chemical shifts in silicates. J Phys Chem 1984;88:1518–22.

Summary

Una de las características más reseñables de los tejidos naturales es su capacidad para regenerar áreas dañadas. Inspirados por esta habilidad de los organismos vivos y los materiales naturales, actualmente se están realizando grandes esfuerzos para desarrollar materiales sintéticos capaces de recuperar su integridad estructural y propiedades físicas tras ser dañados.

Existen numerosas investigaciones en el ámbito de los materiales reparables que incluyen opciones tanto para materiales metálicos, cerámicos o poliméricos. Sin embargo, éstos últimos han centrado principalmente la atención debido a la facilidad con la que pueden ser funcionalizados o la diversidad de propiedades mecánicas que pueden presentar.

El concepto principal utilizado en el desarrollo de materiales poliméricos reparables implica la introducción de agentes activos que, idealmente, deberían de ser capaces de detectar y reparar los daños producidos. De esta forma se puede aumentar la fiabilidad de los materiales durante toda su vida en servicio.

Debido a los múltiples enfoques y alternativas propuestas, la clasificación de los materiales reparables suele ser compleja. Dicha clasificación se suele realizar generalmente teniendo en cuenta las características del proceso de reparación y se suelen diferenciar dos grandes grupos de polímeros reparables.

Los polímeros reparables denominados autonómicos son aquellos materiales capaces de reparar daños sin intervención externa. Esto implica que la generación del daño es responsable de la activación del mecanismo por el que el material será capaz de reparar el daño. Por el contrario, los materiales reparables no autonómicos necesitan la aplicación de un determinado estímulo para activar dicho mecanismo.

El principal objetivo de esta tesis fue el desarrollo de poliuretanos en base agua con propiedades intrínsecas de reparación. Para conseguir dicho objetivo, se seleccionaron tres alternativas diferentes atendiendo a la clasificación general de materiales reparables autonómicos y no autonómicos.

Los materiales no autonómicos sintetizados se basaron en la incorporación de monómeros fotoactivos derivados de la cumarina dentro de la estructura polimérica de poliuretanos en base agua. Estos monómeros son capaces de dimerizar de forma reversible como consecuencia de la aplicación de luz ultravioleta de determinada longitud de onda. La incorporación de dichos monómeros permitió, seleccionando adecuadamente las condiciones de irradiación, unir de manera reversible y controlada las cadenas poliméricas y por lo tanto, aumentar o disminuir de la movilidad molecular en las zonas dañadas, permitiendo así la reparación de dichas zonas.

En cuanto al desarrollo de materiales reparables autonómicos, se seleccionaron dos alternativas diferentes. Por un lado se decidió incorporar estructuras covalentes dinámicas basadas en sulfuros aromáticos en poliuretanos reticulados. Estos grupos han demostrado su capacidad de regenerar materiales dañados por medio de reacciones dinámicas de intercambio de cadena. Así, este trabajo estudia la posibilidad de aplicar este concepto a poliuretanos híbridos orgánico-inorgánicos.

Por otro lado, introdujeron monómeros derivados de la ureidopirimidinona para conseguir materiales reparables en base a interacciones supramoleculares. Dichos monómeros son capaces de generar enlaces de hidrógeno de gran fortaleza y direccionales que pueden dar lugar a estructuras con capacidad de auto-reparación.

Los resultados obtenidos en este estudio se recogen en este manuscrito divididos en seis capítulos.

El primer capítulo introduce el tema de los materiales reparables, destacando los conceptos más significativos así como los factores más relevantes que afectan a las propiedades de reparación. Además se presentan las características específicas de los poliuretanos que los convierten en candidatos ideales para desarrollar este tipo de materiales.

El segundo capítulo describe la síntesis y caracterización de los poliuretanos en base agua. El proceso de síntesis se dividió en diferentes etapas. En la primera

de ellas se obtuvieron monómeros activos capaces de ser incorporados covalentemente en la cadena polimérica. Para ello, se modificaron químicamente derivados de cumarina y ureidopirimidinona comerciales, introduciendo grupos hidroxilos reactivos frente a los grupos isocianato en su estructura. En cambió, para la síntesis de los poliuretanos basados en disulfuros aromáticos se optó por un monómero comercial, el 4,4'-aminofenil disulfuro.

Una vez obtenidos los correspondientes monómeros, la síntesis de los polímeros reparables se realizó de acuerdo al denominado método de la acetona. Este método consta de dos procesos fundamentales. El primero de ellos consistió en la síntesis del poliuretano por adición secuencial de los diferentes monómeros, utilizando como disolvente acetona o THF. Durante esta etapa se introdujeron en la estructura polimérica grupos polares que permitieron la posterior dispersión en agua. Una vez obtenidos los poliuretanos, se adicionó agua de manera controlada para producir una inversión de fases y la precipitación del polímero. Los poliuretanos en base agua se obtuvieron en forma de dispersiones estables de tamaño de partícula nanométrico tras la evaporación de la acetona o THF por destilación a vacío.

Los poliuretanos sintetizados se basaron en la reacción del diisocianato de isoforona (IPDI) con diferentes polioles. La naturaleza y la proporción de dichos polioles condicionaron las propiedades físicas y de dispersión de los polímeros sintetizados. Así, fijaron las proporciones de poliol flexible, en nuestro caso, polipropilen glicol (PPG), y de surfactante interno, el ácido dimetilolpropiónico (DMPA). En cada caso, se introdujo el correspondiente monómero activo (derivados de cumarina o ureidopirimidinona) en diferentes proporciones, ajustando la estequiometria con butanodiol (BD). En el caso de los sistemas basados en disulfuros aromáticos se utilizó un precursor de silicio, el N-(n-butil)-aminopropil trimetoxisilano, para conseguir la reticulación de los materiales mediante redes de silicio y se varió su cantidad en función de la concentración de disulfuro aromático en el sistema.

Mediante el proceso de síntesis propuesto se consiguió introducir los monómeros capaces de inducir procesos de reparación en la estructura de los poliuretanos.

Dicha introducción se confirmó mediante diferentes técnicas espectroscópicas como la espectroscopia de resonancia nuclear de protón (RMN) o la espectroscopia infrarroja de transformada de Fourier (FTIR). En este apartado se estudió también la incorporación de monómeros reparables en la estructura polimérica y su influencia en las características de la dispersión. Se concluyó que la incorporación de dichos grupos funcionales aumentaba el tamaño de partícula de la dispersión para los sistemas basados en cumarina y ureidopirimidinona. En cambio, se determinó que la incorporación de grupos alcoxisilano determinó en mayor medida dicho tamaño de partícula en el caso de los materiales basados en disulfuros aromáticos.

El tercer capítulo se centra en la caracterización de la respuesta a la luz ultravioleta de los diferentes polímeros basados en cumarina. Se sintetizaron dos sistemas basados en cumarina en los grupos fotoactivos se incorporaron en dos formar diferentes. En el primer caso se funcionalizaron ambos extremos de las cadenas de poliuretano mientras que en el segundo los grupos cumarina fueron introducidos como extendedores de cadena en el medio de la estructura polimérica. Como consecuencia de estas diferencias en la estructura polimérica, el proceso de dimerización reversible dio como resultado un aumento del peso molecular o la reticulación reversible dependiendo del sistema.

Teniendo en cuenta las características de cada uno de los sistemas propuestos, el estudio de la respuesta se dividió en tres apartados. En primer lugar se realizó la caracterización espectroscópica del proceso mediante espectroscopia ultravioleta, espectroscopia infrarroja y resonancia magnética nuclear. Este estudio permitió confirmar los cambios estructurales producidos por la acción de la luz así como cuantificar el rendimiento del proceso.

En un segundo paso se caracterizó la respuesta física la respuesta física de los materiales tras la aplicación de diferentes condiciones de irradiación. Este análisis se realizó teniendo en cuenta las características de los sistemas sintetizados y su posible respuesta. Así, el aumento y disminución del peso molecular de los sistemas lineales de cumarina se caracterizó por medio de análisis reológicos y cromatográficos. En cambio, la reticulación reversible de los poliuretanos que

incorporaban los grupos cumarina en el medio de la cadena polimérica se determinó por medio de medidas de contenido en gel.

En tercer lugar se estudiaron las características de la reacción de cicloadición, tratando aspectos como la reversibilidad del proceso, la cinética o la evolución bajo luz solar. Así, se determinó la influencia de la morfología de los diferentes sistemas tanto en la cinética y reversibilidad del proceso. A consecuencia de su morfología separada en fases, los sistemas reticulables mostraron cinéticas de cicloadición independientes de la concentración en las etapas iniciales del proceso y también menor reversibilidad.

El capítulo cuatro se centra a su vez en la caracterización de los materiales reparables autonómicos. Como se ha comentado, la característica principal de estos sistemas es su capacidad de reparar daños sin necesidad de ninguna intervención externa. Esta habilidad está muy influenciada por las propiedades físicas de los materiales en estado sólido, así como las condiciones en las que los materiales son capaces de fluir y reparar daños. Por lo tanto el estudio se centró en el análisis de diferentes factores que determinan las propiedades en estado sólido, como pueden ser las características de reticulación o la morfología de los materiales, así como la caracterización reológica en diferentes condiciones.

Dicho estudio permitió establecer las concentraciones mínimas de precursores de silicio necesarias para obtener grados significativos de reticulación en los sistemas basados en disulfuros aromáticos. Además, el estudio reológico confirmó la capacidad de fluir de ambos sistemas en determinadas condiciones de temperatura. Los materiales basados en interacciones supramoleculares presentaron un comportamiento principalmente viscoso en condiciones de flujo, mientras que la respuesta de los materiales basados en disulfuros aromáticos fue viscoelástica. Al margen de promover esta respuesta viscoelástica, la introducción de estos grupos dinámicos permitió el procesado de estos materiales reticulados por moldeo por compresión, lo que aumenta sus posibilidades de reutilización y reciclado. Sin embargo, dicho proceso alteró sus propiedades físicas. Por último, se caracterizó la morfología de los materiales mediante

microscopía de fuerza atómica y se demostró la separación en fases para ambos sistemas.

El quinto capítulo analiza la capacidad de reparación de los poliuretanos sintetizados. En primer lugar se aplicaron los diferentes materiales en forma de recubrimientos y se determinaron las condiciones en las cuales estos sistemas son capaces de rellenar grietas de varias micras de espesor. Se establecieron tanto las temperaturas mínimas como las condiciones de irradiación necesarias para que el proceso tuviera lugar.

En segundo lugar se determinaron las propiedades de reparación de los mismos materiales, obtenidos en forma de filmes. Dicho estudio se realizó de acuerdo a tres apartados diferentes. En primer lugar se analizaron las propiedades de los materiales de forma cualitativa como prueba de la eficacia del concepto seleccionado. Todos los sistemas fueron capaces de recuperar su integridad estructural después de ser cortados en dos partes. La reparación dio como resultado materiales capaces de ser doblados y de aguantar una masa arbitraria sin romperse.

Después se realizó un análisis de la reparación en la interfase dañada por medio de medidas de permeabilidad. Los resultados mostraron pequeños aumentos de la permeabilidad para los sistemas reparables, siendo más reseñables en el caso de los materiales basados en sulfuros aromáticos. Este comportamiento se achacó a la creación de vías preferenciales de transporte como consecuencia de una ineficiente regeneración en la superficie de ruptura.

Por último se realizó un estudio cuantitativo de la recuperación de las propiedades físicas de los materiales por medio de ensayos de tensión deformación. Estos últimos ensayos permitieron calcular la eficiencia del proceso de reparación de acuerdo a dos propiedades físicas de los materiales, la deformación a rotura y la resistencia del material. Se establecieron eficiencias del primer proceso de reparación por encima del 50% para todos los sistemas. Sin embargo, dicha eficiencia bajó en los siguientes ciclos de ruptura-reparación. En el caso de los polímeros basados en interacciones supramoleculares se

obtuvieron grandes resultados de reparación, pero las propiedades físicas de los materiales limitan su posible aplicación. En cuanto al resto de materiales propuestos, su posible aplicación vendría determinada por las condiciones de reparación y de las necesidades de la aplicación concreta.

Finalmente, el sexto capítulo recoge las conclusiones más relevantes obtenidas de este trabajo. Entre ellas, cabe destacar la posibilidad de aplicar la metodología desarrollada en la síntesis de poliuretanos comerciales para proporcionar propiedades de reparación a los materiales finales.

Estas propiedades dependerán en cada caso del agente de reparación utilizado en cada caso. Así, el uso de monómeros de cumarina permite modificar de manera controlada las propiedades de los materiales finales controlando las condiciones de irradiación. Sin embargo, el proceso está limitado debido a la pérdida de reversibilidad que sufre el proceso fotoquímico al aumentar el número de ciclos. Por otro lado, la incorporación de monómeros basados en disulfuros aromáticos, permiten obtener materiales reticulados con respuesta elástica a temperatura ambiente pero capaces de fluir y ser reprocesados en determinadas circunstancias. Por último, la incorporación de estructuras derivadas de la ureidopirimidinona dio como resultado materiales con una respuesta elástica en condiciones de reposo. Sin embargo, dicha incorporación no parece ser capaz de generar una estructura tridimensional lo suficientemente fuerte como para evitar el flujo del material.

Finalmente, cabe destacar que la introducción de los diferentes agentes propuestos ha dado lugar a materiales con propiedades significativas de reparación. En este sentido, tanto la cantidad de agente activo como las propiedades físicas de la matriz polimérica juegan un papel importante.